Universidad de Extremadura

TESIS DOCTORAL

Medida y modelización de la componente difusa de la radiación solar total y ultravioleta

Guadalupe Sánchez Hernández

Departamento de Física

2017

Universidad de Extremadura

TESIS DOCTORAL

MEDIDA Y MODELIZACIÓN DE LA COMPONETE DIFUSA DE LA RADIACIÓN SOLAR TOTAL Y UV

Guadalupe Sánchez Hernández

DEPARTAMENTO DE FÍSICA

Conformidad del Director:

Fdo: **Antonio Serrano Pérez**

2017

A mis padres

Índice general

Índice de figuras

Resumen

Es necesario contar con medidas precisas de radiación solar sobre la superficie de la Tierra, y en particular de sus componentes difusa y directa, para detectar y cuantificar adecuadamente las variaciones en el balance radiativo terrestre y, con ello, el cambio climático. Además del desarrollo de estudios climáticos, el conocimiento de la distribución de la radiación solar en sus componentes es fundamental en el avance sostenible de las energías renovables, la arquitectura, la ingeniería, la agricultura y la ecología. De especial interés es el análisis de la radiación solar ultravioleta debido a sus efectos sobre los seres vivos, en particular, sobre la salud del ser humano. En este intervalo espectral la componente difusa juega un papel muy importante ya que supone, al menos, el 40 % de la radiación UV que llega a la superficie terrestre.

Con el fin de mejorar las medidas de radiación solar difusa, en esta Tesis Doctoral se han estudiado y analizado las principales fuentes de error en la medida de radiación solar difusa, tanto en el intervalo espectral solar total (radiación solar difusa total) como en el rango de longitudes de onda ultravioleta (radiación solar difusa ultravioleta). La medida de la componente difusa requiere, además del sensor adecuado para el intervalo espectral que se desea medir, un dispositivo de apantallamiento que impida que la radiación solar directa incida sobre dicho sensor. Esto hace que la medida de la componente difusa presente errores derivados tanto del funcionamiento del sensor como del sistema de apantallamiento. Determinar y corregir estas fuentes de error es esencial para la homogeneización de las series de datos de radiación empleadas en el análisis del balance radiativo terrestre y la evaluación del recurso solar disponible.

Entre las principales fuentes de error que afectan a la medida de radiación solar difusa total destaca el error asociado al cero térmico del radiómetro utilizado para su medida (también llamado piranómetro). Gracias al trabajo realizado en esta Tesis Doctoral se ha obtenido el mayor número de valores experimentales de cero térmico registrados hasta el momento mediante la aplicación de la metodología

de tapados. Se han realizado medidas experimentales de distintos modelos de piranómetro midiendo irradiancia global y difusa con y sin ventilación artificial bajo una gran variedad de condiciones ambientales. Las medidas de cero térmico realizadas muestran que su no consideración puede producir un error de hasta un 20 % en la medida de irradiancia difusa total. Además, las diferencias observadas entre los valores del cero térmico de los distintos instrumentos analizados confirman la dificultad de establecer un único método de corrección para todos modelos de piranómetro. En el caso particular de esta Tesis Doctoral se han propuesto varios modelos de corrección del error asociado al cero térmico para el modelo de piranómetro CMP11 ampliamente utilizado en estaciones radiométricas de todo el mundo.

Asimismo, esta Tesis Doctoral ha abordado el análisis y corrección del error introducido por el anillo de sombra, uno de los dispositivos de apantallamiento más utilizados para la medida de la componente difusa. Se trata de un error debido al propio diseño del dispositivo y que puede llegar a provocar una subestimación de la medida de irradiancia difusa total de hasta un 37 % [Kudish e Ianetz, 1993]. En particular, en esta Tesis Doctoral se han comparado seis modelos de corrección del error introducido por el anillo de sombra en las medidas de irradiancia solar difusa total. Cabe destacar que, antes de ser comparados, los modelos han sido particularizados a las características de nuestra localización. Este paso se ha revelado como fundamental a la hora de corregir el error introducido por el anillo de sombra. En esta parte del estudio destaca también la propuesta de modelos originales para la corrección del error debido al uso de bandas de sombra en medidas de irradiancia difusa ultravioleta. Este punto resulta de gran relevancia debido a la escasez de este tipo de modelos en el rango de longitudes de onda ultravioleta.

La obtención de medidas de radiación precisas permite analizar su dependencia con sus principales factores moduladores: aerosoles, nubes y gases atmosféricos. Dicho análisis es un paso fundamental en el desarrollo de modelos empíricos para la estimación de la radiación difusa en localizaciones en las que existen medidas experimentales. Existe gran disparidad en lo referente a la modelización de la radiación solar difusa total y ultravioleta. Los modelos empíricos para la estimación de irradiancia difusa total son numerosos y recogen gran variedad de formas funcionales y dependencias. Por el contrario, el número de modelos empíricos para la estimación de la radiación difusa ultravioleta es muy limitado debido, principalmente, a la escasez de medidas de esta magnitud. Esta Tesis Doctoral supone un importante impulso para la modelización de la radiación difusa

ultravioleta al proponer tres modelos originales para su estimación a partir de medidas de irradiancia global ultravioleta, mucho más habituales.

Summary

Accurate measurements of global, direct, and diffuse solar radiation at the Earth's surface are required to suitably detect and quantify the variations in the earth's radiation balance and, thus, the climate change. In addition to climatic studies, the knowledge of the solar radiation components is essential for the sustainable development of renewable energies, architecture, engineering, agriculture and ecology. Of special interest is the analysis of the solar ultraviolet radiation due to its impact on biological organisms, particularly on human health. In this spectral range the diffuse component diffuse plays a very important role as it comprises, at least, 40 % of the UV radiation reaching the Earth's surface.

In order to improve the accuracy of solar radiation measurements, this Doctoral Thesis analyses the main sources of error in diffuse solar radiation measurements in both the total solar spectral interval (total diffuse solar radiation) and the ultraviolet range (ultraviolet diffuse solar radiation). Measuring the diffuse component requires a sensor suitable for the spectral range to sample and a blocking device that prevents direct solar radiation from reaching the sensor. Thus, diffuse irradiance measurements are affected by errors caused by the functioning of the sensor and the shadow system. It is needed to determine and correct these sources of error for the homogenization of solar radiation data used in the analysis of the terrestrial radiative balance and in the quantification of the available solar resource.

Among the main sources of error affecting the the process of measuring total diffuse solar radiation, the thermal offset of the radiometer (called pyranometer) must be considered. Thanks to the work developed in this Doctoral Thesis, the highest number of experimental thermal offset values recorded by the capping events methodology until now has been obtained. Experimental thermal offset values for different pyranometer models have been obtained while measuring global and diffuse irradiance, with and without mechanical ventilation, under a wide range of environmental conditions. The obtained thermal offset measurements show

that, if neglected, the error in total diffuse irradiance measurements can be up to 20 %. Additionally, the differences in the thermal offset values detected between the different instruments analyzed confirm the difficulty of establishing a single correction method valid for all pyranometer models. This Doctoral Thesis proposes several models for correcting the error associated to the thermal zero in CMP11 pyranometers, which is a model widely used in radiometric stations all around the world.

Additionally, this Doctoral Thesis has addressed the analysis and correction of the error introduced by the shadow ring, one of the shadowing devices most used for measuring the diffuse component. This error is associated to the design of the device itself and may cause an underestimation up to 37 % in the total diffuse irradiance [Kudish and Ianetz, 1993]. In particular, this Doctoral Thesis compares six mathematical models to correct the error introduced by the use of shadow rings for measuring total diffuse solar irradiance. It should be noted that, before being compared, the models have been particularized to the characteristics of our location. This step has revealed as fundamental in correcting the error introduced by the shadow ring. In this part of the study, the proposal of original models to correct the error caused by the use of shadow bands in ultraviolet diffuse irradiance measurements should be highlighted. This point is of great relevance due to the scarcity of this type of mathematical models in the range of ultraviolet wavelengths.

Accurate radiation measurements allow the analysis of its dependence with its main modulating factors: aerosols, clouds and atmospheric gases. This analysis is a fundamental step for developing empirical models to estimate diffuse radiation in locations where experimental measurements are not available. There is great disparity regarding the modeling of total and ultraviolet solar diffuse radiation. There is a plethora of empirical models for the estimation of total diffuse irradiance and they include a wide variety of functional forms and dependences. In contrast, the number of empirical models for the estimation of diffuse ultraviolet radiation is very limited, mainly due to the scarcity of experimental measurements. This Doctoral Thesis three is innovative as it proposes original models to estimate the diffuse ultraviolet irradiance by using global ultraviolet irradiance values, which are much more widely measured worldwide.

Capítulo 1

Información general sobre la Tesis Doctoral

1.1. Justificación y coherencia unitaria de la Tesis Doctoral

Esta Tesis Doctoral versa sobre la medida y simulación de la radiación solar que llega a la superficie terrestre, particularmente sobre la componente difusa de esta radiación, integrada tanto en el espectro solar total como restringida al rango ultravioleta. Este tema se encuadra en la línea de investigación Radiación solar"desarrollada dentro del Grupo de Investigación AIRE (Física de la Atmósfera, Clima y Radiación en Extremadura) del Departamento de Física de la Universidad de Extremadura.

El estudio de la radiación solar tiene una gran vigencia actualmente, incrementada aún más por sus posibles variaciones asociadas al cambio climático. En particular, resulta muy importante disponer de medidas fiables y de gran precisión, no sólo de la irradiancia solar sino también de sus componentes difusa y directa de forma individual. En este sentido cabe indicar que el proceso de medida de la radiación solar difusa no ha gozado de la atención recibida por la radiación solar global y que, actualmente, se presenta como un prometedor campo de mejora del conocimiento. Esta menor abundancia de estudios se acentúa muchísimo en el caso de la radiación solar ultravioleta difusa, la cual es medida en muy pocas estaciones en el planeta.

En este sentido, esta Tesis Doctoral constituye una unidad con un objetivo común, investigando en la mejora de diversos aspectos de la medida de la radiación

solar difusa así como su simulación en función de otras variables meteorológicas. Así, estudia varias fuentes de error de especial importancia para la medida de la radiación solar difusa, como el error térmico y la subestimación asociada al uso de anillos o bandas de sombras para apantallar la radiación directa. Además, propone modelos de corrección de estos errores así como de simulación en función de otras variables habitualmente registradas en las estaciones meteorológicas. Todo ello con el propósito común de mejorar la medida de la componente difusa de la radiación solar, así como su simulación.

La presente memoria de Tesis Doctoral se ha elaborado siguiendo la modalidad "Tesis doctorales presentadas como compendio de publicaciones", de acuerdo con el artículo 46 de la Normativa Reguladora de los Estudios de Doctorado en la Universidad de Extremadura. Según esta modalidad, la Tesis Doctoral se soporta fundamentalmente en trabajos publicados, a los que se acompaña una introducción y un resumen general. Si bien esta modalidad presenta una mayor dificultad en cuanto a la visión unitaria de la Tesis Doctoral, posee, a nuestro parecer, interesantes ventajas como son: 1) el hecho de incorporar todo el enriquecimiento científico derivado de los procesos de discusión con los revisores de los artículos, 2) la garantía de calidad que supone la publicación en revistas de gran impacto, y 3) una mayor difusión internacional de los resultados de la Tesis Doctoral. Por todo ello, esta Tesis Doctoral se ha elaborado conforme a dicha modalidad.

1.2. Objetivo

Esta Tesis Doctoral tiene como principal objetivo contribuir a una mejor estimación de la irradiancia difusa total y UV, tanto en lo relativo a la corrección de sus medidas, como a la propuesta de modelos que permitan su estimación a partir de otras magnitudes. Este objetivo general se concreta en las siguientes aportaciones específicas:

- Cuantificar el error asociado al cero térmico en los piranómetros para la medida de irradiancia difusa total.
- Proponer modelos para la corrección del error asociado al cero térmico en las medidas de irradiancia difusa total.
- Analizar y corregir la subestimación debida al uso de anillos o bandas de sombra para medir la irradiancia difusa total.

- Analizar y corregir la subestimación debida al uso de anillos o bandas de sombra para medir la irradiancia difusa ultravioleta.
- Analizar y proponer modelos para la estimación de la fracción de irradiancia difusa UV.

1.3. Estructura de la memoria

Esta Tesis Doctoral recopila el trabajo descrito en siete artículos, los cuales abordan los objetivos mencionados en la sección anterior. La presente memoria ha sido estructurada en los siguientes bloques y capítulos:

- Este primer capítulo introductorio donde se establece el marco dentro del cual se ha desarrollado este trabajo.
- El Capítulo 2, centrado en el análisis y corrección del error asociado al cero térmico en los piranómetros utilizados para la medida de la irradiancia global y difusa total. Este capítulo agrupa cuatro artículos en los que se han obtenido valores experimentales del cero térmico de distintos modelos de piranómetros midiendo irradiancia global y difusa con y sin ventilación artificial, y donde se han propuesto modelos para la corrección de dicho error.
- El Capítulo 3, agrupa dos artículos en los que se analiza el error asociado al uso de anillos o bandas de sombra en las medidas de irradiancia difusa total y ultravioleta. En el primero de ellos se revisan y mejoran los modelos para la corrección del anillo de sombra en las medidas de irradiancia difusa total. El segundo de los artículos propone modelos para la corrección del error debido al uso de bandas de sombra en medidas de irradiancia difusa ultravioleta.
- El Capítulo 4, incluye por un artículo que propone distintos modelos empíricos para la estimación de la fracción de irradiancia solar difusa en el rango UV del espectro solar.
- Por último, se incluye un capítulo final con los principales resultados y conclusiones de esta Tesis Doctoral.

Cada capítulo, además de contener los artículos correspondientes a su temática concreta, incluye una introducción que pretende poner en valor dichos artículos incidiendo en la motivación que subyace a su estudio y algunos aspectos especialmente interesantes de los mismos. No se trata, sin embargo, de una traducción al castellano del contenido de los mismos, pues los propios artículos son ya parte fundamental de

la Tesis Doctoral en sí misma. Esta introducción pretende ser un espacio de discusión sobre los mismos, que enriquezca el conjunto de artículos con comentarios adicionales y resalte algunos aspectos que, a nuestro parecer, tienen especial relevancia.

Capítulo 2

Introducción

2.1. Origen y características de la radiación solar difusa

La radiación solar constituye la principal fuente de energía del Sistema Climático, siendo el motor de numerosos procesos físicos, químicos y biológicos de gran importancia para la existencia y desarrollo de los ecosistemas y la vida en la Tierra. Así, participa muy activamente en los intercambios de energía y masa entre los diferentes subsistemas climáticos, destacando su importantísimo papel en el balance radiativo terrestre, el ciclo hidrológico y el ciclo del carbono.

Dicha radiación procede, principalmente, de la superficie visible del sol, denominada fotosfera solar. Esta emisión es el resultado último de la actividad del núcleo del sol, donde se producen reacciones termonucleares en las que cuatro núcleos de Hidrógeno se fusionan para dar un núcleo de Helio. La energía liberada mantiene el núcleo a una temperatura alrededor de más de 15×10^6 K. Esta energía se transporta hacia la superficie solar mediante procesos de re-irradiación y convección, manteniendo la temperatura de la fotosfera a unos 5800 K. Finalmente, es fundamentalmente la fotosfera la que emite radiación hacia el espacio.

Esa radiación emitida por el sol llega a la parte superior de la atmósfera terrestre como un haz de rayos aproximadamente paralelos con una distribución espectral asimilable, a grandes rasgos, a la de un cuerpo negro a unos 5800 K situado a 1 U.A., denominándose espectro solar "extraterrestre" (Figura 2.1). Este espectro está compuesto aproximadamente por un 9 % de radiación ultravioleta (UV), rayos X y gamma (menos de 400 nm), un 50 % de radiación visible (400-750 nm) y un 41 % de radiación infrarroja (750-4000 nm). Esta radiación sufre ligeras[1] variaciones

[1]Hay que hacer notar que, aunque las variaciones en la actividad solar producen fluctuaciones

asociadas a la actividad solar (relacionada con las manchas solares) y a la variación anual de la distancia Sol-Tierra.

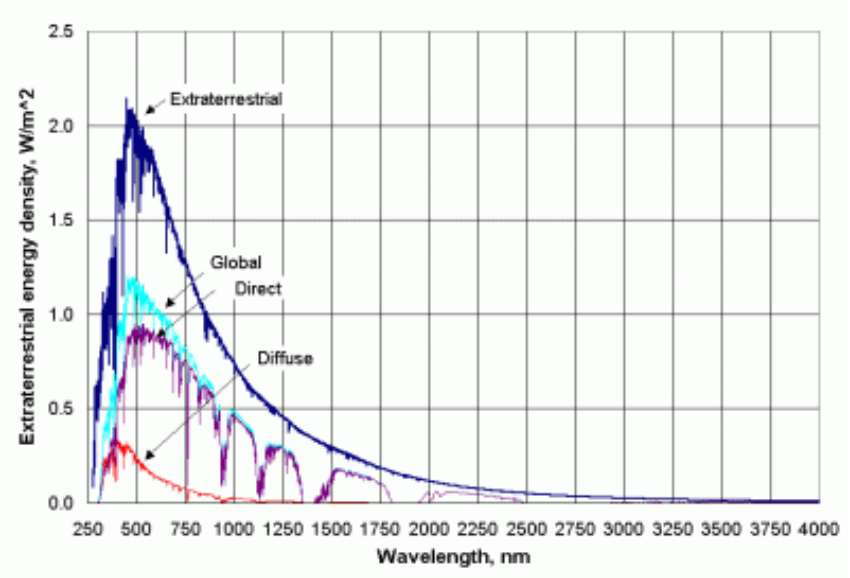

Figura 2.1: Irradiancia solar espectral en el tope de la atmósfera y componentes global, directa y difusa en la superficie terrestre resultantes de los procesos de absorción y dispersión por parte de los gases para una atmósfera estándar.

Cuando esta radiación solar penetra en la atmósfera comienza a interaccionar con los componentes atmosféricos, pudiendo sufrir absorción y dispersión[2], modificándose así su intensidad, distribución espectral y dirección de propagación. Esta interacción va cambiando a medida que la radiación penetra en la atmósfera debido a la variación vertical en la composición de la atmósfera y a los procesos acumulativos de atenuación que va sufriendo la propia radiación. En estos complejos procesos de absorción y dispersión intervienen numerosos gases (como, por ejemplo, O, O_2, O_3, N, N_2, H_2O, CO_2, etc.), así como las nubes y los aerosoles. Hay que mencionar que, debido a la diferencia en tamaño del dispersor, las moléculas de las gases atmosféricos (alrededor de 10^{-4} micras) producen dispersión en el régimen de Rayleigh, mientras que las gotas (la mayoría entre 4

pequeñas en la cantidad total de radiación solar emitida, las variaciones relativas en las longitudes de onda muy cortas pueden ser importantes.

[2]Es conocida la dificultad para la traducción al castellano del término inglés "scattering", que designa el cambio de dirección de propagación de la radiación tras interaccionar con la materia. No existiendo un consenso en la comunidad científica en cuanto al término a emplear en castellano, en la bibliografía específica se encuentran diversas opciones, como, por ejemplo, "dispersión", "difusión" o "esparcimiento". En esta memoria se emplea el término "dispersión" para designar el mencionado fenómeno.

y 50 micras) y cristales (entre 1 y 100 micras) de las nubes, y los aerosoles (gran variedad, entre 10^{-3} y 10^{2} micras), producen dispersión en el régimen Mie. Este hecho es importante pues la dispersión Rayleigh presenta una acusada dependencia con la longitud de onda, dispersándose más las longitudes de onda menores, mientras que la dispersión Mie por una nube no resulta tan selectiva espectralmente.

Como consecuencia de estos complejos procesos de absorción y dispersión, acaba llegando a la superficie terrestre un campo de radiación solar atenuado respecto al que incide en el tope de la atmósfera. Este campo radiativo global está compuesto por: 1) radiación solar que no ha sido dispersada en su recorrido dentro de la atmósfera y que, por tanto, proviene en la dirección del sol (la cual se denomina *radiación solar directa*), y 2) radiación solar que ha sido dispersada una o varias veces y que proviene de todas direcciones (la cual se denomina *radiación solar difusa*). Debido a la dependencia espectral de la absorción y de algunos procesos de dispersión, la distribución espectral de la radiación solar directa y difusa difieren, aportando interesante información sobre dichos procesos de dispersión y, como consecuencia, sobre los componentes atmosféricos que han intervenido. Así, la medida de la radiación solar difusa en superficie en ciertas longitudes de onda permite estimar características de la columna de aerosol [Gueymard, 1998; Foyo-Moreno et al., 2014] y de la nubosidad [Long and Ackerman, 2000; Kaskautis et al., 2008]. Además, la medida de la partición del campo radiativo solar en su componentes directa y difusa resulta esencial para numerosas aplicaciones, como el aprovechamiento del recurso solar como fuente de energía renovable.

La Figura 2.1 presenta un ejemplo de la atenuación que sufre la radiación solar al atravesar la atmósfera. Dicha figura muestra la irradiancia solar espectral global (directa más difusa), directa y difusa que llega a la superficie terrestre suponiendo una atmósfera estándar sin nubes ni aerosoles, suelo con reflectividad nula y un ángulo cenital solar de 42°. Como puede observarse, la radiación que finalmente llega a la superficie terrestre abarca longitudes de onda comprendidas entre los 290 nm y los 4000 nm. A la radiación solar integrada en todo este intervalo espectral se la denomina *radiación solar total*[3]. Este intervalo espectral incluye longitudes de onda del rango ultravioleta (280 nm - 400 nm), visible (400 nm - 700 nm) e infrarrojo (700 - 4000 nm). Se observa además un mayor peso de la componente difusa para las longitudes de onda más cortas, lo cual se debe a su mayor dispersión

[3]En la bibliografía se emplean indistintamente los términos "total" y "global "para designar la radiación solar integrada a todo el espectro solar. En esta memoria se prefiere utilizar "total", reservando el término "global" para referirse a la suma de las componentes directa y difusa de la radiación.

por las moléculas de los gases atmosféricos. En la figura también se advierte el importante papel de los gases atmosféricos en los procesos de absorción, entre los que destacan el ozono (para las longitudes de onda más cortas) y el vapor de agua (numerosas bandas de absorción a partir de 0.5 micras).

La atenuación de la radiación solar por parte de la atmósfera para una localización concreta varía contínuamente dependiendo de la geometría de iluminación solar, los perfiles de concentración de los gases, y de la presencia, distribución espacial y características radiativas de nubes y aerosoles. En el caso de cielo despejado acaba llegando a la superficie terrestre un valor global promedio en torno al 68 % de la radiación solar incidente en el tope de la atmósfera. En el caso de cielo totalmente cubierto el porcentaje global promedio ronda el 28 %. Estos grandes números sólo pretenden dar una idea de la importancia de las nubes en este proceso de atenuación, pues cada situación concreta ha de ser analizada de forma particular, teniendo gran importancia la forma y distribución espacial tridimensional de las nubes, su posición relativa respecto del sol, las propiedades radiativas de las gotas, la distribución de tamaños de gota dentro de la nube y su variación con la altura y con la cercanía a los bordes de la nube, la existencia de distintas fases líquida y sólida dentro de una misma nube, etc. Como ejemplo basta mencionar que, bajo condiciones de nubes rotas, la reflexión de la radiación en las paredes de las nubes puede dar lugar a una focalización de la radiación en distintas áreas del suelo, dando lugar a valores locales de radiación superiores incluso a los correspondientes a la radiación solar en el tope de la atmósfera [Cede et al., 2002; Sabburg and Calbó, 2009; Piedehierro et al., 2014].

2.2. Aplicaciones

2.2.1. Energía solar

Además de su papel fundamental en los procesos climáticos y biológicos, la radiación solar constituye una fuente casi inagotable de energía. La energía solar sobre la superficie terrestre es 10000 veces mayor que la demanda anual de energía mundial. La sociedad científica *Union of Concerned Scientists* sostiene que sólo 18 días de irradiación solar sobre la Tierra contienen la misma cantidad de energía que la acumulada por todas las reservas mundiales actuales de carbón, petróleo y gas natural. Así, la energía solar constituye una prometedora alternativa a las fuentes de energía más utilizadas actualmente, pudiendo contribuir además a un desarrollo más global y sostenible.

La disponibilidad del recurso solar varía de manera importante con la latitud, continentalidad y condiciones meteorológicas de cada localización. Uno de los aspectos decisivos para el correcto aprovechamiento de dicho recurso solar es conocer la partición del campo radiativo en sus componentes directa y difusa. Esta información es esencial para el diseño del sistemas de aprovechamiento solar adecuados a cada localización y condiciones atmosféricas [Posadillo et al., 2009; El-Sebaii et al., 2010; Torres et al. 2010].

En la actualidad existen dos tipos principales de tecnología para aprovechar la energía solar: *termosolar* y *fotovoltaica*. La primera de ellas consiste en utilizar la radiación solar de forma directa para producir calor mediante captadores o colectores térmicos. Dicho calor puede aprovecharse para cocinar alimentos, calentar agua para el consumo doméstico o para generar energía mecánica y, a partir de ella, energía eléctrica. Por otro lado, la tecnología fotovoltaica consiste en transformar la radiación solar en energía eléctrica mediante el uso de dispositivos basados en semiconductores o en una deposición de metales sobre un cierto sustrato.

Ambas formas de aprovechamiento de la energía solar se basan en la incidencia de la radiación solar sobre ciertos dispositivos, lo que requiere el conocimiento preciso de la partición de la radiación solar en sus componentes directa y difusa. Así, por ejemplo, la tecnología fotovoltaica es más adecuada en aquellas regiones en las que la componente difusa es la predominante. Por el contrario, en las zonas con predominio de la componente directa, la tecnología termosolar de concentración presenta un mayor rendimiento.

2.2.2. Arquitectura solar

Además de sus aplicaciones a gran escala para la generación de calor o energía eléctrica, la energía solar se ha hecho un hueco relevante en otras áreas como la arquitectura. Dentro de esta disciplina se ha desarrollado la rama conocida como Arquitectura Solar que emplea técnicas para aprovechar la energía solar en las edificaciones. Para ello resulta fundamental conocer la radiación solar y su distribución en las componentes difusa y directa en cada localización, con el fin de dimensionar, orientar y diseñar edificios que aprovechen la energía solar de forma más eficiente.

Lejos de ser un movimiento reciente, las primeras técnicas de aprovechamiento

solar en edificios datan de la Antigua Grecia. Algunas de esas técnicas como orientar los edificios al sol, seleccionar materiales con propiedades térmicas favorables, diseñar espacios por los que el aire circule de forma natural o usar voladizos, toldos y vegetación con el fin de generar sombra, siguen siendo utilizadas en la actualidad. Este conjunto de técnicas que permiten en uso y control de la energía solar de forma directa, sin transformarla, se denomina *tecnología solar pasiva*. Existe otro tipo de tecnología solar, denominada *tecnología solar activa*, que transforma la energía solar en energía eléctrica o mecánica. Un ejemplo de este tipo de tecnología son la mayoría de los sistemas de agua caliente sanitaria. En la actualidad, lo más habitual es formar sistemas híbridos que combinan el bajo coste de mantenimiento de los sistemas pasivos y el mayor rendimiento de los sistemas térmicos activos.

2.2.3. Salud

A pesar de suponer tan sólo un 5 % del intervalo total de la radiación solar que finalmente llega al suelo, la radiación UV juega un papel fundamental en numerosos procesos biológicos, ecológicos y fotoquímicos. En este intervalo espectral la componente difusa supone una gran contribución. Así, debido a la mayor efectividad de los procesos de dispersión para las longitudes de onda más cortas, al menos el 40 % de la radiación UV que llega a la superficie terrestre lo hace en forma de radiación difusa [Utrillas et al., 2007].

En principio, una dosis adecuada de radiación UV resulta muy beneficiosa para la salud de los seres humanos ya que promueve la síntesis de vitamina D_3, ayuda a mantener los niveles de calcio en la sangre y fortalece el sistema inmunitario [Webb et al., 1988; Glerup et al., 2000; Holick, 2004]. Sin embargo, una exposición excesiva puede tener consecuencias muy negativas, contribuyendo al debilitamiento del sistema inmune, propiciando el desarrollo de trastornos oculares como las cataratas, y favoreciendo la aparición de de eritema[4] y el desarrollo de cánceres de piel [Diffey, 2004; Heisler, 2010]. Para medir los efectos de la radiación UV sobre los seres humanos, en particular su capacidad para producir eritema en la piel humana, se utiliza el conocido como espectro de acción eritemática [McKinlay y Diffey, 1987; CIE, 1998]. A la radiación UV ponderada por este espectro de acción se la denomina radiación ultravioleta eritemática (UVER).

La preocupación por los efectos dañinos de la radiación UV sobre la salud humana se ve acentuada por el importante peso que la componente difusa tiene en

[4]Enrojecimiento de la piel

este intervalo espectral. Además de suponer un elevado porcentaje de la radiación global UV que llega a la superficie terrestre, la radiación difusa UV llega a la superficie procedente de todas direcciones, lo que dificulta su bloqueo. Así por ejemplo, la irradiancia UVER difusa bajo una sombrilla de playa estándar puede alcanzar el 34 % de la irradiancia UVER global [Utrillas et al., 2010] y hasta el 60 % bajo la sombra de un árbol [Parisi et al., 2000].

Con el fin de informar y concienciar a la ciudadanía sobre la importancia de la radiación UV y de sus posibles efectos nocivos para la salud, las autoridades sanitarias de numerosos países han promovido la difusión del denominado Índice Ultravioleta, UVI [ICNIRP, 1995]. Se trata de una información sencilla y fácil de entender que resume en un único número el nivel de radiación solar UVER que llega a la superficie terrestre. Este índice fue estandarizado por la Organización Mundial de la Salud en su Guía "Índice UV" [WHO, 2003], en la cual se incluyen, además, recomendaciones sobre cómo protegerse de la radiación solar UV.

Además de su influencia sobre el ser humano, la radiación UV tiene importantes efectos sobre la salud de numerosos ecosistemas. Por ejemplo, el exceso de radiación UV induce una disminución de la producción de biomasa (plantas, fitoplancton y zooplancton) lo que puede conducir a una reducción de la capacidad de fijación de dióxido de carbono [Zepp et al., 2008]. Además, la cantidad de radiación UV determina los patrones de migración y la pigmentación de algunas especies de zooplancton [Häder et al., 2011, 2015]. Varios estudios han demostrado también que en la etapa larval de algunos peces, la radiación UV puede influir en su desarrollo, aumentar las tasas de mutación, o causar daños en la piel y los ojos y, por tanto, afectar a su capacidad de supervivencia [Häder et al., 2011, 2015].

2.3. Radiación solar difusa en el marco del cambio climático actual

La cambiante actividad humana ha provocado alteraciones importantes en la composición de la atmósfera [Blumthaler et al 1994; Herman, 2010; Bais et al., 2011], aumentando significativamente la abundancia de algunos gases (como el CO_2, CH_4, NO_2, etc.) y de los aerosoles. Este cambio en la composición atmosférica afecta notablemente a los procesos de absorción y dispersión, modificando la distribución de la radiación solar en sus componentes difusa y directa. A su vez, estos cambios en el campo radiativo solar conllevan una modificación del balance radiativo y, en consecuencia, del clima.

Las primeras evidencias de las variaciones seculares en la radiación solar en la superficie de la Tierra fueron detectadas a finales de 1980 y principios de 1990 [Ohmura y Lang, 1989; Dutton et al., 1990]. Desde entonces, numerosos estudios han analizado la tendencia de la irradiancia solar global media en la superficie de la Tierra [Wild, 2009]. Wild et al. [2005] cuantificaron que estas variaciones se encontraban entre -5.1 W/m^2 y -1.6 W/m^2 por década durante el período 1960-1990 y entre +2.2 W/m^2 y +5.1 W/m^2 por década a partir de 1990. Esta tendencia ha sido confirmada por estudios posteriores [Sanchez-Lorenzo et al., 2015; Wild, 2016]. Sin embargo, el responsable de este cambio no está claro, y por lo tanto, la contribución de las nubes y los aerosoles a las variaciones decadales de la irradiancia solar global sigue siendo un tema controvertido [Wild, 2009; Augustine y Dutton, 2013; Mateos et al., 2014].

También se han detectado variaciones en las componentes individuales de la radiación solar y en subintervalos espectrales. Así, recientemente se han detectado tendencias en los valores de radiación solar difusa total y también específicamente en su rango UV. Así, se ha observado una tendencia positiva de +3 W/m^2 por década en los valores de radiación solar difusa total en Estados unidos durante el periodo 1996-2007 [Long et al., 2009]. También se han detectado tendencias negativas, como en Girona (España), donde un estudio reciente cuantifica la tendencia en -1.3 W/m^2 por década para el periodo 1994-2014 [Calbo et al., 2016].

En cuanto al rango UV, los estudios indican la existencia de tendencias positivas en Europa [Krzyscin et al., 2011; Smedley et al., 2012]. En el caso particular de la Península Ibérica se ha detectado una tendencia de +2.1 % por década en los valores de irradiancia UVER en el período 1985-2011 [Roman et al., 2015].

Estas alteraciones en los valores de radiación difusa total y UV tienen importantes consecuencias sobre los ecosistemas. Varios estudios han señalado que existe una estrecha relación entre la cantidad de radiación difusa total y la fotosíntesis, aumentando generalmente su eficiencia cuando la radiación difusa total aumenta [Mercado, 2009; Kannianh, 2012]. Sin embargo, la sobreexposición a la radiación UV reduce el tamaño, productividad y calidad en muchas de las especies de plantas de cultivo el arroz, la soja, el trigo, el algodón o el maíz. El aumento de la radiación UV también implica la reducción de las poblaciones de fitoplancton y la extinción de importantes ecosistemas como los corales [Lesser y Farrell, 2004].

2.4. Medida de la radiación solar difusa

La medida de la radiación solar difusa descansa en la característica diferenciadora de la componente difusa respecto a la directa: que la primera proviene de todas direcciones mientras que la segunda llega solamente en la dirección solar. Por ello, para medir la componente difusa se emplean los mismos instrumentos que para la medida de radiación solar global pero se requiere, además un dispositivo de apantallamiento que impida que la componente directa llegue a dicho sensor. Este requisito adicional sobre la instrumentación explica que la medida de la componente difusa esté mucho menos extendida que la medida de la radiación global. Esta menor abundancia de medidas de la componente difusa es muchísimo más acentuada en el caso del rango UV.

Esta situación está cambiando actualmente pues el interés por la medida de la radiación difusa total ha aumentado notablemente debido a la necesidad de un conocimiento más detallado del balance radiativo y a sus implicaciones para el desarrollo de tecnologías para el aprovechamiento de la energía solar. Entre las iniciativas para la medida de la radiación difusa total hay que señalar los programas como la Baseline Surface Radiation Network (BSRN) o el Atmospheric Radiation Measurements (ARM). A pesar de ello, el número de estaciones en las que se mide irradiancia solar difusa ultravioleta sigue siendo muy escas. Entre el reducido número de estudios que aportan medidas experimentales de irradiancia solar difusa ultravioleta eritemática destacan los desarrollados en Australia [Parisi et al., 2000; Turnbull et al., 2005; Turnbull and Parisi, 2008], Valencia [Utrillas et al., 2007, 2009; Utrillas, 2010; Nuñez et al., 2012].

2.4.1. Radiómetros de banda ancha para la media de irradiancia difusa total y ultravioleta

Existen diferentes magnitudes radiométricas relacionadas con la radiación. En el caso de la medida de la radiación solar difusa la magnitud más interesante es la *irradiancia*. Ésta se define como la energía radiante que llega a una superficie por unidad de tiempo y por unidad de superficie. Podemos decir que se trata pues de una densidad superficial (por unidad de superficie) de potencia (energía por unidad de tiempo). Sus unidades en el Sistema Internacional son W/m^2. En el caso de la medida meteorológica estándar de la irradiancia solar global y difusa se considera una superficie horizontal[5], por lo que los radiómetros deben estar bien nivelados.

[5]Para algunos objetivos particulares puede resultar interesante medir la irradiancia sobre superficies inclinadas, por lo que los instrumentos de medida pueden colocarse inclinados, paralelos a la

Existen distintos tipos de instrumentos para medir la irradiancia solar sobre la superficie terrestre según el rango y la resolución espectral que se desean medir. Atendiendo a esta última característica los instrumentos se clasifican en: 1) espectrorradiómetros, los cuales proporcionan valores espectrales, 2) radiómetros multicanal, aquellos que miden valores de irradiancia en varias bandas estrechas, y 3) radiómetros de banda ancha, los cuales permiten medir valores de irradiancia integrados en un amplio intervalo de longitudes de onda.

En esta Tesis Doctoral nos centraremos en el análisis de la irradiancia medida medidos con instrumentos de banda ancha correspondientes tanto a todo el espectro solar como exclusivamente al rango ultravioleta. Los radiómetros de banda ancha son instrumentos muy robustos adecuados para la medida automática durante largos periodos sometidos a todo tipo de condiciones atmosféricas. Su fácil manejo y mantenimiento y su precio relativamente económico han favorecido la integración de este tipo de instrumentos en estaciones radiométricas repartidas por todo el mundo.

El radiómetro utilizado para medir irradiancia solar global o difusa del espectro solar total recibe el nombre específico de *piranómetro*. Los piranómetros utilizados en esta Tesis Doctoral basan su principio de funcionamiento en el efecto termoeléctrico conocido como efecto Seebeck. La parte visible del sensor es una superficie rugosa pintada de negro que absorbe la radiación incidente calentándose. Esta superficie está en contacto con uno de los extremos de un termopar (unión caliente) que se calienta a su vez. Mientras tanto,el otro extremo del termopar permanece a un temperatura más fría (unión fría) en contacto con el cuerpo del piranómetro. Esta diferencia de temperatura entre ambos extremos de la unión termoeléctrica genera una diferencia de potencial que es lo que se registra, y que es proporcional a la radiación solar incidente. Para proteger el sensor de influencias externas como la lluvia, la suciedad o el viento, el piranómetro posee una doble cúpula de vidrio transparente que permite la transmisión del 98 % de la radiación solar en todas sus longitudes de onda.

En el caso de la medida de radiación ultravioleta los radiómetros deben muy sensibles y precisos ya que la cantidad de radiación llega a la superficie terrestre en estas longitudes de onda es varios órdenes de magnitud menor que en longitudes de onda superiores correspondientes al espectro visible. En los estudios realizados en esta Tesis Doctoral sobre la radiación en este intervalo espectral se han utilizado

superficie en cuestión.

radiómetros UVS-E-T fabricados por Kipp & Zonen. Este instrumento tiene una respuesta espectral que simula el espectro de acción eritemática de la piel humana [ISO 17166:1999/CIE S007/E-1998]. El funcionamiento es algo más complejo que en los piranómetros. La radiación solar atraviesa la cúpula de cuarzo que permite el paso del rango UV. Un filtro absorbe la luz visible e IR y deja pasar los la radiación correspondiente al espectro de acción CIE. La radiación UV transmitida incide sobre una lámina de fósforo sensible a la radiación UV. Este material absorbe la componente UV y la reemite por fluorescencia en el rango visible, predominantemente en longitudes de onda correspondientes al verde [Robertson, 1972; Berger, 1976)]. Un segundo filtro de vidrio transmite la luz reemitida, la cual es medida por un fotodiodo de estado sólido, cuya respuesta máxima está en el verde. Todo este dispositivo se encuentra estabilizado a 25 °C para evitar que su funcionamiento se vea alterado por factores externos.

Todos los instrumentos utilizados en esta Tesis Doctoral satisfacen los estándares de medida establecidos por la Organización Meteorológica Mundial (OMM) para la medida de irradiancia difusa total y UV, respectivamente [WMO, 2014].

2.4.2. Dispositivos para el bloqueo de la radiación solar directa.

Como se indicó anteriormente en la introducción de esta sección, para medir radiación difusa se necesita un dispositivo adicional que bloquee la radiación procedente de la dirección del Sol impidiendo que llegue al sensor. El primer mecanismo diseñado con este objetivo fue el anillo o banda de sombra. Como su propio nombre indica, este dispositivo consiste en un anillo o banda que se dispone paralelo a la trayectoria solar de tal forma que sombrea el sensor del piranómetro durante el movimiento diurno del sol.

El primer modelo de este mecanismo fue fabricado a mediados del siglo pasado por Drummond y Kristen [1951] y se muestra en la Figura 2.2a. Las series de irradiancia difusa más longevas cuentan con medidas obtenidas empleando este dispositivo. En la actualidad su diseño sigue siendo fundamentalmente el mismo. Los fabricantes actuales sólo han añadido ligeros cambios como la introducción de dos brazos móviles que facilitan el manejo del anillo, o la modificación de su perfil para que la sombra que se proyecta sobre el sensor sea aproximadamente constante a lo largo del año. Un ejemplo es el anillo de sombra CM121 fabricado por Kipp & Zonen que se muestra en la Figura 2.2b. No obstante, la necesidad de medir radiación sobre

superficies inclinadas, principalmente de la mano del desarrollo de tecnología para el aprovechamiento de la energía solar, ha dado lugar a innovadores diseños como el desarrollado por Simon et al. [2015] que se muestra en la Figura 2.2c. Este dispositivo permite la medida simultánea de irradiancia difusa en cuatro planos verticales.

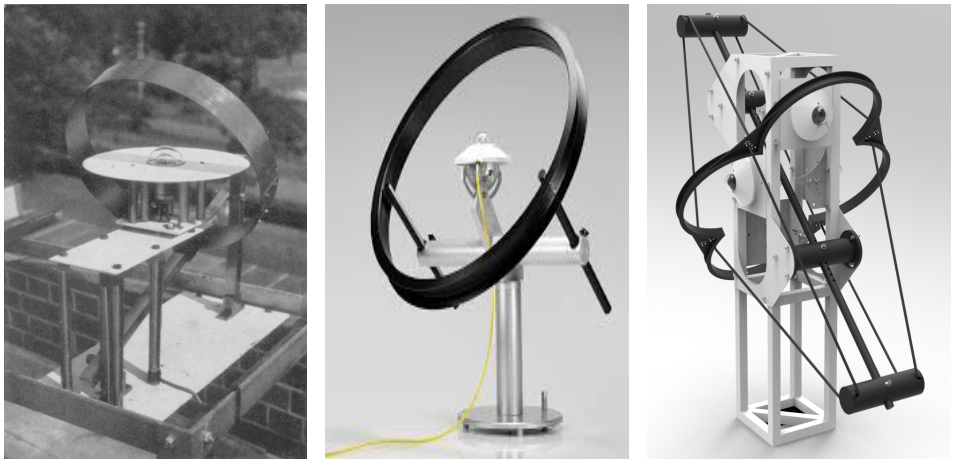

(a) (b) (c)

Figura 2.2: Distintos modelos de anillo de sombra. (a) Modelo original de Drummond y Kristen [1951] (b) Modelo CM121 fabricado por Kipp & Zonen. (c) Dispositivo de sombra diseñado por de Simon et al. [2015] para la medida simulatanea de irradiancia difusa en cuatro planos verticales

El anillo de sombra presenta algunas ventajas sobre otros sistemas que hacen que su uso siga siendo muy extendido en la actualidad. Se trata de un instrumento fácil de operar ya que sólo requiere el ajuste manual de su altura con el fin de adaptarlo a la declinación solar del día en cuestión. La frecuencia con que debe ajustarse esta altura depende de la época del año y de la latitud de la estación. Además, su gran robustez hace que sea el dispositivo más adecuado para la medida de irradiancia difusa en localizaciones con condiciones meteorológicas extremas, como en la Antártida [Serrano et al., 2002]. Otra importante ventaja anteriormente mencionada es la posibilidad de ser adaptado para medir irradiancia difusa sobre superficies inclinadas.

Los nuevos avances tecnológicos han permitido el desarrollo de dispositivos de sombreado más sofisticados. En la actualidad, se ha extendido el uso de seguidores solares equipados con bolas o discos de sombra (Figura 2.3). Estos dispositivos consisten en un cuerpo motorizado con unos brazos móviles acabados en una bola

(o disco) que se mueven solidarios al sol en su movimiento diurno, corrigiendo la altura de las bolas de forma que el sensor del piranómetro permanezca sombreado en todo momento.

Figura 2.3: Seguidor solar Solys2 fabricado por Kipp & Zonen

El seguidor solar presenta algunas ventajas respecto al anillo de sombra, como son su funcionamiento totalmente automático y la menor fracción de cielo ocultada al sensor por parte del apantallamiento. Así, mientras el seguidor solar bloquea exclusivamente el disco solar, el anillo de sombra, debido a su diseño, bloquea, no sólo la componente directa, sino también la irradiancia difusa interceptada por todo el ángulo sólido subtendido por el anillo. Esto conlleva una subestimación de la medida de irradiancia difusa que ha de ser corregida. El análisis de este problema y su corrección será uno de los objetivos de esta Tesis Doctoral.

2.4.3. Precisión en las medidas de irradiancia difusa total y UV

La precisión de las medidas de irradiancia difusa vendrá determinada tanto por las características del instrumento utilizado (sensibilidad, respuesta angular, etc.) y su mantenimiento (calibración, limpieza, control del sombreado, etc.), así como por las características del dispositivo de sombreado.

La Organización Meteorológica Mundial, a través de los estudios realizados por la BSRN, establece que los valores de irradiancia difusa más precisos son aquellos medidos por un piranómetro ventilado instalado en un seguidor solar (de dos ejes)

y sombreado por un disco o bola que proyecte una sombra de 5° desde el centro del sensor. Además los instrumentos deben ser revisados cada día y los datos deben ser sometidos a un control de calidad. Se estima que la incertidumbre en las medidas así obtenidas es de un 2 % (3 W/m^2) [Ohmura et al., 1998; McArthur, 2005]. Sin embargo, la mayoría de las estaciones radiométricas no cuentan con la instrumentación y el personal necesario para la aplicación de un protocolo tan estricto.

Medir radiación ultravioleta es difícil debido a la pequeña cantidad de radiación en este intervalo espectral que llega a la superficie y a la rápida variación de esta cantidad para las distintas longitudes de onda. Debido a ello, el error asociado a la medida de irradiancia UV es notablemente superior al error de la irradiancia total. No contribuye a mejorar este panorama las dificultades en la estandarización de las medidas de irradiancia UV debido, principalmente, a la variedad de instrumentos utilizados para su medida y a los numerosos usos para los que se emplean las medidas [WMO, 2003]. La OMM [2014] establece una error del 10 % en el proceso de calibración de los radiómetros de banda ancha UV. Los radiómetros UV utilizados en esta Tesis Doctoral han sido calibrados siguiendo el procedimiento establecido por Grupo de Trabajo 4 de la Acción COST 726 [Webb et al., 2006; Gröbner et al. 2007; Vilaplana et al., 2009]. Al igual que en el caso de la irradiancia difusa total también el sistema utilizado para sombrear el sensor podría ampliar la incertidumbre las medidas de irradiancia difusa ultravioleta.

2.5. Modelización de la radiación solar difusa

A pesar del incremento en el número de estaciones radiométricas que incorporan la instrumentación necesaria para la medida de la radiación difusa total, su distribución espacial es muy irregular. La situación es aún más crítica en el caso de las medidas de radiancia difusa ultravioleta. Sin embargo, la componente difusa depende de variables medidas de forma rutinaria en estaciones radiométricas y meteorológicas distribuidas por todo el planeta, lo que hace interesante el desarrollo de modelos que permitan su estimación a partir de las medidas disponibles.

Asimismo, la modelización de la radiación difusa constituyen una potente herramienta para entender los complejos procesos que dan lugar a su formación. Los modelos permiten analizar el papel de los distintos constituyentes atmosféricos en los procesos de dispersión así como los posibles efectos derivados de variaciones de dichos constituyentes. La simulación de radiación solar, y en particular de la

componente difusa, es fundamental para entender el cambio climático y sus posibles efectos sobre los seres vivos. Además de su aplicación a estudios climáticos, los modelos de radiación solar difusa son fundamentales en el avance sostenible de las energías renovables, la arquitectura, la ingeniería, la agricultura y la ecología.

Los modelos para la estimación de radiación solar pueden clasificarse en dos categorías: 1) *modelos de transferencia radiativa* y 2) *modelos empíricos*. Como su propio nombre indica, en los modelos de transferencia radiativa, los valores de radiación se obtienen mediante la resolución de las ecuaciones de transferencia radiativa. El método utilizado para resolver dichas ecuaciones y las aproximaciones consideradas determinarán el tipo de modelo dentro de esta categoría (1D, 3D, MonteCarlo, etc.). Estos modelos permiten la estimación de radiación solar global, difusa y directa, espectral o integrada, a diferentes alturas dentro de la atmósfera. Algunos de los modelos de transferencia radiativa más empleados por la comunidad científica son: SBDART, libRadtran o TUV.

Por su parte, los modelos empíricos se construyen mediante el ajuste matemático de valores de radiación y datos de los distintos factores que la modulan en su camino hacia la superficie terrestre. Las formas funcionales y variables implicadas dependen tanto de la componente de la radiación que se desea modelizar como de las variables a partir de las cuales se construirá el modelo. En el caso particular de la componente difusa, entre otros parámetros, resulta imprescindible introducir en el modelos información sobre la posición solar y la capa de aerosoles y/o nubes. Entre las expresiones empíricas para la estimación de irradiancia difusa total se encuentran los modelos Iqbal-C [Iqbal, 1983], REST2 [Gueymard, 2008] o el modeleo por Boland et al. [2008]. Aunque mucho menos numerosos, también se han propuesto para la estimación de la irradiancia difusa ultravioleta entre los que destacan los modelos Grant and Gao [2003], Nuñez et al. [2012] y Silva [2015].

De particular interés resultan los modelos empíricos para la obtención de la fracción de irradiancia difusa, k_d, que se define como el cociente entre la irradiancia difusa y global sobre una superficie horizontal. Trabajar con esta magnitud en lugar de con los valores de irradiancia difusa supone algunas ventajas entre las que destacan: 1) su menor dependencia con la posición solar y 2) su mayor sensibilidad ante pequeñas variaciones en la partición difusa/directa de la radiación solar [Long y Ackerman, 2000]. Este tipo de modelos toman como variable principal los valores de transmisividad de la radiación global en el correspondiente rango de longitudes de onda. Esta magnitud, que se define como el cociente entre la radiación global

sobre una superficie horizontal y la radiación en el tope de la atmósfera, resulta de gran interés ya que se ve afectada por los mismos procesos de absorción y dispersión que la fracción de difusa. Estos modelos pueden introducir además otras variables que complementen la información contenida en el índice de claridad.

Bibliografía

Augustine, J. A., and E. G. Dutton (2013), Variability of the surface radiation budget over the United States from 1996 through 2011 from high-quality measurements, *J. Geophys. Res. Atmos.*, 118, 43–53.

Bais A.F., K.Tourpali, A. Kazantzidis, H. Akiyoshi, S. Bekki, P. Braesicke, M.P. Chipperfield, M. Dameris, V. Eyring, H. Garny, D. Iachetti, P. Jöckel, A. Kubin, U. Langematz, E. Mancini, M. Michou, O. Morgenstern, T. Nakamura, P.A. Newman, G. Pitari, D.A. Plummer, E. Rozanov, T.G. Shepherd, K. Shibata, W. Tian, and Y. Yamashita (2011), Projections of UV radiation changes in the 21st century: impact of ozone recovery and cloud effects, *Atmos. Chem. Phys.*, 11, 7533-7545.

Berger, D.S. (1976), The sunburning ultraviolet meter: design and performance, *Photochemistry and Photobiology*, 24, 587-593.

Blumthaler, M., W. Ambach, and M. Salzgeber (1994), Effects of cloudiness on global and diffuse UV irradiance in a high-mountain area, *Theor. Appl. Climatol.*, 50, 23–30, 1994.

Boland, J., B. Ridley, and B. Brown (2008), Models of diffuse solar radiation, *Renew. Energy*, 33, 575–584.

Cede, A., M. Blumthaler, E. Luccini, R.D. Piacentini, L. Nuñez (2002). Effects of clouds on erythemal and total irradiance as derived from data of the Argentine Network, *Journal of Geophysical Research*, 29, 2223.

Calbó, J., J.A. González, and A. Sanchez-Lorenzo (2016), Building global and diffuse solar radiation series and assessing decadal trends in Girona (NE Iberian Peninsula), *Theor. Appl. Climatol.*.

CIE (1998), Erythema reference action spectrum and standard erythema dose, Vienna, ISO 17166:1999/CIE S007-1998.

de Simón-Martín M., C. Alonso-Tristán, D. González-Peña, M. Díez-Mediavilla (2015), New device for the simultaneous measurement of diffuse solar irradiance on several azimuth and tilting angles, *Solar Energy*, 19, 370-382.

Diffey B.L. (1991), Solar ultraviolet radiation effects on biological systems, *Phys. Med. Biol.*, 36, 299-328.

Diffey, B. L. (2004), Climate change, ozone depletion and the impact on ultraviolet exposure of human skin, *Phys. Med. Biol.*, 49, 1–11.

Drummond, A. J. and M. K. Kristen (1951) The measurement of solar radiation in South Africa, *South African J. Sci.*, 48, I03.

Dutton, E. G., R. S. Stone, D. W. Nelson, and B. G. Mendonca (1990), Recent interannual variations in solar radiation cloudiness, and surface temperature at the South Pole, *J. Clim.*, 4, 848–858.

El-Sebaii A. A. and A. Terabia (2003), Estimation of horizontal diffuse solar radiation in Egypt, *Energy Conversion & Management*, 44, 2471-2482.
Foyo-Moreno,I.,I.Alados,M.Antón, J. Fernández-Gálvez, A. Cazorla, and L. Alados-Arboledas (2014), Estimating aerosol characteristics from solar irradiance measurements at an urban location in southeastern Spain, *J. Geophys.Res. Atmos.*, 119,1845-1859.

Glerup, H., K. Mikkelsen, L. Poulsen, E. Hass, S. Overbeck, and J. Thomsen (2000), Commonly recommended daily intake of vitamin D is not sufficient if sunlight exposure is limited, *J. Intern. Med.*, 247, 260–268.

Grant, R. H., and W. Gao (2003), Diffuse fraction of UV radiation under partly cloudy skies as defined by the Automated Surface Observation System (ASOS), *J. Geophys. Res.*, 108(D2), 4046.

Gröbner, J., G. Hülsen, L. Vuilleumier, M. Blumthaler, J. M. Vilaplana, D. Walker, and J. E. Gil (2007), Report of the PMOD/WRC-COST Calibration and Intercomparison of Erythemal radiometers. Available at: http//i115srv.vuwien.ac.at/uv/COST726/COST726 Dateien/Results/PMOD WRC COST726 campaign 2006 R.pdf.

Gueymard C., F. Vigola (1998), Determination of atmospheric turvidity fromm the diffuse-eam broadband irradiance ratio, *Solar Energy*, 63, 135–146.

Gueymard, C.A. (2008), REST2: High performance solar radiation model for cloudless-sky irradiance, illuminance and photosynthetically active radiation—validation with a benchmark dataset, *Solar Energy*, 82, 272–285.
Häder D.P., E.W. Helbling, C.E. Williamson, and R.C. Worrest (2011), Effects of UV radiation on aquatic ecosystems and interactions with climate change, *Photochem. Photobiol. Sci.*, 10, 242 -260.

Häder D.P., C.E. Williamson, S.Ä. Wängberg, M. Rautio, K.C. Rose, K. Gao, E.W. Helbling, R.P. Sinha, R.C. Worrest (2015), Effects of UV radiation on aquatic ecosystems and interactions with other environmental factors, *Photochem. Photobiol. Sci.*, 14, 108-126.

Heisler, G. M. (2010), Urban forest influence on exposure to UV radiation and potential consequences for human health, in UV Radiation in Global Climate Change. Measurements, Modeling and Effects on Ecosystems, edited by Gao, W., et al., pp. 331–369, Tsinghua University Press, Beijing.
Herman, J. R. (2010), Global increase in UV irradiance during the past 30 years (1979–2008) estimated from satellite data, *J. Geophys. Res.*, 115.

Holick, M. F. (2004), Vitamin D: importance in the prevention of cancers, type 1 diabetes, heart disease and osteoposoris, *Am. J. Clin. Nutr.*, 79, 362–371.

Iqbal, M., (1983), An Introduction to Solar Radiation, Academic Press, Toronto.

ICNIRP (1995), Global Solar UV Index. WHO/WMO/INCIRP recommendation, INCIRP publication no 1/95, Oberschleissheim.

Kaskaoutis D.G., H.D. Kambezidis, S.K. Kharol, K.V.S. Badarinath (2008), The diffuse-to-global spectral irradiance ratio as a cloud-screening technique for radiometric data, *Journal of Atmospheric and Solar-Terrestrial Physics*, 70,1597-1606.

Krzyścin J.W., P.S. Sobolewski, J. Jaroslawski, J. Podgórski, and B. Rajewska-Wiech (2011), Erythemal UV observations at Belsk, Poland, in the period 1976–2008: Data homogenization, climatology, and trends, *Acta Geophysica*, 59,

155-182.

Long C.N., and T.P. Ackerman (2000),Identification of clear skies from broadband pyranometer measurements and calculation of downwelling shortwave cloud effects, *Journal of Geophysical Research*, 105, 609-615.

Long, C.N., E.G. Dutton, J. A. Augustine, W. Wiscombe, M. Wild, S. A. McFarlane, and C. J. Flynn, (2009), Significant decadal brightening of downwelling shortwave in the continental United States, *J. Geophys. Res.*, 114.

Mateos, D., A. Sanchez-Lorenzo, M. Antón, V. E. Cachorro, J. Calbó, M. J. Costa, B. Torres, and M. Wild (2014), Quantifying the respective roles of aerosols and clouds in the strong brightening since the early 2000s over the Iberian Peninsula, *J. Geophys. Res. Atmos.*, 119.

McArthur L. J. B. (2005), Baseline Surface Radiation Network (BSRN). Operations Manual, Version 2.1. WCRP-121, WMO/TD-No. 1274

McKinlay A.F. and B.L. Diffey (1987), Human Exposure to Ultraviolet Radiation: Risks and Regulations Edited by W. F. Passchier and B. F. M. Bosnajakovic, pp.83–87, Elsevier, Amsterdam.
Nuñez, M., M. P. Utrillas, and J. A. Martinez-Lozano (2012), Approaches to partitioning the global UVER irradiance into its direct and diffuse components in Valencia, Spain, *J. Geophys. Res.*, 117.

Ohmura, A., and H. Lang (1989), Secular variation of global radiation over Europe, in Current Problems in Atmospheric Radiation, edited by J. Lenoble and J. F. Geleyn, pp. 98–301, Deepak, Hampton, Va.

Ohmura, A. , E. Dutton, B. Forgan, C. Fröhlich , H. Gilgen, H. Hegner, A. Heimo, G. König-Langlo, B. Mcarthur, G. Müller, R. Philipona, R. Pinker, C.H. Whitlock, and M. Wild (1998), Baseline Surface Radiation Network (BSRN/WRMC), a new precision radiometry for climate research, *Bull. Amer. Meteor. Soc.*, 79, 2115 – 2136.

Parisi, A. V., M. G. Kimlin, J. C. F. Wong, and M. Wilson (2000), Diffuse component of solar ultraviolet radiation in tree shade , *J. Photochem. Photobiol. Biol.*, 54, 116–120.

Parisi, A. V., A. Green, and M. G. Kimlin (2001), Diffuse Solar UV Radiation and Implications for Preventing Human Eye Damage, *Photochem. Photobiol.*, 73, 135–139.

Piedehierro A.A., M. Anton, A. Cazorla, L. Alados-Arboleda L., and F.J. Olmo (2014), Evaluation of enhancement events of total solar irradiance during cloudy conditions at Granada (Southeastern Spain), *Atmospheric Research*, 135-136,1-7.

Posadillo R., R. López Luque (2009), Hourly distributions of the diffuse fraction of global solar irradiation in Córdoba (Spain), *Energy Conversion and Management*, 50, 223-231.

Robertson, D.F. (1972). Solar ultraviolet radiation in relation to human sunburn and skin cancer, Ph. D. thesis, University of Queensland, Australia.

Román R., J. Bilbao and A. de Miguel (2015), Erythemal ultraviolet irradiation trends in the Iberian Peninsula from 1950 to 2011, *Atmos. Chem. Phys.*, 15, 375–391.

Sabburg, J., and J. Calbó (2009), Five years of cloud enhanced surface UV radiation measurements at two sites (in the Northern and Southern Hemispheres), *Atmospheric Research*, 93, 902–912.

Sanchez-Lorenzo, A., M. Wild, M. Brunetti, J. A. Guijarro, M. Z. Hakuba, J. Calbó, S. Mystakidis, and B. Bartok (2015), Reassessment and update of long-term trends in downward surface shortwave radiation over Europe (1939–2012), *J. Geophys. Res. Atmos.*, 120, 9555–9569.

Serrano A., M. Antón, M. L. Cancillo, J. A. García, M. R. Arias, V. L. Mateos, M. Ramos (2002), Medidas de radiación solar en la Isla Decepción (Shetland del Sur, Antártida) durante el verano austral (campaña 2000/2001), Proceedings 3a Asamblea Hispano-Portuguesa de Geodesia y Geofísica, Valencia (España), Tomo II, 1349-1352, ISBN 84-9705-297-8.

Silva A. (2015), The diffuse component of erythemal ultraviolet radiation, *Photochem. Photobiol. Sci.*

Smedley A.R.D., J.S. Rimmer, D. Moore, R. Toumi, and A.R. Webb (2012), Total ozone and surface UV trends in the United Kingdom: 1979–2008, *Int. J Climatol.*, 32, 338-346.

Torres J.L., De Blas M., García A., de Francisco A. (2010), Comparative study of various models in estimating hourly diffuse solar irradiance, *Renewable Energy*, 35, 1325-1332.

Turnbull, D. J., A. V. Parisi, and M. G. Kimlin (2005), Vitamin D effective ultraviolet wavelengths due to scattering in shade, *J. Steroid Biochem. Mol. Biol.*, 96, 431–436.

Turnbull, D. J., and A. V. Parisi (2008), Utilising shade to optimize UV exposure for vitamin D, Atmos. Chem. Phys., 8, 2841–2846.
Utrillas, M. P., M. J. Marín, A. R. Esteve, F. Tena, J. Cañada, V. Estellés, and J. A. Martínez-Lozano (2007), Diffuse UV erythemal radiation experimental values, *Journal of Geophysical Research*, 112

Utrillas, M. P., M. J. Marín, A. R. Esteve, V. Estellés, F. Tena, J. Cañada, and J. A. Martínez-Lozano (2009), Diffuse Ultraviolet Erythemal Irradiance on Inclined Planes: A Comparison of Experimental and Modeled Data, *Phot. Pho.*, 85(5), 1245.

Utrillas, M. P., J. A. Martınez-Lozano, and M. Nuñez (2010), Ultraviolet Radiation Protection by a Beach Umbrella, *Photochem. Photobiol.*, 86, 449–456.

Vilaplana, J. M., A. Serrano, M. Antón, M. L. Cancillo, M. Parias, J. Gröbner, G. Hülsen, G. Zablocky, A. Díaz, and B. A. de la Morena (2009), COST Action 726 – Report of the "El Arenosillo"/INTA-COST calibration and intercomparison campaign of UVER broadband radiometers.

Webb, A. R., L. Kline, and M. F. Holick (1988), Influence of season and latitude on the cutaneous synthesis of Vitamin D3: exposure to winter sunlight in Boston and Edmonton will not promote Vitamin D3 synthesis in human skin, *J. Clin. Endocrinol. Metab.*, 67, 373–378.

Webb, A., J. Gröbner, and M. Blumthaler (2006), A practical guide to operating broadband instruments measuring erythemally weighted irradiance, Produced by the join efforts of WMO SAG UV and Working Group 4 of the COST-726 Action: Long Term Changes and Climatology of the UV Radiation over Europe, vol.EUR 22595/WMO.

Wild, M., G. Hans, A. Roesch, A. Ohmura, C. N. Long, E. G. Dutton, B. Forgan, A. Kallis, V. Russak, and A. Tsvetkov (2005), From dimming to brightening: Decadal changes in surface solar radiation, *Science*, 308, 847–850.

Wild, M. (2009), Global dimming and brightening: A review, *J. Geophys. Res.*, 114.

Wild, M. (2016), Decadal changes in radiative fluxes at land and ocean surfaces and their relevance for global warming, *Wiley Interdiscip. Rev.Clim. Change*, 7, 91–107.

World Meteorological Organization (2003). Índice UV Solar Mundial: Guía Práctica (versión en castellano), 28 pp. Organización Mundial de la Salud (WHO), Organización Meteorológica Mundial (WMO), Programa de las Naciones Unidas para el Medio Ambiente (UNEP), Comisión Internacional de Protección contra la Radiación no Ionizante (ICNIRP), Ginebra.

World Meteorological Organization (2008), Guide to Meteorological Instruments and Methods of Observation, vol. 8, 7th ed., 681 pp.,Secretariat of the World Meteorological Organization, Geneva, Switzerland.

World Meteorological Organization (2014), Guide to Meteorological Instruments and Methods of Observation, vol. 8, 7th ed., 1128 pp.,Secretariat of the World Meteorological Organization, Geneva, Switzerland.

Capítulo 3

Error asociado al cero térmico o "thermal offset"

3.1. Introducción

Una de las principales fuentes de error en las medidas de irradiancia solar realizadas por los piranómetros es la señal asociada al cero térmico (*thermal offset*, en su denominación en inglés). Se denomina cero térmico al voltaje que se genera en el sensor como resultado del flujo neto de radiación establecido entre éste y la cúpula (Figura 3.1). Este voltaje se añade al voltaje correspondiente a la medida de la radiación solar, formando parte de la señal de salida. En la mayoría de los casos la temperatura del sensor es mayor que la de la cúpula, produciendo un voltaje negativo y, así, reduciendo la magnitud de la señal final de salida. La no corrección de esta fuente de error conduce generalmente a una subestimación de la irradiancia solar medida.

Estudios previos han estimado que los valores del cero térmico se encuentran entre -20 W/m^2 y 0 W/m^2 [Bush et al., 2000; Haeffelin et al., 2001][1]. Este valor supera notablemente el límite de -7 W/m^2 aceptado por la OMM en las medidas de irradiancia global y difusa de calidad. En el caso de la irradiancia solar difusa, este valor puede llegar a suponer un error de hasta el 40 % [Dutton et al., 2001], muy por encima del la incertidumbre del 2 % que la establecida por la BSRN para las medidas de irradiancia difusa total [Ohmura et al., 1998; McArthur, 2005].

El cero térmico de cada piranómetro es diferente, pues depende de su diseño y

[1]La bibliografía correspondiente a la sección introductoria de cada uno de los capítulos 2, 3 y 4 se encuentra recogida dentro de los artículos que componen dichos capítulos.

materiales de construcción. También está afectado por las configuración de trabajo (ventilado o no, sombreado o no) y las condiciones meteorológicas del momento. Entre las variables meteorológicas que más influyen se pueden citar, por una parte, aquellas condiciones que determinan la temperatura del sensor (la propia radiación solar que se pretende medir y sus factores moduladores como nubosidad y, en menor medida, aerosoles), y por otra, aquellas condiciones relacionadas con la temperatura de la cúpula (la velocidad del viento, la temperatura ambiente, la humedad relativa, etc.). Todo ello hace que el cero térmico de un piranómetro midiendo en el exterior varíe continuamente adaptándose al forzamiento de los factores externos.

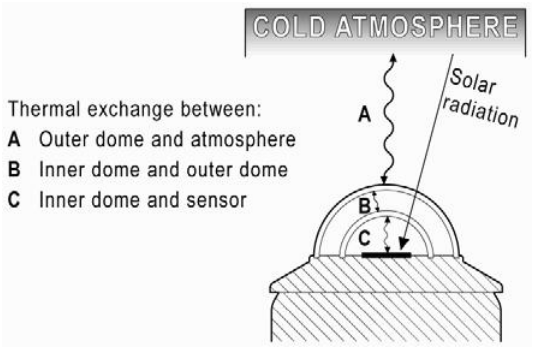

Figura 3.1: Flujo de radiación establecido entre el sensor, las cúpulas y la atmósfera

A pesar de su importancia y de ser una fuente de error conocida desde hace bastante tiempo existen numerosos aspectos del cero térmico aún sin resolver. A continuación se enumeran y describen brevemente los aspectos más destacados aún sin resolver sobre el cero térmico:

- No existe un acuerdo general sobre si el cero térmico de un piranómetro difiere significativamente por el hecho de estar midiendo irradiancia global o difusa. Por un lado, estudios como el realizado por Bush et al. [2000] han detectado valores del error térmico diferentes para un mismo instrumento midiendo global o difusa. Estos resultados son explicados en base al diferente estado térmico en el que el piranómetro trabaja cuando está sombreado y cuando no lo está. Por otros lado, estudios como el desarrollado por Philipona [2002] no han observado tales diferencias.

- Existe una notable controversia sobre la posibilidad de corregir el cero térmico de las medidas diurnas empleando modelos basados en medidas nocturnas. Algunos autores proponen la utilización de la señal nocturna del piranómetro para la corrección del error térmico diurno [Dutton et al., 2001; Younkin y

Long, 2004]. Sin embargo, otros autores señalan que esto no es adecuado debido al importante papel que la radiación solar tiene en el balance final que genera el error térmico [Cess et al., 2000; Haeffelin et al., 2001].

- El efecto de la ventilación artificial en el cero térmico de los piranómetros no está suficientemente estudiado. En general, se espera que la ventilación reduzca la diferencia de temperatura entre las distintas partes del piranómetro y, por tanto, reduzca su cero térmico. Sin embargo, algunos autores han observado el comportamiento opuesto cuando se emplea una fuente de alimentación en corriente alterna para alimentar la unidad de ventilación [Younkin y Long, 2004; Vignola et al, 2007].

- Otro problema no resuelto es la ausencia de una metodología estándar para medir el cero térmico diurno de los piranómetros. Dichas metodologías serán descritas en los correspondientes artículos.

Es importante señalar que estos aspectos están rodeados de una gran controversia científica, derivada de la ausencia de estudios específicos a pesar de su enorme importancia para garantizar la calidad requerida a las medidas de radiación solar.

La metodología empleada para la medida experimental del thermal offset se basa en tapados. Esta técnica consiste en tapar el sensor bloqueando la radiación solar que incidía sobre él, y estudiar la evolución temporal del voltaje de salida del instrumento. Durante el tiempo que dura el tapado dicho voltaje no es sino el resultado del flujo neto de radiación infrarroja entre el sensor y la cúpula, es decir, el cero térmico. El tiempo de tapado debe ser lo suficientemente largo para que el detector responda al bloqueo de la radiación solar pero lo suficientemente breve para que la temperatura de la cúpula no cambie de forma significativa [Bush et al., 2000, Haeffelin et al., 2001, Michalsky et al. 2005, Carlund, 2013].

Varios autores han mostrado que la metodología de tapado permite obtener medidas realistas del cero térmico de piranómetros [Bush et al., 2000; Dutton et al., 2001]. De hecho, ha sido utilizada con frecuencia para obtener valores de cero térmico de referencia con los que calibrar otras metodologías [Bush et al., 2000; Haeffelin et al., 2001; Michalsky et al., 2003]. Además, los tapados tiene la gran ventaja de poder ser aplicados en cualquier localización y a cualquier instrumento. No obstante, la aplicación de esta metodología presenta ciertos requisitos que es necesario considerar. Por un lado, el diseño y materiales de la tapa utilizada para bloquear la radiación solar deben ser elegidos de tal forma que su influencia sobre

la señal sea despreciable. Del mismo modo, el tiempo de tapado debe adaptarse a las características del piranómetro, en particular a los tiempos de respuesta del sensor y la cúpula.

Otra limitación de esta metodología es su escasa operatividad. Los tapados se realizan de forma manual, lo que exige una gran dedicación y trabajo y limita su aplicación a campañas concretas. Este problema se ha subsanado con muchas horas de trabajo, mucha paciencia y la ayuda y apoyo de mi director y mis compañeros.

Los artículos que componen este capítulo presentan los resultados obtenidos durante dos campañas intensivas diseñadas especialmente para la medida experimental del cero térmico. Mientras que la primera de estas campañas fue iniciativa nuestra, la segunda fue sugerida por algunos fabricantes de piranómetros interesados en el tema tras la publicación del Artículo 1. Como resultado de estas dos campañas se ha generado el conjunto más amplio y representativo de medidas de cero térmico obtenidas mediante la metodología de tapados realizadas hasta la fecha.

Por último, debe señalarse que el error asociado al cero térmico no se considera en los radiómetros diseñados para medir radiación UV por dos razones principales. En primer lugar, el proceso de medida es significativamente diferente, empleando un fotodiodo, y no una termopila. Además, estos instrumentos se encuentran termostatizados a una temperatura fija establecida: a 25 °C los Kipp & Zonen UV-S-E-T, a 25 °C los Solar Light UV-Biometer, a 45 °C los YES UVB-1, a 40 °C los NILU-UV, etc. Esta termostatización reduce ostensiblemente las diferencias de temperatura entre las diferentes partes del radiómetro. Por tanto, el estudio y corrección del cero térmico se ha centrado en el caso de los piranómetros de medida de la irradiancia solar total.

3.2. Artículo 1

3.2.1. Datos del artículo

Título: Pyranometer thermal offset: Measurement and analysis

Autores: Guadalupe Sánchez[a]
Antonio Serrano[a]
Mª Luisa Cancillo[a]
José Agustín García[a]

Filiación: [a]Dpto. de Física, Universidad de Extremadura, Badajoz, España

Revista: *Journal of Atmospheric and Oceanic Technology*
Volumen: 32 **Páginas:** 234-246 **Año de publicación:** 2015
doi: 10.1175/JTECH-D-14-00082.1

3.2.2. Principales aportaciones del artículo

Este primer artículo tiene como objetivo medir y analizar los valores de cero térmico en piranómetros. En particular, en este trabajo se ha cuantificado el rango de variación del cero térmico diurno de dos piranómetros Kipp & Zonen modelo CMP11. Además, estos valores han sido comparados con los valores de cero térmico nocturno y también entre ambos instrumentos.

Los valores de cero térmico diurnos fueron obtenidos mediante la metodología de tapados. Por el hecho de ser nuestra primera aproximación a la aplicación de esta metodología, en este trabajo se ha dedicado mucho esfuerzo a su correcta implementación, con el fin de garantizar la calidad de las medidas del cero térmico.

En este sentido, destaca la pre-campaña realizada para analizar los posibles efectos de la tapa y el tiempo de tapado sobre las medidas. Durante esta pre-campaña se realizaron tapados de varias duraciones con el fin de determinar el tiempo óptimo de tapado que finalmente se estimó en 1.5 minutos. Con el fin de evaluar la emisividad de la tapa, se realizaron tapados empleando tapas con distintos diseños y materiales. Además, se realizaron medidas específicas de su emisividad mediante tapados de un pirgeómetro. Estas pruebas demostraron que la tapa finamente empleada en este estudio presentaba una emisividad despreciable de 0.34 W/m^2.

Otro de los aspectos relacionados con la metodología analizado en este trabajo ha sido el criterio para seleccionar el momento durante el tapado que se corresponde con el valor del thermal offset. Los distintos criterios encontrados en la bibliografía

han sido recopilados y comparados sin detectar diferencias significativas entre ellos. Es por ello que finalmente en este trabajo se ha optado por tomar el valor mínimo durante el tapado como valor del cero térmico tal como hizo Bush et al. [2000].

Todo el trabajo realizado en este artículo acerca de la metodología de tapados ha sido empleado como la base de medida de los demás artículos recogidos en este capítulo. Además, este trabajo contribuye muy positivamente a la estandarización de protocolos para la aplicación de esta técnica.

Finalmente, se llevó a cabo una campaña de medida del cero térmico durante nueve días entre marzo y julio en la que se registraron gran variedad de condiciones meteorológicas y radiativas. Durante cada día las medidas fueron tomadas desde primera hora de la mañana hasta última hora de la tarde. Este es el primer estudio en el que se registran medidas de cero térmico mediante tapados distribuidos a lo largo de todo el día. Esto ha permitido la detección de un ciclo diurno en los valores de cero térmico, el cual está asociado, principalmente, a la variación de temperatura del sensor debida a la radiación solar.

Este trabajo cuantifica el rango de variación del cero térmico para los piranómetros Kipp & Zonen modelo CM11, obteniéndose valores desde -19 W/m^2 hasta +0.6 W/m^2. Asimismo relaciona esta variación con la llegada de radiación solar, como factor principal. Ello explica que los valores absolutos máximos (más negativos) se obtengan al mediodía en condiciones de cielo despejado y los mínimos (menos negativos e incluso positivos) bajo cielo cubierto.

Los valores obtenidos en este estudio revelan que el cero térmico de los piranómetro CMP11 analizados pueden suponer entre un 5 % y un 15 % de la medida de irradiancia difusa en días despejados. Este valor está notablemente por encima del 2 % establecido por la OMM como error para estas medidas. Aunque a priori, estos valores sí están dentro del este margen de error en la medida de irradiancia global, debe tenerse en cuenta que los valores absolutos de thermal offset obtenidos en días despejados podrían tener un gran impacto en el análisis del forzamiento radiativo de aerosoles [DiBiagio et al., 2009; DiBiaggio et al., 2010].

Este estudio muestra además que las diferencias detectadas en los valores del thermal offset de los dos instrumentos analizados son significativas al 95 %. Esto sugiere diferencias relevantes incluso entre el mismo modelo de piranómetros. Dado que en este trabajo sólo se han utilizado dos piranómetros sería conveniente ampliar

el estudio a un mayor número de piranómetros tanto del mismo modelo como a otros modelos. Esto permitiría establecer rangos de variación del thermal offset para cada modelo de piranómetro.

También se han resultado significativas al 95 % las diferencias de un mismo instrumento midiendo global o difusa. Esta comparación se ha revelado más complicada de lo que inicialmente se esperaba ya que es realmente difícil que dos días consecutivos coincidan tanto en los valores de radiación como en el resto de variables meteorológicas.

Cabe señalar que, debido a la diferencia en las condiciones atmosféricas, el cero térmico de un piranómetro particular en un lugar puede ser diferente del cero térmico medido en otro lugar. Este hecho enfatiza la importancia de realizar medidas in situ del cero térmico. Sin embargo, aunque nuestros resultados se aplican únicamente a nuestros instrumentos específicos en nuestra ubicación particular, la metodología y las comparaciones descritas en este trabajo pueden utilizarse para desarrollar análisis similares en otros lugares, con otros instrumentos y condiciones ambientales.

3.2.3. Copia original del artículo

Pyranometer Thermal Offset: Measurement and Analysis

G. SANCHEZ, A. SERRANO, M. L. CANCILLO, AND J. A. GARCIA

Department of Physics, University of Extremadura, Badajoz, Spain

(Manuscript received 16 April 2014, in final form 9 October 2014)

ABSTRACT

The reliable estimation of the radiative forcing and trends in radiation requires very accurate measurements of global and diffuse solar irradiance at the earth's surface. To improve measurement accuracy, error sources such as the pyranometer thermal offset should be thoroughly evaluated. This study focuses on the measurement and analysis of this effect in a widely used type of pyranometer. For this aim, a methodology based on capping the pyranometer has been used and different criteria for determining the thermal offset have been applied and compared. The thermal offset of unventilated pyranometers for global and diffuse irradiance has been measured under a wide range of cloud, ambient temperature, wind speed, and radiation conditions. Significant differences in absolute values and variability have been observed between daytime and nighttime, advising against correcting the thermal offset effect based only on nighttime values. Notable differences in the thermal offset between cloudy and cloud-free conditions have been also observed. The main results show that the ambient temperature, the radiation, and its direct/diffuse partitioning are the variables more related to the daytime thermal offset.

1. Introduction

Numerous studies published over the past decades have revealed important differences in the irradiance values estimated by climate or radiative transfer models and those measured with pyranometers at the earth's surface (Garratt 1994; Kato et al. 1997; Halthore et al. 1998; Wild et al. 1998; Valero and bush 1999; Wild 2005). These differences could result in important variations in the subsequent calculation of the radiative forcing and climate trends. Recent studies have estimated a global annual mean solar irradiance at the earth's surface of $184 \pm 10\,\mathrm{W\,m^{-2}}$ (Wild et al. 2013). A widely used pyranometer, such as the Kipp and Zonen CM11 with a manufacturer error of 3% (Kipp and Zonen 2000), would record the above-mentioned global mean irradiance with an absolute error of $\pm 5.5\,\mathrm{W\,m^{-2}}$. This means a very high uncertainty compared to the typical magnitude of the other forcing agents, which has been estimated by the Intergovernmental Panel on Climate Change in the order of $2\,\mathrm{W\,m^{-2}}$ (Pachauri and Reisinger 2007). The mentioned uncertainty is also very large in comparison with the magnitude of the decreasing and increasing trends observed in solar radiation between 1960 and 1990 (dimming period) and after 1990 (brightening period) (Wild et al. 2005). During the dimming and brightening periods, the observed variations ranged in the intervals between -5.1 and $-1.6\,\mathrm{W\,m^{-2}\,decade^{-1}}$, and between 2.2 and $5.1\,\mathrm{W\,m^{-2}\,decade^{-1}}$, respectively (Wild 2009).

Besides climate studies, accurate irradiance measurements are indispensable for the development of solar energy systems. Thus, the efficiency and lifespan of solar systems highly depend on the actual radiation field for each specific location. For instance, a high variability in the solar radiation, occurring mainly under broken cloud conditions, increases the fatigue of materials (Patsalides et al. 2007; Patsalides et al. 2012).

This demand of high-quality radiation values leads to the identification and correction of the main errors in pyranometer measurements. One of the sources of error first detected in solid black pyranometers is the thermal offset error. The thermal offset is a spurious signal due to the difference in temperature between the inner dome and the detector of a pyranometer. In the most common Moll–Gorczynski-type pyranometer, the solar radiation passes through the two glass domes and is absorbed by a black-painted ceramic disk that is intimately bonded to the thermopile detector. However,

Corresponding author address: Guadalupe Sanchez Hernandez, Department of Physics, University of Extremadura, Avenida de Elvas s/n, 06071 Badajoz, Spain.
E-mail: guadalupesh@unex.es

DOI: 10.1175/JTECH-D-14-00082.1

the black ceramic disk absorbs not only the solar radiation transmitted through the domes but also the wavelength infrared radiation emitted by the instrument optics. Thus, the temperature of the inner dome and the detector differ, since they are made of different materials and in contact with different parts of the radiometer: the inner dome with the outer dome, and the detector with the thermopile and the pyranometer case. This different temperature leads to a potentially significant imbalance in the net infrared radiation budget of the detector, subsequently producing a spurious signal that is superimposed on the output signal. This temperature imbalance remains continuously due to the differences in the thermal capacity of the dome and the detector and in the radiation budget of each part of the pyranometer.

True irradiance is underestimated in most occasions, as the detector is at a higher temperature than the dome. It is worth noting that a thermal offset error between -5 and $-30\,W\,m^{-2}$ in diffuse irradiance results in underestimating the irradiance values in 0.7%–4.3% (Reda et al. 2003). It is worth noting that an offset error of $15\,W\,m^{-2}$, which is a typical value under cloud-free conditions, is about 30% of the high-sun Rayleigh diffuse signal (Dutton et al. 2001). Some studies have reported that thermal offset error decreases under cloudy-sky conditions and at nighttime due to the decrease in the dome-detector temperature difference (Bush et al. 2000; Philipona 2002). Additionally, several authors have pointed out the important role played by local and specific factors such as the environment conditions (Long et al. 2003; Vignola et al. 2007, 2008, 2009), the pyranometer model (Cess et al. 2000; Haeffelin et al. 2001; Dutton et al. 2001), the ventilated/unventilated conditions (Philipona 2002), and the radiometric variable measured (global or diffuse) (Bush et al. 2000).

Although being acknowledged as a source of error in solar radiation measurements, there are still numerous uncertainties about the thermal offset and its impact on measurements. For example, there is no general agreement about whether the thermal offset for a pyranometer differs depending on the measurement of global or diffuse irradiance. Thus, while Philipona (2002) found similar thermal offsets for diffuse and global irradiance measurements, Bush et al. (2000) stated that a shaded radiometer operates in a different thermal state than the same instrument in unshaded conditions.

Other unresolved issue is the absence of a standard methodology for measuring the daytime thermal offset of pyranometers. Thus, several methodologies have been applied with that aim (Bush et al. 2000; Dutton et al. 2001; Philipona 2002; Ji and Tsay 2010).

In this framework, this study aims to contribute to a better knowledge of the thermal offset error. It focuses on the measurement and analysis of the daytime thermal offset of unventilated Kipp and Zonen CM11 pyranometers. Although this pyranometer model is extensively used worldwide by international (such as the Baseline Surface Radiation Network) and national radiation networks (deployed by most European national weather services), its thermal offset has not been sufficiently investigated. To measure the daytime thermal offset, the capping methodology has been followed. This technique allows for estimating the thermal offset of a pyranometer by monitoring the response of the output signal when the detector is suddenly covered by a cap. According to this technique, numerous capping events have been conducted under a wide range of air temperature and cloud conditions, and different estimates of the thermal offset have been compared. Additionally, other environmental variables have been simultaneously recorded during the capping events in order to determine the main factors affecting the thermal offset. The analysis has been applied to two similar instruments, so as to account for the variability between instruments of the same type.

2. Instrumentation

This study relies on measurements performed at the radiometric station installed in Badajoz, southwestern Spain (38.9°N, 7.01°W; 199 m MSL), on the roof of the Department of Physics building on the campus of the University of Extremadura, guaranteeing an open horizon. This radiometric station is managed by the research group Atmosphere, Climate and Radiation in Extremadura (AIRE) of the University of Extremadura. This location in western Spain is characterized by a mild Mediterranean climate with very dry and hot summers. During this season measured solar irradiance values are among the highest recorded in Europe.

In this station, global and diffuse irradiance have been measured by two Kipp and Zonen CM11 pyranometers with serial numbers 068948 and 027784 and denoted as pyranometer A and pyranometer B, respectively. The CM11 pyranometer manufactured by Kipp and Zonen is based on the Moll–Gorczynski thermopile and it is formed by 100 thermocouples. The sensing element is a black-painted ceramic (Al_2O_3) disk. Only the border of this disk is in good thermal contact with the pyranometer body. The 100 cold junctions are located along this border, while the 100 hot junctions are near the center in a rotational symmetric arrangement (Kipp and Zonen 2000). These hot junctions are heated by solar radiation,

resulting in a different temperature than the reference temperature of the isolated shielded cold junctions and therefore producing a voltage. The pyranometer is provided with two hemispherical glass domes that are essentially transparent to solar radiation within the interval 0.28–2.8 μm and opaque to longer wavelengths. On the other hand, the thermopile detector is sensitive to both shortwave and longwave radiation (approximately from 0.28 to 100 μm).

The CMP 11 Kipp and Zonen instrument complies with International Organization for Standardization (ISO) 9060 criteria for an ISO secondary standard pyranometer. It is classified as ''high quality'' according to the WMO nomenclature (WMO 2008), with a directional error lower than 10 W m^{-2} for zenith angles up to 80° with a 1000 W m^{-2} beam (Kipp and Zonen 2000). In addition to the manufacturer calibration, both pyranometers participated in two intercomparison campaigns carried out in 2013. The first one took place in April 2013 at the Spanish State Meteorological Agency [Agencia Estatal de Meteorología (AEMET)] station in Badajoz and the second in June 2013 at the Atmospheric Sounding Station [Estación de Sondeos Atmosféricos (ESAt)] of the National Institute for Aerospace Technology [Instituto Nacional de Tecnica Aeroespacial (INTA)] in ''El Arenosillo'' (Huelva, Spain). In these campaigns our two pyranometers were compared to the ventilated Kipp and Zonen CM21 pyranometers 070122 and 041219, respectively, which had been recently calibrated. The calibration factors obtained in the different campaigns and the one provided by the manufacturer notably agree, with relative differences lower than 0.5%, proving the high stability of the response of both pyranometers.

The diffuse solar irradiance was measured by installing the pyranometer (A or B) on a Kipp and Zonen SOLYS2 sun tracker with a shading ball that moves automatically, following the sun's motion and continuously blocking the radiation coming in the sun's direction.

To measure the direct solar radiation, a CHP1 pyrheliometer manufactured by Kipp and Zonen was used. Its first calibration was performed by the manufacturer in 2008 by exact interchange of the test pyrheliometer and the reference pyrheliometer PMO2 of the World Radiation Center (WRC) using the sun as source, resulting in an error sensitivity of ±0.5%. Our pyrheliometer was subsequently calibrated in 2013 at the AEMET Radiometric Laboratory in Madrid, Spain, using the calibrated Kipp and Zonen CH1 pyrheliometer 050408 as reference, which is directly traced to WRC Davos, Switzerland, reference. Both calibrations show a notable agreement, with calibration factors differing in less than 0.1%. The CHP1 pyrheliometer was also installed on the Kipp and Zonen SOLYS2 sun tracker.

Simultaneously, a Kipp and Zonen CG1 pyrgeometer recorded its body temperature (T_p) and the Net IR irradiance on its detector, allowing for the calculating of the downward infrared irradiance (IR) as follows:

$$\mathrm{IR} = \mathrm{Net\ IR} + \sigma T_p^4, \tag{1}$$

where σ is the Stefan–Boltzmann constant. The pyrgeometer CG1 is provided with a 64-thermocouple thermopile detector and has been designed for meteorological measurements of downward atmospheric longwave radiation with good reliability and accuracy. It guarantees an inaccuracy of measurement lower than 20 W m^{-2} and a zero offset lower than 2 W m^{-2} due to a change in temperature of 5 K h^{-1} (Kipp and Zonen 2003). It is very stable, with a sensitivity change per year lower than 1%. It has been calibrated by intercomparison with Kipp and Zonen reference CG1 FT002, resulting in a sensitivity error of ±5% at 20°C and 140 W m^{-2} (Kipp and Zonen 2003).

In addition to the radiative measurements, the ambient temperature during the capping events was monitored by a shadowed and ventilated fast response temperature probe PS-2135 with a precision of 0.1°C and a PASCO GLX datalogger. The temperature probe was located next to the radiometers, being representative of the ambient air temperature at the radiometric station. At the same time, the wind speed was monitored by anemometer model compact 4.3159.00.150 manufactured by THIES. This instrument is installed at the AEMET station in Badajoz, which is located 400 m from our radiometric station.

In its usual configuration, the station records radiation every minute. However, for this particular study, a specific campaign at a temporal frequency of 1 s was performed. Thus, the dataset consists of simultaneous measurements of global, diffuse, direct, and infrared irradiance on a 1-s basis recorded by a Campbell CR1000 acquisition system. The capping events were conducted on seven specific days between March and July 2013, selected according to their atmospheric situations in an attempt to account for a large variety of environment and sky conditions. During these days more than 200 measurements of thermal offset were recorded under different cloud conditions, ambient temperatures, wind speed and solar positions, and operational configurations (measuring global or diffuse). Additionally, the same number of cases was randomly selected at nighttime for each day of study among those measurements registered at solar elevation under −10°. This elevation was selected as the threshold for

nighttime data not affected by solar radiation refracted or scattered by atmospheric components and clouds.

3. Methods

a. Technique for measuring the thermal offset

Although different methodologies have been applied up to date for measuring the thermal offset (Bush et al. 2000; Dutton et al. 2001; Philipona 2002; Ji and Tsay 2010), none of them can be universally recommended, since each method has its specific limitations.

One methodology consists of installing thermistors in the pyranometer for measuring the temperatures of the detector and of the outer/inner dome (Bush et al. 2000; Haeffelin et al. 2001). This method provides a reliable description of the thermal offset behavior, since it directly measures the difference of temperature between the detector and the dome. However, under inhomogeneous radiative fields, temperatures within the dome can vary significantly (Smith 1999) and therefore the temperature measured may not be representative. Moreover, attaching thermometers to the dome can affect the measurements, since they interfere with the incoming radiation.

To avoid the need for attaching a thermistor to the dome, Ji and Tsay (2010) proposed a new technique consisting of installing a barometer inside the pyranometer. This new methodology is based on the relationship between the effective temperature of the dome and the pressure of the air trapped between the outer and inner domes. Then, assuming that the air between the domes behaves as an ideal gas, the thermal offset can be determined. The main drawback of these two methodologies is the need to modify the pyranometer by installing thermometers and barometers inside and/or outside the instrument.

The third method estimates the thermal offset as the difference between the signal of the analyzed pyranometer and a reference pyranometer with a negligible thermal offset (Dutton et al. 2001; Philipona 2002). This method has the advantage of being nonintrusive. However, this procedure generally underestimates the thermal offset, since even the reference pyranometers present a nonzero thermal offset (Ji and Tsay 2010; Dutton et al. 2001). Moreover, this methodology ignores other differences between the reference pyranometer and the pyranometer of study, such as their specific cosine error, spectral response, time response, and temperature dependence.

The fourth methodology for estimating daytime thermal offset relies on conducting capping events. These experiments consist of instantaneously blocking the shortwave (SW) radiation to the detector (a thermopile) of the pyranometer while continuously recording its signal output. The monitoring of the signal evolution once the detector has been blocked allows for determination of the thermal offset. This monitoring is performed until the detector has responded to the SW blocking but before the dome temperature changes significantly. This is a reliable procedure, since the dome temperature has a time constant that is distinguishably longer than the detector (several minutes vs a few seconds) (Bush et al. 2000; Dutton et al. 2001; Haeffelin et al. 2001; Michalsky et al. 2005; Carlund 2013). Its main drawback is the possible effect of the capping on the thermal balance due to the cap emission and the alteration of the circulation of the air (Ji and Tsay 2010).

In the present study this fourth method consisting of capping events was preferred despite being highly demanding. It has the advantage of providing realistic values of the thermal offset independently of other reference instruments and not requiring installation of thermometers in the pyranometers. In this study, the capping events and the cap itself were designed in order to minimize the limitations of the method.

To minimize the effect of IR exchange between the capping device and the domes, a cap with a low-emissivity inner surface was manufactured. The cover was fabricated of polystyrene coated with a reflective material on both inside and outside surfaces (Fig. 1). The emission of the cap was measured covering the pyrgeometer for 5 min (more than 3 times the capping events' duration) during several days under overcast and under cloud-free conditions, and with the temperature ranging between 13.5° and 30°C. The mean net infrared irradiance measured during these experiments was 0.36 $W m^{-2}$. These values are negligible compared to the thermal offset magnitude, as it will be shown in next sections. Additionally, the cap was placed in a refrigerated room before and after each capping event in order to avoid overheating the cap. The cap was built to cover the dome and the screen but not the entire pyranometer body in order to block only the irradiance arriving at the detector. In this way, the temperature of the pyranometer body and the air circulation around it are less affected.

To observe the evolution of the signal of our two pyranometers once capped, a long capping event was essayed. Figure 2 shows a 1-h capping event for pyranometers A and B. It is observed that once the detector was capped, the signal rapidly decreased to negative values and then smoothly increased to approach a stable value. Pyranometer A takes 20 min to reach a stable value around 1.20 $W m^{-2}$, while pyranometer B takes 15 min to stabilize around 2.98 $W m^{-2}$.

b. Criteria for estimating the thermal offset

Although the capping technique has been used by several authors, there is no general agreement about the

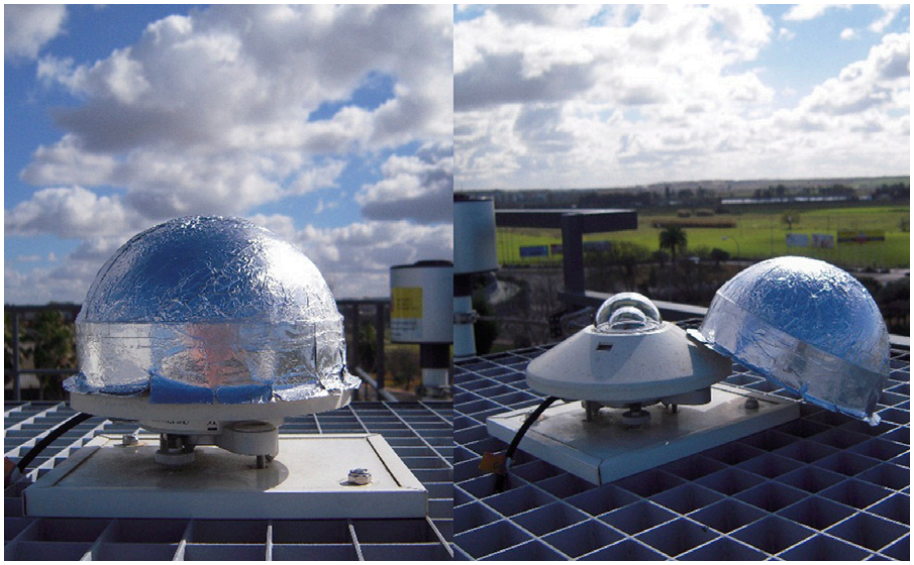

FIG. 1. Cap used for the capping events.

exact time when the output signal reaches the thermal offset value, and different criteria are usually applied. For instance, Bush et al. (2000) and Michalsky et al. (2005) estimated the thermal offset as the minimum signal value reached once the pyranometer is covered. Haeffelin et al. (2001) used the average value within 10 and 20 s after the capping starts. Dutton et al. (2001) used the signal value at 10 times the pyranometer time constant after the capping starts. Recently, Carlund (2013) proposed to calculate the thermal offset as the y intercept of the lineal fit of the output signal versus time within 42 and 84 s after the capping starts.

It must be noted that these criteria were developed for specific instruments and conditions and therefore they need to be adapted to our particular case. Thus, while the criteria proposed by Bush et al. (2000), Michalsky et al. (2005), Dutton et al. (2001), and Carlund (2013) can be appropriately applied in their original version, the criterion used by Haeffelin et al. (2001) is specific for a Precision Spectral Pyranometer (PSP) pyranometer and is unsuitable for Kipp and Zonen CM11 pyranometers. The reason is the longer time constant of the CM11 pyranometers with respect to PSP pyranometers. In the case of the CM11 pyranometers, the output signal is high between 10 and 20 s after the capping event starts. Applying the original version of this criterion overestimates the thermal offset. Therefore, this methodology was adapted to CM11 pyranometers and a time interval between 20 and 40 s was considered.

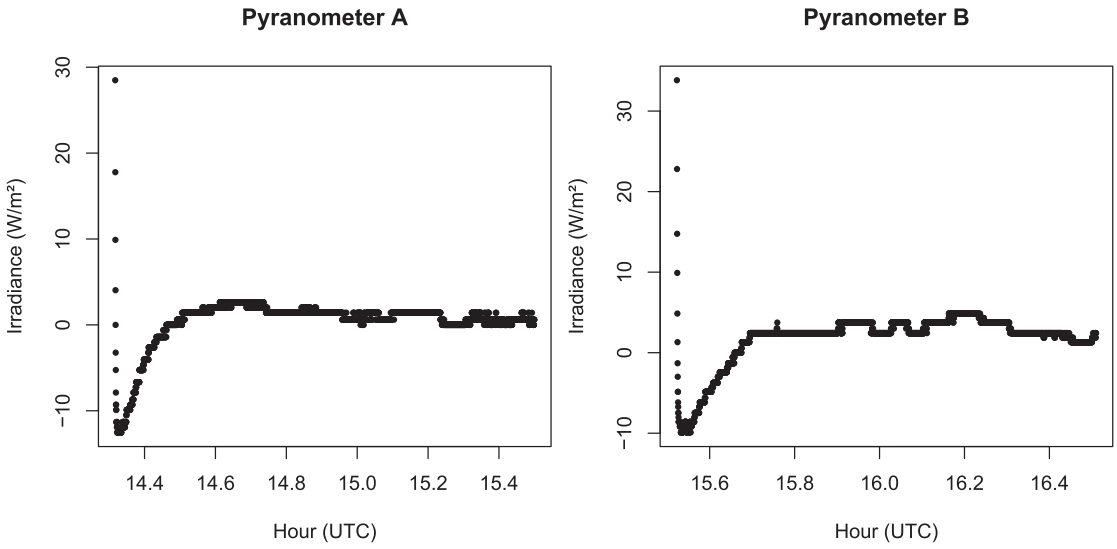

FIG. 2. Long capping events for (a) pyranometer A and (b) pyranometer B.

The selection of a proper lasting time for the capping events had to comply with different requirements. On the one hand, it must be long enough to allow the application of the described methodologies. The methodology that was more demanding was that from Carlund (2013), which requires at least 84 s of capping. On the other hand, the capping must be short enough not to significantly modify the thermal balance between the dome and the detector. To comply with both requirements, we decided to perform capping events lasting 1.5 min. This is the minimum time needed to calculate the thermal offset according to the different criteria described above without significantly affecting the pyranometer temperature imbalance.

Subsequently, numerous 1.5-min-lasting capping events were conducted. The thermal offset of our two pyranometers were measured one after another. The interval between the two consecutive capping events was, at least, 2 min in order to avoid memory effects. The irradiance (global, diffuse, direct, and IR), wind speed, and ambient temperature values ascribed to each capping event were considered as those registered 2 s before capping the pyranometer.

The thermal offset will be calculated by applying these four different criteria under different environment conditions and the results will be analyzed. Finally, a suitable criterion will be chosen.

c. Analysis

Once the most suitable criterion for estimating the thermal offset was selected, the values obtained for the two pyranometers under different conditions were studied in detail. Differences in the thermal offset between daytime and nighttime, under different cloud conditions, and between pyranometers working in the same conditions were analyzed and compared. Differences in thermal offset error between global and diffuse measurements were also investigated.

The relationship between thermal offset and various radiation and environmental variables have been addressed in numerous studies (Bush et al. 2000; Haeffelin et al. 2001; Dutton et al. 2001; Vignola et al. 2007; Ji and Tsay 2010). In particular, the ambient temperature has been reported by many authors as a main factor for the thermal offset (Bush et al. 2000; Dutton et al. 2001; Haeffelin et al. 2001; Philipona 2002; Ji and Tsay 2010). Additionally, the temperature T_p of a collocated pyrgeometer is of special interest, since some authors have indicated its high correlation with the pyranometer temperature due to the similar design of both instruments (Dutton et al. 2001; Ji and Tsay 2010). Moreover, several authors have pointed out the relationship between the thermal offset of a pyranometer and the Net IR measured by a collocated pyrgeometer (Dutton et al. 2001; Haeffelin et al. 2001). These magnitudes are key factors in the local energy balance, which affects the temperature of the pyranometer dome.

In addition, thermal offset dependences on the clearness index k_t and the diffuse fraction K_d were analyzed. These ratios provide information about the relative attenuation suffered by the radiation when crossing the atmosphere. These ratios are defined by the following expressions:

$$k_t = \frac{I_g}{I_{\mathrm{TOA}}}, \tag{2a}$$

$$K_d = \frac{I_d}{I_g}, \tag{2b}$$

respectively, where I_g, and I_d are the global and diffuse irradiance on a horizontal surface on the earth's surface, respectively, and I_{TOA} represents the actual irradiance on a horizontal surface at the top of the atmosphere, which is calculated as follows:

$$I_{\mathrm{TOA}} = 1370\,\mathrm{W\,m^{-2}}\,E_0\cos(\theta), \tag{3}$$

where E_0 stands for the eccentricity correction due to the earth–sun actual distance and θ stands for the solar zenith angle.

d. Schedule of measurements

To investigate the thermal offset of the two pyranometers under different cloud and ambient temperature conditions, measurements with different configurations were performed. Table 1 summarizes the main characteristics of the capping events conducted. It provides information about the date, the cloud condition, the variable measured by each pyranometer (global or diffuse), the number of capping events for each day of measurement, and the ranges of different variables (ambient temperature, wind speed, net infrared irradiance, global solar, and diffuse solar irradiance). The range refers to the interval of variation of each variable corresponding to the capping events conducted each day.

The variety of episodes allowed for studying several aspects of the thermal offset effect. Thus, with the aim to analyze the possible differences in the thermal offset between the two pyranometers, both instruments measured the same variable (global or diffuse) during days 171, 172, 177, and 178. On the other hand, in order to evaluate the main factors affecting the thermal offset, each pyranometer measured the same variable (global or diffuse irradiance) during days with different temperature,

TABLE 1. Date, cloud condition, variable measured, and range of ambient temperature (ΔT_a), wind speed (Δw), Net IR (ΔNet IR), global (ΔI_g) and diffuse (ΔI_d) irradiance during the capping events conducted each day.

	Capping events																			
Date	14 Mar 2013		28 Mar 2013		16 May 2013		20 Jun 2013		21 Jun 2013		26 Jun 2013		27 Jun 2013		18 Jul 2013		19 Jul 2013	
Day of year	73		87		136		171		172		177		178		199		200	
Cloud condition	Clear		Overcast		Overcast		Clear		Cirrostratus		Clear		Clear		Clear		Clear	
ΔT_a (°C)	10°–14°		14°–15°		16°–14.5°		16°–30°		18°–30°		28°–36°		25°–35°		20°–36°		20°–37°	
Wind speed ($m\,s^{-1}$)	1.4–3.4		2.8–4.9		4.5–7.6		1.2–3.8		1.7–4.5		0.6–1.6		1.2–3.2		0.9–3.3		0.5–4.4	
ΔNetIR ($W\,m^{-2}$)	−139, −113		−53, −15		−47, −28		−135, −94		−123, −81		−128, −107		−126, −89		−126, −86		−122, −91	
ΔI_g ($W\,m^{-2}$)	185, 834		125, 860		106, 350		374, 988		300, 1016		577, 958		422, 886		259, 990		303, 971	
ΔI_d ($W\,m^{-2}$)	40, 66		160, 494		106, 350		59, 87		138, 475		116, 176		116, 204		85, 118		72, 126	
	PA	PB	PA	PB	PA	PB	PA	PB	PA	PB	PA	PB	PA	PB	PA	PB	PA	PB
Variable measured	Glo.	Dif.	Glo.	Dif.	Glo.	Dif.	Glo.	Glo.	Dif.	Dif.	Dif.	Dif.	Glo.	Glo.	Glo.	Dif.	Dif.	Glo.
No. of capping events	12	12	10	10	13	13	20	19	16	15	6	6	8	8	15	15	14	14

wind speed, and cloud conditions. For example, pyranometer A measured global irradiance during days 73, 87, 136, 171, 178, and 199 (Table 1). Additionally, in order to study the possible differences in the thermal offset values when the pyranometer measures global or diffuse irradiance, pairs of consecutive days have been used; one day the pyranometer measured global irradiance, while the next day it measured diffuse irradiance. For this comparison, consecutive days with similar temperature, wind speed, and cloud conditions, such as days 199 and 200, were selected. Finally, during some days one pyranometer measured global irradiance, while the other measured diffuse irradiance, with the aim to have enough measurements of all the variables used in the study.

4. Results and discussion

a. Comparison of criteria

The thermal offsets of the two pyranometers were estimated following the original criteria proposed by Bush et al. (2000), Dutton et al. (2001), and Carlund (2013), and the Haeffelin et al. (2001) criterion was adapted as described in section 3.

Figure 3 shows the thermal offset values obtained by applying the four criteria to pyranometer A on an overcast day and a clear day (days 136 and 199, respectively). During both days pyranometer A measured global irradiance. In general, the absolute differences between different criteria are mostly under $1.5\,W\,m^{-2}$ on clear days, and nearly zero on cloudy days. In particular, the results obtained by applying Bush and Dutton's criteria agree overall. In contrast, on clear days, the adapted Haeffelin et al.'s criterion seems to give slightly higher values. These results agree with the paired t tests at a 95% confidence level performed between the two criteria. The tests indicate no statistically significant differences between Bush et al.'s and Dutton et al.'s criteria. On the other hand, Carlund's and Haeffellin et al.'s criteria show significant differences with respect to any other criterion.

In this framework it is worth noting that no best criterion can be established and that the decision must be based on practical considerations. In this study, the Bush et al. (2000) methodology was preferred, since it requires no estimation of any characteristic of the pyranometer, such as its time constant, which can be inaccurate or difficult to determine.

b. Experimental values of the thermal offset

Figure 4, top panels, shows the thermal offset obtained by capping pyranometers A and B under different cloud

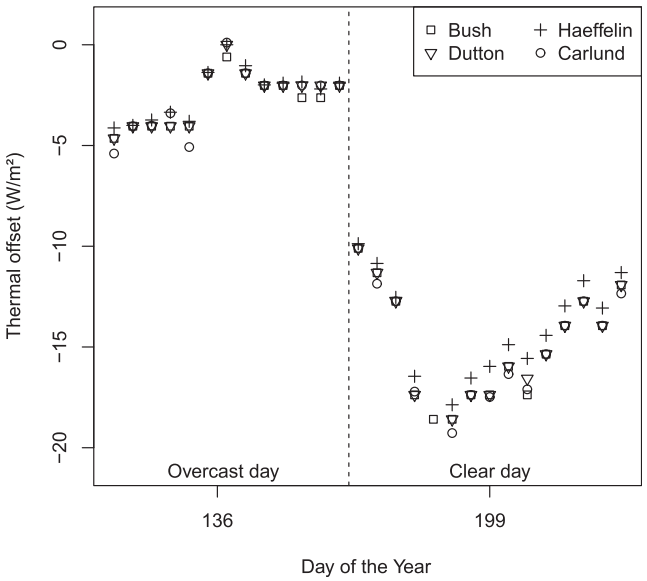

FIG. 3. Thermal offset obtained with different methodologies for pyranometer A when measuring global irradiance on an overcast day (136) and a clear day (199).

conditions along with the corresponding nighttime measurements. In spite of corresponding to the same pyranometer model, significant differences between pyranometers A and B are observed when they were measured under the same environmental conditions (days 171, 172, 177, and 178). The absolute thermal offset of pyranometer A is usually higher than the thermal offset of pyranometer B. This fact can be also observed in Fig. 2. The larger differences, up to 3.48 $W m^{-2}$, occur when both pyranometers measure global irradiance, while the differences decrease to a mean value of 0.37 $W m^{-2}$ when they measure diffuse irradiance. To statistically assess the significance of these differences, two sample t tests were performed. The test resulted in significant differences at a 95% confidence level. This result indicates that the thermal offset must be determined for each instrument individually, even if they correspond to the same manufacturer and model.

The thermal offset of pyranometer A (B) ranges from $-19\,W m^{-2}$ ($-16\,W m^{-2}$) on a cloud-free hot day to $-0.5\,W m^{-2}$ ($+0.6\,W m^{-2}$) on an overcast day with a mild temperature. This decrease in the absolute value of the thermal offset under cloudy conditions agrees with results obtained by other authors (Bush et al. 2000; Dutton et al. 2001) who suggest it is due to the enhancement of downward IR by clouds, heating the pyranometer dome and reducing the dome-detector temperature difference. Under certain atmospheric conditions, the temperature of the dome can be higher than the temperature of the detector, resulting in a positive offset (Bush et al. 2000; Dutton et al. 2001). The thermal offset on clear days (73, 171, 177–200) is notably lower at sunrise/sunset than at noon. At sunrise and sunset, the diffuse fraction K_d is higher because of the longer path traveled by the radiation within the atmosphere. These results point out the important effect on the thermal offset of both the quantity and distribution of the radiation. Figure 4, bottom panels, shows the normalized thermal offset (divided by the irradiance) for daytime measurements. These relative values range from 1% for irradiance during cloudy days to over 15% for diffuse irradiance during cloud-free days.

Figure 4, top panels, shows notable differences in the thermal offset between daytime and nighttime (see, for instance, days 199 and 200). This fact agrees with results reported by several authors for other pyranometer models and locations (Cess et al. 2000; Haeffelin et al. 2001; Philipona 2002; Ji and Tsay 2010). The nighttime offset on different days ranges from 0 to $-5\,W m^{-2}$. In contrast, the daytime thermal offset can reach values under $-15\,W m^{-2}$. There are also notorious differences in the variability. Thus, while the daytime thermal offset under cloud-free conditions can vary up to $8\,W m^{-2}$, during the corresponding nighttime the variability rarely exceeds $2\,W m^{-2}$. These significant differences between day and night advise against the common procedure of using the averaged nighttime measurements as daytime thermal offset.

It is worth noting the differences in thermal offset between days with similar cloud cover, Net IR, and wind speed but different temperature ranges, such as days 73 and 199 (see Table 1). Figure 4, top panels, shows that lower ambient temperatures in day 73 result in lower thermal offset for both pyranometers.

Days 199 and 200 show differences regarding measuring global or diffuse radiation. These differences have been evaluated, and values in the range from 0.61 to 5.86 $W m^{-2}$ for pyranometer A and from 0.56 to 3.74 $W m^{-2}$ for pyranometer B have been obtained. Although these differences are lower than the values obtained by Bush et al. (2000) for a PSP pyranometer (about 8.5 $W m^{-2}$), these differences are significant, as confirmed by a two-sample t test at a 95% confidence level. This finding is counter to results obtained by Philipona (2002) but agrees with Bush et al. (2000) and Cess et al. (2000), who reported differences depending on whether global or diffuse irradiance is measured. This open issue emphasizes the need for studying different pyranometers' families and models.

c. *Relationship with some radiative variables*

The relationship of the experimental thermal offset with some radiative and environment variables was

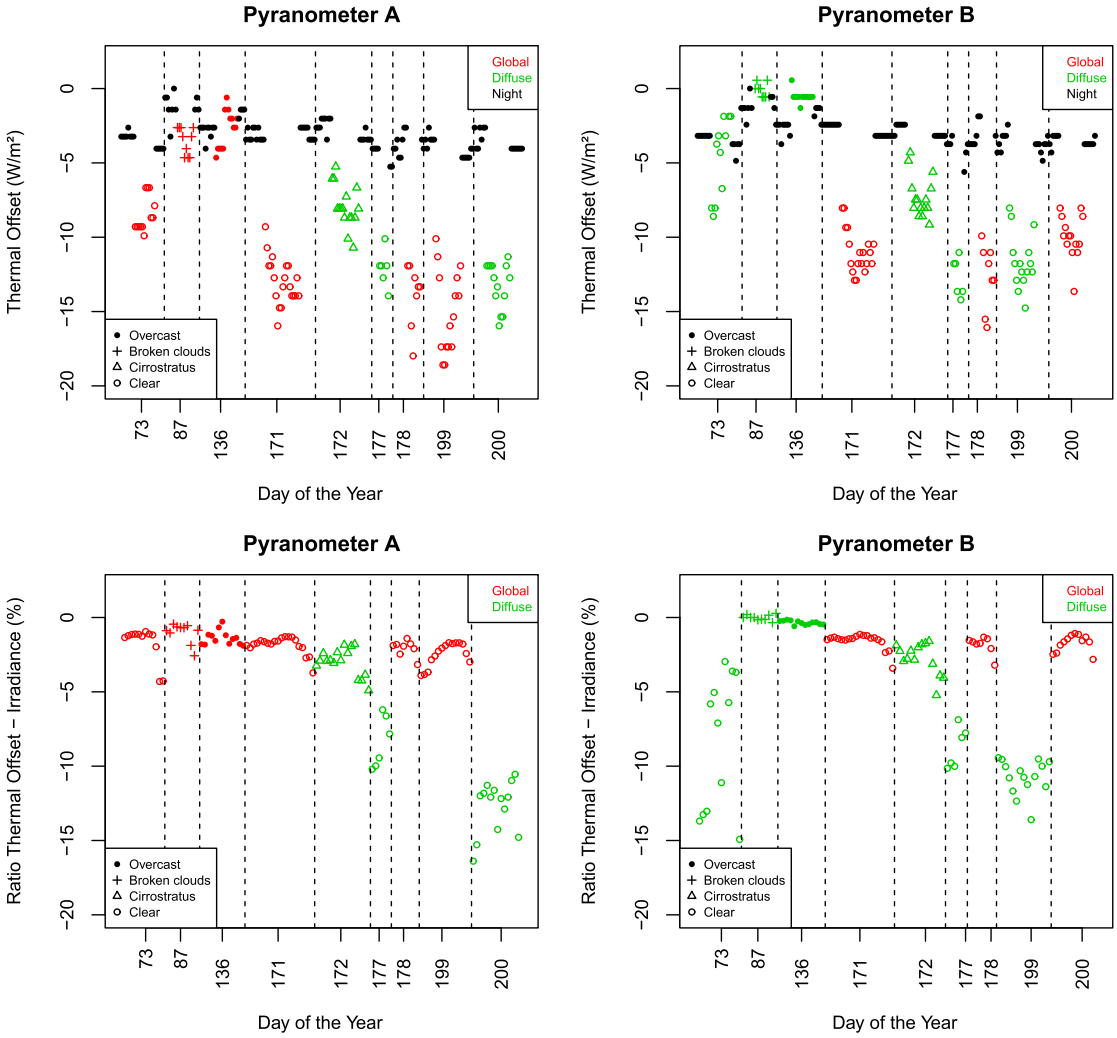

FIG. 4. Nighttime and daytime thermal offset obtained for (top left) pyranometer A and (top right) pyranometer B and daytime thermal normalized (divided by the irradiance) offset for (bottom left) pyranometer A and (bottom right) pyranometer B.

studied. It must be noted that, since the essayed variables are not independent, they are considered individually in the search of a good fit. Figures 5a–f show the daytime thermal offset (gray points) versus the ambient temperature, the clearness index, the diffuse and direct fractions, the Net IR irradiance, the temperature in a collocated pyrgeometer, and the wind speed for pyranometer A. Figures 5e,f show also the nighttime measurements (black points). A clear relationship with ambient and pyrgeometer temperatures and with radiation is found, in agreement with results reported for other pyranometer models (Gulbrandsen 1978; Wardle et al. 1996; Ji and Tsay 2010). Thermal offset decreases when ambient temperature (Fig. 5a), pyranometer temperature (Fig. 5f), and clearness index (Figs. 5c) increase. The diffuse fraction of the radiation plays an important role. Hence, the thermal offset increases when K_d increases (Fig. 5d). The analysis of the Net IR dependence shows similar thermal offset values for cloudy conditions (black points with higher Net IR) and nighttime (gray points) but large differences with daytime values (black points with lower Net IR) (Fig. 5e). A similar result can be observed in the thermal offset versus pyrgeometer temperature relationship (Fig. 5f).

To assess these relationships, least squares regressions between the thermal offset of pyranometer A and each independent variable have been constructed. For this aim the dataset has been split into two subsets: 75% (84 data) for the fitting and the remaining independent 25% (28 data) for the validation. The fittings are moderately good with the coefficient of correlations ranging from 0.64 for the wind to 0.84 for K_d. When these fittings are applied to the independent set, root-mean-square errors (RMSE) under $3.8\,\mathrm{W\,m^{-2}}$ are obtained, showing a moderate predictive skill.

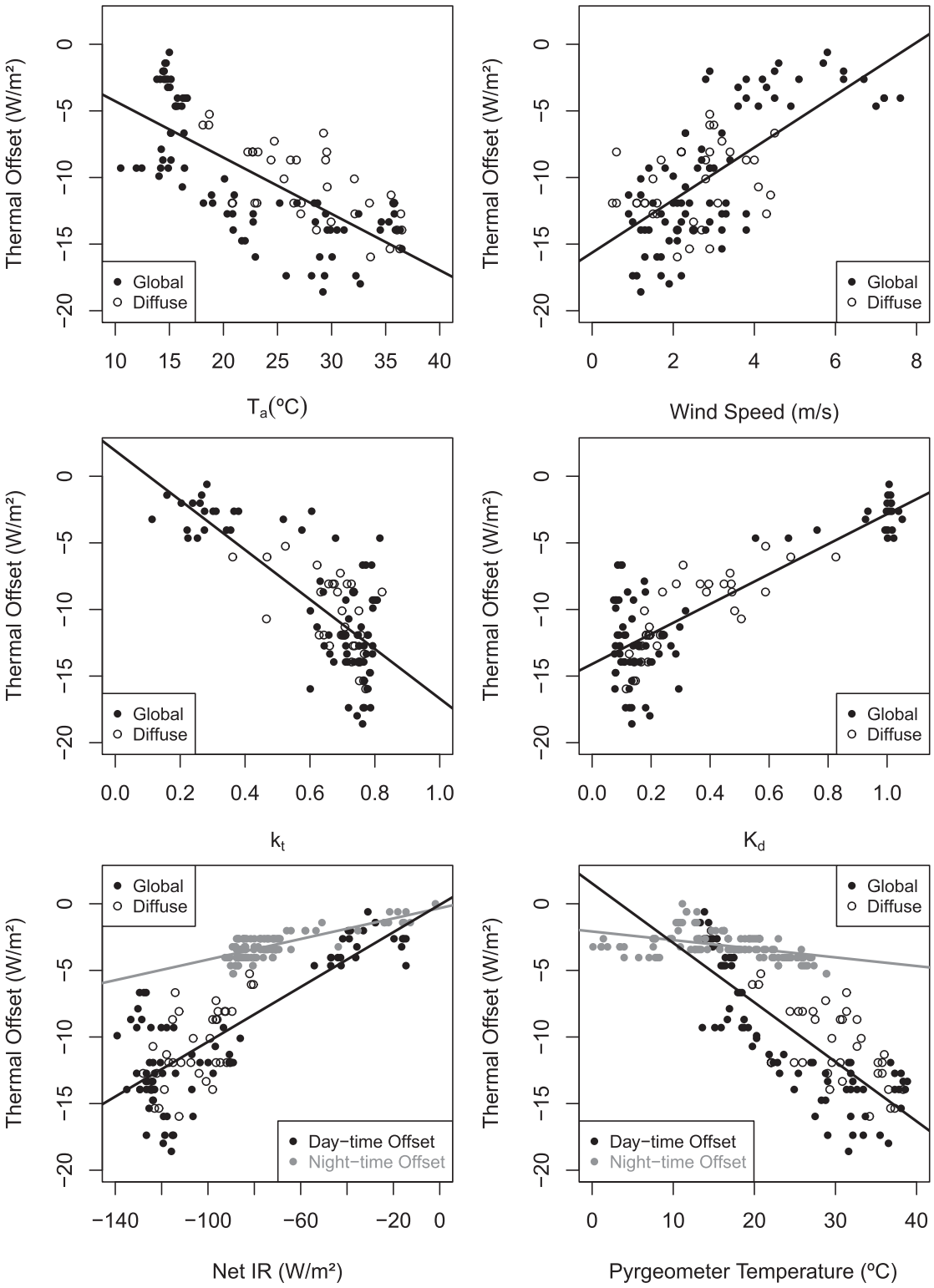

FIG. 5. Pyranometer A thermal offset vs (a) ambient temperature T_a, (b) wind speed, (c) clearness index k_t, (d) diffuse fraction k_d, (e) Net IR, and (f) pyrgeometer temperature T_p.

Figures 5a–f show a complex relationship of the thermal offset with the ambient temperature, the radiation magnitude, and its distribution. Higher thermal offset takes place on clear days around noon, when irradiance, but not the ambient temperature, reaches its maximum value. The simultaneous dependence on temperature and irradiance can be clearly seen in Figs. 6a, where the thermal offset of each pyranometer

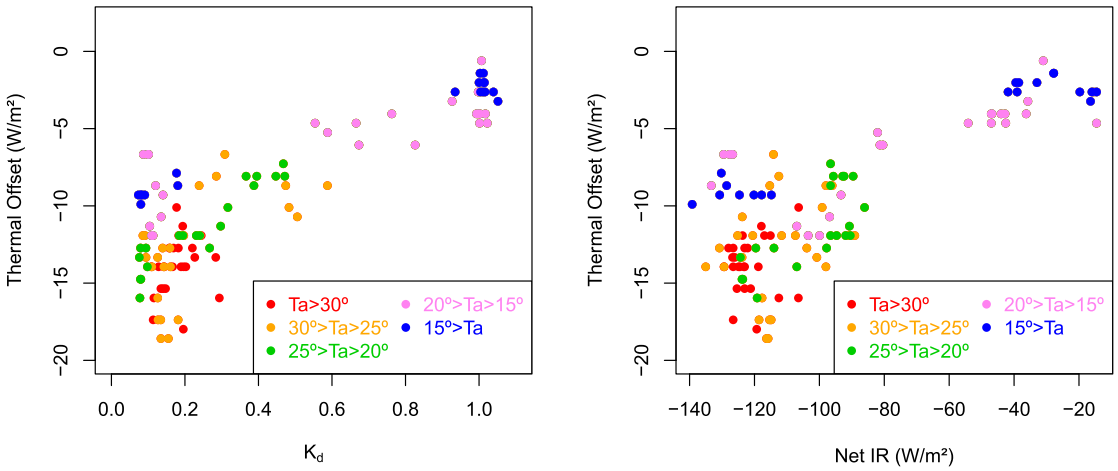

FIG. 6. Pyranometer A thermal offset vs (a) the diffuse fraction and (b) the Net IR for different ambient temperatures.

has been plotted versus the diffuse fraction K_d, using colored symbols to indicate the ambient temperature. It can be seen that the thermal offset is low for high diffuse fraction and low ambient temperature. At the same time, the thermal offset is higher for ambient temperatures above 25°C and diffuse fraction below 0.3, that is, when the direct component is the main irradiance component. A similar behavior can be observed for Net IR, as is shown in Fig. 6b.

5. Discussion and conclusions

In this study, more than 200 experimental measurements have been performed, aimed to investigate the thermal offset of unventilated pyranometers. Thus, capping events under different cloud, wind speed, temperature, and radiation conditions were conducted. The capping methodology was preferred to other methods, since it requires no physical modification of the pyranometers and avoids the nonzero offset and other sources of error that could appear when other instruments are used as reference.

Different criteria to estimate the thermal offset from capping events' measurements (Bush et al. 2000; Dutton et al. 2001; Carlund 2013; Haeffelin et al. 2001) have been applied and compared. Some criteria were adapted to our specific pyranometer model: the Kipp & Zonen CM11. Although all criteria resulted in similar thermal offset values on cloudy days, significant differences for Carlund's and Haeffelin et al.'s criteria with respect to any others have been detected. It was concluded that the convenience of coming to an agreement for establishing a standard procedure would make comparisons easier. In this study, the criterion proposed by Bush et al. (2000) and Michalsky et al. (2005), which consists of selecting the lower signal value after the pyranometer is capped, was chosen because it allows to directly estimate the thermal offset without the need to specify any additional characteristic of the pyranometer.

The significance of differences between the thermal offset of pyranometers A and B has been assessed by means of a two-sample t test. The test indicates statistically significant differences between the means at a 95% confidence level, concluding the need to characterize each radiometer individually.

Significant differences in the thermal offset between daytime and nighttime were also found. This important result agrees well with results reported by Cess et al. (2000), Philipona (2002), and Ji and Tsay (2010) for other pyranometer models and locations. This finding advises against the common procedure of assuming that the nighttime offset constitutes an appropriate estimation for the daytime thermal offset.

Regarding measuring global or diffuse radiation, differences in the range from 0.61 to 5.86 W m^{-2} for pyranometer A and from 0.56 to 3.74 W m^{-2} for pyranometer B have been obtained. These differences were confirmed by a two-sample t test at a 95% confidence level. This finding agrees with Bush et al. (2000) and Cess et al. (2000) but dissents with results obtained by Philipona (2002). This diversity in results is probably related to the different methodology, instrumentation, and location used in these studies. These results argue for the need to develop studies focusing on different pyranometer types.

The relationship between the thermal offset and various characteristics of the environment and radiation conditions have been also examined. There are strong relationships with the ambient temperature, radiation, and the direct/diffuse partitioning. Thus, the highest thermal offset occurs in situations with low diffuse fraction and high ambient temperatures. Conversely, the lower thermal offset is found in situations with high

diffuse fraction and low ambient temperatures. The corresponding least squares regression between the thermal offset and each independent variable has been constructed, showing moderate predictive skill and the relationship with K_d, the one with the best performance, with a correlation coefficient of about 0.84.

This work aims to contribute to better knowledge of the pyranometer thermal offset error, in particular for the widely used Kipp & Zonen CM11. It is worth noting that, due to the difference in atmospheric conditions, the thermal offset of a particular pyranometer at one location may be different from the offset measured at another location. This fact emphasizes the importance of performing on-site measurements of the thermal offset. However, although our results apply solely to our specific instruments at our particular location, the methodology and comparisons described in this paper can be used to develop similar analysis at other locations, with other instruments and environmental conditions. In fact, the complete knowledge of the thermal offset issue will be achieved by a collection of studies that analyze specific instruments at particular locations. This study also suggests directions for future research concerning the development of correction models for the thermal offset.

Acknowledgments. This study was partially supported by the research project CGL2011-29921-C02-01 granted by the Ministerio de Economía y Competitividad from Spain and by Ayuda a Grupos GR10131 granted by Gobierno de Extremadura and Fondo Social Europeo. Guadalupe Sanchez Hernandez thanks the Ministerio de Economía y Competitividad for the predoctoral FPI grant. The Centra Territorial de Extremadura de la Agencia Estatal de Meteorología (AEMET) at Badajoz and the ''El Arenosillo'' Atmospheric Sounding Station (ESAt) of the National Institute for Aerospace Technology (INTA) in Huelva provided suitable facilities for the pyranometer comparisons.

REFERENCES

Bush, B. C., F. P. J. Valero, and A. S. Simpson, 2000: Characterization of thermal effects in pyranometers: A data correction algorithm for improved measurement of surface insolation. *J. Atmos. Oceanic Technol.,* **17,** 165–175, doi:10.1175/1520-0426(2000)017<0165:COTEIP>2.0.CO;2.

Carlund, T., 2013: Baltic region pyrheliometer comparison 2012: 21 May–1 June 2012, Norrköping, Sweden, World Meteorological Organization Rep., Instruments and Observing Methods Rep. 112, 40 pp.

Cess, R. D., T. Qian, and M. Sun, 2000: Consistency tests applied to the measurement of total, direct, and diffuse shortwave radiation at the surface. *J. Geophys. Res.,* **105,** 24 881–24 887, doi:10.1029/2000JD900402.

Dutton, E. G., J. J. Michalsky, T. Stoffel, B. W. Forgan, J. Hickey, D. W. Nelson, T. L. Alberta, and I. Reda, 2001: Measurement of broadband diffuse solar irradiance using current commercial instrumentation with a correction for thermal offset errors. *J. Atmos. Oceanic Technol.,* **18,** 297–314, doi:10.1175/1520-0426(2001)018<0297:MOBDSI>2.0.CO;2.

Garratt, J. R., 1994: Incoming shortwave fluxes at the surface—A comparison of GCM results with observations. *J. Climate,* **7,** 72–80, doi:10.1175/1520-0442(1994)007<0072:ISFATS>2.0.CO;2.

Gulbrandsen, A., 1978: On the use of pyranometers in the study of spectral solar radiation and atmospheric aerosols. *J. Appl. Meteor.,* **17,** 899–904, doi:10.1175/1520-0450(1978)017<0899:OTUOPI>2.0.CO;2.

Haeffelin, M., S. Kato, A. M. Smith, C. K. Rutledge, T. P. Charlock, and J. R. Mahan, 2001: Determination of the thermal offset of the Eppley precision spectral pyranometer. *Appl. Opt.,* **40,** 472–484, doi:10.1364/AO.40.000472.

Halthore, R. N., S. Nemesure, S. E. Schwartz, D. G. Irme, A. Berk, E. G. Dutton, and M. H. Bergin, 1998: Models overestimate diffuse clear-sky surface irradiance: A case for excess atmospheric absorption. *Geophys. Res. Lett.,* **25,** 3591–3594, doi:10.1029/98GL52809.

Ji, Q., and S.-C. Tsay, 2010: A novel nonintrusive method to resolve the thermal dome effect of pyranometers: Instrumentation and observational basis. *J. Geophys. Res.,* **115,** D00K21, doi:10.1029/2009JD013483.

Kato, S., T. P. Ackerman, E. E. Clothiaux, J. H. Mather, G. G. Mace, M. L. Wesely, F. Murcray, and J. Michalsky, 1997: Uncertainties in modeled and measured clear-sky surface shortwave irradiance. *J. Geophys. Res.,* **102,** 25 881–25 898, doi:10.1029/97JD01841.

Kipp and Zonen, 2000: Instruction manual for CM11 and CM14 pyranometer/albedometer, version 0805, 62 pp. [Available online at http://www.kippzonen.com/Download/48/CM-11-Pyranometer-CM-14-Albedometer-Manual.]

——, 2003: Instruction manual for CG1 and CG2 pyrgeometer and net pyrgeometer, version 0204, 63 pp. [Available online at http://www.kippzonen.com/Download/31/CG-1-CG-2-Pyrgeometers-Manual.]

Long, C. N., K. Younkin, K. L. Gaustad, and J. A. Augustine, 2003: An improvement daylight correction for IR loss in ARM diffuse SW measurements. *Proceedings of the Thirteenth Atmospheric Radiation Measurement Science Team Meeting,* D. A. Carrothers, Ed., U.S. Department of Energy, 1–8.

Michalsky, J. J., and Coauthors, 2005: Toward the development of a diffuse horizontal shortwave irradiance working standard. *J. Geophys. Res.,* **110,** D06107, doi:10.1029/2004JD005265.

Pachauri, R. K., and A. Reisinger, Eds., 2007: *Climate Change 2007: Synthesis Report.* Cambridge University Press, 104 pp.

Patsalides, M., and Coauthors, 2007: The effect of solar irradiance on the power quality behaviour of grid connected photovoltaic systems. *Proc. Int. Conf. on Renewable Energy and Power Quality (ICREPQ'07),* Seville, Spain, EA4EPQ, 284. [Available online at http://www.icrepq.com/icrepq07/284-patsalides.pdf.]

——, A. Stavrou, V. Efthymiou, and G. E. Georghiou, 2012: Towards the establishment of maximum PV generation limits due to power quality constraints. *Int. J. Electr. Power Energy Syst.,* **42,** 285–298, doi:10.1016/j.ijepes.2012.03.043.

Philipona, R., 2002: Underestimation of solar global and diffuse radiation measured at Earth's surface. *J. Geophys. Res.,* **107,** 4654, doi:10.1029/2002JD002396.

Reda, I., T. Stoffel, and D. Myers, 2003: A method to calibrate a solar pyranometer for measuring reference diffuse irradiance. *Sol. Energy,* **74,** 103–112, doi:10.1016/S0038-092X(03)00124-5.

Smith, A. M., 1999: Prediction and measurement of thermal exchange within pyranometers. M.S. thesis, Dept. of Mechanical Engineering, Virginia Polytechnic Institute and State University, 64 pp.

Valero, F. P., and B. C. Bush, 1999: Measured and calculated clear-sky solar radiative fluxes during the Subsonic Aircraft Contrail and Cloud Effects Special Study (SUCCESS). *J. Geophys. Res.,* **104,** 27 387–27 398, doi:10.1029/1999JD900947.

Vignola, F., C. N. Long, and I. Reda, 2007: Evaluation of methods to correct for IR loss in Eppley PSP diffuse measurements. *Optical Modeling and Measurements for Solar Energy Systems,* D. R. Myers, Ed., International Society for Optical Engineering (SPIE Proceedings, Vol. 6652), 66520A, doi:10.1117/12.73447.

——, ——, and ——, 2008: Modeling IR radiative loss from Eppley PSP Pyranometers. *Optical Modeling and Measurements for Solar Energy Systems II,* B. K. Tsai, Ed., International Society for Optical Engineering (SPIE Proceedings, Vol. 7046), 70460E, doi:10.1117/12.796457.

——, ——, and ——, 2009: Testing a model of IR radiative losses. *Optical Modeling and Measurements for Solar Energy Systems III,* B. K. Tsai, Ed., International Society for Optical Engineering (SPIE Proceedings, Vol. 7410), 741003, doi:10.1117/12.826325.

Wardle, D. I., and Coauthors, 1996: Improved measurements of solar irradiance by means of detailed pyranometer characterisation. Int. Energy Agency Rep. IEA-SHCP-9C-2, 364 pp.

Wild, M., 2005: Solar radiation budgets in atmospheric model intercomparison from a surface perspective. *Geophys. Res. Lett.,* **32,** L07704, doi:10.1029/2005GL022421.

——, 2009: Global dimming and brightening: a review. *J. Geophys. Res.,* **114,** D00D16, doi:10.1029/2008JD011470.

——, A. Ohmura, H. Gilgen, E. Roeckner, M. Giorgetta, and J. J. Morcrette, 1998: The disposition of radiative energy in the global climate system: GCM-calculated versus observational estimates. *Climate Dyn.,* **14,** 853–886, doi:10.1007/s003820050260.

——, and Coauthors, 2005: From dimming to brightening: Decadal changes in surface solar radiation. *Science,* **308,** 847–850, doi:10.1126/science.1103215.

——, D. Folini, C. Schar, N. Loeb, E. G. Dutton, and G. Konig-Langlo, 2013: The global energy balance from a surface perspective. *Climate Dyn.,* **40,** 3107–3134, doi:10.1007/s00382-012-1569-8.

WMO, 2008: Guide to meteorological instruments and methods of observation. 7th ed. No. 8, Secretariat of the World Meteorological Organization, 681 pp.

3.2.4. Informe del Director de la Tesis Doctoral

El artículo "Pyranometer thermal offset: Measurement and analysis", fue publicado en la revista *Journal of Atmospheric and Oceanic Technology* en el año 2015, teniendo la revista un factor de impacto de 2.159 y estando incluida en el primer cuartil (Q1, ranking 2 de 14 revistas) dentro de la categoría "Engineering, Ocean".

La participación de la doctoranda Dña. Guadalupe Sánchez Hernández en este artículo ha sido muy elevada y diversa, colaborando muy activamente en todas las etapas desarrolladas para la obtención del artículo, desde la concepción de la idea original hasta la propuesta, diseño y toma de medidas, el análisis de resultados y la elaboración del manuscrito. Merece la pena destacar el gran trabajo y esfuerzo que ha dedicado a la realización de experimentos de tapado, lo que ha exigido creatividad e iniciativa para resolver los problemas que surgen al implementar una metodología por primera vez.

Todas estas las tareas han sido desarrolladas por la doctoranda bajo mi dirección y supervisión, pudiendo dar fe de que todo lo aquí expuesto es verídico.

Fdo.: El Director de la Tesis Doctoral

Por otra parte, D. Antonio Serrano Pérez, Dña. María Luisa Cancillo Fernández y D. José Agustín García García, coautores de este artículo, afirman mediante este escrito que han colaborado en este artículo pero que éste forma parte íntegra de la Tesis Doctoral de Dña. Guadalupe Sánchez Hernández y que no va a ser utilizado por ellos como parte de sus respectivas tesis doctorales.

Dña. Mª Luisa Cancillo Fernández D. José Agustín García García

3.3. Artículo 2

3.3.1. Datos del artículo

Título: Correcting daytime thermal offset in unventilated pyranometers

Autores: Antonio Serrano[a]
Guadalupe Sánchez[a]
Mª Luisa Cancillo[a]

Filiación: [a]Dpto. de Física, Universidad de Extremadura, Badajoz, España

Revista: *Journal of Atmospheric and Oceanic Technology*
Volumen: 32 **Páginas:** 2088 - 2099 **Año de publicación:** 2015
doi: 10.1175/JTECH-D-15-0058.1

3.3.2. Principales aportaciones del artículo

El principal objetivo de este trabajo es la propuesta de modelos empíricos para la corrección del cero térmico en las medidas diurnas de irradiancia difusa y global en piranómetros sin ventilación artificial. En este trabajo se han analizado tanto modelos de una sola variable como distintas combinaciones lineales de varias de ellas. Asimismo, se ha analizado la posibilidad de utilizar modelos desarrollados a partir de datos nocturnos para predecir los valores de cero térmico diurno. Además, la utilización en este estudio de dos piranómetros del mismo modelo ha permitido analizar la generalidad de los coeficientes de los modelos finalmente propuestos.

Para este trabajo se han utilizado los valores de cero térmico obtenidos mediante la metodología de tapados descritos en el Artículo 1. Estas medidas fueron tomadas bajo una gran variedad de condiciones atmosféricas lo que garantiza la representatividad del estudio.

Los modelos empíricos propuestos en este trabajo incluyen diversas variables meteorológicas que influyen en la diferencia de temperatura entre el sensor y la cúpula del piranómetro, que es, finalmente, el origen del cero térmico. Las variables ensayadas han sido la temperatura ambiente, la velocidad de viento, la humedad relativa, la radiación infrarroja descendente, la radiación infrarroja neta, la temperatura de un pirgeómetro cercano, el índice de claridad y la fracción de irradiancia difusa. Estas magnitudes presentan además la ventaja de ser frecuentemente medidas en las estaciones radiométricas.

Entre los modelos de una variable propuestos en este estudio destacan aquellos

cuya variable independiente es la fracción de irradiancia difusa (k_d) o la temperatura de un pirgeómetro instalado junto al piranómetro (T_p). El primero de estos modelos, denominado Modelo k_d es este artículo, destaca por permitir la corrección del cero térmico a partir de las propias medidas de irradiancia global y difusa, sin necesidad de instrumentación adicional. Los modelos de una variable han sido analizados también para valores nocturnos de thermal offset. Los valores del RMSE obtenidos al aplicar los coeficientes nocturnos a los datos diurnos son superiores a 7.3 W/m^2 para todos los modelos. Esto indica que la aplicación de los modelos obtenidos a partir de datos nocturnos solo corrigen parcialmente el thermal offset diurno.

Para la propuesta de modelos con varias variables se partió de un conjunto inicial de 223 modelos que surge de la combinación de las todas variables consideradas en modelos de entre dos y ocho variables. Sin embargo, algunas de estas combinaciones presentaban una elevada autocorrelación entre sus variables que podría afectar a la estabilidad de los coeficientes de ajuste. Para detectar y descartar los modelos en los que aparecía autorcorrelación se recurrió al uso de herramientas estadísticas adecuadas.

Con el análisis estadístico de la autocorrelación el número de modelos se redujo a 46 de los cuales finalmente se analizaron los diez con el mayor valor del coeficiente de determinación. Entre estas diez combinaciones lineales finalmente propuestas destaca la formada por k_d y t_p y la formada por k_d e IR. Además de las medidas de irradiancia global y difusa, estos modelos requieren de las medidas simultáneas de un pirgeómetro. No obstante, las otras combinaciones también muestran buenos resultados, lo que permite seleccionar el modelo más adecuado en función de las variables disponibles.

Aunque el uso de los piranómetros CMP11 utilizado en este estudio está muy extendido, debemos reconocer que los resultados obtenidos en este trabajo son específicos para este instrumento y para nuestra localización. Tanto las dependencias funcionales como los coeficientes empíricos aquí mostrados podrían variar tanto con el modelo de piranómetro como con la localización. Es por ello que resulta de gran interés evaluar la generalidad de los modelos propuestos en este trabajo con otros modelos de piranómetros y/o en otras localizaciones.

3.3.3. Copia original del artículo

Correcting Daytime Thermal Offset in Unventilated Pyranometers

A. SERRANO, G. SANCHEZ, AND M. L. CANCILLO

Department of Physics, University of Extremadura, Badajoz, Spain

(Manuscript received 25 March 2015, in final form 21 July 2015)

ABSTRACT

A main source of error in solar radiation measurements is the thermal offset inherent to pyranometers. Despite acknowledgment of its importance, its correction has been widely ignored for several decades. This neglect may have caused a generalized underestimation in solar radiation measurements. This study focuses on the correction of this error in solar irradiance measurements. For this aim a plethora of correction models built as a linear combination of several environmental variables related to the ambient temperature and to the incoming radiation were proposed. The models are fitted to experimental measurements obtained during capping events and, finally, their performance is evaluated and compared. The main results indicate that models with only one independent variable moderately correct the thermal offset error. These simple models are useful when no additional instrumentation other than the pyranometer is available. On the other hand, the more complex models show the best performance, with a coefficient of determination R^2 over 0.8, an RMSE under 2 W m^{-2}, and an absolute value of mean bias error (MBE) under 0.5 W m^{-2}. Additionally, these models are used to study the differences between nighttime and daytime correction, revealing the unsuitability of using nighttime-fitted models to correct the daytime thermal offset. The general validity of the models is tested by their application to two different pyranometers. Results indicate that, whereas the factors involved in the best-performing models are the same, the values of the loading coefficients differ and therefore must be specifically calculated for each pyranometer.

1. Introduction

In recent years, scientific research and emerging solar energy technologies demand an increase in the accuracy of solar radiation measurements. Thus, some studies have shown the dependence of climatic results on the measuring methodology used and on the quality of radiation measurements (Wang et al. 2013). Equally important is the role played by high-quality measurements of the radiation income at the earth's surface for the use of solar radiation as a renewable energy. The vertiginous increase of energy demand requires improving both quantity and quality of solar systems. The design of a solar system suitable for a certain location depends highly on the characteristics of the local solar radiation field, where the partitioning of direct/diffuse radiation is of particular importance (Patsalides et al. 2007, 2012).

High-quality radiation values require identification and correction of the main errors in pyranometer measurements. One of the sources of uncertainty first detected in solid black pyranometers was the thermal offset. This error is caused by the temperature difference between the dome of the pyranometer and its detector, which produces a spurious signal superimposed on the output signal (Drummond and Roche 1965; Gulbrandsen 1978). In most cases, the detector has a temperature higher than the dome, producing a negative signal and, as a result, an underestimation of the radiation. This signal has been quantified to be between −30 and −5 W m^{-2} depending on the instrument design and environmental conditions (Reda et al. 2003; Ji and Tsay 2010). Additionally, several studies have shown notable differences between thermal offsets measured at nighttime or daytime, under cloud or clear conditions, and with high or low temperatures (Bush et al. 2000; Haeffelin et al. 2001; Dutton et al. 2001; Ji and Tsay 2010; Sánchez et al. 2015). Despite having been widely discussed, this error has been ignored for several decades. Philipona (2002) estimated that this neglect may have produced an underestimation between 3% and 8% in solar radiation measurements. However, the process is affected by various environmental factors that make it difficult to propose a thermal offset correction valid for all instrument designs, locations, and environments (Bush et al. 2000).

Corresponding author address: Antonio Serrano, Department of Physics, University of Extremadura, Avda. de Elvas s/n, 06071 Badajoz, Spain.
E-mail: asp@unex.es

DOI: 10.1175/JTECH-D-15-0058.1

Nevertheless, different approaches to correct this error have been proposed. Some corrections focus on the temperature difference between the dome and the detector (Bush et al. 2000; Haeffelin et al. 2001) or on related magnitudes, such as the pressure of the air trapped between the outer and the inner domes (Ji and Tsay 2010). The popular model developed by Dutton et al. (2001) relies on the dome-detector temperature difference and includes an additional term that relates the thermal offset with the net infrared (IR) irradiance measured by a collocated pyrgeometer. A main limitation of this model appears for an inhomogeneous radiation field, when the temperature measured by the pyrgeometer may not be representative (Smith 1999). Additionally, nowadays, the great majority of pyranometers lack temperature and pressure detectors, and their installation can disturb the measurements by interfering with the incoming radiation. Therefore, other correction approaches need to be used.

Dutton et al. (2001) showed that, under cloudy conditions, the net IR term of their model could be used alone to correct the thermal offset of solar diffuse radiation measured by Eppley Precision Spectral Pyranometers (PSPs). However, this approach is not suitable for other conditions and other pyranometer types, such as the widely used unventilated Kipp & Zonen CM11 (Dutton et al. 2001; Carlund 2013). Therefore, other authors have attempted to correct the thermal offset using different methodologies and tentative relationships, mainly based on ambient temperature, relative humidity, and wind velocity (Vignola et al. 2007, 2008, 2009). However, these relationships have been tested only under very specific conditions and instruments, and no thorough comparison has been conducted yet.

The main objective of this paper is to propose models for correcting the daytime pyranometer thermal offset error. Toward this aim, capping events were conducted to measure the daytime thermal offset of two unventilated CM11 pyranometers under different cloud conditions, ambient temperature, solar elevation, and operational configuration (measuring global or diffuse solar radiation). Simultaneously, radiative and environmental magnitudes such as global and diffuse solar irradiance, ambient temperature, downward total and net terrestrial IR irradiance, temperature of the pyrgeometer, wind speed, and relative humidity were measured. Different correction models using these factors have been proposed and compared. Some of these models have been fitted using daytime or nighttime data in order to investigate their possible differences. Additionally, the performance of the models when applied to two different pyranometers was compared so as to assess their possible wider applicability.

2. Data

a. *Instrumentation*

This empirical study is based on measurements of global and diffuse solar irradiance, ambient temperature, downward total and net terrestrial infrared irradiances, and detector temperature of a pyrgeometer registered at the main radiometric station operated by the research group Atmosphere, Climate and Radiation in Extremadura (AIRE) of the University of Extremadura. This station is placed on the roof of the Physics Building at the university campus in Badajoz, Spain (38.9°N; 7.01°W; 199 m MSL). It includes a range of radiometric instrumentation and benefits from an open horizon, which guarantees the reliability of the measurements.

Global and diffuse solar irradiance were measured by two CM11 pyranometers with serial numbers 068948 and 027784, manufactured by Kipp & Zonen (pyranometer A and pyranometer B, respectively). The CM11 model complies with International Organization for Standardization (ISO) 9060 criteria for an ISO secondary standard pyranometer being classified as ''high quality'' by WMO (1996). It guarantees a directional error lower than 10 $W m^{-2}$ for zenith angles up to 80° and a 1000 $W m^{-2}$ radiation beam (Kipp & Zonen 2000). In addition to the original calibration performed by the manufacturer, both pyranometers participated in two intercomparison campaigns hosted by the Spanish State Meteorological Agency [Agencia Estatal de Meteorología (AEMET)] in Badajoz in April 2013 and by the National Institute for Aerospace Technology [Instituto Nacional de Técnica Aeroespacial (INTA)] in its Atmospheric Sounding Station ''El Arenosillo,'' Huelva, in June 2013. In these campaigns the two pyranometers benefited from their comparison to two well-conditioned and recently calibrated Kipp and Zonen CM21 pyranometers with serial numbers 070122 and 041219, respectively. The calibration factors obtained in both campaigns are in good agreement with the values provided by the manufacturer, showing relative differences under 0.5% and therefore ensuring the temporal stability of the pyranometers.

Diffuse solar irradiance measurements were obtained by shading the pyranometer detector by a ball that moves in synchronization with the sun motion so as to continuously block the direct radiation. The pyranometer and the shading ball were installed on the sun tracker model SOLYS2 manufactured by Kipp & Zonen (2008).

The temperature of the ambient air at the station was monitored by a fast response temperature probe (model PS-2135) connected to a PASCO GLX datalogger. The temperature probe has a precision of 0.1°C (PASCO 2014). It was shadowed and ventilated in order to guarantee the reliability of its measurements. The probe was installed next to the pyranometers, being representative of the air temperature at the station.

The radiometric station also includes a Kipp & Zonen CG1 pyrgeometer for measuring downward atmospheric infrared irradiance. In fact, it measures the net radiation (NetIR), defined as the difference between the downward infrared radiation emitted from the atmosphere and the upward irradiance of the detector. To take the emission of the detector into account, the internal temperature (T_p) is also registered. Thus, the total downward atmospheric infrared irradiance (IR) is derived as follows:

$$\mathrm{IR} = \mathrm{NetIR} + \sigma T_p^4, \tag{1}$$

where σ is the Stefan–Boltzmann constant. The CG1 pyrgeometer has been designed to provide highly reliable and accurate measurements of atmospheric infrared radiation. It guarantees measurements with an error lower than $20\,\mathrm{W\,m^{-2}}$ and a zero offset lower than $2\,\mathrm{W\,m^{-2}}$, even under changing temperature conditions of $5\,\mathrm{K\,h^{-1}}$ (Kipp & Zonen 2003). It is also very stable in time, with the change in sensitivity lower than $1\%\,\mathrm{yr^{-1}}$. It has been calibrated by Kipp & Zonen using the CG1 FT002 pyrgeometer as a reference, resulting in a sensitivity error of 5% under conditions of a temperature of 20°C and an irradiance of $140\,\mathrm{W\,m^{-2}}$ (Kipp & Zonen 2003).

All these data were recorded every minute except for solar irradiance, measured by the pyranometers, which was acquired every second in order to allow for accurate determination of the thermal offset during the capping events.

Additionally, wind speed and relative humidity were monitored every 10 min at a nearby meteorological station located 400 m away from our radiometric station. This station belongs to AEMET and follows WMO standard protocols and procedures for calibration and measurement. Wind speed is measured by a Thies Compact anemometer with serial number 4.3159.00.150. The relative humidity is measured by a Thies Compact sensor model 1.1025.55.700 with 0.1° resolution and ±2% accuracy. This sensor operates inside a Stevenson wooden louver to prevent from heating by direct radiation.

b. Capping events

For the present study, a specific campaign was performed consisting of determining the daytime thermal offset by capping the pyranometers. The capping events were conducted during 9 days between March and July 2013 (days of the year 73, 87, 136, 171, 172, 177, 178, 199, and 200). These particular days were selected so as to cover a wide range of cloud cover, temperature, wind, and radiation conditions. All environmental variables listed above were measured concurrently with these capping events.

The capping methodology relies on obtaining the thermal offset value analyzing the time evolution of the output signal of the pyranometer once its detector is suddenly capped. This technique has been widely applied to different pyranometers (Bush et al. 2000; Dutton et al. 2001; Haeffelin et al. 2001; Michalsky et al. 2005; Carlund 2013). The reliability of this methodology has been proved by Bush et al. (2000) and Haeffelin et al. (2001) comparing its results with the difference of temperature between the dome and the detector, which is the main cause of the thermal offset. This methodology presents the advantage of being nonintrusive since there is no need to attach thermometers neither to the detector nor to the dome, avoiding interfering with the incoming radiation and therefore affecting the measurements. In the current study, following the criteria suggested by Bush et al. (2000) and Michalsky et al. (2005), the thermal offset was obtained as the minimum value reached by the signal once the pyranometer detector is capped. For a clear identification of the minimum, the signal was recorded every 1 s, and each capping event conducted in this study took 1.5 min. Figure 1 clearly illustrates the identification of the thermal offset in a long capping event. The measurements registered during the capping events showed that, for our Kipp & Zonen CM11 pyranometers, this minimum was reached about 25–35 s after the detector was capped, and then the output signal remains constant for about 20 s before starting to increase. For CM11 pyranometers, 1.5 min is long enough to detect the reaction of the detector and identify the minimum but short enough to prevent significant changes in the dome temperature or in the environmental conditions.

To obtain reliable estimations of the thermal offset by using the capping methodology, a specific cap of polystyrene was built. This cap was designed to cover the detector and dome while allowing for air circulation around the pyranometer. The inside and outside of the cap were covered with a reflective material. The cap was maintained shadowed and refrigerated before each capping event in order to minimize the IR exchange with the domes. Further details about the capping events conducted and the estimation of the thermal offset can be found in Sanchez et al. (2015).

A total of 114 capping events with pyranometer A and 100 with pyranometer B were conducted; all of them

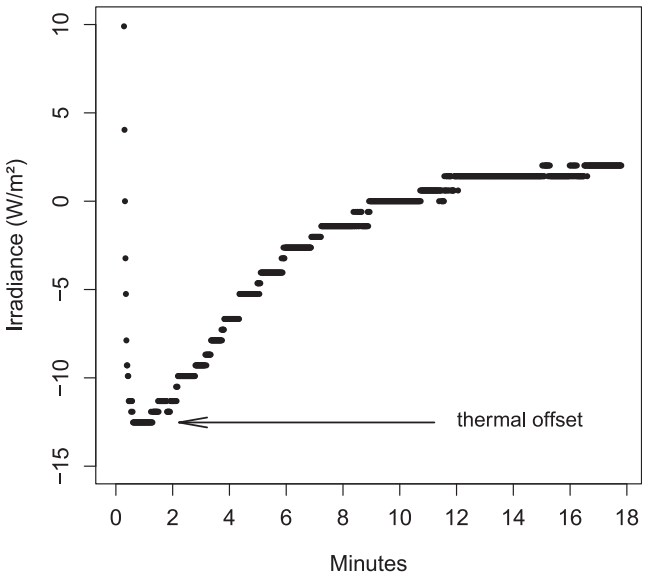

FIG. 1. Evolution of the signal once the detector is capped and identification of the thermal offset as the minimum value is reached.

with a solar zenith angle lower than 80°. In each capping event, an estimate of the thermal offset was obtained.

Additionally, the most representative measurements of the environmental variables available for each capping event were included in the dataset to be used for the development of correction models. Thus, values of global and diffuse solar irradiances, downward and net IR irradiances, and pyrgeometer temperature correspond to the measurement registered just 2 s immediately before the capping event. Air temperature was obtained as the mean of the instantaneous measurement taken 1 s before the capping event starts and the instantaneous measurement taken 1 s after the capping event finishes. For wind speed and relative humidity, the 10-min average value nearest to the central time of the capping event was considered.

3. Methodology

To correct the thermal offset, several mathematical models built as a linear combination of different factors were proposed, fitted to the experimental measurements, compared, and finally ranked according to their performance.

a. Main factors

The Kipp & Zonen CM11 pyranometer used in this study is based on the Moll–Gorczynski thermopile. This thermopile was designed by Dr. W. J. Moll of Utrecht University and later used by Professor L. Gorczynski of the Polish Meteorological Institute to construct pyrheliometers and pyranometers in 1924. The Moll thermopile is made up of many (100 in the case of Kipp & Zonen CM11) thermocouples (Kipp & Zonen 2000) and has a rapid response to changes of incident radiation. It offers a linear relationship between radiation intensity and instrumental response. In this type of pyranometer, the solar radiation passes through two glass domes and is almost completely absorbed by a sensing element consisting of a ceramic disk painted in black. The 100 cold (passive) junctions are located along the border of this disk, being in good thermal contact with the pyranometer housing, which serves as a heat sink. On the other hand, the 100 hot (active) junctions are located beneath the blackened receiver surface, symmetrically arranged near the center, and are heated by the radiation absorbed in the black coating, resulting in a different temperature than the isolated shielded cold junctions and therefore producing a voltage. The pyranometer is provided with two hemispherical glass domes for protecting the black detector coating from the environment. These domes are essentially transparent to solar radiation up to 2.8 μm but opaque to longer wavelengths.

On the other hand, the domes and the detector have different thermal capacity, and their temperatures usually differ due to ambient temperature changes, conduction and convection in the vicinity of the detector, and an infrared exchange between surfaces of different temperatures (Dutton et al. 2001). This temperature imbalance, responsible for the mentioned thermal offset, is affected by external conditions, such as ambient air temperature, air humidity, wind, etc. These variables are potential factors to be considered for the characterization of the thermal offset. Among them, this study includes experimental measurements of the variables pointed out by several authors as the main factors for the daytime thermal offset of the unventilated pyranometers.

The experiments conducted by Bush et al. (2000), Haeffelin et al. (2001), and Ji and Tsay (2010) showed ambient air temperature (T_a) influences the thermal balance of the dome and the detector of the pyranometer, significantly affecting its thermal offset. Additionally, other environmental factors, such as wind speed (W) and relative humidity (RH), directly related to ambient temperature, have been also suggested as influencing factors (Bush et al. 2000; Haeffelin et al. 2001; Vignola et al. 2007, 2008, 2009). Therefore, ambient temperature, wind speed, and relative humidity are considered as main factors in this study.

Several studies of thermal offset have also pointed out the key role played by the solar radiation reaching the detector (Gulbrandsen 1978; Bush et al. 2000; Ji and Tsay 2010; Sanchez et al. 2015). An increase in solar irradiance affects the dome and the detector differently,

thus modifying the temperature imbalance. Additionally, several studies document changes in thermal offset related to different direct/diffuse partitioning of the incoming radiation (Vignola et al. 2009; Sanchez et al. 2015). To take into account this influence, the clearness index (k_t) and the diffuse fraction (K_d) were also included as factors in the models as they provide information on the relative attenuation and scattering, respectively, suffered by the radiation when crossing the atmosphere. They are defined as follows:

$$k_t = \frac{I_g}{I_{\mathrm{TOA}}} \quad \text{and} \tag{2.a}$$

$$K_d = \frac{I_d}{I_g}, \tag{2.b}$$

respectively, where I_g and I_d are the global and diffuse solar irradiance arriving on a horizontal surface at the earth's surface, respectively; and I_{TOA} is the actual solar irradiance on a horizontal surface at the top of the atmosphere. Term I_{TOA} is calculated as follows:

$$I_{\mathrm{TOA}} = S\varepsilon_0 \cos\theta, \tag{3}$$

where S is the solar constant and is equal to 1370 W m^{-2}; ε_0 is the eccentricity correction, which accounts for the actual distance from Earth to the sun; and θ is the solar zenith angle.

Additionally, the thermal offset is affected by other sky conditions. Thus, the infrared downward irradiance at ground level increases under a cloudy sky, heating the dome, and consequently reducing the difference in temperature between the dome and the detector. Under these conditions, the absolute value of the thermal offset will decrease (Bush et al. 2000). Several authors have quantified this influence using NetIR as measured by a thermopile pyrgeometer (Dutton et al. 2001; Haeffelin et al. 2001; Michalsky et al. 2005; Gueymard and Myers 2009). This methodology was originally proposed by Dutton et al. (2001) and Haeffelin et al. (2001) based on the high correlation between the net (NetIR) and the total downward infrared irradiance (IR). These authors have analyzed this dependence only for nighttime measurements. In this study, the relevance of this magnitude for the daytime thermal offset will be investigated. To suitably account for this dependence, both magnitudes—NetIR and IR—will be independently considered as factors to be included in the correction models.

Haeffelin et al. (2001), Dutton et al. (2001), Michalsky et al. (2005), and Gueymard and Myers (2009) analyzed the thermal offset dependence with NetIR but only for nighttime measurements. They studied this dependence for different instruments (PSP and CM21/CM22), and they observed that the results depend on each instrument.

On the other hand, the pyrgeometer temperature (T_p) shows good agreement with the thermal offset, as reported by Ji and Tsay (2010), and recently confirmed by Sanchez et al. (2015). For the Kipp & Zonen CG1 pyrgeometer, this magnitude is measured by a thermistor installed within the instrument, near the detector, resulting in good estimation of the temperature detector.

For this article, variables are expressed in their standard units: T_a and T_p in degrees Celsius, W in meters per second, RH in percent, NetIR and IR in watts per square meter, and k_t and K_d are unitless. Units of each loading coefficient are therefore the inverse units of its factor.

b. Model approaches

Once the main factors to be included are identified, the next step is to propose the mathematical relationships (models) to be used for correcting the daytime thermal offset. The preliminary plots of thermal offset versus each factor showed an almost linear tendency with considerable scatter. Then, linear regressions were developed between the thermal offset as the dependent variable and the factors as the independent variables.

The most elementary models essayed correspond to simple linear regression with only one variable. Thus, eight one-variable models were built with each factor (T_a, W, RH, k_t, K_d, NetIR, T_p, and IR) as the independent variable.

Several authors have pointed out the distinct behavior of the thermal offset between nighttime and daytime (Bush et al. 2000; Cess et al. 2000; Haeffelin et al. 2001; Philipona 2002; Ji and Tsay 2010; Carlund 2013). These results suggest possible differences between models developed with nighttime and daytime measurements. This aspect will be assessed with the one-variable model proposed.

In addition to those simple expressions, more informative models simultaneously involving several factors were proposed. These models were built as multiple linear regressions with combinations of the eight factors as the independent variables. In principle, 223 different combinations are possible, ranging from two to eight variables included. However, some factors are highly correlated, providing redundant information. In these cases, this multicollinearity could lead to ill-conditioned regressions. To detect multicollinearity in the models, the variance inflation factor (VIF) for each factor included in each model was calculated as follows (Stine 1995; Allison 1999):

$$\mathrm{VIF}_i = \frac{1}{1 - R_i^2}, \tag{4}$$

where R_i^2 is the coefficient of determination of the regression of factor i on all other factors included in the

model. The statistical index VIF measures the increase in uncertainty of an estimated regression coefficient due to collinearity.

The suitable cutoff value for VIF depends on the specific problem (Stine 1995).The most common value ranges from 10 to the most restrictive 2.5 (Allison 1999). In this study, a threshold value of 3 has been adopted as the limit for multicollinearity. This value rejected ill-conditioned models while retaining a substantial number of models for the comparison. Thus, models with a VIF higher than 3 in any of the factors involved have been rejected; 46 models were finally selected among the initial 223 possible combinations of factors, whereas the remaining 177 were rejected due to multicollinearity.

c. *Analysis*

To develop the linear regressions corresponding to the different models, the dataset corresponding to pyranometer A (114 cases) was randomly divided into two subsets: the first one comprising 75% of the measurements (86 data) for model fitting, and the second one comprising the remaining 25% (28 data) for validation and comparison purposes. The reason for this asymmetric distribution (75%/25%) is to guarantee a reliable number of cases for the fitting. They are named ''fitting'' and ''validation'' subsets, respectively.

For each model, the goodness of fit of the linear regression was quantified by R^2. This statistic measures how well the observed outcomes are replicated by the model.

Subsequently, the regressions were tested by applying each fitted model to the validation subset, and by calculating the root-mean-square error (RMSE) and the mean bias error (MBE). These two statistics provide information about the magnitude of the difference between modeled and measured values, and about their mean deviation, respectively.

To statistically assess the significance of the differences between models, paired t tests were applied. This statistical test compares two paired samples and determines whether both samples originate from the same statistical population.

The complete analysis has been developed also for pyranometer B. The best-performing models have been subsequently compared with those obtained for pyranometer A with the aim to assess the general validity of the models studied. This comparison applies not only to the main factors involved in the regressions but also to the values of their loading coefficients.

Additionally, the performance of models fitted only with nighttime measurements for estimating the daytime thermal offset has been addressed. This is an interesting topic that has been widely discussed by several authors (Bush et al. 2000; Cess et al. 2000; Haeffelin et al. 2001; Philipona 2002; Ji and Tsay 2010; Carlund 2013). Its interests derive from the possibility to estimate the thermal offset of a pyranometer as the output signal measured during nighttime without the need for conducting specific experiments that interfere with daytime measurements. To address this issue, the daytime thermal offset was estimated by applying nighttime-fitted models to daytime conditions. These estimations were subsequently compared to the experimental values of the thermal offset obtained in the capping events. This comparison was performed by applying paired t tests.

For the development of the nighttime-fitted models, a new dataset comprising 114 nighttime cases (the same number of values as daytime measurements) was built, as well as its division into fitting (75% data) and validation (25% data) subsets. These data were randomly selected among nighttime measurements registered at solar elevation under $-10°$. This elevation was used as the threshold for nighttime data not affected by solar radiation refracted nor scattered by atmospheric components and clouds.

4. Results and discussion

a. *One-variable models*

Eight one-variable linear models were proposed based on the relationship between the thermal offset and ambient temperature, wind speed, relative humidity, clearness index, diffuse fraction, net and downward IR irradiances, and pyrgeometer temperature. In this study, the models are given the same name as the independent variables used in the linear relationships.

Figure 2 depicts the experimental measurements and the fittings obtained with each model. The daytime thermal offset ranges from 0 to $-20\,\mathrm{W\,m^{-2}}$, with a mean value of $-10\,\mathrm{W\,m^{-2}}$. A significant dependence of the thermal offset with each variable can be observed. Models K_d, NetIR, and T_p show lower RMSE than models W, RH, and IR. The overall trend can be positive or negative. Thus, whereas the thermal offset increases with wind, relative humidity, NetIR irradiance, and diffuse fraction, it decreases with ambient air and pyrgeometer temperatures, downward IR irradiance, and clearness index.

This dependence of the thermal offset with NetIR conforms with published results from other authors (Dutton et al. 2001; Haeffelin et al. 2001; Michalsky et al. 2005; Gueymard and Myers 2009) who also found a positive trend although with reference to nighttime values.

Table 1 shows the values of the coefficients of the fitted models along with R^2 for each one-variable model proposed. It also includes the RMSE and MBE obtained over the validation subset. RMSE ranges from 2.4 to

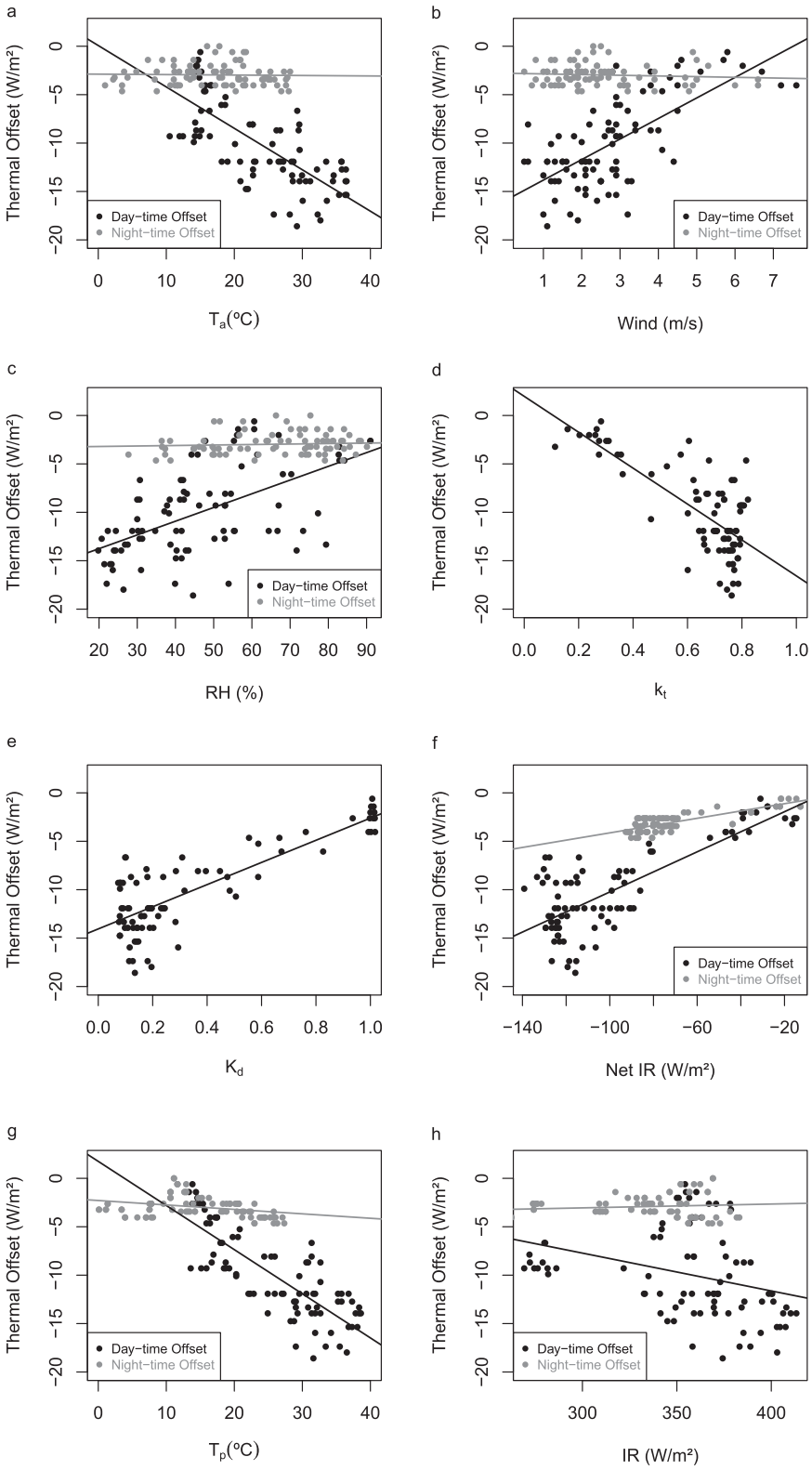

FIG. 2. Thermal offset vs the eight factors of study. Experimental daytime (black circles) and nighttime (gray circles) measurements, and their fittings (black for daytime measurements and gray for nighttime measurements) are plotted.

TABLE 1. Fitting and validation results for pyranometer A of the eight one-variable models proposed. The models are named according to the independent variable. They are ranked by their value of R^2 obtained in the fitting.

	Proposal		Fitting (86 data pairs)			Validation (28 data pairs)	
Rank	Model	Formula	a_0	a_1	R^2	RMSE ($W\,m^{-2}$)	MBE ($W\,m^{-2}$)
1	K_d	$a_0 + a_1 \times K_d$	−14.053	11.444	0.689	2.428	0.680
2	T_p	$a_0 + a_1 \times T_p$	1.753	−0.456	0.655	2.954	0.162
3	NetIR	$a_0 + a_1 \times$ NetIR	0.125	0.104	0.629	2.649	0.763
4	k_t	$a_0 + a_1 \times k_t$	1.979	−18.546	0.555	2.958	0.655
5	T_a	$a_0 + a_1 \times T_a$	0.073	−0.427	0.533	3.303	0.280
6	W	$a_0 + a_1 \times W$	−15.945	2.121	0.461	3.625	0.789
7	RH	$a_0 + a_1 \times$ RH	−16.588	0.142	0.321	3.864	0.434
8	IR	$a_0 + a_1 \times$ IR	3.999	−0.039	0.100	4.369	0.224

4.3 $W\,m^{-2}$ and MBE ranges from 0.2 to 0.8 $W\,m^{-2}$, indicating sound fittings. Models K_d, T_p, and NetIR perform notably well, with R^2 over 0.6 and RMSE under 3 $W\,m^{-2}$. The good performance of the model T_p (second in the ranking) confirms the suitability of data from a temperature detector of a collocated pyrgeometer, as reported by Ji and Tsay (2010). NetIR has also been previously investigated as a factor for the thermal offset but only for nighttime measurements (Haeffelin et al. 2001; Dutton et al. 2001; Michalsky et al. 2005; Gueymard and Myers 2009). On the contrary, models W, RH, and IR show poor fittings (R^2 under 0.4) and large RMSE values around 4 $W\,m^{-2}$. These figures indicate the secondary role played by these latter three factors.

By comparison, models T_a and k_t perform moderately well. Model k_t is of particular interest since it relies only on the irradiance measured by the pyranometer. Thus, it offers the advantage of providing thermal offsets without the need of additional data from other instruments. Model T_a is based on the ambient temperature, which is routinely measured at standard meteorological stations. These two models can be good candidates to retrieve offset data from past measurements, when additional instrumentation is unavailable.

b. *Daytime versus nighttime thermal offset*

Several authors have attempted to estimate the thermal offset using exclusively nighttime measurements (Dutton et al. 2001; Michalsky et al. 2005; Gueymard and Myers 2009). In the absence of solar radiation, the thermal offset is simply obtained as the output signal given by the pyranometer. Therefore, this approach offers the advantage of measuring the thermal offset without the need for additional daytime measurements.

In this study the representativeness of the nighttime thermal offset is analyzed. Thus, Figs. 2b,c,e,f,g, and h depict also nighttime data and their corresponding linear fittings. The daytime and nighttime offsets are very different, with the nighttime offsets showing much less variability. The linear fits reflect these characteristics. To quantify the performance of nighttime-fitted models for estimating the daytime values, Table 2 shows the fitting and validation results for pyranometer A when using nighttime measurements. The low variability of the thermal offset during the night impacts its low RMSE values. However, the R^2 values are remarkably low, indicating poor predictive relationships with any variable except for NetIR. Although the fitting with NetIR as an independent variable can be considered reliable, its predictions of daytime offsets might be poor given differences in NetIR from daytime to nighttime.

Table 3 shows how the models with their nighttime-acquired coefficients perform in estimating daytime thermal offsets. RMSE and MBE values are calculated with respect to true values experimentally obtained by capping events. Additionally, paired t tests were developed to assess how significant the differences between nighttime and daytime thermal offsets are. Thus, Table 3 also shows the p value obtained in paired t tests between the experimental daytime thermal offset and estimates provided by nighttime-fitted models.

RMSE and MBE values (Table 3) are notably higher than those obtained for daytime-fitted models (Table 1). MBE indicates an underestimation of about 7 $W\,m^{-2}$ in the absolute value of the daytime thermal offset. RMSE is also remarkable, being twice higher than in analogous daytime-fitted models (Table 1). The paired t tests show statistically significant values at the 99% confidence level for all models, indicating the unsuitability to use nighttime-fitted models for estimating the daytime thermal offset.

Results have proved that, while the nighttime-fitted models can be useful for night conditions (Table 2), their use is unsuitable for estimating the thermal offset during daytime (Table 3). This result confirms the important role played by the incoming solar radiation in creating a temperature imbalance between the dome and the detector and therefore in the daytime thermal offset (Gulbrandsen 1978; Bush et al. 2000; Ji and Tsay 2010; Sanchez et al. 2015). Since solar radiation is a strong

TABLE 2. Models proposed, and fitting and validation results for pyranometer A with nighttime measurements.

	Proposal		Fitting (86 data pairs)			Validation (28 data pairs)	
Rank	Model	Formula	a_0	a_1	R^2	RMSE ($W\,m^{-2}$)	MBE ($W\,m^{-2}$)
2	T_p	$a_0 + a_1 \times T_p$	−2.500	−0.044	0.108	1.180	−0.465
3	NetIR	$a_0 + a_1 \times$ NetIR	−0.254	0.040	0.615	0.520	−0.050
5	T_a	$a_0 + a_1 \times T_a$	−2.796	0.022	0.024	1.316	−0.624
6	W	$a_0 + a_1 \times W$	−2.825	0.147	0.037	1.293	−0.653
7	RH	$a_0 + a_1 \times$ RH	−4.593	0.021	0.130	1.386	−0.676
8	IR	$a_0 + a_1 \times$ IR	−3.463	0.001	0.001	1.183	−0.606

influencing factor for the daytime offset, relationships derived at night are only valid for the nighttime offset. Furthermore, the application to daytime use of those regression coefficients derived at night presents an additional limitation since the range of air temperature, wind speed, relative humidity, and net IR might, in general, be notably different between day and night.

c. Models with more than one variable

Table 4 summarizes the fitting and validation results for the 10 best models for pyranometer A. These models perform remarkably well, with R^2 values over 0.8, RMSE values under 2.3 $W\,m^{-2}$, and MBE values under 0.53 $W\,m^{-2}$. The factor K_d is included in nine best models, usually accompanied by IR or T_a or T_p, and another variable that can be W or RH. The variables T_a and T_p are highly correlated ($R = 0.987$) and therefore can be used interchangeably. These results provide flexibility in the instrumentation employed depending on whether a pyrgeometer or an ambient thermometer is available.

Wind speed and relative humidity also influence the correction, but they play less of a role than the other factors. In general, no large improvement in R^2, RMSE, and MBE is achieved when using three-variable models instead of their shorter version with only two variables (Table 4). Table 4 presents six relationships that support this argument: IR_K_d versus IR_K_d_W/RH, T_p_K_d versus T_p_K_d_W/RH, and T_a_K_d versus T_a_K_d_W/RH. In all cases, the two-variable model is preferred since it performs equally as well while requiring less additional instrumentation.

Taking into account practical considerations such as the availability of the instrumentation required by each model to be applied, models T_a_k_t and T_a_RH_W should be considered. In addition to their good performance ($R^2 > 0.75$; RMSE $< 2.7\,W\,m^{-2}$; MBE $< 0.57\,W\,m^{-2}$), they have the advantage of requiring measurements of additional variables routinely registered at standard meteorological stations, such as ambient temperature, wind speed, and relative humidity.

d. Model generalization to other pyranometers

To address the generalization of the models to other pyranometers of the same type, a complete analysis was developed also for pyranometer B using the same days and following the same methodology as for pyranometer A. The main factors involved in the best-performing regressions and the loading coefficients for pyranometer B were compared with those obtained for pyranometer A.

The performance values for one-, two-, and three-variable models fitted for pyranometer B were similar to those obtained for pyranometer A. Table 5 shows the fitting and validation results for the 10 best-performing models. It is interesting to note that, although the formulas are the same as those for pyranometer A (Tables 4 and 5), the loading coefficients show notable differences.

The possible generalization of the models was evaluated by applying the models fitted for pyranometer A to the pyranometer B validation dataset, and comparing the predicted offsets with the experimental measurements. A paired t test to assess the significance of the differences between these two dataset was developed.

Table 6 shows the RMSE and MBE values between the modeled and measured thermal offsets of pyranometer B, together with the results of the paired t tests.

Notable increases in MBE ($2\,W\,m^{-2}$ higher) and RMSE ($1\,W\,m^{-2}$ higher) are observed (Tables 5 and 6), indicating a worsened performance. The paired t test confirmed that these differences are statistically significant at the 95% confidence level (Table 6), indicating that the model fitted for pyranometer A is unsuitable for pyranometer B.

TABLE 3. Validation results of nighttime-fitted models applied to estimate the daytime thermal offset, and the paired t test result between the true experimental daytime thermal offset and estimates provided by nighttime-fitted models.

Model	RMSE ($W\,m^{-2}$)	MBE ($W\,m^{-2}$)	p value
T_p	7.959	6.788	5.5×10^{-9}
NetIR	7.315	6.462	2.2×10^{-10}
T_a	8.651	7.416	4.2×10^{-9}
W	8.709	7.363	1.1×10^{-8}
RH	8.337	7.125	6.1×10^{-9}
IR	8.795	7.559	4.2×10^{-9}

TABLE 4. Fitting and validation results for the 10 best-performing models for pyranometer A.

Rank	Proposal		Fitting (86 data pairs)					Validation (28 data pairs)	
	Model	Expression	a_0	a_1	a_2	a_3	R^2	RMSE ($W\,m^{-2}$)	MBE ($W\,m^{-2}$)
1	IR_K_d_W	$a_0 + a_1 \times \text{IR} + a_2 \times K_d + a_3 \times W$	2.711	−0.049	11.113	0.281	0.855	2.121	0.376
2	T_p_K_d_W	$a_0 + a_1 \times T_p + a_2 \times K_d + a_3 \times W$	−6.347	−0.270	6.368	0.374	0.853	2.183	0.452
3	IR_K_d	$a_0 + a_1 \times \text{IR} + a_2 \times K_d$	3.620	−0.050	12.012	—	0.851	2.141	0.343
4	IR_K_d_RH	$a_0 + a_1 \times \text{IR} + a_2 \times K_d + a_3 \times \text{RH}$	3.598	−0.050	12.004	0.0002	0.851	2.142	0.343
5	T_p_K_d	$a_0 + a_1 \times T_p + a_2 \times K_d$	−5.523	−0.276	7.456	—	0.846	2.245	0.414
6	T_p_K_d_RH	$a_0 + a_1 \times T_p + a_2 \times K_d + a_3 \times \text{RH}$	−4.466	−0.293	7.672	−0.015	0.848	2.167	0.412
7	T_a_K_d_W	$a_0 + a_1 \times T_a + a_2 \times K_d + a_3 \times W$	−7.934	−0.248	7.373	0.408	0.841	2.226	0.546
8	T_a_K_d	$a_0 + a_1 \times T_a + a_2 \times K_d$	−7.094	−0.253	8.595	—	0.833	2.280	0.507
9	T_a_K_d_RH	$a_0 + a_1 \times T_a + a_2 \times K_d + a_3 \times \text{RH}$	−6.625	−0.260	8.737	−0.007	0.833	2.246	0.509
10	NetIR_IR_W	$a_0 + a_1 \times \text{NetIR} + a_2 \times \text{IR} + a_3 \times W$	11.672	0.086	−0.043	0.804	0.807	2.298	0.527

Therefore, while the best-performing formulas are the same, with slight changes in the ranking order the loadings notably differ. This result suggests the need for calculating the coefficients individually for each pyranometer. This finding is in line with previous studies (Cess et al. 2000; Dutton et al. 2001; Haeffelin et al. 2001; Michalsky et al. 2005; Gueymard and Myers 2009) that commented that the thermal offset is specific for each instrument.

5. Conclusions

This study provides a sound and methodical analysis of the correction of the daytime thermal offset of pyranometers. Eight influencing factors were considered and a plethora of expressions were built with the aim to correct the daytime thermal offset of Kipp & Zonen CM11 pyranometers. The dependence on the individual factors was investigated individually as well as in combination involving several (two and three) variables.

This thorough approach to the thermal offset correction considered all 223 possible combinations of eight main factors as opposed to previous studies, which usually analyzed only one or two expressions. Thus, this study presents a complete comparison of models not previously examined.

The use of the VIF value to prevent multicollinearity has proved to be successful, reducing the original 223 expressions to 46 well-conditioned models.

The one-variable models K_d, and T_p performed reasonably well, estimating the thermal offset even better than the widely used Dutton et al. (2001) model based on NetIR. These models resulted in an R^2 over 0.6 and an RMSE under 3 $W\,m^{-2}$ but showed the need for including more factors to reliably estimate the thermal offset. Models involving only k_t or T_a showed R^2 over 0.5 and could be of particular use for a series of past measurements when no additional instrumentation is available.

The nighttime-fitted models were shown to be unsuitable for predicting the daytime thermal offset, emphasizing the important role played by the daytime incoming radiation in the temperature imbalance between the dome and the detector, which is the original cause for the thermal offset.

Several modes with more than one independent variable performed really well, with IR_K_d_W and T_p_K_d_W being the two best. Taking into account the convenience of parsimonious expressions, the models IR_K_d and T_p_K_d were finally preferred. However, the current study showed different options that could

TABLE 5. Fitting and validation results for the 10 best-performing models for pyranometer B.

Rank	Proposal Model	Fitting (75 data pairs)					Validation (25 data pairs)	
		a_0	a_1	a_2	a_3	R^2	RMSE ($W\,m^{-2}$)	MBE ($W\,m^{-2}$)
1	IR_K_d_W	10.387	−0.064	10.673	0.297	0.876	1.713	−0.029
2	IR_K_d_RH	12.204	−0.067	12.112	−0.009	0.872	1.758	0.059
3	IR_K_d	11.341	−0.065	11.856	—	0.871	1.735	0.129
4	T_p_K_d_W	−1.811	−0.344	3.988	0.531	0.861	1.468	0.192
5	T_p_K_d_RH	2.824	−0.413	6.352	−0.046	0.859	1.503	0.166
6	T_a_K_d_W	−3.650	−0.326	5.098	0.591	0.855	1.820	0.228
7	T_p_K_d	−0.808	−0.348	6.023	—	0.846	1.598	0.481
8	T_a_K_d	−2.628	−0.327	7.406	—	0.844	1.935	0.309
9	T_a_K_d_RH	−0.063	−0.374	7.874	−0.036	0.844	1.935	0.309
10	NetIR_IR_W	17.786	0.079	−0.057	0.850	0.843	1.610	0.216

TABLE 6. Results of applying pyranometer B data to those models fitted with pyranometer A data: RMSE, MBE, and p values of the paired t test between modeled and experimental values.

Model	RMSE (W m^{-2})	MBE (W m^{-2})	p value
IR_K_d_W	2.793	−2.243	2.7×10^{-7}
IR_K_d_RH	2.758	−2.156	9.1×10^{-7}
IR_K_d	2.760	−2.157	9.0×10^{-7}
T_p_K_d_W	2.516	−2.042	1.6×10^{-7}
T_p_K_d_RH	2.526	−2.004	4.7×10^{-7}
T_a_K_d_W	5.950	−5.352	7.6×10^{-11}
T_p_K_d	2.477	−1.921	1.3×10^{-8}
T_a_K_d	2.590	−1.823	2.9×10^{-5}
T_a_K_d_RH	19.829	17.947	3.7×10^{-11}
NetIR_IR_W	24.450	24.013	2.2×10^{-6}

be used depending on the additional instrumentation available.

The general validity of the models was addressed by applying pyranometer A–fitted models for estimating the daytime thermal offset of pyranometer B. These estimations were compared to experimental values measured by conducting capping events. The results indicate significant differences, establishing the need to derive specific models for each pyranometer. While the best-performing formulas were found to be the same for both pyranometers, with slight changes in the ranking order, the values of the loading coefficients significantly differed, emphasizing the need to calculate the coefficients individually for each pyranometer.

Although being of great interest due to the extensive use of this model of pyranometers, it must be recognized that the results obtained in this study are specific for CM11 Kipp & Zonen pyranometers. Therefore, this study suggests directions for research, and future work should attempt to replicate these results for other families of pyranometers.

Acknowledgments. This study was partially supported by the research projects CGL2011-29921-C02-01 and CGL2014-56255-C2-1-R granted by the Ministerio de Economía y Competitividad from Spain. Guadalupe Sánchez Hernández thanks the Ministerio de Ciencia e Innovación for her predoctoral FPI grant. The Centro Territorial de Extremadura de la Agencia Estatal de Meteorología (AEMET) in Badajoz (Spain) and the Estación de Sondeos Atmosféricos El Arenosillo (ESAt) del Instituto Nacional de Técnica Aeroespacial (INTA) in Huelva (Spain) provided suitable facilities for pyranometer intercomparison campaigns. AEMET also provided wind and relative humidity data.

REFERENCES

Allison, P. D., 1999: *Multiple Regression: A Primer.* Pine Forge Press, 202 pp.

Bush, B. C., F. P. J. Valero, and A. S. Simpson, 2000: Characterization of thermal effects in pyranometers: A data correction algorithm for improved measurement of surface insolation. *J. Atmos. Oceanic Technol.*, **17**, 165–175, doi:10.1175/1520-0426(2000)017<0165:COTEIP>2.0.CO;2.

Carlund, T., 2013: Baltic region pyrheliometer comparison 2012, WMO Instruments and Observing Methods Rep. IOM 112, 46 pp.

Cess, R. D., Q. Taotao, and S. Moguo, 2000: Consistency tests applied to the measurement of total, direct, and diffuse shortwave radiation at the surface. *J. Geophys. Res.*, **105**, 24 881–24 887, doi:10.1029/2000JD900402.

Drummond, K. L., and J. J. Roche, 1965: Corrections to be applied to measurements made with Eppley (and other) spectral radiometers when used with Schott colored glass filters. *J. Appl. Meteor.*, **4**, 741–744, doi:10.1175/1520-0450(1965)004<0741:CTBATM>2.0.CO;2.

Dutton, E. G., J. J. Michalsky, T. Stoffel, B. W. Forgan, J. Hickey, D. W. Nelson, T. L. Alberta, and I. Reda, 2001: Measurement of broadband diffuse solar irradiance using current commercial instrumentation with a correction for thermal offset errors. *J. Atmos. Oceanic Technol.*, **18**, 297–314, doi:10.1175/1520-0426(2001)018<0297:MOBDSI>2.0.CO;2.

Gueymard, C. A., and D. R. Myers, 2009: Evaluation of conventional and high-performance routine solar radiation measurements for improved solar resource, climatological trends and radiative modeling. *Sol. Energy*, **83**, 171–185, doi:10.1016/j.solener.2008.07.015.

Gulbrandsen, A., 1978: On the use of pyranometers in the study of spectral solar radiation and atmospheric aerosols. *J. Appl. Meteor.*, **17**, 899–904, doi:10.1175/1520-0450(1978)017<0899:OTUOPI>2.0.CO;2.

Haeffelin, M., S. Kato, A. M. Smith, C. K. Rutledge, T. P. Charlock, and J. R. Mahan, 2001: Determination of the thermal offset of the Eppley precision spectral pyranometer. *Appl. Opt.*, **40**, 472–484, doi:10.1364/AO.40.000472.

Ji, Q., and S.-C. Tsay, 2010: A novel nonintrusive method to resolve the thermal dome effect of pyranometers: Instrumentation and observational basis. *J. Geophys. Res.*, **115**, D00K21, doi:10.1029/2009JD013483.

Kipp & Zonen, 2000: Instruction manual for CM11 pyranometer and CM14 albedometer. Version 0805, 62 pp.

——, 2003: Instruction manual for CG1 pyrgeometer and CG2 net pyrgeometer. Version 0204, 63 pp.

——, 2008: Instruction manual for SOLYS 2, 2-Axis Sun Tracker. Version 0811, 66 pp.

Michalsky, J. J., and Coauthors, 2005: Toward the development of a diffuse horizontal shortwave irradiance working standard. *J. Geophys. Res.*, **110**, D06107, doi:10.1029/2004JD005265.

PASCO, 2014: Fast Response Temperature Probe manual. Instruction sheet for the PASCO models PS-2135, 012-08475E, 2 pp.

Patsalides, M., and Coauthors, 2007: The effect of solar irradiance on the power quality behaviour of grid connected photovoltaic systems. *Proc. Int. Conf. on Renewable Energy and Power Quality (ICREPQ'07)*, Seville, Spain, University of Vigo, 284. [Available online at http://www.icrepq.com/icrepq07/284-patsalides.pdf.]

——, A. Stavrou, V. Efthymiou, and G. E. Georghiou, 2012: Towards the establishment of maximum PV generation limits due to power quality constraints. *Int. J. Electr. Power Energy Syst.*, **42**, 285–298, doi:10.1016/j.ijepes.2012.03.043.

Philipona, R., 2002: Underestimation of solar global and diffuse radiation measured at Earth's surface. *J. Geophys. Res.*, **107**, 4654, doi:10.1029/2002JD002396.

Reda, I., T. Stoffel, and D. Myers, 2003: A method to calibrate a solar pyranometer for measuring reference diffuse irradiance. *Sol. Energy*, **74**, 103–112, doi:10.1016/S0038-092X(03)00124-5.

Sanchez, G., A. Serrano, M. L. Cancillo, and J. A. Garcia, 2015: Pyranometer thermal offset: Measurement and analysis. *J. Atmos. Oceanic Technol.*, **32**, 234–246, doi:10.1175/JTECH-D-14-00082.1.

Smith, A. M., 1999: Prediction and measurement of thermal exchange within pyranometers. M.S. thesis, Dept. of Mechanical Engineering, Virginia Polytechnic Institute and State University, 64 pp.

Stine, R. A., 1995: Graphical interpretation of variance inflation factors. *Amer. Stat. Assoc.*, **49**, 53–56.

Vignola, F., C. N. Long, and I. Reda, 2007: Evaluation of methods to correct for IR loss in Eppley PSP diffuse measurements. *Optical Modeling and Measurements for Solar Energy Systems*, D. R. Myers, Ed., International Society for Optical Engineering (SPIE Proceedings, Vol. 6652), 66520A, doi:10.1117/12.734474.

——, ——, and ——, 2008: Modeling IR radiative loss from Eppley PSP pyranometer. *Optical Modeling and Measurements for Solar Energy Systems II*, B. K. Tsai, Ed., International Society for Optical Engineering (SPIE Proceedings, Vol. 7046), 70460E, doi:10.1117/12.796457.

——, ——, and ——, 2009: Testing a model of IR radiative losses. *Optical Modeling and Measurements for Solar Energy Systems III*, B. K. Tsai, Ed., International Society for Optical Engineering (SPIE Proceedings, Vol. 7410), 741003, doi:10.1117/12.826325.

Wang, K., R. E. Dickinson, Q. Ma, J. A. Augustine, and M. Wild, 2013: Measurement methods affect the observed global dimming and brightening. *J. Climate*, **26**, 4112–4120, doi:10.1175/JCLI-D-12-00482.1.

WMO, 1996: *Guide to Meteorological Instruments and Methods of Observation.* 6th ed. WMO-8, 501 pp.

3.3.4. Informe del Director de la Tesis Doctoral

El artículo "Correcting daytime thermal offset in unventilated pyranometers", fue publicado en la revista Journal of Atmospheric and Oceanic Technology en el año 2015, teniendo la revista un factor de impacto de 2.159 y estando incluida en el primer cuartil (Q1, ranking 2 de 14 revistas) dentro de la categoría "Engineering, Ocean".

La participación de la doctoranda Dña. Guadalupe Sánchez Hernández en este artículo ha sido elevada y diversa, colaborando muy activamente en todas las etapas desarrolladas para la obtención del artículo, como el diseño y realización de los experimentos de medida, la propuesta de modelos de corrección y su implementación y cálculo, el análisis de resultados y la preparación del manuscrito.

Todas estas las tareas han sido desarrolladas por la doctoranda bajo mi dirección y supervisión, pudiendo dar fe de que todo lo aquí expuesto es verídico.

Fdo.: El Director de la Tesis Doctoral

Por otra parte, D. Antonio Serrano Pérez y Dña. María Luisa Cancillo Fernández, coautores de este artículo, afirman mediante este escrito que han colaborado en este artículo pero que éste forma parte íntegra de la Tesis Doctoral de Dña. Guadalupe Sánchez Hernández y que no va a ser utilizado por ellos como parte de sus respectivas tesis doctorales.

Dña. Mª Luisa Cancillo Fernández D. Antonio Serrano Pérez

3.4. Artículo 3

3.4.1. Datos del artículo

Título: An intercomparison of the thermal offset for different pyranometers

Autores: Guadalupe Sánchez[a]
Mª Luisa Cancillo[a]
Antonio Serrano[a]

Filiación: [a]Dpto. de Física, Universidad de Extremadura, Badajoz, España

Revista: *Journal of Geophysical Research - Atmospheres*

Volumen: 121 **Páginas:** 7901-7912 **Año de publicación:** 2016

doi: 10.1002/2016JD024815

3.4.2. Principales aportaciones del artículo

Este artículo amplía nuestros estudios previos sobre el cero térmico aplicando la metodología de tapado a diversos modelos de piranómetro de diferentes fabricantes. Con este fin se organizó una campaña en la que participaron tres de los principales fabricantes de piranómetros, cada uno de las cuales cedió de forma temporal dos de sus instrumentos más utilizados. El objetivo último fue el estudio de las diferencias en magnitud, comportamiento diurno y dependencia de las condiciones ambientales del cero térmico de los piranómetros participantes en la campaña. Cabe destacar que esta es la campaña de intercomparación de valores de cero térmico con mayor número de tapados realizada hasta el momento.

Teniendo en cuenta los resultados de los dos artículos anteriores, se decidió realizar esta nueva campaña durante dos días despejados de verano. Estos días las variables que determinan el cero térmico, como la temperatura o la propia radiación solar, presentan un amplio rango de variación. Además, es en días despejados cuando se esperan los valores más elevados de cero térmico. La distribución de los tapados a lo largo de todo el día permitió además la obtención de valores de cero térmico bajo condiciones similares de radiación pero diferentes condiciones de temperatura, humedad relativa y viento.

Aprovechando que esta nueva campaña requería de la fabricación de más tapas, se volvió a pensar en el diseño y el proceso de fabricación de las mismas. Aunque finalmente se conservó el diseño original, en esta ocasión fabricó un molde con ayuda de una impresora 3D el cual se rellenó con un material aislante. La emisividad

y posible influencia de las tres nuevas tapas se evaluó mediante varios tapados largos sobre los piranómetros y varios tapados sobre el pirgeómetro de la nuestra estación. Estas pruebas revelaron que la emisividad promedio de las tres tapas es de 0.4 W/m^2. El estudio confirmará que este valor está muy por debajo de los valores de cero térmico medidos por lo que su efecto puede considerarse despreciable.

Los resultados muestran notables diferencias entre los valores de cero térmico de los piranómetros analizados. En las horas centrales del día estas diferencias pueden llegar a alcanzar hasta 8 W/m^2. Además de las diferencias en los valores del cero térmico se han observado también importantes diferencias en su comportamiento diurno. Si bien el cero térmico de todos los piranómetro muestran un ciclo diurno, éste mucho más acusado en unos piranómetros que en otros. Estas diferencias entre piranómetros son de gran relevancia tanto en la comparación de estudios realizados con diferentes instrumentos como en la continuidad de series largas de radiación y los estudios sobre posibles tendencias en los valores de radiación derivados de su análisis.

Este estudio ratifica las importantes diferencias detectadas en nuestros estudios anteriores entre el cero térmico nocturno y diurno en el piranómetro CMP11 y revela que los nuevos instrumentos analizados en esta campaña también muestran esas mismas diferencias. Este resultado advierte sobre la inexactitud que podría cometerse si se corrigen los valores diurnos de cero térmico a partir de los valores nocturnos.

No menos importantes son las diferencias observadas en las dependencias del cero térmico de cada piranómetro respecto a las variables meteorológicas y radiativas analizadas. Este resultado pone de manifiesto la importancia del diseño y los materiales empleados en la fabricación del piranómetro sobre el cero térmico. Además, este resultado muestra la dificultad de establecer un modelo de corrección común para todos los piranómetros a partir de variables meteorológicas y/o radiativas. Esto sugiere que los modelos obtenidos en el Artículo 2 podrían no ser válidos para todos los instrumentos. Por tanto, se requieren estudios específicos para definir la forma más adecuada de corregir el cero térmico en cada tipo de piranómetro.

Un resultado no esperado de este estudio es la no viabilidad de la metodología de tapados para la medida del cero térmico en uno de los piranómetros inicialmente considerados. No obstante, la metodología ha podido ser aplicada a cinco de los seis instrumentos con los que se inició el estudio. Por tanto se puede seguir considerando

una metodología de aplicación general.

A pesar del enorme esfuerzo hecho para medir valores de cero térmico en un amplio rango de valores de temperatura, radiación, humedad relativa y velocidad viento este estudio no contempla distintas situaciones nubosas o temperaturas por debajo de los 15 °C. Aunque en estas situaciones cabría esperar valores más bajos tanto del cero térmico de cada piranómetro como de las diferencias entre ellos, sería conveniente ampliar el número de medidas en tales condiciones. Estas nuevas medidas son imprescindibles para la obtención de modelos de corrección del cero térmico para cada piranómetro.

Dadas las limitaciones de nuestra estación no pudo hacerse una comparativa simultánea del cero térmico de los cinco piranómetros midiendo difusa. Esta comparativa requiere al menos la instalación de dos seguidores solares mientras que nuestra estación solo cuenta con uno. Una comparativa de este tipo podría ayudar a esclarecer la existencia o no de diferencias en los valores de cero térmico entre las medidas de irradiancia global y difusa.

3.4.3. Copia original del artículo

AGU PUBLICATIONS

JGR

Journal of Geophysical Research: Atmospheres

RESEARCH ARTICLE
10.1002/2016JD024815

Key Points:
- First intensive intercomparison campaign of pyranometer thermal offset with the main manufacturers
- Daytime thermal offset differs between instruments, ranging mostly between 0 and -10 W/m^2
- Daytime thermal offset in clear skies shows a diurnal cycle being wind speed a key factor

Correspondence to:
G. Sanchez,
guadalupesh@unex.es

Citation:
Sanchez, G., M. L. Cancillo, and A. Serrano (2016), An intercomparison of the thermal offset for different pyranometers, *J. Geophys. Res. Atmos.*, *121*, 7901–7912, doi:10.1002/2016JD024815.

Received 18 JAN 2016
Accepted 12 JUN 2016
Accepted article online 15 JUN 2016
Published online 4 JUL 2016

An intercomparison of the thermal offset for different pyranometers

G. Sanchez[1], M. L. Cancillo[1], and A. Serrano[1]

[1]Department of Physics, University of Extremadura, Badajoz, Spain

Abstract An unprecedented intensive intercomparison campaign focused on the experimental measurement of the thermal offset of pyranometers has been conducted at Badajoz (Spain) with the participation of three main manufacturers. The purpose of this study is to compare the thermal offset of six commercially available pyranometers, being some of them widely used and others recently commercialized. In this campaign, the capping methodology has been used to experimentally measure the daytime thermal offset of the pyranometers. Thus, a short but intense campaign has been conducted in two selected summer days under clear-sky conditions, covering a large range of solar zenith angle, irradiance, and temperature. Along the campaign, a total of 305 capping events have been performed, 61 for each pyranometer. The daytime thermal offset obtained for different pyranometers ranges between 0 and −16.8 W/m^2 depending on the environmental conditions, being sometimes notably higher than values estimated indoors by manufacturers. The thermal offset absolute value of all instruments shows a diurnal cycle, increasing from sunrise to central hours of the day and decreasing from midafternoon to sunset. The analysis demonstrates that thermal offset is notably higher and more variable during daytime than during nighttime, requiring specific daytime measurements. Main results emphasize the key role played by wind speed in modulating the thermal offset.

1. Introduction

Very accurate measurements of global irradiance on the Earth's surface are currently demanded in order to detect small variations in the incoming solar radiation and therefore changes in climate. Thus, variations in the amount of solar energy reaching the Earth's surface could have profound environmental, social, and economic implications [*Wild*, 2009]. A first evidence of secular variations in solar radiation on the Earth's surface was reported in late 1980s and early 1990s [*Ohmura and Lang*, 1989; *Russak*, 1990; *Dutton et al.*, 1990]. From then on, numerous studies have analyzed the trend of mean global irradiance on the Earth's surface [*Wild*, 2009]. *Wild et al.* [2005] quantified these variations to be between −5.1 W/m^2 and −1.6 W/m^2 per decade during the dimming period (1960–1990) and between +2.2 W/m^2 and +5.1 W/m^2 per decade during the brightening period (after 1990). This trend has been confirmed by later studies [*Sanchez-Lorenzo et al.*, 2015; *Wild*, 2016]. However, the responsible for this change is not clear, and thus, the contribution of clouds and aerosols to the decadal variations of global irradiance is still a controversial topic [*Wild*, 2009; *Augustine and Dutton*, 2013; *Mateos et al.*, 2014].

This growing interest for accurate irradiance measurements on the Earth's surface has favored the deployment of a great number of ground-based radiation networks (Global Energy Budget Archive, Baseline Surface Radiation Network, Surface Radiation, Atmospheric Radiation Measurement Program, etc.). Pyranometers installed in these radiometric stations must satisfy quality requirements established by *World Meteorological Organization* (*WMO*) [2008] to provide high quality; however, each manufacturer chooses specific designs and materials to comply with these requirements. The final design and materials have relevant influence on the pyranometer performance and therefore on the uncertainty of its measurements.

An important source of uncertainty is their thermal offset error [*Philipona*, 2002]. Thermal offset is an spurious signal caused by the difference in temperature between the dome and the detector of a pyranometer. The thermal offset has been quantified to be between −30 W/m^2 and −5 W/m^2 depending on the instrument design and environmental conditions [*Reda et al.*, 2003; *Ji*, 2007]. Several studies [*Bush et al.*, 2000; *Sanchez et al.*, 2015] have reported notable differences in thermal offset between overcast or cloud-free conditions. The effect of thermal offset in irradiance values could range from 1% for irradiance during cloudy days to 15% for diffuse irradiance during cloud-free days [*Sanchez et al.*, 2015]. The decrease in thermal offset under cloudy conditions is mainly due to the enhancement of downward IR by clouds, which reduces the dome-detector temperature difference. Additionally, a direct relationship between thermal offset and ambient

temperature has been suggested by several authors [*Haeffelin et al.*, 2001; *Dutton et al.*, 2001; *Ji and Tsay*, 2010; *Sanchez et al.*, 2015; *Serrano et al.*, 2015]. The uncertainty caused by the thermal offset can be very large compared with trends observed in mean global irradiance at the Earth's surface and therefore must be accounted for in radiative forcing studies.

The thermal offset effect is a well-known issue for pyranometers. Indeed, it was detected in the early operations of pyranometers [*Drummond and Roche*, 1965], but its effect in the uncertainty of shortwave irradiance measurements has been ignored until recently. Additionally, most previous studies treated the thermal offset as an additional correction in a preprocessing stage [*Philipona*, 2002; *Michalsky et al.*, 2003, 2005; *Carlund*, 2013] or focused on a particular pyranometer model under specific conditions [*Bush et al.*, 2000; *Haeffelin et al.*, 2001; *Ji and Tsay*, 2010; *Ji et al.*, 2011]. Only a few studies have compared various pyranometers [*Philipona*, 2002; *Michalsky et al.*, 2003, 2005; *Ji*, 2007; *Carlund*, 2013], and they have the drawback of comparing against a zero-thermal offset reference, ignoring other sources of differences among instruments.

The limitations in previous studies and the introduction of new and improved pyranometer models in radiometric stations worldwide motivates a updated approach to the study of thermal offset. Additionally, a comprehensive study of the thermal offset requires comparing different pyranometer models under the same environmental and radiative conditions. Such intercomparison is needed to put into agreement the conclusions reported by different authors using different types of pyranometers.

Thus, this paper presents an intercomparison of the thermal offset between different unventilated pyranometers. Toward that aim, a specific intensive campaign was organized and the main manufacturers were invited to send their instruments. Six pyranometers participated in the campaign, being four of them widely used instruments and the other two new models recently commercialized. During this campaign, the thermal offset of the six pyranometers were measured simultaneously by means of the capping methodology, and subsequently compared. This study aims at analyzing differences in magnitude, diurnal behavior, and dependence on environmental conditions. This is, to our knowledge, the first intensive thermal offset intercomparison for pyranometers using the capping methodology. This analysis could have profound implications in the homogenization of long-term radiation series for climate and radiative forcing analysis.

2. Instrumentation

The measurements were performed in June 2015 at the radiometric station installed in Badajoz, southwestern Spain (38.98°N, 7.018°W; 199 m above sea level), on the roof of the Department of Physics' building at the campus of the University of Extremadura, guaranteeing an open horizon. This radiometric station is managed by the "Atmosphere, Climate and Radiation in Extremadura" research group of the University of Extremadura. Badajoz is located in south-western Spain, being characterized by a mild Mediterranean climate with very dry and hot summer and solar irradiance values among the highest recorded in Europe in summer.

In order to perform a comprehensive study, the main manufacture of pyranometers were invited to participate in the campaign and six instruments, provided by Eppley (SPP and GPP), Hukseflux (SR20 and SR25), and Kipp & Zonen (CMP11 and CMP22), were compared. Each manufacturer contributed with two different pyranometers: a widely used model and a new or improved version. All these pyranometers comply with International Organization for Standardization (ISO) 9060 criteria for an ISO secondary standard pyranometer, being classified as "high quality" according to the World Meteorological Organization (WMO) nomenclature [*WMO*, 2008]. These pyranometers are calibrated according to procedures detailed in *International Organization for Standardization* (*ISO*) 9847 [1992]. Table 1 summarizes their main characteristics as reported in the corresponding pyranometer manuals and manufacturer websites [*Kipp and Zonen*, 2013; *Hukseflux*, 2014, 2015; https://eppleylab.com].

The fundamental basis of operation for the participating pyranometers is the thermoelectric principle. Their sensing elements are made up of a large number of thermocouples junction pairs connected in series. While the reference junction keeps at a fixed temperature, the active junction is exposed to the solar radiation. Bonded on the active junctions to the thermocouples there is a black-painted ceramic disk that help to absorb the incident solar radiation. When the incoming radiation passes through the two glass domes, it is absorbed by the black ceramic disk making the temperature of the active junctions increases. The differential temperature between the active and the reference junctions produces an electromotive force directly proportional to the differential temperature created, and subsequently a voltage signal.

Table 1. Main Characteristics of the Participating Pyranometers[a]

Manufacturer	Eppley		Hukseflux		Kipp & Zonen	
Model	SPP	GPP	SR20	SR25	CMP11	CMP22
Serial number	38172	38188	3727	2499	080493	150173
Spectral range (nm) (50% points)	295–2800	295–2800	285–3000[b]	285–3000[b]	285–2800	200–3600
Temperature sensor	Yes	No	Yes	Yes	No	Yes
Inner dome	glass	glass	glass	glass	glass	quartz
Outer dome	glass	glass	glass	sapphire	glass	quartz
Body material	bronze	aluminum	aluminum	aluminum	aluminum	aluminum
Offset A (W/m^2)	5	5	5	1	<7	<3

[a]Thermal offset is commonly denominated as "offset A" in pyranometer manuals. Daily uncertainty values have been reproduced here as they appear in the corresponding manuals. Note that they could have been obtained using different methodologies, and therefore, no direct comparison can be made between them.
[b]Spectral range for 20% transmission points.

However, this signal is affected by the thermal offset error. This error is produced by the difference in temperature between the dome and the sensor. Thus, the outer dome cools to space; this cools the inner dome to a temperature generally lower than the temperature of the pyranometer's body that serves as the reference junction of the thermopile. This difference in temperature produces a infrared flux radiation imbalance, which results in a signal superimposed on the output signal. This spurious signal is known as the thermal offset of the pyranometer.

The detector is protected by two concentric hemispherical domes. Using two domes guarantees a better thermal equilibrium between the sensor and the the inner dome, thus reducing the thermal offset. The thermal offset is also affected by the material the domes are made of. While domes in pyranometers SPP, GPP, SR20, and CMP11 are made of glass, SR25 combines a glass inner dome with a sapphire outer dome. In the case of CMP22 both domes are made of quartz.

The body of a pyranometer is designed to provide high mechanical and thermal stability to the instrument. The pyranometers participating in the campaign showed differences in their bodies, mainly in the material used and their design. Thus, SPP has a bronze heavy body, while the the rest of the pyranometers have lighter bodies made of aluminum. The pyranometers usually have a plastic screen attached to the body. This screen protects the external parts from rainfall and reduces solar heating to the body. All pyranometers had their own screen, except the GPP. To obtain comparable measurements, a screen was built for the GPP pyranometerand used throughout the campaign.

Co-located measurements of global, diffuse, direct, and infrared irradiance were performed simultaneously to the capping events. These measurements describe the radiative condition when capping events were conducted.

Global and diffuse irradiances were measured by two Kipp and Zonen CM11 pyranometers with serial numbers 068948 and 027784. A CHP1 pyrheliometer, with serial number 080031, and a CG1 pyrgeometer, with serial number 990143, both manufactured by Kipp and Zonen, were used to measure direct and net infrared irradiance (Net IR), respectively. All these instruments were mounted on a solar tracker (Kipp & Zonen Solys 2) during this campaign. The solar tracker is equipped with a shading ball assembly that continuously prevents the direct solar irradiance for reaching the diffuse irradiance sensor. All these instruments have been recently calibrated against a higher standard [*ISO 9847*, 1992] in an outdoor comparison. In its usual configuration, the station records radiation every minute. However, for this particular study, a temporal frequency of 1 s was performed. Thus, the data set consists of simultaneous measurements of global, diffuse, direct, and infrared irradiance and all participating pyranometers signal on a 1 s basis. All data were recorded by a Campbell CR1000 acquisition system.

Additionally, ambient temperature, relative humidity, and wind speed were monitored at a nearby meteorological station, which is only 400 m away from our radiometric station. This station belongs to the Spanish Meteorological Agency (AEMET) and follows WMO standard protocols and procedures for calibration and measurement. Wind speed was measured by a Compact anemometer manufactured by THIES with serial number 4.3159.00.150. The ambient temperature and relative humidity were measured by a Compact probe model 1.1025.55.700, manufactured also by THIES. This sensor operates inside a Stevenson wooden shelter to prevent heating by direct radiation.

Figure 1. Participating pyranometers. From left to right:(top) SPP, SR20, and CMP11 and (bottom) GPP, SR25 and CMP22 (bottom).

3. Methodology

3.1. Capping Events

In this study the thermal offset was estimated by a methodology based on capping the pyranometer sensor. This methodology consists of instantaneously blocking the shortwave (SW) radiation incident on the sensor of the pyranometer while continuously recording its signal output. This monitoring is performed until the detector has responded to the shortwave blocking but before the dome temperature changes significantly. This widely used methodology has the advantage of providing realistic values of the thermal offset independently of other reference instruments without requiring installing thermometers inside the pyranometers. For these reasons measurements obtained by means of capping events have been used as reference to validate other methodologies [*Bush et al.*, 2000; *Dutton et al.*, 2001; *Haeffelin et al.*, 2001; *Michalsky et al.*, 2003, 2005] or as the main procedure to get thermal offset values [*Carlund*, 2013; *Sanchez et al.*, 2015; *Serrano et al.*, 2015].

To minimize the IR exchange between the cap used to cover the pyranometer and its domes, three caps with low emissivity were manufactured. The cover was fabricated in polystyrene and coated inside and outside with a reflective material. The caps were designed to cover the dome but not the entire pyranometer body, just to block the irradiance arriving at the detector. In this way, the temperature of the pyranometer body and the air circulation around it are not affected. The caps were kept shadowed outdoors before and after each capping event with the aim of maintaining the caps at ambient temperature.

3.2. Preliminary Measurements

The capping event methodology assumes that the detector response is fast enough in relation to the time needed for the change in the dome temperature. Previous studies showed that once the instrument is covered, the signal sharply decreases, reaches a minimum, and then smoothly increases to approach a stable value [*Bush et al.*, 2000, Figure 6; *Sanchez et al.*, 2015, Figure 2]. According to *Bush et al.* [2000] and *Michalsky et al.* [2005], this minimum value constitutes a good estimate of the thermal offset. This criterion compares well with other estimations [*Sanchez et al.*, 2015] while requiring no estimation of the time constant of the pyranometer, which can be difficult to determine. In this study, this criterion was considered.

Six preliminary measurements were performed for each instrument to determine their individual reaction when covered. All the pyranometers with the exception of SR25 showed the expected behavior described above. As an example, Figure 1 shows the output signal of each pyranometer, recorded at 1 s resolution during a preliminary capping event. The vertical lines have been plotted to illustrate the time when each instrument reaches its minimum value, i.e., the thermal offset.

Pyranometers CMP11 and CMP22 showed a well-defined thermal offset (Figure 2). While pyranometers CMP11 and CMP22 took 10 and 14 s in average, respectively, to reach the minimum, GPP, SPP, and SR20 took 22 s, 33 s,

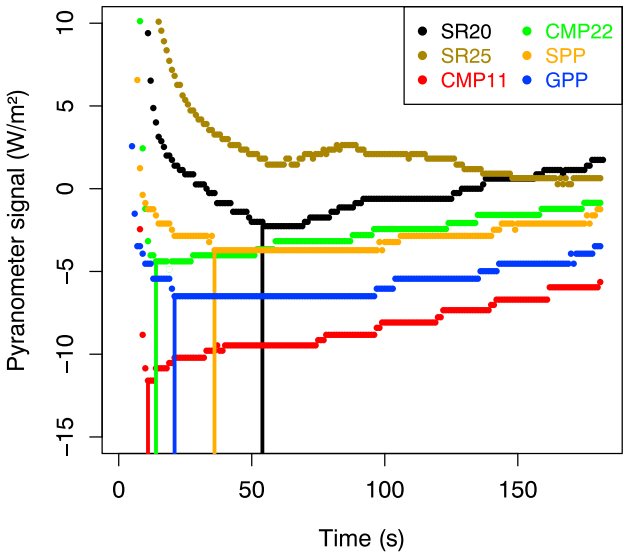

Figure 2. Evolution of the output signal for each pyranometer during a capping event.

and 57 s, respectively. It has been also observed that these latter instruments remain in their thermal offset value for several seconds.

The output signal of the pyranometer SR25 decreases smoothly when it is suddenly covered, fluctuating while the signal approaches a constant value which depends mainly on the environmental and radiative conditions. This final constant value was analyzed during the preliminary campaign, and it was found to range between $-1.87\ W/m^2$ and $5.38\ W/m^2$. Due to the presence of oscillations, a minimum cannot be determined, making the capping methodology unsuitable for this instrument. This oscillating pattern, different from other pyranometers, might be likely due to the sapphire (instead of glass) outer dome in the SR25 pyranometer, used to improve the thermal coupling between body and domes.

3.3. Schedule of Measurements

According to the information provided by the preliminary measurements, 4 min capping events were conducted for pyranometers CMP11, CMP22, SPP, GPP, and SR20, but not for SR25, for which the capping event methodology revealed unsuitable.

The campaign was conducted on June 2015, and measurements were concentrated on days 26th and 30th (days 177 and 181 of the year, respectively). These two summer days were selected due to their clear-sky conditions and their high temperature and irradiance values. Several studies point out that the higher thermal offset values are expected under these conditions [*Bush et al.*, 2000; *Dutton et al.*, 2001; *Sanchez et al.*, 2015; *Serrano et al.*, 2015].

Thus, 305 capping events (61 for each instrument) were conducted between 06:00 UTC and 19:30 UTC on June 26 and between 07:15 UTC and 19:40 UTC on June 30. Measurements spanned a solar zenith angle range between 15.5 and 85.0°; therefore, ensuring capping events covered an almost complete diurnal cycle.

Figures 3a–3d shows the evolution of ambient temperature (T_a), relative humidity (RH), wind speed (W), global (G) and diffuse (D) shortwave irradiance, and net infrared (Net IR) irradiance for days 177 and 181 as measured simultaneously to the capping events.

Sky was clear during both days with global irradiance showing almost identical behavior and reaching around $1000\ W/m^2$ at noon. The ambient temperature ranged between 18°C and 38°C along the period of measurements. Prior to 10:00 UTC all radiative and environmental conditions between days 177 and 181 were similar, except wind speed (Figure 3). More precisely, wind speed ranged from 0.5 to 2 m/s on day 177 and from 3 to 6 m/s on day 181. Conversely, measurements of relative humidity, diffuse SW and net IR irradiances, and wind speed after 10:00 UTC significantly differ between both days, tending to be higher on day 181. Therefore, the time period before 10:00 UTC will allow the analysis of the individual effect of the wind speed on the thermal offset.

4. Results and Discussion

4.1. Nighttime Thermal Offset

Figures 4a and 4b show all pyranometer nighttime signals for days 177 and 181, respectively. Since there is no shortwave radiation, this signal corresponds to the nighttime thermal offset. In this study, nighttime has been considered as the period when solar elevation is under −10°. In order to have a similar number of nighttime values than during daytime, 30 nighttime measurements were selected for each instrument and each day. It

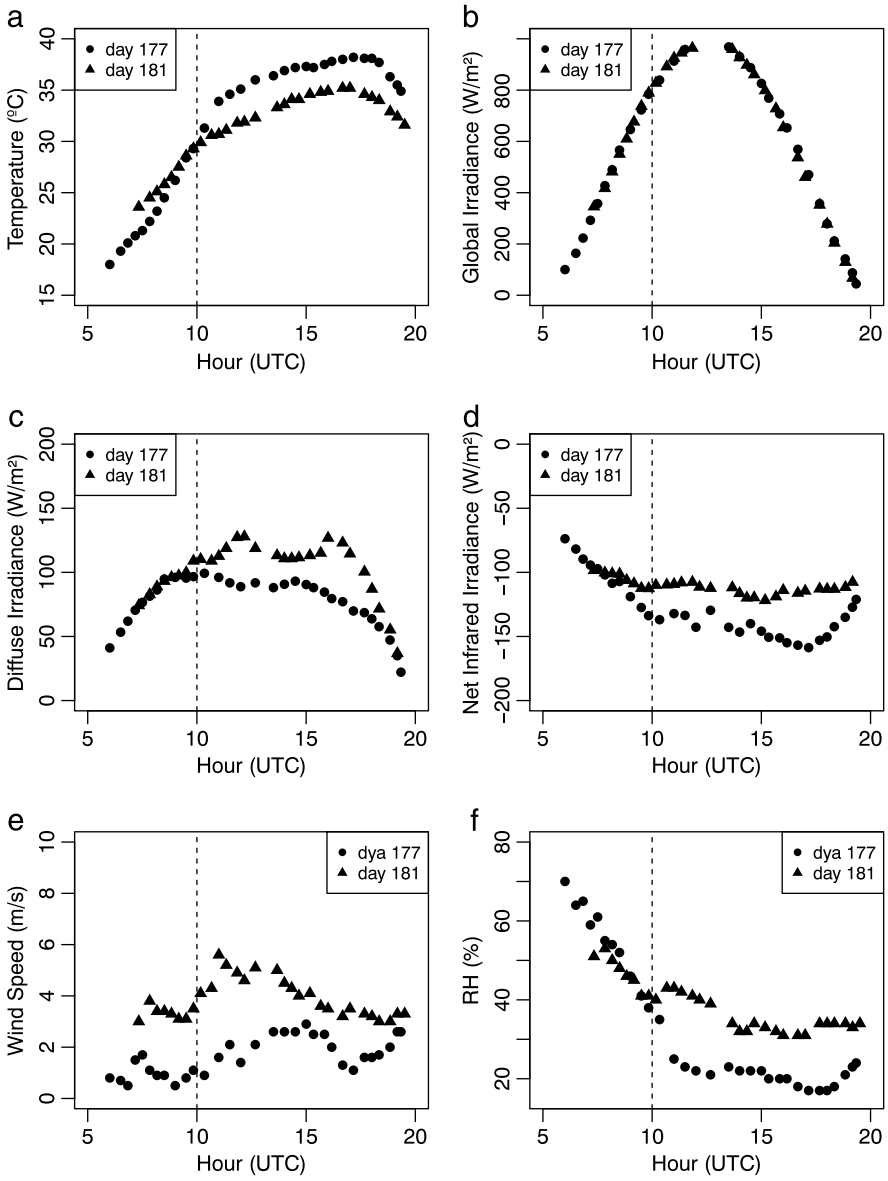

Figure 3. Daily evolution of ambient temperature, global, diffuse, and net IR irradiance, wind speed, and relative humidity for the two days of cappings (days 177 and 181), measured simultaneously to the capping events.

can be seen that this nighttime thermal offset is very stable as compared with the daytime estimations obtained by capping events (Figures 4c and 4d). The standard deviation of the nighttime thermal offset ranges from 0.30 to 0.61 W/m^2. Nighttime thermal offset absolute values are also notably lower than those measured during daytime. According to the nighttime mean values, the pyranometers clustered into three groups: (1) SR25, with a mean value around 0.4 W/m^2; (2) SR20 and CMP22, with a mean value around -1.5 W/m^2; and (3) CMP11, SPP, and GPP, with a mean value of -3.5 W/m^2, more than twice the value of the first group. These notable differences between nighttime and daytime thermal offset behavior indicate the important role played by the radiative and environmental conditions.

4.2. Daytime Thermal Offset

Figures 4c and 4d show the daytime thermal offset obtained by capping events on days 177 and 181. It shows a marked diurnal cycle with a variation 2 or 3 times higher than those observed for nighttime values.

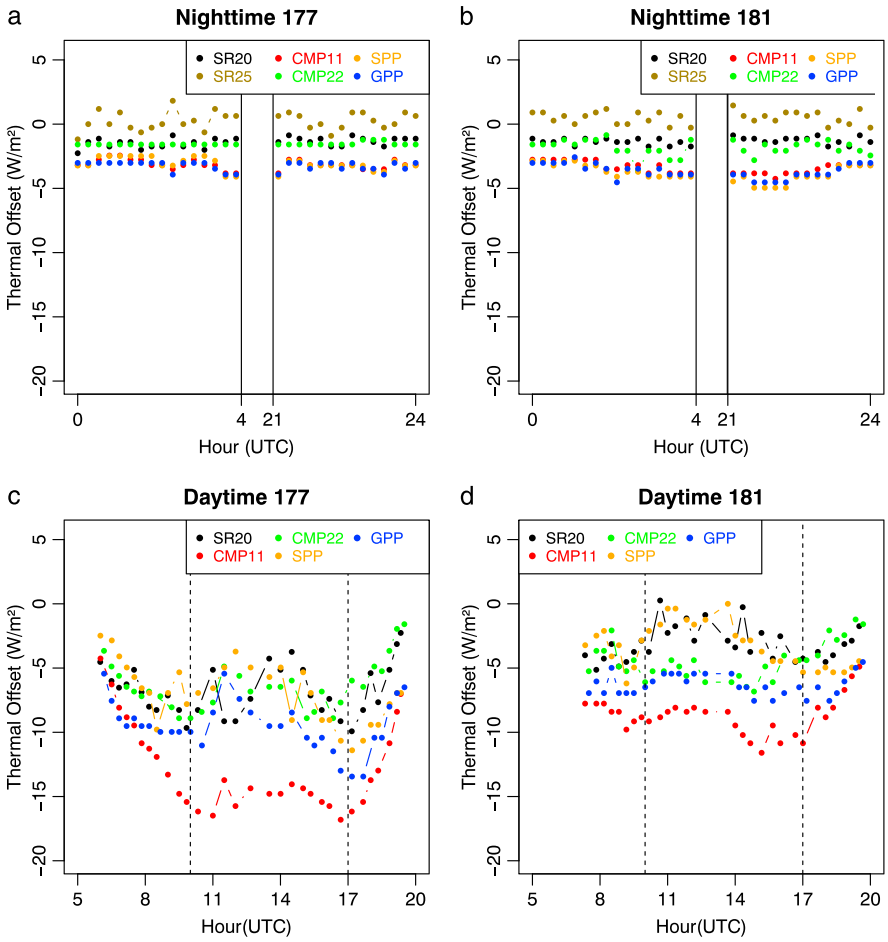

Figure 4. Thermal offset measured (top row) nighttime and (bottom row) daytime during days 177 and 188.

The vertical lines have been drawn in Figures 4c and 4d to separate time periods when thermal offset shows different overall behavior. Before around 08:00 UTC, absolute values of thermal offset tend to increase for all instruments. This increase is particularly notable for CMP11, with positive trend until 10:00 UTC. All environmental and radiative magnitudes showed high variations during this time period of increasing absolute thermal offset, except the wind speed which remained fairly constant. Increasing ambient temperatures, global and diffuse irradiances, simultaneously to decreasing net IR irradiance and relative humidity, favor the increase in the absolute value of the thermal offset [*Sanchez et al.*, 2015; *Serrano et al.*, 2015]. The opposite situation occurs around sunset, explaining the decrease in the absolute thermal offset observed from around 17:00 UTC onward.

During the central hours of the day, no overall trend is found, although thermal offset significantly fluctuates around the mean value. This high variability agrees with results reported by *Haeffelin et al.* [2001] for a PSP pyranometer. They explained this variability by the turbulent convective heat exchange between the ambient air and the pyranometer, affecting differently the dome and the body. Some main statistics (mean and standard deviation) of the thermal offset measured between 10:00 UTC and 17:00 UTC are shown in Table 2 for each pyranometer. Large differences in the thermal offset between pyranometers and time of the day are observed. CMP11 shows the highest mean absolute value in both days, followed by GPP and CMP22. On day 177, CMP11 shows notably higher absolute values than the other pyranometers, reaching a maximum absolute value of 16.8 W/m^2 while the others remain under 10.0 W/m^2. On the other hand, pyranometers SR20 and SPP show the minimum mean absolute thermal offset but also the highest variability for both days. These two pyranometers show very similar statistics for both days.

Table 2. Mean Values and Standard Deviation (SD) of the Thermal Offset for Each Instrument on Days 177 and 181 for the Time Period Between 10:00 and 17:00 UTC

	Day 177 (10:00–17:00 UTC)		Day 181 (10:00–17:00 UTC)	
Instrument	Mean (W/m^2)	SD (W/m^2)	Mean (W/m^2)	SD (W/m^2)
SR20	−6.9	2.0	−2.4	1.4
CMP11	−15.2	1.0	−9.4	1.1
CMP22	−7.2	1.3	−5.4	0.9
SPP	−6.8	2.1	−2.3	1.5
GPP	−9.6	2.0	−6.2	0.8

It is interesting to note the notable reduction on the absolute value of the thermal offset of pyranometer CMP22 with respect to CMP11, both manufactured by Kipp & Zonen. Thus, mean absolute value at central hours of the day for CMP22 is 8 W/m^2 lower than for CMP11 on day 177 and 4 W/m^2 on day 181 (Table 2). These high differences could be due to the different design and material of their domes; while CMP11 has two 2 mm thick domes made of glass, CMP 22 has two 4 mm thick domes made of quartz.

Regarding pyranometers SPP and GPP manufactured by Eppley, differences around 3.5 W/m^2 have also been observed. Since both pyranometers have the same type of thermopile and domes, the differences must be associated with their different body's material. Thus, while GPP's body is made of aluminum, SPP's body is made of bronze being therefore notably heavier than GPP and showing a lower thermal conductivity.

It is interesting to note that the absolute value of thermal offset obtained experimentally in this study can be significantly higher than those offset A values provided by manufacturers (see Table 1). The main reason for these differences is that manufacturers generally measure the offset A under specific conditions, which could be notably different from those affecting the instruments outdoors once installed. When a pyranometer is installed outdoors at a station additional factors affect its response such as the relative humidity and wind speed. It is also important to note that these factors show different behavior between day and night. A thorough analysis about these factors will be developed in section 4.3.

4.3. Dependence on Environmental Magnitudes

In addition to the diurnal cycle, thermal offset varied between days, being remarkably higher on day 177 than on day 181. Also, day 171 showed a larger variability than day 181.

It is not easy to identify the main factors explaining the differences in thermal offset between days 177 and 181 since many radiative and environmental variables generally differ between the two days. However, there is a rather interesting time period before 10:00 UTC, when all radiative and environmental conditions except the wind speed behave similarly on days 177 and 181 (Figure 3). Thus, for this time period, differences in thermal offset between both days can be attributed to the effect of wind speed.

In order to analyze the effect of this and other environmental magnitudes, a thorough analysis has been performed. Figure 5 show the daytime and nighttime thermal offset versus wind speed, Net IR irradiance, ambient temperature, and relative humidity for each pyranometer.

Significant differences in behavior are observed between day and nighttime thermal offset and between their relationships with the environmental conditions. A main limitation is the short range of variation of environmental conditions during night, showing no clear trend and therefore preventing developing any linear regression. During nighttime the thermal offset tends to smoothly oscillate around the mean value given in section 4.1. An additional difference bewteen day and nighttime thermal offset is the lack of solar radiation during the night, which is acknowledged as a main contribution to the differential heating of the dome and the sensor and, subsequently, to the thermal offset [*Sanchez et al.*, 2015]. This different behavior between daytime and nighttime is in agreement with results reported by several other authors who prevent correcting daytime thermal offset using empirical models developed with nighttime data [*Cess et al.*, 2000; *Haeffelin et al.*, 2001; *Philipona*, 2002; *Ji and Tsay*, 2010; *Serrano et al.*, 2015].

A general negative trend in daytime thermal offset with respect to the ambient temperature can be observed for all pyranometers. Thus, the absolute value of the thermal offset increases as ambient temperature increases. On the contrary, a positive trend is observed in daytime thermal offset with respect to relative humidity, Net IR, and wind speed for all pyranometer. These findings agree with results reported by other authors such as *Dutton et al.* [2001] and *Serrano et al.* [2015] and confirm that thermal offset increases under

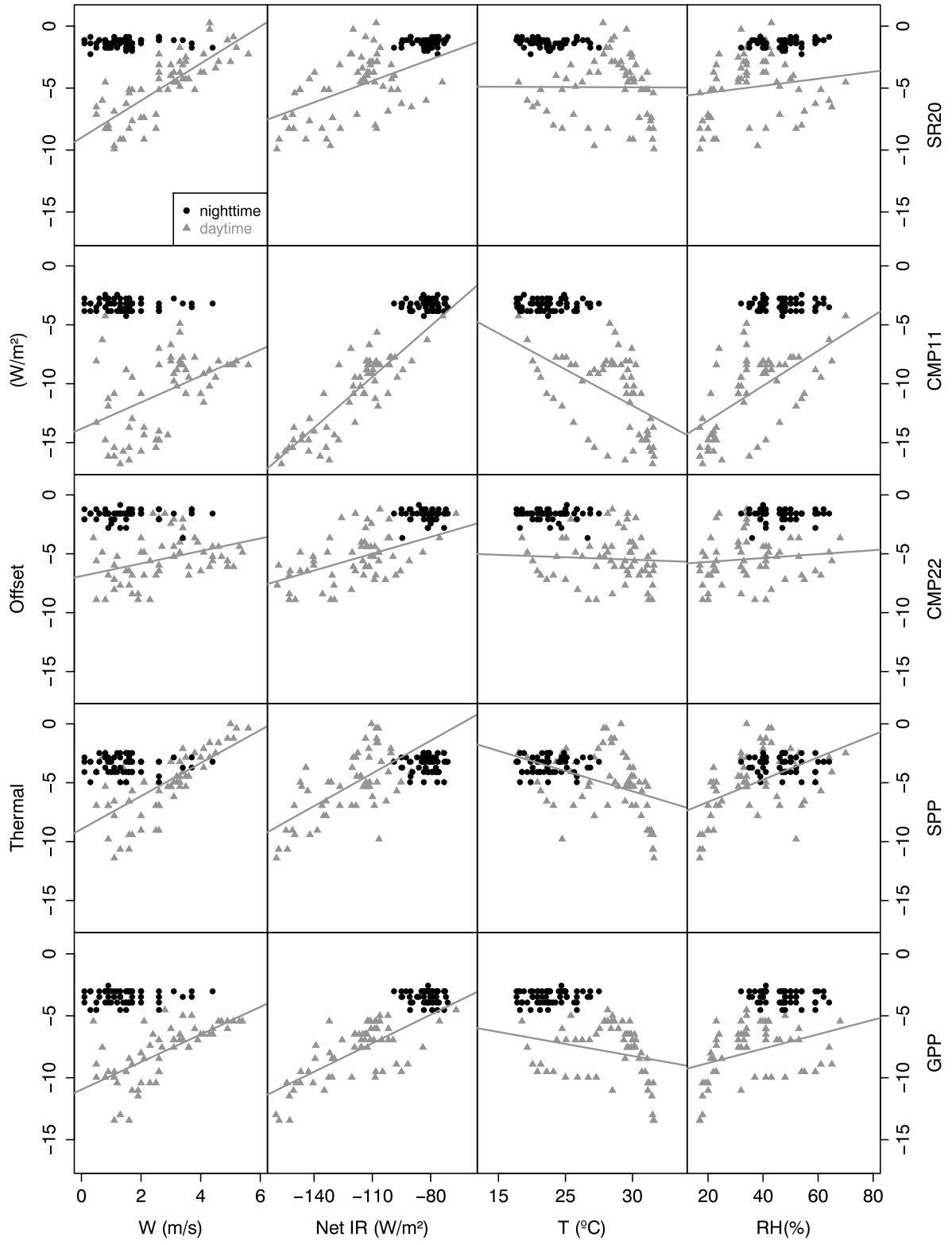

Figure 5. Thermal offset relationship with ambient temperature, Net IR, relative humidity, and wind speed for daytime (grey triangles) and nighttime (black points) data.

Table 3. Coefficient of Determination, R^2, for the Relationships Between the Daytime Thermal Offset and the Environmental Magnitudes

Instrument	Wind Speed	Net IR	Ambient Temperature	Relative Humidity
SR20	0.640	0.208	0.022	0.024
CMP11	0.202	0.739	0.260	0.366
CMP22	0.136	0.240	0.003	0.013
SPP	0.470	0.423	0.120	0.220
GPP	0.470	0.490	0.060	0.125

cloud-free conditions, low relative humidity, low wind speed, and high temperature. The least squares regression analysis has been conducted to assess the significance of the relationships. The coefficients of determination for these fittings are summarized in Table 3.

The relationships between the thermal offset and ambient temperature and relative humidity are not statistically significant, showing values of R^2 below 0.4 for all pyranometers. Three pyranometers show R^2 values higher than 0.4 for fittings with respect to the Net IR being the CMP11 pyranometer, the instrument with the most significant value (0.739). The relationship with respect to the wind speed is particularly clear for pyranometers SR20, SPP, and GPP, with coefficients of determination of 0.64, 0.47, and 0.47, respectively. Therefore, the wind speed appears as a main factor for reducing the absolute value of the thermal offset. This result agrees with *Dutton et al.* [2001], *Michalsky et al.* [2005], *Ji* [2007], and *Serrano et al.* [2015].

5. Conclusions

In order to thoroughly analyze the thermal offset of different pyranometers, an intensive campaign of measurements was conducted at Badajoz (Spain) in June 2015. Pyranometers SR20 and SR25, manufactured by Hukseflux; SPP and GPP, manufactured by Eppley; and CMP11 and CMP22, manufactured by Kipp & Zonen, participated in the intercomparison campaign. These pyranometers are a significant representation of widely used and new pyranometer models of the main manufacturers. In this campaign, the thermal offset was estimated following the nonintrusive capping methodology.

Preliminary measurements revealed the unsuitability of the capping methodology to be applied to pyranometer model SR25 since a clear minimum could not be identified during the capping events. When this instrument is covered, its output signal decreases and then tends to oscillate between $-1.87\,W/m^2$ and $5.38\,W/m^2$, depending on the environmental and radiative conditions. Therefore, alternative methodologies, such as its comparison with an instrument with negligible thermal offsets or invasive methods as attaching the installation of temperature sensors on its detector and dome to measure their temperature difference could be considered.

Regarding nighttime thermal offset, pyranometers clustered into two groups: (1) SR20 and CMP22, with a mean value around $-1.5\,W/m^2$, and (2) CMP11, SPP and GPP, with a mean value of $-3.5\,W/m^2$. These values are notably lower and more stable than those observed during daytime. These values agree with those reported by *Cess et al.* [2000], *Philipona* [2002], *Ji and Tsay* [2010], and *Sanchez et al.* [2015] for several unventilated pyranometer models and locations. This finding advises, as suggested by *Serrano et al.* [2015] for CMP11 pyranometers, against the common procedure of estimating diurnal thermal offset from nighttime data for unventilated pyranometers. However, it should be note that different results could be found for ventilated pyranometer, as suggested by *Michalsky et al.* [2003, 2005].

During the campaign, more than 300 capping events were conducted on clear-sky days 177 and 181 covering a wide range of solar zenith angle. As a result, a large number of daytime thermal offset values were estimated for pyranometers SR20, SPP, GPP, CMP11, and CMP22 under different environmental and radiative conditions. These measurements revealed a diurnal overall pattern in the absolute values of thermal offset: increasing until around 08:00 UTC or 10:00 UTC, oscillating around a mean value during central hours of the day, and decreasing after 17:00 UTC. This diurnal behavior is more notable for CMP11, and its amplitude likely depends on the environmental and radiative conditions. This diurnal pattern has not been reported previously. Therefore, correcting the thermal offset error requires complex expressions, which account for this diurnal variation, and not only the addition of a constant factor.

On average, during the central hours of the day, SPP and SR20 show the lowest absolute value of thermal offset followed by CMP22 and GPP, while CMP11 tends to show higher absolute values. On the contrary, CMP11, CMP22, and GPP show lower standard deviation than SR20 and SPP. The mean thermal offset during central hours of the day ranges between $-2.3\,W/m^2$ and $-15.2\,W/m^2$. Meanwhile, its standard deviation ranges between $0.8\,W/m^2$ and $2.1\,W/m^2$. It is important to note that a high variability makes it difficult to correct the thermal offset, while a high but constant value is easier to correct.

During these two days the measured thermal offset resulted in relative errors between 1% and 3%. These values could result in systematic uncertainties of the order of the 2% established by WMO for daily achievable uncertainty for high-quality pyranometers [*WMO*, 2008]. This fact emphasizes the need for correcting this source of error.

The relationship between the themal offset of each pyranometer versus several environmental magnitudes has been analyzed for both daytime and nighttime data. Notable differences in the thermal offset trends between daytime and nighttime were detected. This important result agree with results reported by *Cess et al.* [2000], *Philipona* [2002], *Ji and Tsay* [2010] and, more recently, *Sanchez et al.* [2015] and *Serrano et al.* [2015]. This finding prevent correcting daytime thermal offset using empirical models developed with nighttime data.

Positive general trends with respect to Net IR, wind speed, and relative humidity and negative trend with respect to ambient temperature have been found for daytime thermal offset. However, not all these relationships are actually significant, and only SR20 thermal offset versus wind speed and CMP11 versus Net IR show R^2 values higher than 0.6. Additionally, SPP and GPP thermal offset versus both Net IR and wind speed have R^2 values around 0.45. Thus, daytime values of Net IR and wind speed could be considered in order to develop a model for correcting these instruments as suggested *Serrano et al.* [2015]. Additionally, this results revealed that wind speed is a main factor for reducing the magnitude of the thermal offset. This result agrees with previous studies which suggested that wind speed homogenizes the temperature balance and therefore contributes to reduce the absolute value of the thermal offset [*Bush et al.*, 2000; *Haeffelin et al.*, 2001; *Michalsky et al.*, 2005; *Ji*, 2007].

This unprecedented campaign contributes to a better knowledge of the thermal offset of pyranometers by comparing different instruments under actual measuring conditions outdoors. It provides useful information that completes the indoor measurements performed by the manufacturers. Therefore, it favors the precise measurement of the Earth's radiation balance and aerosol radiative forcing, for instance. This study also suggests interesting directions for future research concerning the behavior of the thermal offset when the pyranometer is ventilated.

Acknowledgments
This study was partially supported by the research projects CGL2011-29921-C02-01 and CGL2014-56255-C2-1-R granted by the Ministerio de Economía y Competitividad from Spain and by Ayuda a Grupos GR15137 granted by Junta de Extremadura and Fondo Social Europeo (FEDER). Authors thank Eppley, Hukseflux, and Kipp & Zonen for providing their instrument to this study and to the Spanish Agencia Estatal de Meteorología (AEMet) for the provision of meteorological data. Guadalupe Sanchez Hernandez thanks the Ministerio de Economía y Competitividad for the predoctoral FPI grant. The data analyzed in this study are available from authors upon request (guadalupesh@unex.es).

References

Augustine, J. A., and E. G. Dutton (2013), Variability of the surface radiation budget over the United States from 1996 through 2011 from high-quality measurements, *J. Geophys. Res. Atmos.*, *118*, 43–53, doi:10.1029/2012JD018551.

Bush, B. C., F. P. J. Valero, and A. S. Simpson (2000), Characterization of thermal effects in pyranometers: A data correction algorithm for improved measurement of surface insolation, *J. Atmos. Oceanic Technol.*, *17*, 165–175.

Carlund T. (2013), Baltic Region Pyrheliometer Comparison 2012, World Meteorological Organization, Rep. 112, pp. 10–35, Geneva, Switzerland.

Cess, R. D., T. Qian, and M. Sun (2000), Consistency test applied to the measurement of total, direct, and diffuse shortwave radiation at the surface, *J. Geophys. Res.*, *105*, 24,881–24,887.

Drummond, K. L., and J. J. Roche (1965), Corrections to be applied to measurements made with Eppley (and other) spectral radiometers when used with Schott colored glass filters, *J. Appl. Meteorol.*, *4*, 741–744.

Dutton, E. G., R. S. Stone, D. W. Nelson, and B. G. Mendonca (1990), Recent interannual variations in solar radiation cloudiness, and surface temperature at the South Pole, *J. Clim.*, *4*, 848–858.

Dutton, E. G., J. J. Michalsky, T. Stoffel, B. W. Forgan, J. Hickey, D. W. Nelson, T. L. Alberta, and I. Reda (2001), Measurement of broadband diffuse solar irradiance using current commercial instrumentation with a correction for thermal offset errors, *J. Atmos. Oceanic Technol.*, *18*, 297–314.

Haeffelin, M., S. Kato, A. M. Smith, C. K. Rutledge, T. P. Charlock, and J. R. Mahan (2001), Determination of the thermal offset of the Eppley precision spectral pyranometer, *Appl. Opt.*, *4*, 472–484.

Hukseflux (2014), User manual SR20 secondary standard pyranometer, Manual v1407.

Hukseflux (2015), User manual SR25 secondary standard pyranometer with sapphire outer dome, Manual v1508.

International Organization for Standardization (ISO) 9847 (1992), Solar energy—Calibration of field pyranometers by comparison to a reference pyranometer.

Ji, Q. (2007), A method to correct the thermal dome effect of pyranometers in selected historical solar irradiance measurements, *J. Atmos. Oceanic Technol.*, *24*, 529–536.

Ji, Q., and S.-C. Tsay (2010), A novel nonintrusive method to resolve the thermal-dome-effect of pyranometers: Instrumentation and observational basis, *J. Geophys. Res.*, *115*, D00K21, doi:10.1029/2009JD013483.

Ji, Q., S.-C. Tsay, K. M. Lau, R. A. Hansell, J. J. Butler, and J. W. Cooper (2011), A novel nonintrusive method to resolve the thermal-dome-effect of pyranometers: Radiometric calibration and implications, *J. Geophys. Res.*, *116*, D24105, doi:10.1029/2011JD016466.

Kipp & Zonen (2013), Instruction manual CMP series pyranometers and CMA series albedometers.

Mateos, D., A. Sanchez-Lorenzo, M. Antón, V. E. Cachorro, J. Calbó, M. J. Costa, B. Torres, and M. Wild (2014), Quantifying the respective roles of aerosols and clouds in the strong brightening since the early 2000s over the Iberian Peninsula, *J. Geophys. Res. Atmos.*, *119*, 10,382–10,393, doi:10.1002/2014JD022076.

Michalsky, J. J., et al. (2003), Results from the first ARM diffuse horizontal shortwave irradiance comparison, *J. Geophys. Res.*, *108*(D3), 4108, doi:10.1029/2002JD002825.

Michalsky, J. J., et al. (2005), Toward the development of a diffuse horizontal shortwave irradiance working standard, *J. Geophys. Res.*, *110*, D06107, doi:10.1029/2004JD005265.

Ohmura, A., and H. Lang (1989), Secular variation of global radiation over Europe, in *Current Problems in Atmospheric Radiation*, edited by J. Lenoble and J. F. Geleyn, pp. 98–301, Deepak, Hampton, Va.

Philipona, R. (2002), Underestimation of solar global and diffuse radiation measured at Earth's surface, *J. Geophys. Res.*, *107*(D22), 4654, doi:10.1029/2002JD002396.

Reda, I., T. Stoffel, and D. Myers (2003), A method to calibrate a solar pyranometer for measuring reference diffuse irradiance, *Sol. Energy*, *74*, 103–112.

Russak, V. (1990), Trends of solar radiation, cloudiness and atmospheric transparency during recent decades in Estonia, *Tellus Ser. B*, *42*, 206–210.

Sanchez, G., A. Serrano, M. L. Cancillo, and J. A. Garcia (2015), Pyranometer thermal offset: Measurement and analysis, *J. Atmos. Oceanic Technol.*, *32*, 234–246, doi:10.1175/JTECH-D-14-00082.1.

Sanchez-Lorenzo, A., M. Wild, M. Brunetti, J. A. Guijarro, M. Z. Hakuba, J. Calbó, S. Mystakidis, and B. Bartok (2015), Reassessment and update of long-term trends in downward surface shortwave radiation over Europe (1939–2012), *J. Geophys. Res. Atmos.*, *120*, 9555–9569, doi:10.1002/2015JD023321.

Serrano, A., G. Sanchez, and M. L. Cancillo (2015), Correcting daytime thermal offset in unventilated pyranometers, *J. Atmos. Oceanic Technol.*, *38*, 2088–2099.

Wild, M. (2009), Global dimming and brightening: A review, *J. Geophys. Res.*, *114*, D00D16, doi:10.1029/2008JD011470.

Wild, M. (2016), Decadal changes in radiative fluxes at land and ocean surfaces and their relevance for global warming, *Wiley Interdiscip. Rev. Clim. Change*, *7*, 91–107.

Wild, M., G. Hans, A. Roesch, A. Ohmura, C. N. Long, E. G. Dutton, B. Forgan, A. Kallis, V. Russak, and A. Tsvetkov (2005), From dimming to brightening: Decadal changes in surface solar radiation, *Science*, *308*, 847–850, doi:10.1126/science.1103215.

World Meteorological Organization (2008), *Guide to Meteorological Instruments and Methods of Observation*, vol. 8, 7th ed., 681 pp., Secretariat of the World Meteorological Organization, Geneva, Switzerland.

3.4.4. Informe del Director de la Tesis Doctoral

El artículo "An intercomparison of the thermal offset for different pyranometers", fue publicado en la revista Journal of Geophysical Research - Atmospheres en el año 2016, teniendo la revista un factor de impacto en 2015 de 3.318 y estando incluida en el primer cuartil (Q1, ranking 27 de 184 revistas) dentro de la categoría "Geosciences, Multidisciplinary".

La participación de la doctoranda Dña. Guadalupe Sánchez Hernández en este artículo ha sido muy elevada y diversa, colaborando muy activamente en todas las etapas desarrolladas para la obtención del artículo, desde la propuesta de la idea original, hasta el diseño y realización de la campaña de medidas específica para estos estudios, el análisis de resultados, la comparativa, la extracción de conclusiones y la elaboración del manuscrito. Es de justicia resaltar el gran trabajo y esfuerzo que ha dedicado la doctoranda a la realización de la campaña de medida, consistiendo ésta en el mayor número de eventos de tapado que hayan sido publicados en la bibliografía existente hasta la fecha.

Todas estas las tareas han sido desarrolladas por la doctoranda bajo mi dirección y supervisión, pudiendo dar fe de que todo lo aquí expuesto es verídico.

Fdo.: El Director de la Tesis Doctoral

Por otra parte, Dña. María Luisa Cancillo Fernández y D. Antonio Serrano Pérez, coautores de este artículo, afirman mediante este escrito que han colaborado en este artículo pero que éste forma parte íntegra de la Tesis Doctoral de Dña. Guadalupe Sánchez Hernández y que no va a ser utilizado por ellos como parte de sus respectivas tesis doctorales.

Dña. Mª Luisa Cancillo Fernández D. Antonio Serrano Pérez

3.5. Artículo 4

3.5.1. Datos del artículo

Título: Effect of mechanical ventilation on the thermal offset of pyranometers

Autores: Guadalupe Sánchez[a]
Antonio Serrano[a]
Mª Luisa Cancillo[a]

Filiación: [a]Dpto. de Física, Universidad de Extremadura, Badajoz, España

Revista: *Journal of Atmospheric and Oceanic Technology*

Estado: En revisión

3.5.2. Principales aportaciones del artículo

El principal objetivo de este artículo es evaluar el efecto de la ventilación artificial sobre el cero térmico de distintos piranómetros. Para este estudio se contó con tres piranómetros y su correspondientes unidades de ventilación cedidos de forma temporal por tres importantes fabricantes. En este estudio se han analizado valores de cero térmico de piranómetros midiendo irradiancia global y difusa con y sin ventilación artificial. Debe señalarse que este es el primer estudio en el que se comparan valores de cero térmico de un mismo piranómetro instalado en su correspondiente unidad de ventilación y fuera de ella.

De nuevo se organizó una campaña específica en la que las medidas del cero térmico fueron obtenidas mediante tapados. Con el fin de comparar los valores del cero térmico de los piranómetros midiendo irradiancia global con y sin ventilación se seleccionaron las medidas registradas durante dos días consecutivos de características similares (radiación, temperatura, humedad relativa, velocidad de viento). Se hizo lo mismo para comparar los valores de cero térmico de los piranómetros midiendo difusa con y sin ventilación artificial. Distribuidos a lo largo de los cuatro días finalmente seleccionados se obtuvieron 372 medidas experimentales de cero térmico. Esto ha permitido analizar el comportamiento diurno del cero térmico de los distintos piranómetros en las diferentes configuraciones (global/difusa con/sin ventilación) en un amplio rango de temperatura, radiación, humedad relativa y velocidad de viento.

Los resultados de este estudio muestran que, de forma general, la ventilación artificial reduce los valores de cero térmico y su variabilidad en todos los piranómetros analizados. También se ha observado una notable disminución de las diferencias

entre los valores de cero térmico de los distintos piranómetros cuando estos son ventilados de forma artificial. La reducción del cero térmico al aplicar la ventilación artificial se ha cuantificado entre 1.3 W/m^2 y 9 W/m^2. Este resultado es de gran relevancia en la homogeneización de series largas de radiación. Las diferencias detectadas en este estudio para un mismo instrumentos con y sin ventilación son del orden de magnitud de las tendencias detectadas en los valores de radiación global durante los periodos 1960-1990 y a partir de 1990 [Wild et al., 2009] o las tendencias detectadas sobre la radiación difusa [Long et al., 2009; Calbo et al., 2016].

Otro importante resultado a destacar en este estudio son las importantes diferencias halladas en las dependencias respecto a las variables analizadas entre los distintos piranómetros. Esto pone de manifiesto la dificultad de encontrar un modelo de corrección común para todos los modelos de piranómetros. Por tanto, los modelos sugeridos en el Artículo 2 de esta tesis podría no ser de validez general. Los modelos más adecuados para cada tipo de piranómetro podrían variar tanto en los dependencia funcionales como en los coeficientes empíricos. Esto indica nuevas líneas de trabajo para buscar formas de corrección adecuadas para cada instrumento.

Aunque en este estudio hemos intentado validar el modelo de corrección del cero térmico propuesto por Dutton et al. [2001] con los piranómetros analizados en este estudio, los resultados obtenidos no son concluyentes debido a la falta de casos con valores de irradiancia infrarroja neta del pirgeómetro más elevados durante las noches analizadas. Tanto esta validación del modelo de Dutton et al. [2001] como la búsqueda de otros posibles modelos de corrección para el cero térmico requieren ampliar la toma de medidas a otro tipo situaciones (temperaturas más bajas o cielos con distintos tipos de nubosidad).

3.5.3. Copia original del artículo

EFFECT OF MECHANICAL VENTILATION ON THE THERMAL OFFSET OF PYRANOMETERS

G. Sanchez[1], A. Serrano[1], M.L. Cancillo[1]

[1]Department of Physics, University of Extremadura, Badajoz, Spain

Corresponding author: Guadalupe Sanchez (guadalupesh@unex.es)

Abstract.- Thermal offset is a major source of uncertainty for solar radiation measurements. This study assesses the influence of mechanical ventilation on the daytime thermal offset of pyranometers. Towards this goal, an intensive unprecedented campaign of measurements was conducted in Badajoz (Spain) during four selected summer days under clear sky conditions, covering a large range of solar zenith angle, irradiance and temperature. Three leading manufacturers participated in the campaign providing secondary standard pyranometers and compatible ventilation units. The thermal offset was experimentally measured following the capping methodology. A total of 372 capping events were conducted, the largest number ever reported in the literature. Each pyranometer was tested under different operational conditions (with/without ventilation and measuring global/diffuse irradiance). Results show that mechanical ventilation generally reduces the thermal offset. The magnitude of this reduction is different for each pyranometer model and depends on whether the instrument is shadowed (for measuring diffuse irradiance) or not (for measuring global irradiance). Mechanical ventilation tends to homogenize the temperature around the pyranometer and, therefore, reduces the impact of environmental conditions on the thermal offset. CMP11 and SPP pyranometers show notable tendencies in the thermal offset even when mechanical ventilation is applied. The Dutton et al.'s model (2001) aimed to correct the daytime thermal offset is evaluated. Results show this model performs well for the SPP pyranometer but underestimates the absolute value of thermal offset for CMP11 and SR20 pyranometers.

Keywords.- thermal offset, pyranometer, ventilation, global, diffuse

1.- Introduction

The incoming solar irradiance and its partitioning into its direct and diffuse components governs many climate processes such as the hydrological cycle, plant photosynthesis and changes in surface temperature due to Earth's energy budget (Roderick et al., 2001; Gu *et al.*, 2003; Wild, 2009). Thus, changes in clouds and aerosols can modify the solar irradiance amount and its direct/diffuse partitioning, with notable consequences on local, regional and global climates. However, the role of clouds and aerosols as they affect the variability and distribution of solar radiation at the Earth's surface remains unclear. Thus, while Long et al. (2009) claimed that the solar brightening over the United States after 1990 was caused by a general decrease in cloud cover, Wild (2012) attributed it to a decrease in aerosols. Therefore, highly accurate measurements of solar irradiance are required in order to detect small variations in the incoming solar radiation and its response to a range of factors.

A number of studies have examined the operation of pyranometers in order to accurately measure global and diffuse irradiance (Michalsky et al., 2005; Long and Shi, 2008; Gueymard and Myers, 2009). One of the main sources of uncertainty is the thermal offset caused by a difference in temperature between the detector and the inner dome of pyranometers. In fact, the overarching environmental cause is the difference between the instrument body temperature (thermopile cold junction) and the sky blackbody brightness temperature. This temperature difference causes an energy flow through the thermopile (generating a negative voltage signal) out the top of the detector to the inner dome, then from the inner dome to the outer dome, and then radiated to the sky. This thermal imbalance generates an exchange of infrared flux which is absorbed by the detector and is superimposed on the output signal. Neglecting the thermal offset could cause an underestimation of up to 40% in measurements of diffuse irradiance (Reda et al., 2003).

The temperatures of the detector and the inner dome are highly dependent on the physical characteristics of the pyranometer (Cess et al. 2000; Haeffelin et al. 2001; Dutton et al. 2001; Philipona 2002; Bush et al. 2000). The design and the material of each pyranometer component determine the temperature and the thermal coupling between them, and, therefore, the thermal offset. Thus, different designs produced by manufacturers exhibit different thermal offset values. For example, while the

thermal offset for diffuse irradiance measurements under clear skies can reach -20 W/m² for an unventilated Eppley PSP pyranometer (Haeffelin et al., 2001), it is around -17 W/m² for an unventilated CM11 pyranometer (Sanchez et al., 2015).

Due to its relevance, some authors have proposed empirical models to correct the daytime thermal offset with the aim to improve the quality of recorded data. Some of these models rely on nighttime relationships between the offset and the Net IR (Dutton et al., 2001; Younkin and Long, 2004). Other approach is to develop statistical relationships using daytime radiative and environmental magnitudes recorded simultaneously to the pyranometer measurements (Vignola et al., 2007, 2008 and 2009; Serrano et al., 2015).

Several authors (Bush et al., 2000; Haeffelin et al., 2001; Vignola et al. 2007, 2008 and 2009) have studied the influence of environmental conditions on the thermal offset, with wind speed being an important factor. Based on these results, some authors have suggested that thermal offsets could be minimized with adequate ventilation systems which would force ambient airflow around the body and the domes (Dutton et al., 2001; Philipona, 2002; Michalsky et al., 2003). Thus, Ji (2007) reported that mechanical ventilation with a standard 115 VAC fan reduced by 13 W/m² the thermal offset of a PSP pyranometer while measured at noon in a clear day.

Until now, two main approaches have been followed to study the effect of ventilation on the thermal offset: 1) comparing ventilated to unventilated pyranometers (Dutton et al., 2001; Michalsky et al., 2003), and 2) turning on and off in an alternating pattern the ventilation unit of a pyranometer (Philipona, 2002; Ji, 2007). However, these methodologies exhibit important drawbacks. Studies comparing different pyranometers with and without ventilation ignore properties of the pyranometers which could contribute to differences in the signals such as their time responses, cosine error and the pyranometer design. On the other hand, turning off the ventilation unit does not reproduce the actual conditions of common unventilated pyranometers since the ventilation unit modifies the environmental conditions around the pyranometer.

Within this framework, our study aims to evaluate the effect of ventilation units on the thermal offset of different pyranometers and their impact on instrument performance. Towards this goal the main

manufacturers were invited to send their pyranometers along with their corresponding ventilation units to participate in an unprecedented inter-comparison campaign to be held in Badajoz (Spain) during June and July 2015. Among the pyranometers analyzed, the CMP11 manufactured by Kipp & Zonen is studied. This instrument is used worldwide at global and national radiometric networks as Baseline Surface Radiation Network (BSRN), Global Energy Balance Archives (GEBA), Southern African Universities Radiometric Network (SAURAN) and Servicio Meteorológico Nacional in Mexico (SMN-AWS). Other two new models recently commercialized participated in this campaign: the SPP pyranometer manufactured by Eppley, and the SR20 pyranometer manufactured by Hukseflux. It is worth mentioning that the SPP pyranometer has been designed by Eppley as the substitute for the previous model PSP, which has been one of the main instruments used by the BSRN network.

This intensive campaign was conducted during four selected cloud-free summer days when very high thermal offset values were expected. A total of 124 capping events were performed for each pyranometer participating in the campaign. The thermal offset was obtained for the pyranometers measuring under four different operational conditions: measuring global irradiance while mechanical ventilation is being applied, measuring global irradiance while no mechanical ventilation is being applied, measuring diffuse irradiance while mechanical ventilation is being applied, and measuring diffuse irradiance while no mechanical ventilation is being applied. The present work focuses on studying the thermal offset regarding its magnitude, its diurnal evolution and its relationship with environmental conditions. To our knowledge, this is the first study comparing the thermal offset of different pyranometers under such a number of different configurations in actual field conditions.

Additionally, this study evaluates the performance of Dutton et al.'s model (2001) to correct the daytime thermal offset error. This model proposes using a nighttime-fitted linear relationship between the net infrared irradiance and the thermal offset to estimate the daytime thermal offset. The validity of this model is controversial. It has been tested mainly for diffuse irradiance measurements, showing differences between ventilated and unventilated pyranometers (Dutton et al., 2001; Michalsky et al., 2003 and 2005; Carlund, 2013). Our study evaluates the performance of this model when applied to each participating unventilated pyranometer while measuring global or diffuse.

2.- Data

Measurements were made at the rooftop of the Physics Department building, University of Extremadura in Badajoz (Spain), with coordinates 38.98ºN, 7.018ºW; 199 m a.s.l.. This location guarantees an open horizon in the non-industrialized outskirts of the city. The region is characterized by a generally mild Mediterranean climate with hot and cloud-free conditions during summer, when high solar irradiance values are reached.

Thermal offset was measured by means of capping events conducted on 26 and 27 June 2015, and 21 and 22 July 2015. These dates will be hereafter named by their corresponding day of the year (days 176, 177, 202 and 203, respectively). A total of 372 capping events, 124 for each pyranometer, were conducted during these four days, being the highest number of capping events ever reported in the literature.

Since most interesting cases are those with a large thermal offset, the campaign of measurements was performed during summer days. The four selected days showed high irradiance values and, therefore, a large thermal offset was expected. Additionally, these days were selected because of their high stability and similar environmental and radiative conditions. The intense campaign focused on these four selected days allows also to study the diurnal evolution of the thermal offset, which has never been addressed using the capping methodology. The solar zenith angle sampled ranged from 15.5º to 82.0º.

Table 1 gives a fairly complete description of conditions during the actual data collection period for each day, including the ranges of air temperature (with the time when those extreme temperatures occurred), sky brightness temperature, relative humidity, wind speed, and global, diffuse and net infrared irradiances. During the four days of the campaign, global and diffuse irradiance presented very similar diurnal evolution with maximum values at noon of around 1000 W/m² and 100 W/m², respectively. As expected for clear days in this location, ambient temperature quickly rose during the early morning and reached its maximum around 16:00 UTC, remaining close to this maximum value until sunset. Air temperature ranged between 18.0ºC and 37.4ºC during the campaign. The relative humidity and net infrared irradiance also showed similar magnitude and evolution during the four campaign days. During these four days the relative humidity ranged between 22% and 80%, and the net

infrared irradiance between -138.0 W/m² and -71.0 W/m². On days 176-177 wind was significantly different from days 202-203, remaining below 3.2 m/s during days 176 and 177 but reaching values of up to 6.0 m/s during days 202 and 203. In order to compare days with similar wind conditions, days 176 and 177 were used to study the effect of ventilation on the thermal offset in global irradiance measurements, and days 202 and 203 to study the effect of mechanical ventilation on the thermal offset in diffuse irradiance measurements. Thus each pair of days guarantees similar environmental and radiative conditions. Since moderate winds up to 4.9 and 5.8 m/s were found on days 202 and 203 respectively, the thermal offset in diffuse irradiance is compared between mechanically ventilated and naturally ventilated by significant winds.

3. Instruments

3.1.- Pyranometers

Three manufacturers lent secondary standard pyranometers with their compatible ventilation units for the duration of the campaign. They were: 1) a SR20 pyranometer (#3727) with its VU01 ventilation unit provided by Hukseflux (The Netherlands), 2) a CMP11 pyranometer (#080493) and its CVF4 ventilation unit provided by Kipp & Zonen (The Netherlands), and 3) a SPP pyranometer (#38172) with its VEN ventilation unit provided by Eppley Laboratories (U.S.A.). These models are widely used in meteorological stations worldwide.

All the pyranometers used in this study comply with the International Organization for Standardization ISO 9060 criteria for an ISO secondary standard pyranometer, being classified as ‘‘high quality’’ according to the WMO nomenclature (WMO, 2008). They had been calibrated following standard WMO procedures according to ISO 9847 (1992). It is to note that this is the first time the thermal offset of these instruments is simultaneously measured and compared.

The pyranometers studied consist of: 1) a black-coated thermopile acting as a sensor, 2) two concentric hemispherical domes to protect the sensor, 3) the body or case, which holds the key parts of a pyranometer, and 4) a sun screen to protect the body and reduce solar heating. Table 2 shows their main

characteristics as described in the manufacturers' instruction manuals and websites (Kipp and Zonen, 2013; Hukseflux, 2014; https://eppleylab.com).

The pyranometer sensors are based on the thermoelectric principle. Although the detector construction differs between models, the same fundamental working principle is applicable to all of them. The sensing elements are made up of a large number of thermocouples junction pairs connected in series. While the reference junction keeps at a fixed temperature, the active junction is exposed to the solar radiation. Bonded on the active junctions to the thermocouples there is a black-painted ceramic disk that helps to absorb the incident solar radiation. Blackened thermopile detector is preferred over others due to its flat spectral response, fast time response and good angular behavior. The temperature of the active junctions increases when the incoming radiation passes through the two glass domes and is absorbed by the black ceramic disk. The temperature difference between the active and the reference junctions produces a small voltage which is a function of the absorbed irradiance.

The sensor is easily affected by environmental factors and the delicate black coating must be protected; therefore, the sensor is covered by domes. The use of two domes instead of one results in a better thermal equilibrium between the sensor and the inner dome, therefore reducing the thermal offset. The pyranometers participating in this study have glass domes with different size: The diameter of the outer dome is 60 mm in SPP pyranometer, 50 mm in CMP11, and 40 mm in SR20.

The body of a pyranometer is designed to provide high mechanical and thermal stability to the instrument. The pyranometers participating in the campaign showed differences both in the material and the design. For example, SR20 and CMP11 have light aluminum bodies while SPP has a heavy body made of bronze.

There is a screen attached to the body designed to protect it from the rainfall and to reduce solar heating. The material and design of this screen could play an important role regarding the thermal offset. On the one hand, it is in contact with the body, therefore affecting the thermal stability. On the other hand, its size and shape modify the airflow around the pyranometer. Thus, while SR20 and CMP11 have a screen made of plastic with a diameter of 150 mm, SPP has a flatter screen made of aluminum with a notably longer diameter of 190 mm.

During the campaign the pyranometers were installed on a Kipp & Zonen Solys 2 solar tracker (Figure 1.a.) equipped with shading balls. These balls were only installed on days 202 and 203 in order to measure diffuse irradiance. Similarly, ventilation units were only installed on days 176 and 203 in order to obtain measurements under mechanically ventilated conditions. The output signals of the pyranometers were recorded by a Campbell CR1000 data logger every second.

3.2. Ventilation units

Ventilation units are primarily aimed at preventing dew and frost deposition on the domes which could disturb the measurements. As a beneficial side effect, ventilation favors the thermal equilibrium between different parts of a pyranometer, thereby reducing the thermal offset (Kipp and Zonen, 2013; Hukseflux, 2014).

Three ventilation units participated in our campaign. Their main characteristics are summarized in Table 3. These ventilation units consist of a base holding a cover and a fan designed to work at 12 volts DC. Their size, shape and material determine how the air is blown around the body and domes of the pyranometer, therefore affecting the thermal offset.

The base of the ventilation unit holds the fan and has available space to install the pyranometer. The ventilation unit bases of our study are made of aluminum, but their sizes and shapes differ. While VEN and VU01 have a circular base with a diameter of 23.0 cm and 16.5 cm, respectively, the CVF4 has a circular base of 23.0 cm diameter and an additional branch (Figure 1.b). The shape of the base is determined by the relative position of the fan with respect to the pyranometer. In VEN and VU01 the fan is placed under the pyranometer, continuously blowing air upwards over the case and the dome. In contrast, the CVF4 ventilation unit uses a “squirrel cage” design with the fan located aside the pyranometer.

The VEN ventilation unit manufactured by Eppley uses a bladed fan which generates an airflow of 85 m^3/h. The Huskeflux V01 ventilation unit uses a DC centrifugal fan. The intake of air is in the axial

direction and the exhaust is centrifugal. In that sense, the working principle most closely resembles the "squirrel cage" design. This is called a "radial" fan to differentiate it from "axial" fans, which have an intake and exhaust both in the axial direction. The fan uses a backward-curved impeller. The fan airflow is 84 m^3/h at a nominal voltage of 12 V. The manufacturer has estimated an effective airflow of 50 m^3/h at the VU01 cover outlet (personal communication). The VCF4 ventilation unit manufactured by Kipp & Zonen follows a squirrel cage design. It generates an air-free airflow of 28 m^3/h.

The annular area available between the outer dome and the ventilation cover outlet limits the air blown by the fan that arrives at the dome. The size of this annual area is determined by the difference of diameter between the outer dome (Table 2) and the ventilation cover outlet (Table 3). This area is 14.2 mm wide for SR20+V01, 11.5 mm for CMP11+CVF4, and nearly zero for SPP+VEN. These different sizes and the fan airflow rates help to explain the feeling that the airflow is stronger for VU01, followed by CVF4, and finally by VEN.

3.3.- Additional measurements

The campaign was performed at the Badajoz radiometric station. This station is equipped with a CG1 pyrgeometer to measure the downward infrared irradiance. The pyrgeometer was not ventilated during the campaign. This pyrgeometer is designed to provide highly reliable and accurate measurements of infrared irradiance with an error lower than 20 W m-2 under changing temperature conditions up to 5 K/h . It guarantees stability in time, with the change in sensitivity lower than 1% yr–1 (Kipp & Zonen 2003). The calibration factors provided by the manufacturer Kipp & Zonen for the pyrgeometer CG1 were applied. This calibration used a CG1 pyrgeometer as a reference, resulting in a sensitivity error of 5% under conditions of a temperature of 20ºC and an irradiance of 140 W m-2 (according to the Kipp & Zonen calibration sheet for our pyrgeometer). Additionally, in order to confirm the stability of their calibration factors, the pyrgeometer was compared with a CG4 pyrgeometer located at a nearby (400 m from our station) meteorological station managed by the Spanish Meteorological Agency (AEMET). The AEMET pyrgeometer is periodically calibrated every two years by intercomparison with the AEMET reference, which in turn is calibrated every two years by the World Radiation Centre in Davos. The AEMET radiometric network follows WMO standard protocols and procedures for calibration and

measurement, as certified according to ISO 9001:2008. The comparison between our pyrgeometer and the AEMET pyrgeometer extended over the period August to December 2015, and showed a very good agreement, with a mean relative difference of 2%.

Figure 2 shows a local time based time series plot of the difference between the pyrgeometer case temperature (Tcase) and the sky brightness temperature (Tsky). This difference is a descriptor of the infrared imbalance between the pyrgeometer and the air, which provides interesting information to understand the thermal offset of the pyranometers. A similar diurnal pattern is found between days 176 and 177, and slightly less similar between days 202 and 203. All days show an increase of the difference in temperature between the pyrgeometer and the sky along the day. On day 177 the difference decreases at late evening.

The direct irradiance is measured by a CHP1 pyrheliometer installed on a solar tracker Solys 2, all of them manufactured by Kipp & Zonen. This pyrheliometer was calibrated in 2013 at the AEMET Radiometric Laboratory in Madrid, Spain. For this calibration, the Kipp and Zonen CH1 pyrheliometer #050408, which is directly traced to WRC-Davos, was used as reference. The calibration factor obtained in this campaign differs in less than 0.1% respect to that provided by the manufacturer.

The station is also equipped with two Kipp and Zonen CM11 pyranometers, one for measuring global irradiance and the other one, mounted on a CM121 shadow ring, for measuring diffuse irradiance. These two pyranometers comply with the specifications of the first-class World Meteorological Organization classification (WMO, 2008) for this instrument. Both pyranometers participated in the inter-comparison campaign carried out in June 2013 at the “El Arenosillo” Atmospheric Sounding Station of the National Institute for Aerospace Technology (Huelva, Spain). In this campaign our two pyranometers were compared to the ventilated Kipp and Zonen CM21 pyranometer #041219 which had been recently calibrated. The calibration factors obtained in this campaign and the one provided by the manufacturer notably agree, with relative differences lower than 0.5%, proving the high stability of the response of both pyranometers.

The diffuse irradiance measurements have been corrected from the shadow ring error according to the methodology developed by Sanchez et al. (2012).

In this station, radiometric data are recorded by a Campbell CR1000 data-logger usually every minute. However, this study required higher temporal frequency and, therefore, data were recorded every second during the campaign. These measurements give valuable information about the radiation field when capping events were being conducted.

Additionally, measurements of ambient temperature, relative humidity and wind speed were registered every ten minutes at a nearby meteorological station managed by the Spanish Meteorological Agency (AEMET). This station is only 400 m away from our radiometric station and follows WMO standard protocols and procedures for calibration and measurement. Wind speed is measured by a THIES Compact anemometer while ambient temperature and relative humidity are jointly measured by a THIES Compact probe. Temperature and relative humidity sensors operate inside a Stevenson wooden shelter to protect against precipitation and direct radiation. The accuracy is ±2% for relative humidity measurements and ±0.15K for temperature measurements. These measurements describe the environmental conditions while capping events were being performed.

4.- Methodology

4.1.- Capping events

In this study thermal offset measurements have been obtained following the capping methodology. This technique consists of recording the pyranometer output signal while the incoming solar radiation is blocked by a cap that covers the dome. When no solar radiation arrives at the sensor, the output signal is a measure of the exchange of infrared flux between the dome and the sensor, that is, the thermal offset. The capping event should last until the detector has responded to the blocking of shortwave radiation, but it should be short enough to prevent significant changes in the temperature of the dome.

It must be noted that this study has performed the highest number of capping events ever reported in the literature. In fact they are many more than the measurements reported in the previous studies that have used the same methodology, such as in Haeffelin (2001), Michalsky (2003), Michalsky (2005),

and Bush et al. (2000). The low number of capping events conducted in previous studies is probably due to the great effort required to apply this methodology. Other alternative methodologies can easily provide more estimations of the thermal offset, but suffer from other additional drawbacks. Thus, installing thermistors or barometers inside the pyranometer are intrusive methods which can affect the measurements, mainly if a thermometer is attached to the dome. On the other hand, using a negligible thermal offset pyranometer as reference generally underestimates the thermal offset since the thermal offset of the reference is not strictly zero (Ji and Tsay 2010; Dutton et al. 2001). Moreover, other differences between the reference pyranometer and the pyranometer of study (such as their specific cosine error, spectral response, time response, and temperature dependence) are ignored.

Therefore, in the present study the capping methodology was preferred despite being highly demanding since it has the advantage of providing realistic values of the thermal offset independently of other reference instruments and not requiring installation of thermometers nor barometers inside the pyranometers. This methodology has been extensively used for determining the thermal offset and has proven to provide reliable results (Bush et al. 2000, Dutton et al. 2001, Haeffelin et al. 2001, Michalsky et al. 2005, Carlund 2013, Sánchez et al. 2015).

Three caps were specially manufactured for this experiment. The caps were made of polystyrene and coated outside and inside with laminated aluminum (Figure 3). These materials were used in order not to affect the dome and detector temperature when the pyranometer was capped. Thus, the polystyrene was used to insulate the dome and detector from the environment. Moreover, its external side was coated with laminated aluminum to reflect the radiation incoming from outside. The inside of the cap was also coated with aluminum because of its low IR emissivity (0.04), so as to reduce its emission. During the experiments, the caps were kept shadowed outdoors at the same ambient temperature than the pyranometers. Additionally, in order to study the possible radiative effect of the caps their emission was measured. Towards this goal, the pyrgeometer was covered three times by each cap for 10 minutes on days 18 and 19 June 2015. The net infrared irradiance measured was similar for the three caps, with a mean value of 0.39 W m^{-2}, which is negligible compared with the thermal offset values. The caps were designed to just cover the dome and part of the shield while not modifying the air circulation around the pyranometer.

Previous studies have shown that once the pyranometer is covered, the output signal decreases, reaches a minimum and then smoothly increases to approach a stable value (Bush et al. 2000; Sanchez et al. 2015). In the current study the thermal offset was obtained as the minimum value reached by the signal during the capping event, as it was suggested by Bush et al. (2000). This criterion compares well with other estimations (Sanchez et al., 2015) while requiring no estimation of the time constant of the pyranometer, which can be difficult to determine.

In order to analyze the evolution of the output signal when the pyranometer is covered, preliminary long capping events were carried out. Six long capping events were conducted with each pyranometer, three of them with mechanical ventilation and other three without mechanical ventilation. As a result of the information obtained from the preliminary measurements, following capping events were decided to last five minutes. The capping events were performed approximately every 40 minutes to prevent memory effects from happening. The three pyranometers were covered simultaneously to guarantee the measurements were performed under the same environmental conditions.

4.2.- Analysis

Previous studies have reported relationships between thermal offset and environmental variables (Bush et al. 2000; Haeffelin et al. 2001; Dutton et al. 2001; Sanchez et al., 2015). Among the main factors affecting the thermal offset, several authors pointed out the role played by the infrared downward irradiance at ground level. An increase of downward IR irradiance heats the dome and consequently reduces the difference in temperature between the dome and the detector. Several authors have quantified this influence using Net IR as measured by a pyrgeometer and/or the difference of temperature between the pyrgeometer case and the sky brightness temperature (Dutton et al. 2001;Haeffelin et al. 2001; Younkin and Long, 2004; Michalsky et al. 2005; Gueymard and Myers 2009).

Additionally, the thermal offset is affected by the ambient temperature (Ta), relative humidity (RH) and wind speed (W) (Bush et al. 2000; Dutton et al. 2001; Haeffelin et al. 2001; Philipona 2002; Michalsky et al., 2003; Sanchez et al. 2015). The impact of these factors on thermal offset will mainly depend on the pyranometer design. For example, the wind affects both the dome and body but, while the dome is

completely exposed, the body is partially protected by the pyranometer sun screen.

The dependence of daytime thermal offset on these environmental variables and the influence of mechanical ventilation have been thoroughly evaluated for the three pyranometers participating in the campaign.

Additionally, the performance of the model proposed by Dutton et al. (2001) to correct the thermal offset was evaluated. This model proposes a relationship between the thermal offset of a pyranometer and the net infrared irradiance measured by a collocated pyrgeometer, *Net IR,* as follows:

$$Thermal\ Offset = a + b \cdot Net\ IR \qquad (1)$$

According to the Dutton et al.'s proposal, the coefficient *b* is estimated using nighttime measurements and the obtained model is applied to correct the daytime thermal offset. The Dutton et al.'s method is intended to use the pyrgeometer as a tracer of the pyranometer. Therefore, in order to most accurately mimic the conditions that the pyranometer is experiencing, they both must operate under the same ventilation conditions. Since the pyrgeometer used in this study was unventilated, the analysis is only applied to measurements registered by unventilated pyranometers. Nighttime data were selected as those measurements registered when solar altitude was below -10º during nights 177 and 202 (no ventilation was applied).

Ordinary linear least square fittings have been obtained for each pyranometer and the coefficient of determination R^2 was calculated to quantify the goodness-of-fit. This statistic measures how well the observed outcomes are replicated by the model. Additionally, fittings with the intercept forced through (0,0) have also been analyzed. This is a common practice since a zero offset is expected when Net IR equals zero, i.e., when the dome and the sensor of the pyrgeometer have the same temperature. Afterwards, the nighttime-fitted model was employed to estimate the diurnal thermal offset. The differences between modeled and measured thermal offset values will be analyzed for unventilated pyranometers while measuring global or diffuse irradiance.

5.- Results and discussion

Section (5.1) shows the results of preliminary capping events. In section 5.2, the daytime thermal offset measured for each pyranometer and operational configuration is analyzed. Next, the relationship between the thermal offset and several environmental factors is discussed (Section 5.3). Finally, the performance of the Dutton et al.'s model to correct the daytime thermal offset is evaluated (Section 5.4). It should be noticed that, as offsets are usually negative, a reference to increasing offset means more negative and vice versa.

5.1.- Preliminary capping events

Figure 4.a shows an example of the output signal measured by each pyranometer during a preliminary capping event conducted without mechanical ventilation. Vertical lines are plotted to highlight the time that each pyranometer takes to reach its thermal offset.

In all these six preliminary long capping events, the unventilated CMP11 pyranometer shows a sharp minimum with a well-defined thermal offset, taking a mean time of 10.1 s (standard deviation is 1.5 s) to reach the minimum. Meanwhile, the unventilated SPP and SR20 pyranometers requiring a mean time of 33.2 s (standard deviation is 5.9 s) and 63.8 s (standard deviation is 10.0 s) to reach their respective minimum values, taking several seconds to start increasing again.

Figure 4.b. shows an example of the evolution of the output signal measured by each pyranometer during a preliminary capping event while applying ventilation. The time needed by the CMP11 and SPP pyranometers to reach their minimum signal was similar to the values corresponding to the unventilated case. On the contrary, the time needed by SR20 pyranometer notably increases when it is mechanically ventilated. The average time taken by this instrument to reach its minimum value while being ventilated was 150.5 s (with a standard deviation of 18.8 s). This long period of time could significantly affect the estimation of the thermal offset: the temperature of the dome could decrease, causing an underestimation of the thermal offset prior to the capping. In spite of this behavior, the ventilated SR20 has been included in this study; however, its results should be taken with caution.

5.2. Thermal offset measurements

5.2.1. Thermal offset for unventilated pyranometers while measuring global irradiance (UG)

Figure 5.a shows the thermal offset values measured on day 177 by unventilated pyranometers measuring global irradiance. All pyranometers show a clear diurnal cycle, being more pronounced for the CMP11. This diurnal pattern shows three stages: 1) at early morning hours the absolute thermal offset clearly increases (becomes more negative), 2) between mid-morning and around 17:00 UTC the thermal offset oscillates around a constant value, and 3) afterwards the absolute thermal offset decreases (becomes less negative). A similar pattern has been previously reported for two CM11 pyranometers by Sanchez et al. (2015), who suggested that this behaviour during cloudless summer days could be explained by the diurnal variation in the direct/diffuse partitioning.

The mean value of the UG measurements registered during the central period of day 177 is around -6.85W/m² (standard deviation of 2.0W/m²) for the SPP and SR20 pyranometers, but reaches -15.0W/m² for the CMP11 pyranometer. These values fall in the range of thermal offset derived by Bush et al. (2000) for an unventilated PSP measuring global irradiance under cloudless skies. They estimated the thermal offset using measurements of the temperature of the dome and the body, obtaining values between -17.0 W/m² and -6.5 W/m². It must be noted that, although unventilated CMP11 shows the highest absolute thermal offset (most negative), it is very stable during the central hours of the day, with the standard deviation being 1.0W/m² .

5.2.2. Thermal offset for ventilated pyranometers while measuring global irradiance (VG)

Figure 5.b shows the thermal offset measured on day 176 by mechanically ventilated pyranometers measuring global irradiance. The main difference with respect to the unventilated case is the removal of the diurnal cycle. Instead, the VG for SR20 oscillates around -4.5 W/m² all day long. The absolute value of the VG for the CMP11 slightly rises from the early morning to around 15:00 UTC and then, vaguely decreases until the sunset. Meanwhile, the absolute values of the thermal offset for the ventilated SPP pyranometer slightly decreases during the day.

There is a significant reduction in the absolute value of thermal offset when the pyranometers are

mechanically ventilated. The average absolute value of VG is 4.04 W/m² for SR20, 5.16 W/m² for SPP and 5.77 W/m² for CMP11 during the central period of the day. These values mean a reduction of 61% for CMP11 and 25% for SPP. In the case of the SR20 pyranometer, the 41% reduction obtained could be overestimated taking into account the long time needed by this instrument to reach the thermal offset when it is ventilated.

A notable reduction in the variability between consecutive measurements of thermal offset has been also found for the three pyranometers. The standard deviation is reduced to 1.3W/m² for the SR20, to 0.81W/m² for the CMP11 and to 1.5W/m² for the SPP. In addition, the thermal offset values of different pyranometers are very similar. This higher similarity becomes relevant for comparisons of values reported for different pyranometers. Therefore, in general, installation of ventilation units is warranted considering the reduction in absolute thermal offset.

5.1.3. Thermal offset for unventilated pyranometers while measuring diffuse irradiance (UD)

Figure 5.c. shows the thermal offset values measured on day 202 by unventilated pyranometers measuring diffuse irradiance. In contrast with UG, a diurnal cycle is not evident for the UD values of the SPP. Instead, UD values for SPP pyranometer oscillate around a mean value of -3.5W/m² during the entire day with a standard deviation of 2.5W/m². Meanwhile values of UD for CMP11 and SR20 are around -7.0 W/m² before 10 UTC, reach -11.5 W/m2 around noon and then become less negative towards sunset. In both cases, this diurnal evolution is less marked when compared to the diurnal pattern observed for the UG. The mean thermal offset value for the SR20 and CMP11 pyranometers is -8.7W/m² and the standard deviation is around 2.0W/m².

Previous studies are inconclusive regarding the effect of global versus diffuse irradiance in affecting thermal offsets. While Philipona (2000) found no difference in thermal offset between global and diffuse measurements, Bush et al. (2001) reported significant differences. In this study, notably different diurnal pattern is found between days 177 and 202. However, this comparison must be taken with caution since both days showed different environmental conditions. The main difference between the thermal offset for global and diffuse measurements is the effect of direct radiation on the temperatures of dome and sensor. The fast change in the direct component at early morning and later

evening could be the main factor determining the increase and decrease in UG. In the absence of direct irradiance in unventilated diffuse measurements, this tendency disappears in the morning and is smoother during the afternoon. This result about the effect of the direct/diffuse partitioning on the thermal offset tends to agree with several studies (Bush, 2000; Cess, 2000; Sanchez et al., 2015). However, opposite conclusions have been also reported (Younkin and Long, 2004; Vignola et al., 2007, 2008, 2009; Philipona, 2002) and the issue remains controversial. This diversity in results is probably related to the distinct methodology, instrumentation, and location used in the different studies. Thus, further analysis are needed to assess possible differences in the thermal offset of pyranometers depending on whether they are measuring global or diffuse irradiance.

Most UD values obtained for the three pyranometers are less negative than the value -20W/m² given by Haeffelin et al. (2001) for a PSP pyranometer or the value -11.0W/m² reported by Dutton et al. (2001) for two CM21 pyranometers.

5.2.4. Thermal offset for ventilated pyranometers while measuring diffuse irradiance (VD)

Figure 5.d shows the thermal offset measured on day 203 by mechanically ventilated pyranometers measuring diffuse irradiance. Ventilation affects the thermal offset of diffuse irradiance measurements similarly than it was observed for global irradiance measurements. One of its most noticeable effects is the reduction in the variability between consecutive measurements of the thermal offset for all the pyranometers.

The thermal offset of the SR20 pyranometer oscillates around a mean value of -6.17W/m² during the day, with a standard deviation of 1.1W/m². However, this value could be higher considering the time needed by this instruments to reach the minimum when it is covered. In the case of the CMP11 pyranometer, the absolute value of the thermal offset rises from the early morning to around 14:00 UTC and then, decreases towards sunset. This pyranometer shows the largest reduction in the absolute thermal offset with a mean value of 3.4W/m² and a standard deviation of 2.0W/m². A decrease of around 50% in the maximum VD has been observed for the CMP11 with respect to that obtained when it was measuring UD. At the same time, a clear tendency is detected in VD for the SPP pyranometer. The absolute thermal offset of this pyranometer increases smoothly during the day and reaches a

maximum value of 9.0 W/m² during sunset. Its mean value for that day is 4.4W/m² and the standard deviation 2.5W/m². A possible explanation for this increase could be the small outlet of the ventilation unit, that allows no airflow supplied by the fan to reach the dome. With this design, the air driven by the fan circulates only around the body, while the dome is exposed to natural air circulation and to the environmental conditions. The effect of the artificial ventilation on the thermal offset dependence on the environmental conditions will be thoroughly analyzed in the next section. The CMP11 and SPP pyranometers showed similar VD patterns than those observed for VG. This issue will be analyzed in the next section.

Other studies have obtained experimental VD values on cloudless skies by means of capping events (Dutton et al., 2001; Haeffelin et al., 2001; Michalsky et al., 2003). Haeffelin et al. (2001) and Dutton et al. (2001) reported thermal offset values between -15 and -5 W/m² for a PSP pyranometer. These values differ from the results obtained in this study for the CMP11, SPP and SR20 pyranometers. These differences between pyranometer models emphasize the need to individually characterize each instrument and the environmental conditions surrounding each experiment.

5.3. Effect of mechanical ventilation on the influence of environmental conditions

Mechanical ventilation modifies the air circulation around the pyranometers, particularly, around the body and the dome. This change could directly affect the thermal offset and its relationship with the natural environmental conditions. In this section, the effect of ventilation on the relationship between the thermal offset and the environmental variables is examined. To assess these relationships, regression models between the thermal offset of each pyranometer and each independent variable were fitted using the least squares approach.

Figure 6 depicts the behavior of the thermal offset values vs wind speed (W), ambient temperature (Ta), relative humidity (RH), net infrared irradiance (Net IR) and the difference between the pyrgeometer case temperature and the sky brightness temperature (Tcase-Tsky). Data when the pyranometers were measuring global irradiance with and without mechanical ventilation are shown.

The thermal offset in the unventilated CMP11 pyranometer measuring global irradiance shows a

positive tendency with respect to the Net IR irradiance (with $R^2 = 0.713$) and relative humidity (with $R^2 = 0.475$). It shows a negative tendency with respect to ambient air temperature (with $R^2 = 0.5$) as expected, since relative humidity and air temperature are anticorrelated. This behavior agrees with the behavior observed by Serrano et al. (2015) for two unventilated CM11. Similarly, a negative tendency with respect to the Tcase-Tsky difference is expected since this variable is anticorrelated with the Net IR. These tendencies are however less evident for the SPP (with R^2 below 0.43), and imperceptible for the SR20 (with R^2 values below 0.22).

When the pyranometers are measuring global irradiance while being ventilated (grey points in Figure 6) the decrease in the thermal offset described in Section 5.1.b is confirmed. While SR20 shows no clear patterns (with R^2 below 0.38), the CMP11 and SPP pyranometers show similar tendencies to those observed for unventilated measurements (UG), but notably smoother. The CMP11 pyranometer shows the largest attenuation of these tendencies due to ventilation. In general, it is observed that the air generated by the fan seems to homogenize the conditions around the pyranometer favoring the reduction of the thermal offset and its dependence on the environmental conditions.

The persistence of the trends on the CMP11 and SR20 when these two pyranometers are ventilated could be likely related to the actual air volume rate out of their corresponding ventilation units. There are many factors involved in the actual amount of ventilation finally flow around the dome, such as the fan volume and type (bladed/squirrel/radial) and its design. As it was described in Section 3.2., the SR20-VU01 has a fan with a very high volume rate, and a large annular area between the dome and the ventilation cover outlet. Conversely, CMP11-CVF4 and SPP-VEN have lower volume rate fans, and the annular areas available for the airflow to reach the dome are notably smaller.

Figure 7 shows the thermal offset vs wind speed (W), ambient temperature (T), relative humidity (RH) and net infrared irradiance (Net IR) when the pyranometers were measuring diffuse irradiance with and without ventilation. One of the most important results observed for UD is the lack of tendencies with respect to the environmental variables being analyzed, with R^2 being below 0.22 for all pyranometers. A certain diurnal pattern is only observed for the CMP11 pyranometer. This result confirms the importance of the direct/diffuse partitioning on the daily thermal offset behaviour as suggested in Section 5.1.c.

The SR20 pyranometer shows no clear tendency respect to any environmental variable while measuring diffuse irradiance and being ventilated (R^2 below 0.10). On the contrary, the CMP11 and SPP pyranometers show marked relationships with respect to several environmental variables. The thermal offset of diffuse irradiance measurements tends to increase with wind speed, ambient temperature and Tc-Ts difference, and to decrease with Net IR irradiance and relative humidity when the pyranometers are ventilated.

5.4.- Thermal offset correction obtained from nighttime data

5.4.a.- Nighttime fittings

Nighttime thermal offset vs the Net IR values and its corresponding linear least squares fit (solid grey line) are shown in Figure 8 for each pyranometer. The fittings coefficients are summarized in Table 4 together with the root-mean-squared-error (RMSE) and the coefficient of determination (R^2).

The SPP pyranometer shows a slope of 0.0337, which is similar to the values reported by Haeffelin (2001) and Michalsky (2005) for a ventilated PSP. However, the coefficient of determination R^2 is below 0.16 in all cases, indicating that most of the variance is not explained by the linear model. Several authors have previously reported no trend between the nighttime offset and Net IR (Michalsky et al., 2003; Michalsky et al., 2005; Gueymard, 2009). In our particular case, it is difficult to conclude this since the low significance of the fitting could be likely due to the lack of cases with small values of Net IR during the analyzed nights.

In usual practice, the intercept is forced through (0,0) since a zero offset is expected when Net IR equals zero, i.e., when the dome and the sensor of the pyrgeometer are at the same temperature. The no-intercept regression line for each pyranometer has been plotted as a dashed black line in Figure 8.

The slopes obtained for the no-intercept fittings are 0.01 for the SR20 pyranometer, and 0.04 for the CMP11 and SPP pyranometers. All regression coefficients were statistically significant at 95% level of confidence. Dropping the intercept results in a small change in the fitting for SPP since it was the one to show the smallest intercept in the non-forced-to-zero fitting. The CMP11 fitting gets closer to the

SPP fitting when the intercept is forced to be zero.

5.4.b.- Application to correct the daytime thermal offset

The zero-intercept regression models obtained in the previous section were applied to daytime Net IR irradiance measurements and the resulting daytime thermal offset was compared to the experimental values measured using capping events. Figure 9 shows the absolute differences found between the modeled and the measured daytime thermal offset values for days 177 (UG) and 202 (UD).

It can be observed that Dutton et al.'s model notably underestimates the absolute value of the daytime thermal offset for the SR20 and CMP11 pyranometers. This underestimation is larger when the CMP11 pyranometer measures global irradiance than when it is shadowed, and it shows a marked relationship with the solar zenith angle. A similar pattern was reported by Vignola et al. (2007) when measuring diffuse irradiance with a PSP pyranometer while being ventilated.

The regression model obtained with nighttime data performs better for the SPP pyranometer, with absolute differences between modeled and measured values being lower than 5 W/m² and almost uniformly scattered around the zero line. Thus, although our results apply to unventilated pyranometers, these results for the SPP pyranometer are in line with the widely application of Dutton et al.'s model for the ventilated PSP pyranometer, manufactured also by Eppley.

The previous studies that apply the Dutton et al.'s model mainly focussed on diffuse irradiance measurements (Dutton et al., 2001; Michalsky et al., 2005 and 2007). They have reported differences in the daytime thermal offset between model and capping-event measurements of around 1.5 W/m² for ventilated pyranometers and 7 W/m² for unventilated pyranometers. Thus, our results for SPP and SR20 pyranometers fall within the expected range. On the other hand, the CMP11 pyranometer shows somewhat larger differences up to 11 W/m², and notable differences between global and diffuse measurements are found as well.

6.- Conclusions

An intensive campaign to assess the effect of artificial ventilation on the thermal offset of pyranometers was carried out during selected cloudless days in June and July 2015 in Badajoz (Spain). The SR20 (Hukseflux), CMP11 (Kipp & Zonen) and SPP (Eppley) secondary standard pyranometers with their corresponding VU01, CVF4 and VEN ventilation units participated in this campaign. Daytime thermal offset was experimentally measured by means of capping events for each pyranometer while measuring global or diffuse irradiance, and with and without ventilation. To our knowledge, this is the first study to measure and compare the thermal offset of the CMP11, SPP and SR20 pyranometers, on such configurations and in actual field conditions.

Preliminary measurements revealed limitations to apply the capping methodology to the SR20 pyranometer while being ventilated. In this configuration the output signal takes 150s to reach the minimum once the pyranometer is capped. This long period of time could significantly affect the temperature of the dome, resulting in an underestimation of the thermal offset prior to its capping.

The comparison between unventilated and ventilated thermal offset when the pyranometers are measuring global or diffuse irradiance shows interesting results. Generally, mechanical ventilation tends to homogenize the temperature between the sensor and the domes and, therefore, to reduce the thermal offset. Additionally, a notable decrease in the short-term variability of the thermal offset was detected when the pyranometers were ventilated.

Results obtained in this study confirm the differences in the thermal offset between different pyranometer models as reported by previous studies (Dutton et al., 2001; Michalsky et al., 2003) but also reveal notable disparities in their daytime behavior. These differences between pyranometer models are generally reduced when mechanical ventilation is applied. This homogenization of the thermal offset becomes relevant for the comparison of different pyranometers.

In order to correct the daytime thermal offset, several authors have suggested mathematical expressions based on environmental variables (Vignola et al., 2007, 2008, 2009; Dutton et al., 2001; Serrano et al., 2015). Along these lines, the present study shows important differences in the relationships with

environmental magnitudes depending on whether the pyranometer is ventilated or not. The tendencies detected for the CMP11 and SPP pyranometers while ventilated could be related to the small size of the outlet of the ventilation unit, which hinders the airflow to reach the dome.

Additionally, the correction model proposed by Dutton et al. (2001) was essayed in this study. The relationship between the nighttime thermal offset and the Net IR irradiance was analyzed for each pyranometer under unventilated conditions. No significant relationship were found (R^2 below 0.16 for all regression fittings), being in line with other authors (Michalsky et al., 2003; Gueymard and Myers, 2009). However, the low significance could be also related to the lack of cases with Net IR values close to zero. Additionally, regression models forced through (0,0) were also fitted to nighttime data. Then, the fitted models were applied to estimate the daytime thermal offset. Differences between modeled and measured daytime values indicated that Dutton et al.'s model performs well for the unventilated SPP but it is unsuitable for CMP11 and SR20.

The analysis performed in this study highly recommends the general use of ventilation units. However, it must be emphasized that each pyranometer model must be individually studied with its ventilation unit under actual working conditions.

This study aims to contribute to a better knowledge of the thermal offset error in pyranometers, focusing on the effect of ventilation. The methodology and comparisons described in this paper can be applied at other locations, with other instruments and environmental conditions. The findings can be specially relevant for long-term historical radiation series recorded worldwide by networks such as BSRN, GEBA, SAURAN, SMN-AWS, etc. The reduction in the thermal offset when mechanical ventilation is applied has been quantified to be between 1.3 W/m² and 9 W/m². This value is in the order of the general changes in global radiation occurred during the 1960–1990 dimming period (variation between -5.1 and -1.6 W m^{-2} $decade^{-1}$) and the later brightening period (variation between +2.2 and +5.1 W m^{-2} $decade^{-1}$) (Wild et al., 2009). And also similar to the trend (+3 W m^{-2} $decade^{-1}$) in the diffuse irradiance in USA for the period 1996-2007 reported by Long et al. (2009), and to the trend (-1.3W m^{-2} $decade^{-1}$) in Girona (Spain) for the period 1994-2014 recently reported by Calbo et al. (2016). Thus, neglecting the thermal offset error could hinder the detection of these long trends, and the mechanical ventilation has been revealed in this study as an efficient method to reduce such error.

This study also suggests directions for future research concerning the development of models to correct the daytime thermal offset based on environmental and radiative magnitudes. It would be useful in further work to assess offset and ventilation characteristics with instruments of the same type. This might provide some general relationships typical of the pyranometer model.

7.- Acknowledgements

This study was partially supported by the research projects CGL2011-29921-C02-01 and CGL2014-56255-C2-1-R granted by the Ministerio de Economía y Competitividad from Spain and by Ayuda a Grupos GR15137 granted by Junta de Extremadura and Fondo Social Europeo (FEDER). Authors thank to Eppley, Hukseflux and Kipp & Zonen for providing their instrument to this study and to the Spanish Agencia Estatal de Meteorología (AEMet) for the provision of meteorological data. Guadalupe Sanchez Hernandez thanks the Ministerio de Economía y Competitividad for the predoctoral FPI grant BES-2012-054975. The data analyzed in this study are available from authors upon request (guadalupesh@unex.es).

8.- References

Bush, B.C., F.P.J. Valero, and A.S. Simpson, 2000: Characterization of thermal effects in pyranometers: A data correction algorithm for improved measurement of surface insolation. *J. Atmos. Oceanic Technol.*, **17**, 165-175.

Calbó, J., González, JA. & Sanchez-Lorenzo, A. (2016), Building global and diffuse solar radiation series and assessing decadal trends in Girona (NE Iberian Peninsula). Theor Appl Climatol (2016). doi:10.1007/s00704-016-1829-3

Cess, R.D., Q. Taotao, S. Moguo, 2000: Consistency tests applied to the measurement of total, direct, and diffuse shortwave radiation at the surface, *Journal of Geophysical Research: Atmospheres*, **105**, D20, doi:10.1029/2000JD900402.

Carlund T., 2013: Baltic Region Pyrheliometer Comparison 2012. World Meteorological Organization, Rep. 112, pp. 10-35, Geneva, Switzerland.

Dutton, E.G., J.J. Michalsky, T. Stoffel, B.W. Forgan, J. Hickey, D.W. Nelson, T.L. Alberta, and I. Reda, 2001: Measurement of broadband diffuse solar irradiance using current commercial instrumentation with a correction for thermal offset errors. *J. Atmos. Oceanic Technol.*, **18**, 297-314.

https://eppleylab.com

Gu, L. H., D. D. Baldocchi, S. C. Wofsy, J. W. Muger, J. j. Michalsky, S. P. Urbanski, T. A. Boden, 2003: Response of a deciduous forest to the Mount Pinatubo eruption: enhanced photosynthesis, *Science*, **299**, 2035-2038.

Gueymard CA, Myers DR (2009) Evaluation of conventional and high-performance routine solar radiation measurements for improved solar resource, climatological trends, and radiative modeling. Sol Energy 83:171–185

Haeffelin, M., S. Kato, A.M. Smith, C.K. Rutledge, T.P. Charlock, and J.R. Mahan, 2001: Determination of the thermal offset of the Eppley precision spectral pyranometer. *Applied Optics*, **4**, 472-484.

Hukseflux, 2014; User manual SR20 secondary standard pyranometer. Manual v1407.

International Organization for Standardization (ISO) 9060, 1990: Solar energy -- Specification and classification of instruments for measuring hemispherical solar and direct solar radiation.

International Organization for Standardization (ISO) 9847, 1992 :Solar energy -- Calibration of field pyranometers by comparison to a reference pyranometer.

Ji, Q., 2007: A method to correct the thermal dome effect of pyranometers in selected historical solar irradiance measurements, *Journal of Atmospheric and Oceanic Technology,* **24**, 529-536.

Kipp & Zonen, 2013: Instruction manual CMP series pyranometers and CMA series albedometers.

Long, C. N., and Y. Shi (2008), An automated quality assessment and control algorithm for surface radiation measurements, Open Atmos. Sci. J. ,2, 23–37, doi:10.2174/1874282300802010023

Long, C.N., E.G. Dutton, J. A. Augustine, W. Wiscombe, M. Wild, S. A. McFarlane, and C. J. Flynn, 2009: Significant decadal brightening of downwelling shortwave in the continental United States, *J. Geophys. Res.*, **114**, D00D06, doi: 10.1029/2008JD011263.

Michalsky, J.J., R. Dolce, E.G. Dutton, M. Haeffelin, G. Major, J.A. Schlemmer, D.W. Slater, J. Hickey, W. Q. Jeffries, A. Los, D. Mathias, L.J.B. McArthur, R. Philipona, I.Reda, and T. Stoffel, 2003: Results from the first ARM diffuse horizontal shortwave irradiance comparison, *J. Geophys. Res.*, **108**, 4108, doi:10.1029/2002JD002825.

Michalsky, J. J., et al. (2005), Toward the development of a diffuse horizontal shortwave irradiance working standard, J. Geophys. Res., 110, D06107, doi:10.1029/2004JD005265.

Philipona, R., 2002: Underestimation of solar global and diffuse radiation measured at Earth's surface. *J. Geophys. Res.*, **107**, 4654, doi: 10.1029/2002JD002396.

Reda, I., T. Stoffel and D. Myers, 2003: A method to calibrate a solar pyranometer for measuring reference diffuse irradiance. *Sol. Ener.*, **74**, 103-112.

Roderick, M. L., G. D. Farquhar, S. L. Berry, and I. R. Noble, 2001: On the direct effect of clouds and atmospheric particles on the productivity and structure of vegetation, Oecologia, **129**, 21-30.

Sanchez, G., A. Serrano, M.L. Cancillo, and J.A. Garcia, 2015: Pyranometer thermal offset: Measurement and analysis. *J. Atmos. and Oceanic Tech.*, **32**, 234-246. doi: 10.1175/JTECH-D-14-00082.1

Serrano, A., Sanchez, G., & Cancillo, M. L., 2015: Correcting daytime thermal offset in unventilated pyranometers. *Journal of Atmospheric and Oceanic Technology,* **32**, 2088 - 2099.

Vignola F, C.N. Long, and I Reda. 2007. Evaluation of Methods to Correct for IR Loss in Eppley PSP Diffuse Measurements. *Optical Modeling and Measurements for Solar Energy Systems Proceedings* Volume 6652, DR Meyers, ed. DOI: 10.1117/12.734474.

Vignola, F., C. Long, I. Reda, 2008: Modeling IR Radiative Loss from Eppley PSP Pyranometers. Proceeding in *Society of Photo-Optical Instrumentation Engineers (SPIE) conference*, San Diego, California.

Vignola, F., C. Long, I. Reda, 2009: Testing a model of IR radiative losses. Proceeding in *Society of Photo-Optical Instrumentation Engineers (SPIE) conference*, San Diego, California, NREL.

Wild M., 2009: Global dimming and brightening: a review. *J. Geophys. Res.*, **114**, doi: 10.1029/2008JD011470.

Wild, M., 2012: Enlightening global dimming and brightening. B*ull. Am. Meteorol. Soc.*, **93**, 27-37.

Tables

Table 1. Main characteristics during the actual data collection period for each day.

Operational mode	**GLOBAL**				**DIFFUSE**			
	Ventilated		**Unventilated**		**Unventilated**		**Ventilated**	
Day of the year	176		177		202		203	
	min	**max**	**min**	**max**	**min**	**max**	**min**	**max**
Data collection period (Hour UTC)	5.5	17.7	6.0	19.3	6.7	17.5	6.2	17.8
Air Temperature (ºC)	14.3	36.3	18.0	38.2	20.8	36.8	20.4	38.3
Sky brightness temperature (ºC)	13.7	37.9	17.8	40.9	21.3	37.1	19.0	38.5
Relative Humidity (%)	23	87	17	70	29	81	20	82
Wind speed (m/s)	0.3	3.2	0.5	2.9	1.7	4.9	0.8	5.8
Global irradiance (W/m²)	23.1	984.7	44.4	990.2	177.9	976.9	79.3	977.7
Diffuse irradiance (W/m²)	15.2	95.0	22.1	99.3	41.6	77.7	30.0	65.0
Net IR irradiance (W/m²)	-138.0	-66.5	-158.7	-73.8	-117.0	-81.6	-135.8	-62.2

Table 2. Main characteristics of the participating pyranometers provided by the manufacturers in their corresponding manuals and websites. Thermal offset in this table is commonly denominated as “Offset A” in pyranometer manuals.

Model	**SPP**	**SR20**	**CMP11**
Manufacturer	Eppley	Hukseflux	Kipp & Zonen
Serial number	38172	3727	080493
Spectral range (nm) (50% points)	295-2800	285-3000*	285-2800
Dome material	glass	glass	glass
Body material	bronze	aluminum	aluminum
Shield material	aluminum	aluminum	plastic
Outer dome diameter (mm)	50	40	50
Unventilated Offset A (W/m²)	5	5	<7
Ventilated Offset A(W/m²)	--	2.5	50% reduction

* Spectral range for 20% transmision points

Table 3. Main characteristics of the ventilation units provided by the manufacturers in their corresponding manuals and websites .

Ventilation Unit	**VEN**	**VU01**	**CVF4**
Manufacturer	Eppley	Hukseflux	Kipp & Zonen
Pyranometer	SPP	SR20	CMP11
Base Material	aluminium	aluminium	aluminium
Cover material	plastic+aluminum	aluminum	plastic
Dimensions (base diameter (cm) x height (cm))	23.0 x 16.2	16.5 x 12.4	23.0 x 13.0
Fan position	Under the pyranometer	Under the pyranometer	On one side of the pyranometer
Hole in the cover for the pyranometer outer dome (mm)	50	68.5	73

Table 4. Fitting coefficients, root-mean-squared-error, RMSE, and coefficient of determination, R^2 for the nighttime thermal offset and Net IR linear fittings. Coefficients with a significance higher than the 95% have been highlighted.

	a	**s(a)**	**b**	**s(b)**	**R^2**	**RMSE**
SR20	-2.18	0.02	0.0118	0.0002	0.043	0.36
CMP11	-1.50	0.02	0.0215	0.003	0.133	0.38
SPP	-0.63	0.03	0.0337	0.004	0.160	0.54

Figures

Figure 1.a.

Figure 1.b.

Figure 1. Instruments participating in the campaing. From left to right in (a) pyranometers CMP11, SPP and SR20 and in (b) pyranometers inside their corresponding ventilation units CVF4, VEN and VU01.

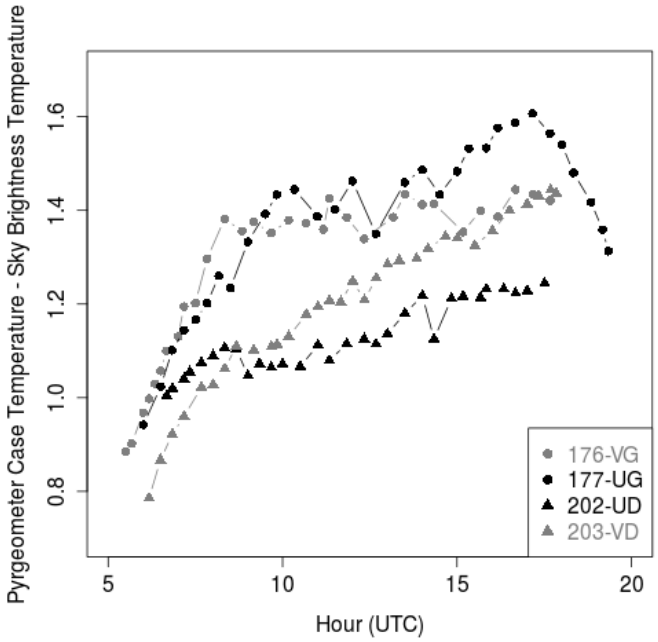

Figure 2. Diurnal evolution of pyrgeometer case – sky brightness temperature

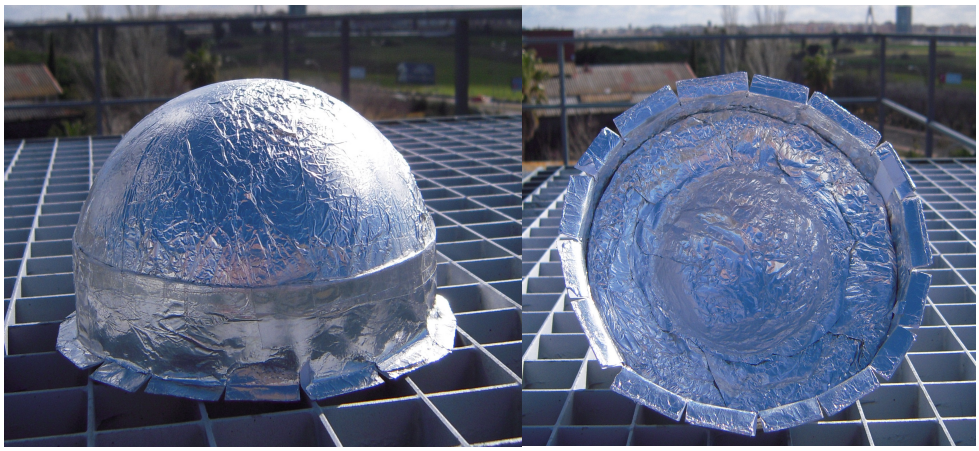

Figure 3. Caps

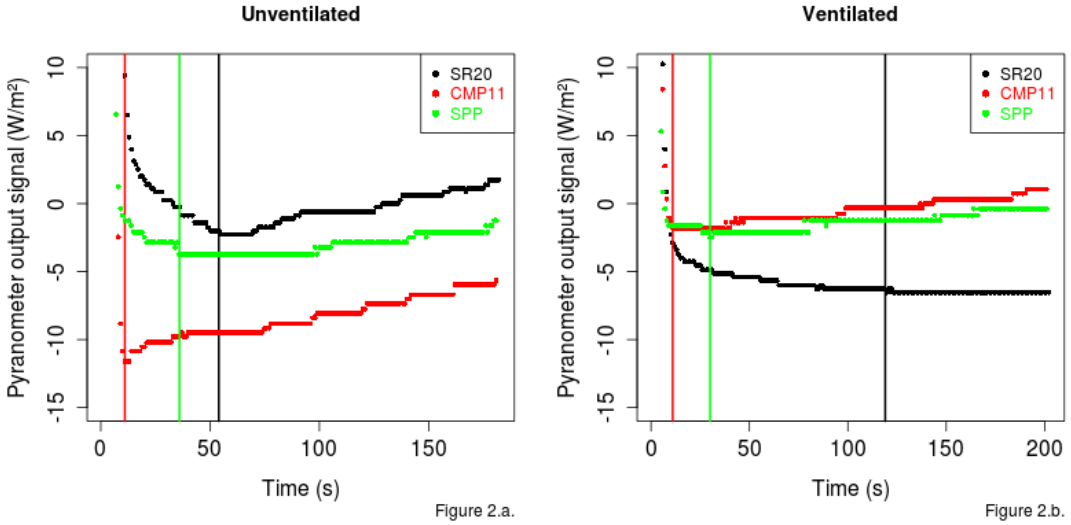

Figure 4. Output signal for each pyranometer during a preliminary capping event for (a) unventilated and (b) ventilated operational modes.

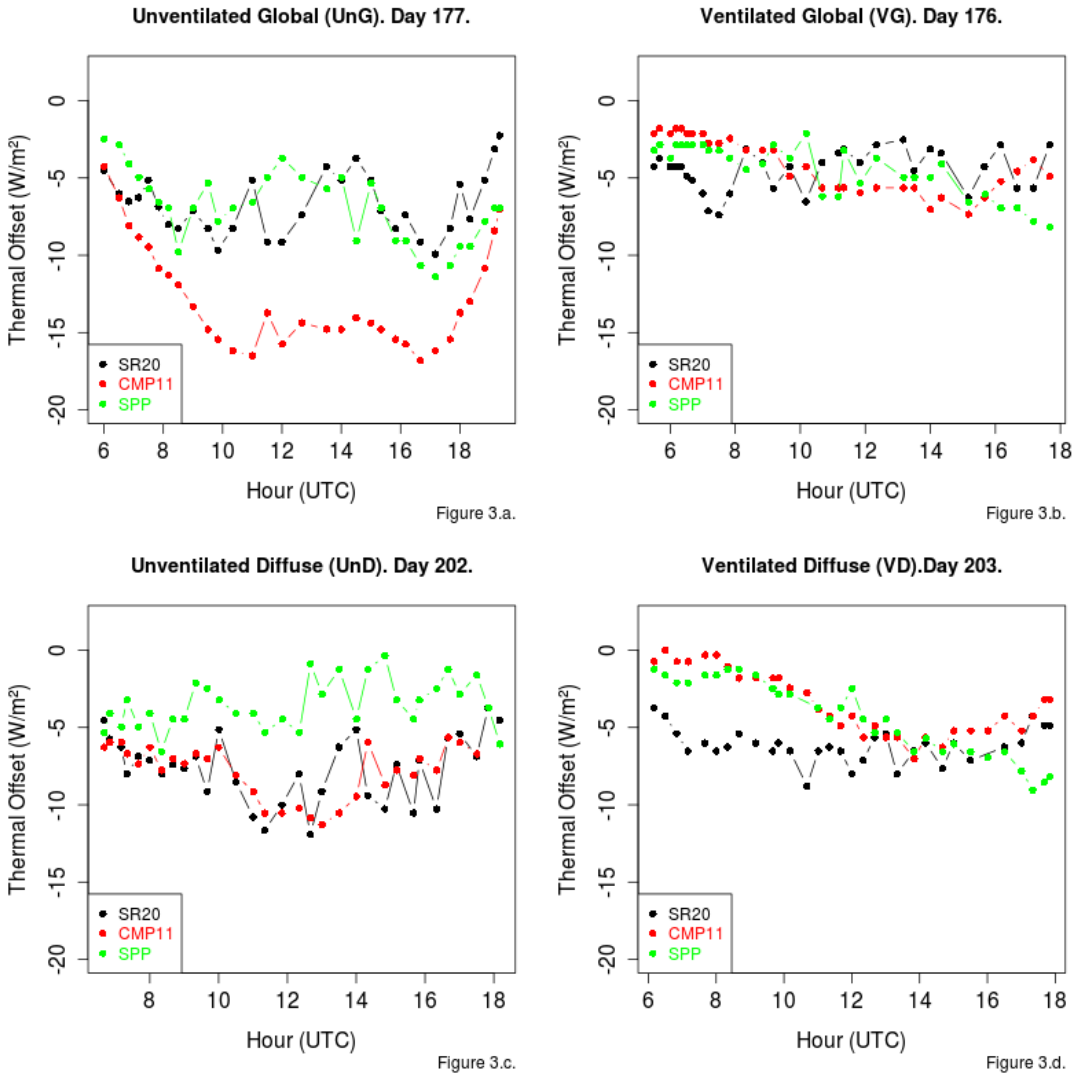

Figure 5. Daily evolution of the thermal offset measurements for (a) Unventilated Global, UG, (b) Ventilated Global, VG, (c) Unventilated Diffuse, UD, and (d) Ventilated Diffuse, VD, for each pyranometer model.

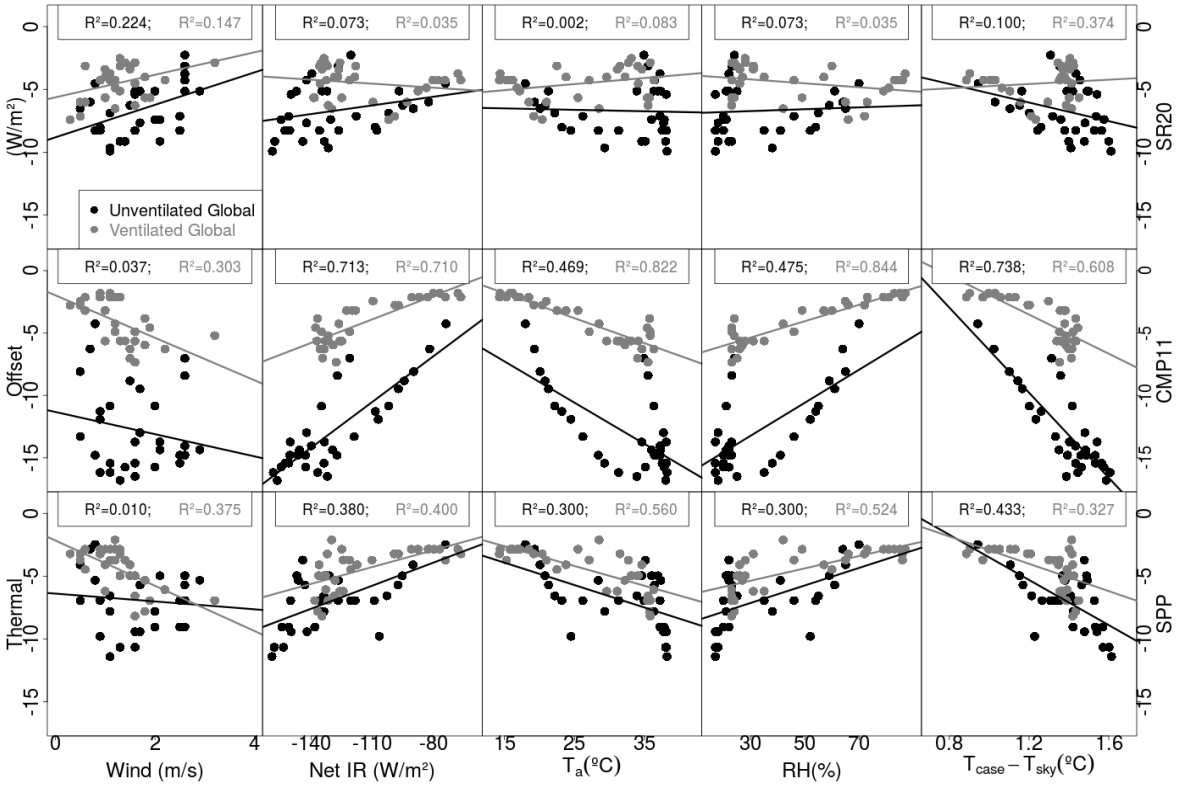

Figure 6. Dependence on the environmental conditions when the pyranometers are measuring global irradiance with ventilation (red points) and without ventilation (black points)

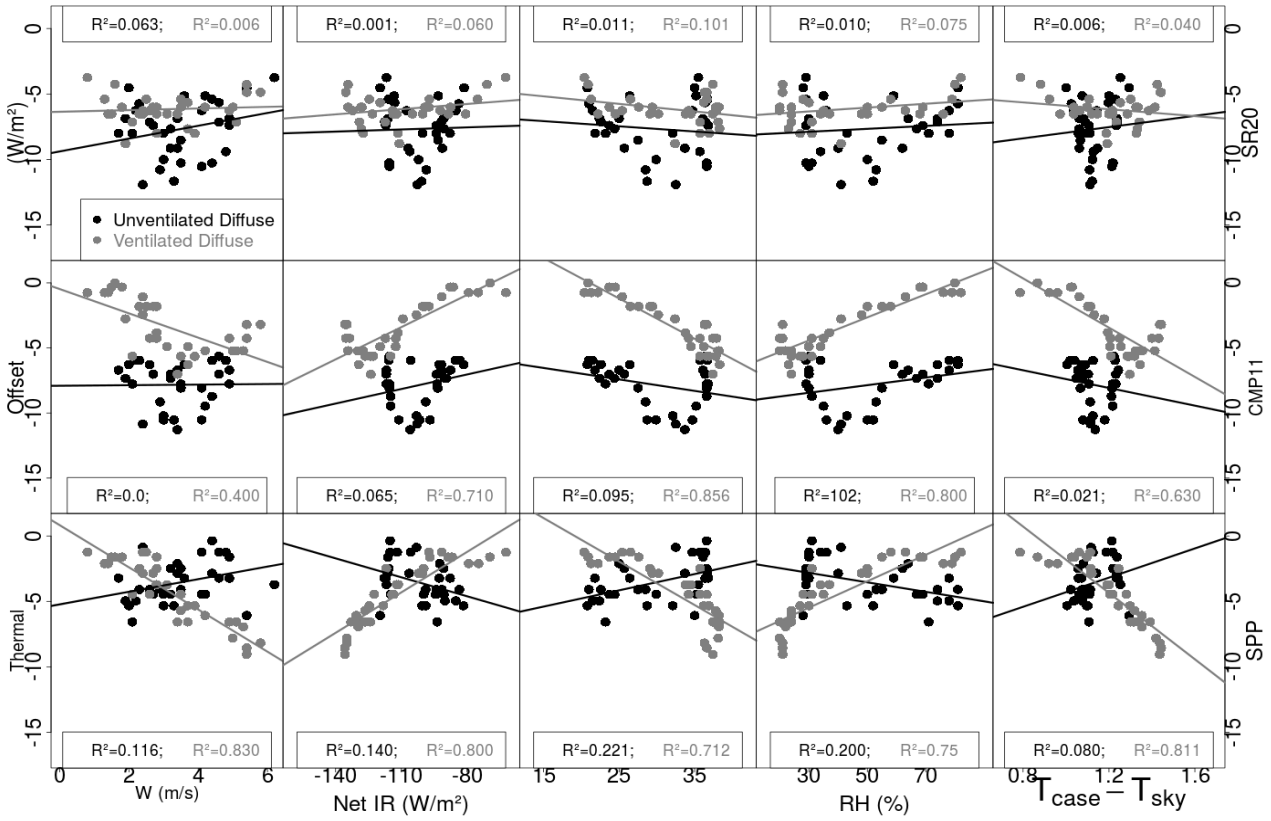

Figure 7. Dependence on the environmental conditions when the pyranometers are measuring diffuse irradiance with ventilation (red points) and without ventilation (black points)

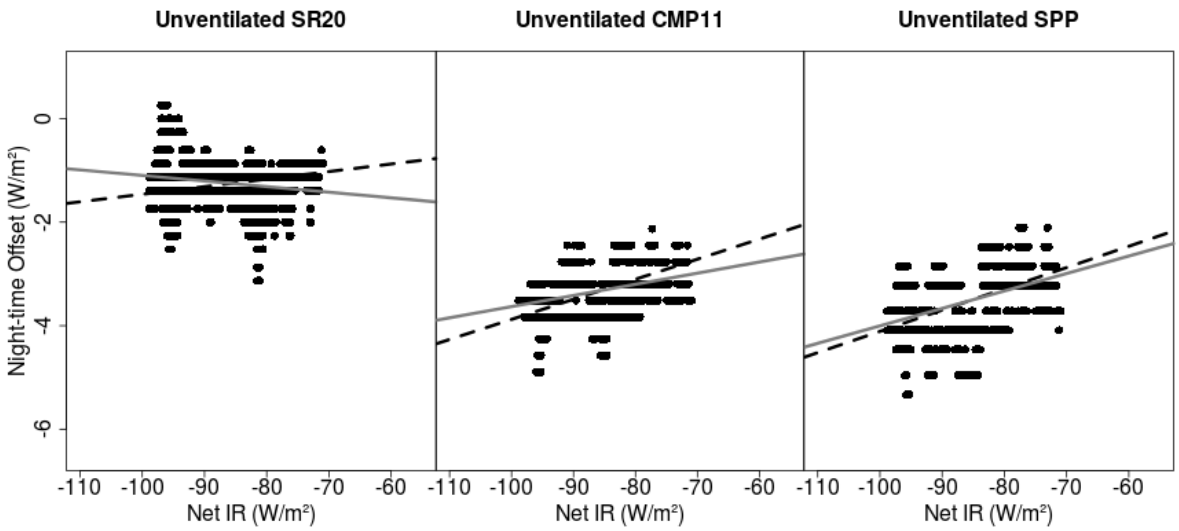

Figure 8. Unventilated nighttime thermal offset versus Net IR irradiance. Solid grey line correspond to the fitting forzed thtough (0,0) while dashed black line represent the no-forced fitting.

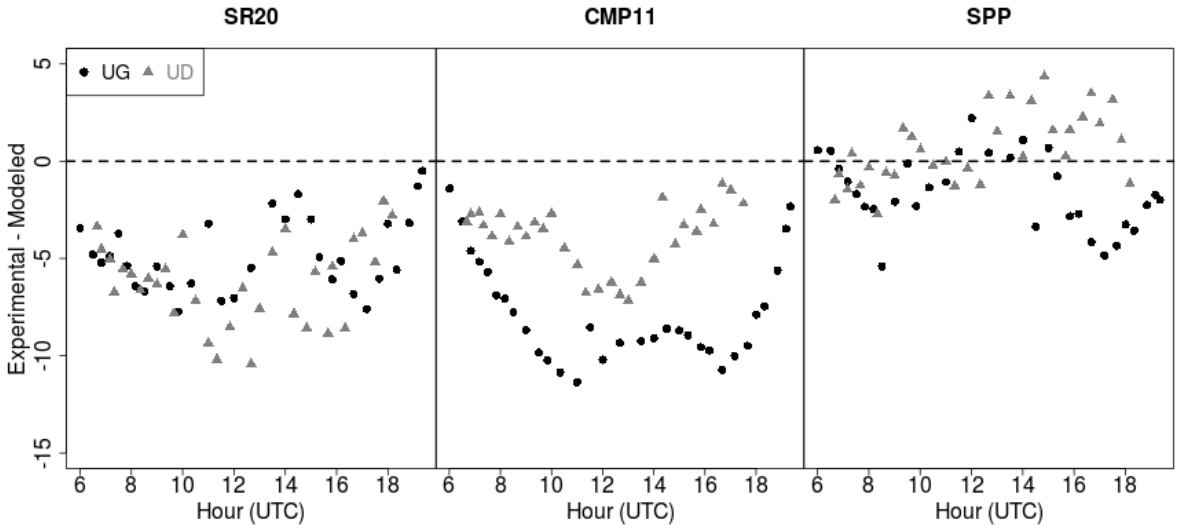

Figure 9. Absolute difference between daytime experimental thermal offset and those values estimated by the application of the Dutton et al.'s methodology (fitting forzed through (0,0)).

3.5.4. Informe del Director de la Tesis Doctoral

El artículo .Effect of mechanical ventilation on the thermal offset of pyranometers", está finalizando el proceso de revisión en la revista Journal of Atmospheric and Oceanic Technology, siendo previsible su publicación definitiva durante el año 2017, teniendo la revista un factor de impacto de 2.159 y estando incluida en el primer cuartil (Q1, ranking 2 de 14 revistas) dentro de la categoría "Engineering, Ocean".

La participación de la doctoranda Dña. Guadalupe Sánchez Hernández en este artículo ha sido muy elevada y diversa, colaborando muy activamente en todas las etapas desarrolladas para la obtención del artículo, como el diseño y realización de las medidas, el análisis de resultados y comparativa, la extracción de conclusiones y la elaboración del manuscrito. Merece la pena destacar el gran esfuerzo invertido por la doctoranda para llevar a cabo la exigente toma de medidas diseñada para el trabajo.

Todas estas las tareas han sido desarrolladas por la doctoranda bajo mi dirección y supervisión, pudiendo dar fe de que todo lo aquí expuesto es verídico.

Fdo.: El Director de la Tesis Doctoral

Por otra parte, D. Antonio Serrano Pérez y Dña. María Luisa Cancillo Fernández, coautores de este artículo, afirman mediante este escrito que han colaborado en este artículo pero que éste forma parte íntegra de la Tesis Doctoral de Dña. Guadalupe Sánchez Hernández y que no va a ser utilizado por ellos como parte de sus respectivas tesis doctorales

Dña. Mª Luisa Cancillo Fernández D. Antonio Serrano Pérez

Capítulo 4

Corrección del error introducido por el anillo de sombra

4.1. Introducción

Como ya se comentó en el Capítulo 1, debido a su diseño el anillo de sombra bloquea, además de la componente directa, la irradiancia difusa interceptada por el anillo. Esto conlleva una subestimación de la medida de irradiancia difusa por lo que estas medidas han de ser corregida.

La corrección del error asociado al uso del anillo de sombra depende de numerosos factores y varía con cada medida. Por un lado, las dimensiones del anillo y su localización geográfica determinan el ángulo sólido subtendido por el mismo [Drummond, 1956]. Por otro lado, las condiciones atmosféricas y la posición solar determinan la distribución direccional del campo de irradiancia difusa [Steven, 1984; LeBaron et al., 1990; Batlles et al., 1995]. Todos estos factores hacen que la subestimación de los valores de irradiancia total difusa medidos con este dispositivo pueda llegar a suponer entre el 9 % y el 38 % de la medida [Kudish e Ianetz, 1993]. Este error supera notablemente el valor de incertidumbre del 2 % exigido por la OMM para las medidas de irradiancia difusa de calidad [Ohmura et al., 1998; McArthur, 2005; WMO, 2014].

Dada la importancia del error producido por el anillo de sombra varios autores han propuesto diferentes modelos para su corrección. De este modo, los valores reales de irradiancia difusa ($I_{d,r}$) pueden obtenerse mediante la aplicación de un factor de corrección (C) a las medidas tomadas por un piranómetro instalado en un anillo de sombra ($I_{d,u}$) tal como refleja la siguiente expresión:

$$I_{d,r} = C \cdot I_{d,u} \tag{4.1}$$

Como una primera aproximación al problema, Drummond [1956] propuso la aplicación de un factor de corrección, C_D, basado exclusivamente en cálculos de geometría solar y bajo la hipótesis de una distribución isótropa del campo de radiación difusa. Este modelo teórico proporciona una estimación muy precisa del ángulo sólido subtendido por el anillo y puede ser aplicado en cualquier localización e intervalo espectral.

Sin embargo, la presencia y distribución espacial de nubes y aerosoles así como la variación de la posición solar hacen que la hipótesis de isotropía para el campo de radiación difusa raramente se cumpla. El propio Drummond [1956] estimó que las medidas de irradiancia difusa una vez corregidas con su modelos requerían una corrección adicional del 7 % en caso de cielos despejados y del 3 % en casos cubiertos debido a la anisotropía de la radiación. Estudios posteriores en diferentes localizaciones estimaron el valor de esta corrección adicional entre un 14 % y 30 % [Stanhill, 1985; Kudish e Ianetz, 1993].

Con el fin de corregir el efecto de la anisotropía, algunos autores propusieron nuevos modelos para la corrección del error debido al anillo de sombra. Estos nuevos modelos proponen expresiones para el factor de corrección que incorporan información sobre la distribución del campo de radiación difusa. Esta información se introduce de dos formas diferentes: 1) utilizando modelos teóricos para la distribución del campo de radiación y 2) mediante parámetros empíricos calculados a partir de datos de radiación. Entre ellos destacan el modelo teórico propuesto por Muneer y Zhang [2002] y los modelos empíricos propuestos por Steven [1984], LeBaron et al. [1990] y Batlles et al. [1995].

La revisión de los trabajos anteriormente mencionados junto con otros estudios posteriores sobre la corrección del error introducido por el anillo de sombra puso de manifiesto la existencia de importantes aspectos aún sin resolver entre los que destacan:

- Las escasez de estudios comparativos de los distintos modelos propuestos bajo las mismas condiciones meteorológicas. Aunque estos modelos han sido aplicados en numerosas ocasiones por separado, son muy pocos los estudios en los que han sido comparados [Batlles et al., 1995; Lopez et al., 2004a, 2004b; Kudish y Evseev, 2008].

- El uso de valores de irradiancia difusa estimados como diferencia de irradiancia global y directa como valores de referencia. Los valores de irradiancia difusa así estimados presentan una gran incertidumbre debido, principalmente, a la limitaciones en la respuesta angular (error coseno) del piranómetro que mide los valores de irradiancia global [Michalsky et al., 1999].

- La aplicación de los coeficientes empíricos del modelo original. A pesar del importante error que podría suponer no adaptar los modelos empíricos a las características locales propias de cada ubicación son muy escasos los estudios que han llamado la atención sobre este aspecto [Dehne, 1984].

- La ausencia de modelos para la corrección del error introducido por el anillo de sombra en medidas de irradiancia difusa ultravioleta. Entre la amplia bibliografía analizada sólo el trabajo realizado por Utrillas et al. [2007] trata este aspecto.

Todos estos aspectos han sido analizados con detalle en los dos artículos que componen este capítulo. Ambos trabajos suponen una importante contribución a la caracterización del error introducido por el anillo de sombra en las medidas de irradiancia difusa total y UV, respectivamente.

4.2. Artículo 5

4.2.1. Datos del artículo

Título: Comparison of shadow-ring correction models for diffuse solar irradiance

Autores: Guadalupe Sánchez[a]
Antonio Serrano[a]
Mª Luisa Cancillo[a]
José Agustín García[a]

Filiación: [a]Dpto. de Física, Universidad de Extremadura, Badajoz, España

Revista: *Journal of Geophysical Research-Atmosphere*
Volumen: 117 **Año de publicación:** 2012
doi: 10.1029/2011JD017346

Este artículo fue además seleccionado como "Spotlight Research". Se trata de una mención especial que reciben, de entre todos los artículos publicados en revistas de la American Geophysical Union, aquellos que destacan por la calidad de su aportación científica. Este reconocimiento dio lugar a una nota sobre nuestro artículo, titulada "New corrections for skylight estimates", publicada en la revista Eos, volumen 93, número 31, página 308, el 31 de julio de 2012.

4.2.2. Principales aportaciones del artículo

Este estudio tiene como objetivo seleccionar el modelo más adecuado para la corrección del error introducido por el anillo de sombra en las medidas de irradiancia difusa total. Con este fin se ha seleccionado un conjunto de modelos representativo de las distintas formas funcionales y variables propuestas en la bibliografía. Los modelos finalmente seleccionados han sido los propuestos por Drummond [1956], Steven [1984], LeBaron et al. [1990], Batlles et al. [1995] y Muneer y Zhang [2002].

Para este estudio se ha utilizado un año completo de datos horarios, lo que garantiza trabajar con una gran variedad de situaciones meteorológicas. A diferencia de los estudios anteriores en los que los valores de irradiancia difusa de referencia eran estimados como diferencia de irradiancia global y directa, en este trabajo, los valores de irradiancia difusa de referencia han sido medidos con un piranómetro instalado en un seguidor solar.

El primer paso, y uno de los puntos a destacar en este estudio, ha sido la reproducción de las metodologías propuestas por Steven [1984], LeBaron et al.

[1990] y Batlles et al. [1995] con medidas de nuestra estación. Con ello se han obtenido los correspondientes coeficientes empíricos para las expresiones propuestas por Steven [1984] y Batlles et al. [1995] y los factores de corrección para cada una de las 256 categorías establecida por LeBaron et al. [1990]. Aunque la particularización de estos modelos a las medidas locales pueda parecer algo trivial, no es una práctica habitual en estudios similares y podría derivar en errores importantes. Una vez los modelos empíricos fueron particularizados se han comparado con los modelos teóricos propuestos por Drummond [1956] y Muneer y Zhang [2002].

El análisis desarrollado en este artículo revela que el factor de corrección que debe aplicarse a las medidas de irradiancia total difusa medidas con anillo de sombra (4.1) en nuestra estación toma valores comprendidos entre 0.88 y 1.32. La subestimación anual promedio en las medida de irradiancia difusa fue estimada en torno a un 10.8 % pudiendo llegar a suponer hasta un 20 % en situaciones de cielos despejados. Estos valores son similares a los obtenidos previamente por otros autores [Kudish e Ianetz; 1993; Lopez et al., 2004b; Kudish y Evseev, 2008].

Como era de esperar, la adaptación a las condiciones locales de los modelos empíricos propuestos por Steven [1984], LeBaron et al. [1990] y Batlles et al. [1995], supone una mejora tanto en su tendencia central como en su dispersión. Además, dicha adaptación elimina posibles dependencias de los residuos respecto a factores como la posición solar o el índice de claridad, las cuales sí se observan en estudios en los que los modelos no son adaptados [Lopez et al., 2004a; Kidish y Evseev, 2008]. También debe mencionarse que los modelos teóricos propuestos por Drummond [1956] y Muneer y Zhang [2002] muestran un comportamiento similar al de los modelos empíricos sin adaptar. Por tanto, en caso de no ser posible la adaptación de los modelos empíricos, los modelos teóricos son igualmente válidos.

La comparación de los modelos teóricos propuestos por Durmmond [1956] y Muneer y Zhang [2002] junto con los modelos empíricos adaptados de Steven [1984], LeBaron et al. [1990] y Batlles et al. [1995] revela un mejor comportamiento de éstos últimos. El valor medio de las diferencias relativas de 10.8 % en las medidas sin corregir se reduce a 0.6 % al aplicar los modelos empíricos adaptados. Con la aplicación de estos modelos de corrección las diferencias relativas de las medidas se encuentran dentro del error del 2 % requerido por la OMM en las medidas de calidad.

4.2.3. Copia original de artículo

Comparison of shadow-ring correction models for diffuse solar irradiance

G. Sánchez,[1] A. Serrano,[1] M. L. Cancillo,[1] and J. A. García[1]

Received 20 December 2011; revised 23 March 2012; accepted 28 March 2012; published 9 May 2012.

[1] Reliable and accurate measurements of diffuse solar irradiance are needed in order to partition global irradiance into its direct and diffuse components. Diffuse irradiance is commonly measured using sun tracking systems or shadow rings. Data obtained using a shadow ring must be corrected for the portion of diffuse irradiance blocked by the ring. In this paper we have examined and evaluated six of the most widely used correction models. Approaches that account for radiation anisotropy perform notably better than those using only geometric corrections. Our results also argue for the need to adjust empirical models to local conditions. Empirical approaches developed by LeBaron et al. (1990) and by Batlles et al. (1995) perform best when compared with the more theoretical models.

Citation: Sánchez, G., A. Serrano, M. L. Cancillo, and J. A. García (2012), Comparison of shadow-ring correction models for diffuse solar irradiance, *J. Geophys. Res.*, *117*, D09206, doi:10.1029/2011JD017346.

1. Introduction

[2] Many solar radiation studies rely on a good knowledge of not only global radiation but on its direct and diffuse components as well. The accurate assessment of global and diffuse solar radiation is essential for estimating the radiation intercepted by horizontal and tilted surfaces such as hills, buildings, vegetation, and animals. In addition to meteorological studies, solar radiation data is used in many applications such as in architecture, engineering, agriculture and ecology.

[3] The amount of diffuse radiation reaching the earth's surface and its proportion to global radiation is mainly determined by the solar zenith angle, the composition of the atmosphere, and surface albedo. Most of the atmospheric constituents are relatively constant in time and space with the exception of aerosols and clouds. Their interaction with solar radiation is complex and any change of these constituents in a changing climate will affect the amount of direct and diffuse radiation reaching the earth's surface and consequently, the surface energy balance. Therefore, very accurate measurements of global, direct, and diffuse solar radiation at the earth's surface are required to suitably detect and quantify the effect of climate change on the earth's radiation balance [*Hansen et al.*, 2005; *Wild et al.*, 2005].

[4] Information on the relative amount of direct and diffuse solar irradiance that is available is also required in the rapidly developing field of renewable energy. There are presently considerable efforts being devoted to improving the efficiency of solar collectors, relying mainly on better collecting systems. An accurate knowledge of the direct and diffuse components of the radiation field is absolutely essential to achieve this goal.

[5] There are different instruments and methodologies aimed to measure solar diffuse radiation. The most precise method consists of shading the pyranometer with a small disc or ball synchronized with the sun's apparent motion. However, the technique is costly, requiring much maintenance and is unstable under strong winds. A more practical and widely used approach is to measure diffuse radiation using a shadow-ring/band. This is a robust mechanism consisting in a ring/band parallel to the sun path that blocks the direct irradiance and prevents it from reaching the sensor. It is an easy-to-operate stationary device that only requires manual adjustment of the sliding bar every few days to account for changing solar declination. The shadow band system is the most common method for measuring diffuse radiation at meteorological stations worldwide. Thus, long time series of diffuse radiation measurements using shading rings exist since the first half of the last century. Some studies have shown that measurements with shadow rings are comparable to those given by more sophisticated tracking devices under totally cloudy skies whereas in clear sky conditions some differences appear [*Ineichen et al.*, 1984].

[6] The shadow ring screens not only the sun's disc but also a substantial portion of the sky and, therefore, its measurements must be corrected for the diffuse radiation intercepted by the ring. This error can, for example, result in a monthly average error of up to 24% [*Drummond*, 1956], significantly affecting any subsequent calculation of other radiometric variables. Thus, a 5% error in the measurement of the horizontal diffuse irradiance will propagate to more than 20% in the calculated direct normal irradiance at zenith angles greater than 75° [*LeBaron et al.*, 1990]. The needed correction factor has been estimated to be between 8.9% and 37.7% [*Kudish and Ianetz*, 1993], depending on the latitude, the weather conditions and the type of the shadow ring

[1]Department of Physics, University of Extremadura, Badajoz, Spain.

Corresponding author: G. Sánchez, Department of Physics, University of Extremadura, Avda. de Elvas s/n, E-06006 Badajoz, Spain. (guadalupesh@unex.es)

0148-0227/12/2011JD017346

[*Steven*, 1984]. This uncertainty limits the accuracy of diffuse radiation measurements and makes it difficult to compare measurements performed at different locations or different seasons [*Drummond*, 1956; *Steven*, 1984]. To emphasize the importance of this correction, it must be noted that it is higher than the variation in solar radiation observed between 1961 and 1990, estimated to be around the 4–6% [*Liepert*, 2002], and higher than the accuracy of ±3% required by the World Meteorological Organization for a particular measurement to be classified as high quality [*World Meteorological Organization* (*WMO*), 2008].

[7] As a first approach to the problem, *Drummond* [1956] proposed a first correction factor as a function of the solid angle subtended by the shadow ring and its altitude above the pyranometer horizon. This model is exclusively based on solar geometry calculations and assumes an isotropic sky radiation distribution. It provides a fairly good estimation of diffuse irradiance occluded by the ring and may be applied anywhere on earth. However, the assumption of isotropy is not generally fulfilled since sky radiance directional distribution notably depends on sun elevation, atmospheric turbidity, cloudiness and usually changes with weather conditions during the day. Thus, *Drummond* [1956] estimated differences of about 7% for cloudless skies and 3% for overcast conditions between its corrected diffuse irradiance values and the reference values due to the anisotropy. Other subsequent studies quantified the additional correction for anisotropic conditions to be between 14% and 30% above the isotropic correction [*Stanhill*, 1985]. Several models have been developed in order to correct for the anisotropy effect. A straightforward modification to the Drummond's model was proposed by *Steven* [1984], who assumed a sky radiance distribution as the sum of a uniform background and a circumsolar component. On the other hand, *LeBaron et al.* [1990] developed a model which classified the different sky conditions into 256 categories as a function of three parameters describing the anisotropic contribution and the fraction of the sky hemisphere occluded by the shadow ring as estimated by *Drummond* [1956]. Using the same parameters than Le Baron et al., *Batlles et al.* [1995] proposed two correction factors as multivariate-lineal functions of these parameters. More recently, *Muneer and Zhang* [2002] have developed a new model based on the anisotropic sky-diffuse distribution theory proposed by *Moon and Spencer* [1942].

[8] Comparative studies are required in order to assess the performance and limitations of these models and their suitability at different locations in the world. However, to our knowledge, there are few comparative studies [*López et al.*, 2004a, 2004b; *Kudish and Evseev*, 2008], and even fewer for regions with similar climatic characteristics as our study site in southwestern Europe. Additionally, most recent studies applied the models using the original values of local parameters as they were proposed by their respective authors, although *Dehne* [1984] noted the need to use coefficients applicable to the local study areas. Failure to do so may create large errors since some of these models have been developed empirically and their correction factors depend on the geographical and climatic characteristics of each location.

[9] Therefore, the main objectives of this paper are to assess the performance of the models proposed by *Drummond* [1956], *Steven* [1984], *LeBaron et al.* [1990], *Batlles et al.* [1995] and *Muneer and Zhang* [2002] in estimating diffuse irradiance measured with a pyranometer and a shadow-ring at Badajoz (southwestern Spain) and to examine how the coefficients of these empirical models need to be adapted to new sites. These models will be called DR (Drummond), ST (Steven), LB (LeBaron et al.), BA or BB (Models A and B by Batlles et al.), and MZ (Muneer and Zhang) hereafter. All the mentioned models have been extensively used in different climatic regions throughout the world [*López et al.*, 2004a, 2004b; *Kudish and Evseev*, 2008] and are well considered by the scientific community. In this study we evaluate the suitability of the empirical models ST, LB, BA and BB to our study site and examine the sensitivity of the various coefficients to the estimate of diffuse radiation. Finally, these adjusted models are compared with the theoretical models DR and MZ.

2. Data

[10] Data used in this study have been acquired at the radiometric station installed in Badajoz, southwestern of Spain (38.9° N; 7.01° W; 199 m a.s.l). The site has an open horizon, free of obstacles and is operated by the Physics Department of the University of Extremadura, guaranteeing careful maintenance. The local climate is characterized by high noon solar elevation, mainly in summer, and by a high number of sunshine hours per year, with our site having one of the highest instantaneous and annual irradiance values in Europe.

[11] The data set consists of one-minute measurements of horizontal global irradiance and two simultaneous measurements of diffuse irradiance using two different methods. The diffuse solar irradiance was measured using a Kipp & Zonen CMP11 pyranometer which was shaded using a Kipp & Zonen CM121 shadow-ring with 620 mm diameter and 55 mm width. Simultaneous measurements of diffuse solar irradiance were taken by another CMP11 pyranometer mounted on a solar tracker (Kipp & Zonen Solys 2). The solar tracker has a ball that prevents the direct solar irradiance to reach the sensor. The ball only shadows the pyranometer sensor and does not obstruct any other sky portion. The correction factor for these measurements is negligible [*Ineichen et al.*, 1984] and therefore they have been used as a reference. A third Kipp & Zonen CMP11 pyranometer was used to measure global irradiance. The study period encompassed an entire year, from 7 August 2010 to 8 August 2011, therefore ensuring that a variety of seasonal processes and meteorological conditions were sampled.

[12] To guarantee the quality and comparability of measurements, both pyranometers were previously inter-compared and calibrated in a field campaign which took place in September 2009 at the Atmospheric Sounding Station of the National Institute for Aerospace Techniques (ESAt/ INTA) located at "El Arenosillo," Huelva, Spain (37.10° N, 7.06° W). The pyranometers were calibrated by intercomparison with a reference pyranometer (Kipp & Zonen CM11 pyranometer, #027771) which had been previously calibrated at the World Radiation Centre (WRC) in Davos, Switzerland. First, signals were corrected for thermal offsets estimated as the averages of values recorded for solar zenith angles higher than 100°. Then, ratios of our pyranometer signal to the signal from the reference pyranometer were estimated for a range of conditions. They proved to be largely constant so that calibration factors

were calculated as average ratios obtained during the field campaign.

[13] Additionally, the data set corresponding to the study period was subjected to a quality control procedure in order to detect and eliminate possible erroneous measurements. The data was subsequently averaged on an hourly basis and used for the analysis. This time interval is widely used in solar radiation studies since it shows the daily variations without been affected by the very fast short-term fluctuations. The hourly data set was randomly divided into two subsets. One of them, containing 75% of all data, was used to construct the empirical models and their coefficients. The second subset, consisting of the remaining 25% of the data, was used for validation purposes as well as for the analysis and model comparison.

3. Methodology

[14] The models DR and MZ result from theoretical studies which make certain assumptions regarding the sky radiance distribution. However, the only parameters involved in these models are the size of the shadow ring and the geographic coordinates, and therefore both models can be used at any location just as originally proposed by their authors. Conversely, the models ST, LB, BA and BB involve empirical local coefficients which were obtained for specific locations. In the present study, these local empirical models have been adjusted using the irradiance data acquired at the radiometric station of Badajoz. This allows us to estimate diffuse irradiance using the empirical models with and without local adjustments. Furthermore, adjusting the empirical models with local coefficients provides a better framework with which to judge their performance. For this analysis, the functional expressions for the correction factor proposed by Steven and by Batlles et al. (models ST, BA and BB) have been fitted to the 75% of the hourly data set and new regression coefficients have been estimated. In the case of the model LB, the correction factors have been calculated following the steps described in detail in the original study [*LeBaron et al.*, 1990]. The differences between original and adjusted models have been tested on the remaining 25% of the data set and the models which performed best have been selected. Subsequently, these selected locally fitted empirical models have been included, together with the globally applicable models DR and MZ in a final comparison using the second subset consisting of the remaining 25% of the data.

[15] The evaluation of the performance of the models was undertaken by graphical and statistical means. For the statistical analysis the relative root mean square error (rRMSE) and the relative mean bias error (rMBE) were calculated in order to numerically quantify the performance of the models. These statistics are defined by the follow expressions:

$$rRMSE = \sqrt{\frac{1}{N}\left(\frac{I_{i,corr} - I_{i,ref}}{I_{d,ref}}\right)^2} \quad (1)$$

$$rMBE = \frac{1}{N}\sum_{1}^{N}\left(\frac{I_{i,corr} - I_{i,ref}}{I_{i,ref}}\right) \quad (2)$$

where N is the total number of measurements, $I_{i,corr}$ is the ith-corrected measurement and $I_{i,ref}$ is the ith-reference value of diffuse irradiance as measured by the pyranometer mounted in the sun tracker device. The statistic rRMSE is a measure of the relative differences between corrected and reference values. On the other hand, the rMBE quantifies the mean bias between the corrected and reference data sets. Positive values indicate overestimation with respect to the reference measurements while negative values mean underestimation. Best models are those with these statistics close to zero.

[16] To complete the statistical analysis, the Taylor diagram [*Taylor*, 2001] was obtained. These diagrams provide a way of graphically summarizing how closely a model matches the reference observations.

[17] Differences between the reference diffuse irradiance measurements and the diffuse irradiance corrected using the original and adjusted models have been evaluated. In addition to the magnitude of the differences, their behavior versus time and other parameters such as the clearness index, the diffuse portion, and the solar zenith angle have been also analyzed.

4. Shadow Ring Correction Models

[18] The error in the diffuse irradiance measurements caused by the use of a shadow ring has been extensively studied. This error causes an underestimation of the measurement because the ring blocks a certain amount of sky radiance that should be incident on the sensor. The corrected diffuse irradiance on an horizontal surface $I_{d,c}$ may then be written as:

$$I_{d,c} = C \cdot I_{d,u} \quad (3)$$

where C is the correction factor and $I_{d,u}$ is the uncorrected horizontal diffuse irradiance measured by the pyranometer installed on a shadow ring.

[19] Several authors have proposed different models for this correction factor. The main characteristics of the six widely used models analyzed in this paper are presented in the following sections. A more detailed description can be found in the literature [*Drummond*, 1956; *Steven*, 1984; *LeBaron et al.*, 1990; *Batlles et al.*, 1995; *Muneer and Zhang*, 2002].

4.1. Drummond: Model DR

[20] *Drummond*'s [1956] model estimates the fraction F of diffuse irradiance that is blocked by a shadow ring with an axis parallel to the polar axis. This model was developed under the following assumptions: (1) the ring width is small compared to its radius, (2) the sensor is negligible in size compared to the other dimensions, (3) there is no back-reflection of radiation from the inner surface of the ring, and (4) the sky radiance distribution was isotropic. With these conditions the diffuse fraction F may be written as:

$$F = \left(\frac{2b}{\pi r}\right)\cos^3\delta(\omega_s \sin\phi \sin\delta + \cos\phi\cos\delta\sin\omega_s) \quad (4)$$

where r is the radius and b is the width of the ring, ω_s the hour angle at sunset in radians, δ the solar declination, and ϕ

the latitude of the location. The correction factor proposed in this model is:

$$C_D = \frac{1}{1-F} \tag{5}$$

4.2. Steven: Model ST

[21] Based on previous studies, *Steven* [1984] proposed a new model for the correction factor to use under clear conditions. This model introduces an additional anisotropy factor independent of the geometrical correction. The main hypothesis is that the sky radiance distribution is the sum of a uniform background and a circumsolar component. The correction factor proposed is:

$$C_S = \frac{I_{d,ref}}{I_{d,u}} = \frac{1}{1-FQ} \tag{6}$$

where F is the fraction of diffuse irradiance occluded by the ring given by the equation (4) and Q is the anisotropy correction factor calculated using the follow expressions:

$$Q = 1 - C'\xi + \frac{C'}{f} \tag{7}$$

$$f = \omega_s \sin\phi \sin\delta + \cos\phi \cos\delta \sin\omega_s \tag{8}$$

where C′ expresses the relative strength of the circumsolar component and ξ is the angular width of the circumsolar region. These coefficients can be obtained by means of a regression analysis of Q values (calculated from equation (6) as a function of the reference diffuse irradiance, uncorrected diffuse irradiance and the portion of diffuse irradiance blocked by the ring) versus 1/f values.

4.3. LeBaron et al.: Model LB

[22] The model proposed by *LeBaron et al.* [1990] describes anisotropic sky conditions by means of three parameters. One of these parameters, ε, describes the cloud conditions and is defined as:

$$\varepsilon = \frac{I_{d,u} + I_{nb}}{I_{d,u}} \tag{9}$$

where $I_{d,u}$ is the uncorrected diffuse irradiance and I_{nb} is the uncorrected direct normal irradiance which can be calculated from the global and uncorrected diffuse irradiance.

[23] The second parameter Δ is a brightness index which is a function of the cloud thickness or aerosol loading [*Perez et al.*, 1990]. It is defined as:

$$\Delta = \frac{I_{d,u} \cdot m}{I_0} \tag{10}$$

where m is the relative optical air mass and I_0 is the irradiance at the top of the atmosphere.

[24] The third parameter is the solar zenith angle θ. These three parameters, together with the isotropy correction C_D proposed by *Drummond* [1956], are used to classify the different sky conditions into 256 categories. These categories are the results of the combination of the four possible values that each parameter can take. The range of each parameter was divided in four subintervals. Subsequently, the reference and uncorrected diffuse irradiance measurements were classified according to the categories defined by the combination of the parameters and, finally, the correction factor for each category was obtained as the average of the ratio between the reference diffuse irradiance measurements and the uncorrected diffuse irradiance measurements. More details can be found in *LeBaron et al.* [1990].

4.4. Batlles et al.: Models BA and BB

[25] Based on the same parameters utilized in model LB, *Batlles et al.* [1995] built two new models to correct the diffuse irradiance measured with shadow rings. Both models use a multiple linear regression of these parameters to obtain the correction factors. In this paper these models will be called BA and BB.

4.4.1. Model BA

[26] This first model proposes an unique expression of the correction factor for all sky conditions:

$$C_{BA} = aC_D + b\log\Delta + c\log\varepsilon + de^{(-1/\cos\theta)} \tag{11}$$

where C_D, ε and Δ were defined in equations (5), (9) and (10) respectively and a, b, c, and d areempirical parameters.

4.4.2. Model BB

[27] After the geometric correction, the parameter ε is the second most significant parameter in the correction factor analysis. Based on this fact, *Batlles et al.* [1995] proposed different multiple linear regressions with appropriate functions of C_D, Δ, and θ for different ranges of ε. The resultant model is described by the following set of equations:

$$C_{BB} = a_1 C_D + b_1 \log\Delta + d_1 e^{(-1/\cos\theta)} \quad \varepsilon \le 3.5 \tag{12a}$$

$$C_{BB} = a_2 C_D + b_2 \log\Delta + d_2 e^{(-1/\cos\theta)} \quad 3.5 < \varepsilon \le 8 \tag{12b}$$

$$C_{BB} = a_3 C_D + b_3 \log\Delta \quad 8 < \varepsilon \le 11 \tag{12c}$$

$$C_{BB} = a_4 C_D + b_4 \log\Delta \quad 11 < \varepsilon \tag{12d}$$

where a_1, b_1, d_1, a_2, b_2, d_2, a_3, b_3, a_4, and b_4 are obtained by regression analysis. More details can be found in *Batlles et al.* [1995].

4.5. Muneer and Zhang: Model MZ

[28] *Muneer and Zhang* [2002] developed a methodology similar to the one applied in model DR but using a new irradiance distribution. This irradiance distribution was based on the model proposed by *Moon and Spencer* [1942] and revised by *Muneer* [1990]. According to this model, the sky radiance distribution is two dimensional and function of any given sky patch geometry (sky patch altitude and azimuth) and the position of the sun. This new irradiance distribution can be used to estimate the total diffuse irradiance that is blocked by the shadow ring as follows:

$$D = \frac{b}{r} L_z \cos^3\delta \left[\frac{I_1 + b_1 I_2}{1 + b_1}\right] \tag{13}$$

Table 1. The rRMSE and rMBE Values for the Original and Adjusted Models

		Original Models		Adjusted Models	
Model	Author	rRMSE (%)	rMBE (%)	rRMSE (%)	rMBE (%)
ST	Steven	4.02	1.19	3.35	−0.04
LB	LeBaron et al.	4.67	−1.20	2.61	0.01
BA	Batlles et al.	4.47	0.65	3.42	0.05
BB	Batlles et al.	4.39	0.78	3.20	0.01

where L_z is the zenith radiance, b is the width of the shadow ring, r is its radio, and δ is the solar declination. Parameters I_1 and I_2 are defined by the follow expressions:

$$I_1 = \omega_s \sin\phi \sin\delta + \cos\phi \cos\delta \sin\omega_s \tag{14}$$

$$I_2 = \omega_s \sin^2\phi \sin^2\delta + 2 \sin\omega_s \sin\phi \cos\phi \sin\delta \cos\delta + \cos^2\phi \cos\delta \left[\frac{\omega_s}{2} + \frac{\sin 2\omega_s}{4}\right] \tag{15}$$

Using this same irradiance distribution, the total diffuse irradiance I_d is calculated by means of numerical integration which gives the following expression:

$$I_d = \frac{\pi L_z}{6}\left[\frac{3 + 2b_1}{1 + b_1} + \frac{3 + 2b_2}{1 + b_2}\right] \tag{16}$$

where b_1 and b_2 are radiance distribution indices for the sky quadrants containing the sun and the opposed quadrant, respectively, which are estimated as follows:

$$\text{If} \quad k_t > 0.2 \quad b_1 = \frac{3.6 - 10.46k_t}{-0.4 + 6.974k_t} \tag{17a}$$

$$b_2 = \frac{1.565 - 0.990k_t}{0.957 + 0.660k_t} \tag{17b}$$

$$\text{If} \quad k_t \le 0.2 \quad b_1 = b_2 = 1.68 \tag{18}$$

Finally, the correction factor given by this model is:

$$C_M = \frac{1}{1 - \frac{D}{I_d}} \tag{19}$$

5. Results and Discussion

5.1. Fitting Local Models

[29] The empirical models ST, LB, BA and BB were fitted to local conditions and the resulting parameters compared with the original parameters listed by the authors in order to assess their general validity. The new correction factors of the models ST, BA and BB were obtained by means of regression analyses using 75% of the data measured at our radiometric station. Similarly, the model LB was adjusted to local conditions using the same 75% data set. Subsequently, the new adjusted models were compared with the original models using the remaining 25% of the data.

[30] Diffuse irradiance corrections using the original and modified methods are compared next. Differences in the estimation of diffuse irradiance between the original and the adjusted model ST can be up to 4.7% and with a mean of 3.1%. The mean difference is 3.2% for the model LB, although individual values can exceed 16.0% and differences are higher than 5% in 15.7% of the cases examined. Mean differences of 1.7% and 2.0% are obtained for models BA and BB with largest differences of up to 15% and 9.2% respectively being reached in high solar zenith angle conditions. The generally low values in the mean difference found for models BA and BB could be explained by the fact that these models were originally developed for two Spanish sites in a geographical region similar to ours. However, dispersion is high when considering individual differences in all of the above three models. One possibility could be that errors are introduced by the parameters ε and Δ, related to cloud cover and brightening conditions, and which might not be totally applicable and valid for our region.

[31] In the above paragraph we examined how the modified models differed from the originals. Here we assess the performance of these modified models against a reference diffuse measurement which is considered a true value. The rRMSE and rMBE values with respect to the reference measurements were obtained for the original and for the adjusted models (Table 1). The aim of this analysis is to check the improvement achieved by the adjusted models. It may be observed that the biases shown by the original models are largely eliminated in the adjusted models which approach zero. The rRMSE values improve by 0.67% for the model ST (from 4.02% to 3.35%) and by 2.06% for the model LB (from 4.67% to 2.61%). It may be concluded that use of empirical models with locally derived coefficients considerably improves the diffuse correction process in shadow-ring measurements. This supremacy of adjusted models relies on their ability to be adapted to locally specific atmospheric and surface albedo conditions.

[32] *Kudish and Ianetz* [1993] estimated the magnitude of the shadow-ring correction factor to be between 8.9% and 37.7%. In our study we obtained a mean difference of 10.8% between the uncorrected and the reference diffuse irradiance measurement. These differences are considerable and therefore any improvement in the correction methodology is valuable and justified. An overall assessment is performed in the next section where the locally fitted version of the empirical models are compared with the globally valid theoretical models DR and MZ.

5.2. Comparative Analysis of the Models

[33] Figures 1a–1g show the uncorrected and corrected diffuse irradiances versus the reference diffuse irradiances for the six models. In general, the measurements exhibit a better performance when corrections are applied. However, although the correction applied by the model DR notably improves the estimation of diffuse irradiance, it still underestimates the reference values. Conversely, this underestimation is no longer evident in the correction models which consider anisotropy. However, all model/reference differences feature much scatter when diffuse irradiance values are high. This is likely due to the large variety of possible diffuse radiation values associated with cloudy conditions.

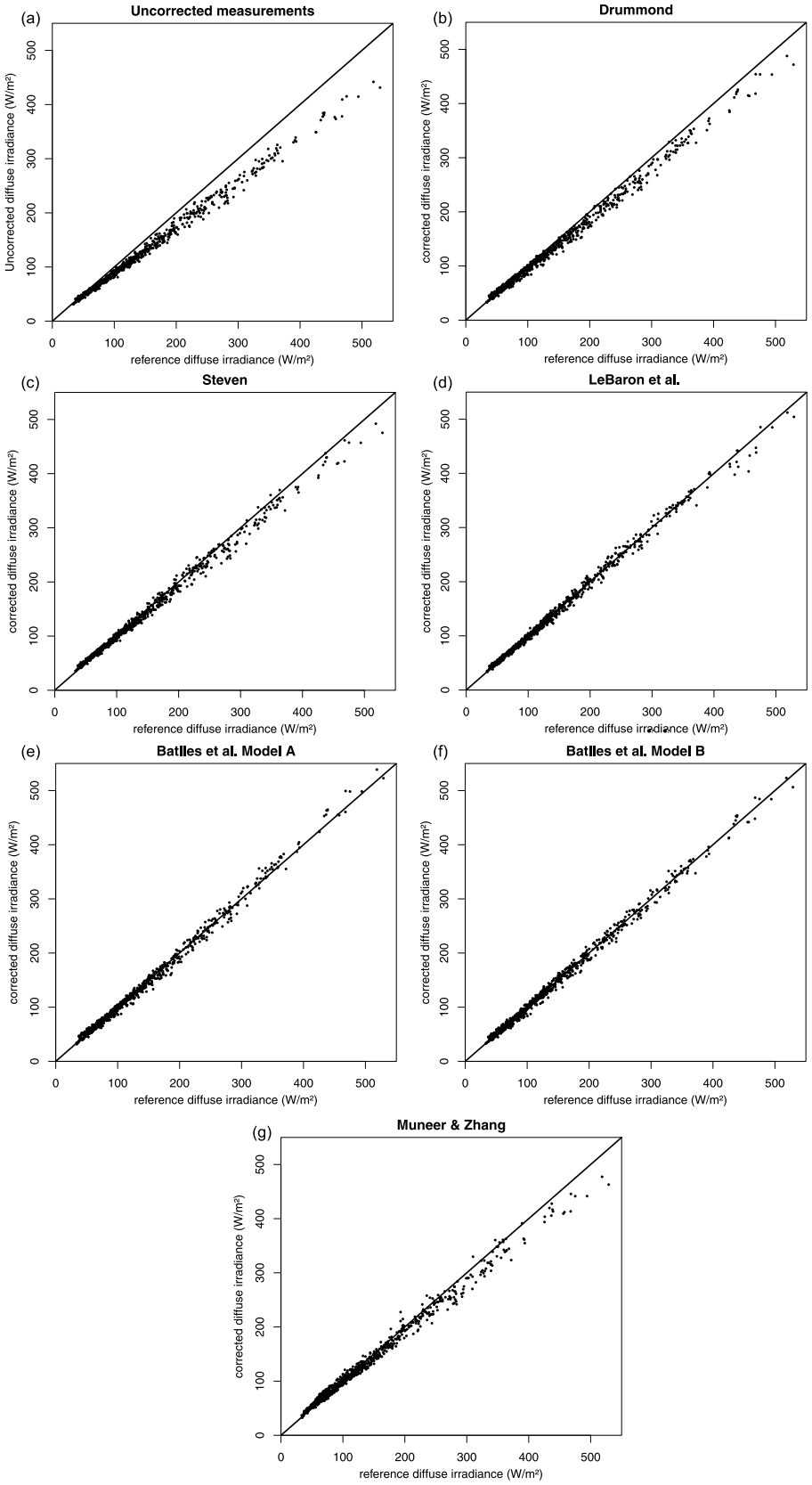

Figure 1. (a) Uncorrected and (b–g) corrected diffuse irradiances versus the reference diffuse irradiances for the six models.

Table 2. Values of rRMSE and rMBE for Uncorrected Measurement and for Corrected Measurements Using the Correction Models Shown Here

Model	rRMSE (%)	rMBE (%)
Uncorrected	7.48	−4.29
DR	4.35	−1.43
ST	3.35	−0.04
LB	2.61	0.05
BA	3.42	0.01
BB	3.20	0.01
MZ	4.34	0.06

[34] Table 2 shows the statistics rRMSE and rMBE for the uncorrected measurements and the various correction models versus the reference measurements. While the rRMSE for uncorrected measurements is about 7.48%, it decreases to values between 2.61% and 4.34% for the corrected measurements. According to this statistic, the model with the best performance is model LB (2.61%) followed by the model BB (3.20%). By contrast the models with the highest rRMSE values are the globally valid theoretical models DR and MZ. All models with the exception of DR estimate diffuse irradiance with a low rMBE. The model DR shows an underestimation in the rMBE of −1.4% as it does not consider the anisotropy in the spatial distribution of the radiation field.

[35] Results also indicate that the locally fitted empirical models (ST, LB, BA and BB) perform better than the globally valid theoretical models (DR and MZ). We also note the fairly good performance shown by the model ST despite being originally developed for cloudless conditions. This good general behavior may be related to the fact that cloudless conditions are very frequent in our region. The best performance is achieved by the model LB followed by the models Ba and BB. These three models feature the parameters ε and Δ that seem to describe the anisotropy effect better than other model parameters such k_t in the model MZ, or the circumsolar region characteristics, C and ξ, in the model ST. The main difference between these two best-performing models is that, while the model LB estimates the correction factor as a direct average of a certain subset of the experimental data, models BA and BB propose specific functional expressions which are fitted by regression. On the negative side we note that the model LB needs a considerable amount of computation to obtain a calibration factor for each of the 256 categories.

[36] In order to have a complete comparison of the performance of the different models, the Taylor diagram was plotted (Figure 2). This diagram provides a graphical summary of different aspects of the performance of a model, such as the centered root-mean square error, the correlation and the magnitude of its differences with respect to the reference values [*Taylor*, 2001]. Therefore, it is a suitable tool for model comparison. Figure 2 shows the very good performance of the models LB, BB and BB, followed by the models ST, DR and MZ, and ending with the uncorrected measurements.

[37] An additional analysis was performed in order to better understand the reasons for the differences between the various models and the reference measurement. These differences were analyzed as a function of the solar zenith angle, the clearness index, and the ratio of diffuse-to-global solar irradiance k_d. No significant dependence was found with the solar altitude or with the clearness index, but certain differences between models appeared in the case of k_d (Figure 3). While the models LB, BB and BA suitably account for the dependence with k_d, the models DR, ST and MZ correct for this dependence only partially.

6. Conclusions

[38] In this study, the six most widely used models for correcting horizontal diffuse irradiance measured with a shadow ring have been analyzed and compared. First, the

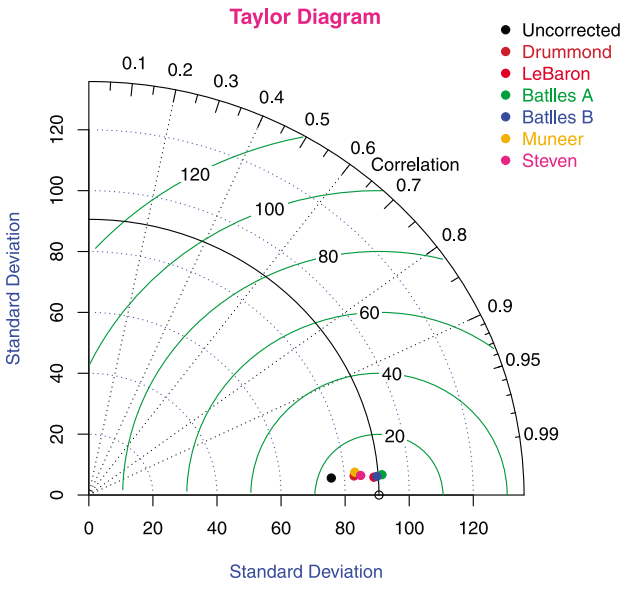

Figure 2. Taylor diagram.

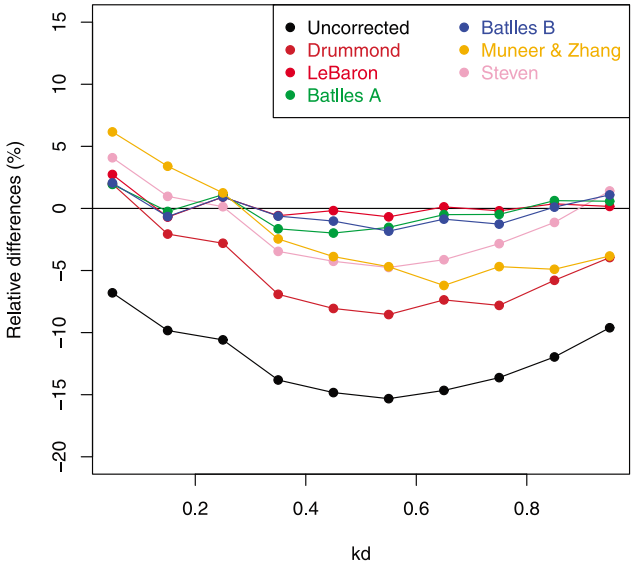

Figure 3. Dependence of relative differences on the ratio of diffuse-to-global solar irradiance k_d.

parameters of the empirical models ST, LB, BA and BB were adjusted for local conditions as determined by our radiometric measurements in Badajoz, southwestern Europe. The locally fitted versions of the original empirical models significantly improved the estimation as determined by the central tendency (quantified by rMBE) and the dispersion (quantified by rRMSE). We conclude that adjusting the empirical coefficients for local atmospheric and surface albedo conditions is warranted and recommend this procedure in other environments that may differ from ours or from the environment associated with the original model development.

[39] These locally fitted versions of the empirical models were subsequently compared with the globally valid theoretical models DR and MZ. Results show the remarkable improvement achieved by the models which account for radiation anisotropy as contrasted with the model DR which considers only a geometrical correction factor. The locally fitted empirical models perform notably better than the globally valid theoretical models. In particular, the models LB, BB and BA performed best, exhibiting the lowest values of both the rRMSE and rMBE statistics. All these results are also confirmed by the global comparison performed by means of the Taylor diagram.

[40] The analysis of residuals shows that they are independent of both solar zenith angle and clearness index in all models. However, the models ST, DR and MZ proposed by Steven, Muneer and Zhang, and by Drummond show certain dependence of their residuals on k_d, while the models LB, BB and BA show no dependence.

[41] All these results argue for the use of locally adjusted empirical models in order to correct for errors caused by the shadow ring when measuring solar diffuse irradiance. The model LB developed by LeBaron et al., and the models BB and BA by Battles et al. performed best for our specific location.

[42] This study has made a positive contribution to the methodology of measuring accurately the diffuse solar irradiance at the earth's surface. Therefore, it provides useful information for future studies which focus on estimating precisely the earth's radiation balance or studies which attempt to quantify the solar radiation resource for renewable energy applications.

[43] **Acknowledgments.** This study was partially supported by the research projects CGL2008-05939-C03-02/CLI and CGL2011-29921-C02-01 granted by the "Ministerio de Ciencia e Innovación" from Spain. The authors thank Manuel Nunez for proofreading the text.

References

Batlles, F. J., F. J. Olmo, and L. Alados-Arboleda (1995), On shadow band correction methods for diffuse irradiance measurements, *Sol. Energy*, *54*, 105–114, doi:10.1016/0038-092X(94)00115-T.

Dehne, K. (1984), Diffuse solar radiation measured by the shade ring method improved by a correction formula, *Rep. 15*, World Meteorol. Org., Geneva, Switzerland.

Drummond, A. J. (1956), On the measurement of sky radiation, *Arch. Meteorol. Geophys. Bioklimatol., Ser. B*, *7*, 413–436, doi:10.1007/BF02242969.

Hansen, J., et al. (2005), Earth's energy imbalance: Confirmation and implications, *Science*, *308*, 1431–1435, doi:10.1126/science.1110252.

Ineichen, P., J. M. Gremaud, O. Guisan, and A. Mermoud (1984), Study of the corrective factor involved when measuring the diffuse solar radiation by use of the ring method, *Sol. Energy*, *32*, 585–590, doi:10.1016/0038-092X(84)90133-6.

Kudish, A. I., and E. G. Evseev (2008), The assessment of four different correction models applied to the diffuse radiation measured with a shadow ring using global and normal beam radiation measurements for Beer Sheva, Israel, *Sol. Energy*, *82*, 144–156, doi:10.1016/j.solener.2007.06.006.

Kudish, A. I., and A. Ianetz (1993), Analysis of diffuse radiation data for Beer Sheva: Measured (shadow ring) versus calculated (global-horizontal beam) values, *Sol. Energy*, *51*, 495–503, doi:10.1016/0038-092X(93)90134-A.

LeBaron, B. A., J. J. Michalsky, and R. Perez (1990), A simple procedure for correcting shadow band data for all sky conditions, *Sol. Energy*, *44*, 249–256, doi:10.1016/0038-092X(90)90053-F.

Liepert, B. G. (2002), Observed reductions of surface solar radiation at sites in the United States and worldwide from 1961 to 1990, *Geophys. Res. Lett.*, *29*(10), 1421, doi:10.1029/2002GL014910.

López, G., T. Muneer, and R. Claywell (2004a), Assessment of four shadow band correction models using beam normal irradiance data from the United Kingdom and Israel, *Energy Convers. Manage.*, *45*, 1963–1979, doi:10.1016/j.enconman.2003.11.001.

López, G., T. Muneer, and R. Claywell (2004b), Comparative study of four shadow band diffuse irradiance corrections algorithms for Almeria, Spain, *J. Sol. Energy Eng.*, *126*, 696–701, doi:10.1115/1.1666895.

Moon, P., and D. E. Spencer (1942), Illumination from a non-uniform sky, *Trans. Illum. Eng. Soc.*, *37*, 707–725.

Muneer, T. (1990), Solar radiation model for Europe, *Build. Serv. Eng. Res. Technol.*, *11*, 153–163.

Muneer, T., and X. Zhang (2002), A new method for correcting shadow band diffuse irradiance data, *J. Sol. Energy Eng.*, *124*, 34–43, doi:10.1115/1.1435647.

Perez, R., P. Ineichen, R. Seals, J. J. Michalsky, and R. Steward (1990), Modelling daylight availability and irradiance components from direct and global irradiance, *Sol. Energy*, *44*, 271–289, doi:10.1016/0038-092X(90)90055-H.

Stanhill, G. (1985), Observations of shade-ring corrections for diffuse sky radiation measurements at the dead sea, *Q. J. R. Meteorol. Soc.*, *111*(470), 1125–1130, doi:10.1256/smsqj.47012.

Steven, M. D. (1984), The anisotropy of diffuse solar radiation determined from shade-ring measurements, *Q. J. R. Meteorol. Soc.*, *110*, 261–270, doi:10.1002/qj.49711046317.

Taylor, K. E. (2001), Summarizing multiple aspects of model performance in a single diagram, *J. Geophys. Res.*, *106*, 7183–7192, doi:10.1029/2000JD900719.

Wild, M., H. Gilgen, A. Roesch, A. Ohmura, C. N. Long, E. G. Dutton, B. Forgan, A. Kallis, V. Russak, and A. Tsvetkov (2005), From dimming to brightening: Decadal changes in solar radiation at Earth's surface, *Science*, *308*, 847–850, doi:10.1126/science.1103215.

World Meteorological Organization (WMO) (2008), *Guide to Meteorological Instruments and Methods of Observation*, 7th ed., Geneva, Switzerland.

4.2.4. Informe del Director de la Tesis Doctoral

El artículo Çomparison of shadow-ring correction models for diffuse solar irradiance", fue publicado en la revista Journal of Geophysical Research - Atmospheres en mayo de 2012, teniendo la revista un factor de impacto en 2012 de 3.174 y estando incluida en el primer cuartil (Q1, ranking 23 de 172 revistas) dentro de la categoría "Geosciences, Multidisciplinary".

La participación de la doctoranda Dña. Guadalupe Sánchez Hernández en este artículo ha sido muy elevada y diversa, colaborando muy activamente en todas las etapas desarrolladas para la obtención del artículo, destacando su trabajo en la toma de medidas, implementación de los diferentes modelos y cálculo, análisis de los resultados y comparativa entre modelos, extracción de conclusiones y elaboración del manuscrito.

Todas estas las tareas han sido desarrolladas por la doctoranda bajo mi dirección y supervisión, pudiendo dar fe de que todo lo aquí expuesto es verídico.

Fdo.: El Director de la Tesis Doctoral

Por otra parte, D. Antonio Serrano Pérez, Dña. María Luisa Cancillo Fernández y D. José Agustín García García, coautores de este artículo, afirman mediante este escrito que han colaborado en este artículo pero que éste forma parte íntegra de la Tesis Doctoral de Dña. Guadalupe Sánchez Hernández y que no va a ser utilizado por ellos como parte de sus respectivas tesis doctorales.

Dña. Mª Luisa Cancillo Fernández D. José Agustín García García

4.3. Artículo 6

4.3.1. Datos del artículo

Título: Shadow-band correction for diffuse ultraviolet radiation measurements

Autores: Guadalupe Sánchez[a]
Antonio Serrano[a]
Mª Luisa Cancillo[a]

Filiación: [a]Dpto. de Física, Universidad de Extremadura, Badajoz, España

Revista: *Journal of Geophysical Research-Atmosphere*

Volumen: 118 **Páginas:** 1-10 **Año de publicación:** 2013

doi: 10.1002/jgrd.50361

4.3.2. Principales aportaciones del artículo

Este trabajo tiene como principal objetivo proponer modelos para la corrección del error introducido por una banda de sombra en medidas de irradiancia difusa UV. Para ello se han tomado como punto de partida algunos de los modelos propuestos para la corrección de este error en medidas de irradiancia difusa total.

Los modelos elegidos como puntos de partida para este estudio fueron los propuestos por Drummond [1956], Steven [1984] y Batlles et al. [1995]. En este trabajo no ha sido incluido el modelo propuesto por Muneer y Zhang [2002], ya que dicho modelo parte del modelo de distribución del campo de radiación difusa para el espectro solar total propuesto por Moon y Spencer [1942]. Por tanto los coeficientes y expresiones que finalmente se obtuvieron para el modelo de Muneer y Zhang son propias del espectro solar total y, en principio, podrían no ser adecuadas para el rango de longitudes de onda del UV. Basándonos en los resultados del Artículo 5, también decidimos no incluir el modelo propuesto por LeBaron et al. [1990]. Se trata de un modelo complejo a nivel computacional lo que dificulta su aplicación. Al mismo tiempo, los modelos propuestos por Batlles et al. [1995] incorporan sus mismos parámetros para la descripción de la anisotropía del campo de radiación difusa y su adaptación es mucho más sencilla. Es por ello que ser prefirió la incorporación de estos últimos a este nuevo estudio.

La banda de sombra utilizada en este estudio fue cedida por el centro territorial de AEMet en Extremadura y su uso habitual hasta entonces había sido la medida de irradiancia difusa total. Es por ello que esta banda tuvo que ser adaptada para la medida de irradiancia difusa UV tendiendo en cuenta la diferencia en altura de los

piranómetros y los radiómetros de UV. Finalmente se ha trabajado con dos años de datos horarios de medidas simultáneas de irradiancia difusa medida con esta banda de sombra y con un seguidor solar. Estas últimas son las medidas tomadas como referencias, lo que supone una importante mejora respecto a estudios anteriores.

Otro de los aspectos a destacar de este estudio es la revisión de las dependencias propuestas en los modelos empíricos originales y su adaptación al rango de longitudes de onda UV. Debe tenerse en cuenta que tanto la proporción y como la distribución espacial de la componente difusa total y UV pueden ser notablemente diferentes debido a la mayor efectividad de los procesos de dispersión para longitudes de onda más cortas [Ireland y Sacher, 1996; Grant y Heisler, 1997; Grant y Gao, 2003]. Ambos aspectos juegan un papel fundamental en el error inducido por el anillo de sombra, y por lo tanto, tanto los coeficientes como las dependencias funcionales de los modelos empíricos podrían variar notablemente como ha demostrado este estudio. Este análisis ha llevado, por ejemplo, a prescindir del Modelo B propuesto por Batlles et al. [1995] ya que no se observa un comportamiento a trozos respecto a una de las variables del modelo en el rango de longitudes de onda UV.

De la comparación de las medidas de irradiancia UV difusa medidas con anillo de sombra y las medidas de referencia se ha obtenido valores del factor de corrección comprendidos entre 1 y 1.3. Este rango de valores es similar al obtenido en el Artículo 5 para el factor de corrección que debe aplicarse a las medidas de irradiancia difusa total medidas con anillo de sombra. El valor medio de las diferencias relativas del error introducido por la banda de sombra en este intervalo espectral es de un 14.0 %.

Finalmente, se han propuesto dos modelos empíricos para la corrección del error del anillo de sombra en las medidas de irradiancia difusa UV. Estos han sido comparados con el modelo teórico propuesto por Drummond [1956] el cual no requiere ningún tipo de adaptación a este nuevo intervalo espectral de estudio. Los modelos empíricos Steven* y Batlles A* propuestos en este trabajo muestran los mejores resultados. Sin embargo, no es sencillo cuál de ellos es el mejor. Mientras que el modelo Steven* muestra los valores más bajos de los estadísticos rMBE y rRMSE, sólo las diferencias relativas entre las medidas corregidas con modelo Batlles A* son independientes de las distintas variables analizadas.

Este estudio confirma la idoneidad de la banda de sombra para la medida de irradiancia difusa ultravioleta. Dado el bajo coste de este dispositivo y su robustez su incorporación en estaciones radiométricas de todo el mundo podría impulsar la

obtención de medidas de irradiancia difusa UV. A su vez, estas nuevas podrían ser utilizadas para validar los modelos propuestos en este trabajo en otras localizaciones.

4.3.3. Copia original de artículo

JOURNAL OF GEOPHYSICAL RESEARCH: ATMOSPHERES, VOL. 118, 1–10, doi:10.1002/jgrd.50361, 2013

Shadow-band correction for diffuse ultraviolet radiation measurements

G. Sánchez,[1] A. Serrano,[1] and M. L. Cancillo[1]

Received 27 November 2012; revised 20 March 2013; accepted 21 March 2013.

[1] Although the correction of shadow-band solar total diffuse measurements has been extensively studied, the case of diffuse ultraviolet measurements has not been properly addressed. This study analyzes the correction factor to be applied to experimental measurements performed adapting a shadow-band to a UV radiometer at a radiometric station in Badajoz (Spain). Three different models, based on approaches widely used for correcting total diffuse measurements, have been revised and adapted for the ultraviolet spectral range. Results reveal that some aspects of the correction proposed for total diffuse radiation are not suitable for ultraviolet diffuse radiation. The mathematical expressions are consequently modified to match the behavior in the ultraviolet range. Thus, three correction models particularized for ultraviolet diffuse measurements are proposed and validated against experimental data. The two models adapted from the original expressions proposed by Battles et al., and Steven show the best performance, with rRMSE of 2.74% and 2.20% and rMBE of 1.53% and 0.46%, respectively.

Citation: Sánchez, G., A. Serrano, and M. L. Cancillo (2013), Shadow-band correction for diffuse ultraviolet radiation measurements, *J. Geophys. Res. Atmos.*, *118*, doi:10.1002/jgrd.50361.

1. Introduction

[2] Monitoring the solar ultraviolet (UV) radiation that reaches the earth's surface after crossing the atmosphere is of great interest due to its impact on biological organisms, particularly on human health. Although low doses of UV radiation are beneficial for the synthesis of vitamin D3 [*Webb et al*., 1988; *Glerup et al*., 2000; *Holick*, 2004], an excessive exposure has adverse consequences favoring skin cancer, immune suppression, DNA damage, erythema, and eye disorders [*CIE*, 1987; *Diffey*, 2004; *Heisler*, 2010]. In addition, an increase in UV radiation doses can cause detrimental effects on plant growth, photosynthesis, and aquatic ecosystems [*Diffey*, 1991; *Musil et al*., 2002; *McKenzie et al*., 2003; *Häder* et al., 2011].

[3] This topic acquires even more interest in the framework of the long-term changes of the UV solar radiation, mainly driven by changes in total ozone, with QBO and stratospheric depletion as principal sources of variability [*Zerefos et al*., 1998]. Thus, after the monotonic negative decline from the late 1970s to the mid 1990s due to the release of Chlorofluoro-carbons, Halons, and other ozone-depleting substances, total ozone has not decreased further [*WMO*: *Scientific Assessment of Ozone Depletion*, 2010] or even increased [*Harris et al*., 2008; *Zerefos et al*., 2012]. Now it is interesting to observe whether surface UV radiation decreases as stratospheric ozone levels increase, as reported by *Zerefos et al*., 2012 over Canada, Europe, and Japan.

[4] To effectively protect ourselves from solar UV radiation overexposure, not only the global UV radiation reaching the earth's surface but also its partitioning into direct and diffuse components must be accurately known [*Parisi et al*., 2001; *Turnbull et al*., 2005]. Thus, while the direct component is easy to block with hats, umbrellas, trees, and urban structures, the diffuse component comes from all directions, and its effects are more difficult to minimize [*Utrillas*, 2010; *Kudish et al*., 2011]. The importance of the diffuse component is stressed by the fact that, in summer, erythemal UV radiation can be up to 60% in a tree shade [*Parisi et al*., 2000]. The amount and direct/diffuse partitioning of the solar UV radiation reaching the earth's surface is modulated by several factors such as solar zenith angle [*Ireland and Sacher*, 1996], total ozone content [*Bais et al*., 1993], cloud amount and their spatial distribution [*Blumthaler et al*., 1994; *Alados-Arboledas et al*., 2003; *Calbó et al*., 2005], aerosols [*Kylling et al*., 1998; *Krzyścin and Puchalski*, 1998], and surface albedo [*Blumthaler and Ambach* 1988].

[5] Although global solar UV radiation is frequently registered at many radiometric stations worldwide, its diffuse fraction is scarcely measured, and therefore, information about the direct-to-diffuse partitioning is usually unavailable. To our knowledge, only few studies have reported experimental solar UV diffuse measurements [*Parisi et al*., 2000, 2001; *Grant and Gao*, 2003; *Utrillas et al*., 2007, 2009; *Utrillas*, 2010; *Turnbull et al*., 2005; *Turnbull and Parisi*, 2008; *Nuñez et al*., 2012].

[6] In general, shadow band is the most common device used to measure solar diffuse irradiance worldwide. Due to its structure, this device causes an underestimation in the

[1]Department of Physics, University of Extremadura, Badajoz, Spain.

Corresponding author: G. Sánchez, Department of Physics, University of Extremadura, Avda. de Elvas s/n, 06071-Badajoz, Spain. (guadalupesh@unex.es; asp@unex.es; mcf@unex.es)

2169-897X/13/10.1002/jgrd.50361

Figure 1. Shadow-band adapted for the UVS-E-T pyranometer.

measurements because the band blocks the path of a certain portion of diffuse irradiance to the sensor, and therefore, its measurements must be corrected. This correction depends on the geometry of illumination, shadow-band dimensions, and anisotropy of the radiation field [*Drummond*, 1956; *LeBaron et al*., 1980].

[7] For the particular case of total solar diffuse radiation measured by pyranometers, i.e., diffuse radiation spectrally integrated throughout the whole solar interval (0.285–2.800 μm), several authors have proposed different correction models [*Drummond*, 1956; *Steven*, 1984; *LeBaron et al*., 1990; *Batlles et al*., 1995; *Muneer and Zhang*, 2002]. These models have been validated by comparison with experimental measurements at different locations [*López et al*., 2004a, 2004b; *Kudish and Evseev*, 2008; *Sánchez et al*., 2012] and are widely accepted to provide accurate and reliable total solar irradiance values.

[8] However, the correction in the UV range has not been sufficiently broached. It is worth noting that diffuse fraction can be significantly different in the UV range, as a consequence of the more intense scattering by molecules and small particles at shorter wavelengths. Therefore, the angular distribution of the diffuse component [*Ireland and Sacher*, 1996; *Grant and Heisler*, 1997] and the diffuse fraction [*Grant and Gao*, 2003] can be notably different for the total solar spectrum when compared to the UV region. Both aspects highly affect the error induced by the shadow band, and therefore, correction models specific for the ultraviolet region are needed.

[9] As far as we are aware, only one paper analyzes this issue [*Utrillas et al*., 2007], aimed at reporting reliable diffuse UVER experimental values at a coastal station near the Mediterranean Sea. That study calculates the correction of the diffuse UVER irradiance measured by a band-shadowed YES UVB-1 broadband radiometer. The authors estimated the reference UVER diffuse irradiance as the difference between the global UVER irradiance measured by a YES UVB-1 broadband radiometer and the direct UVER irradiance calculated convolving with the CIE spectrum the spectral direct irradiance measured by an Optronic OL754 spectroradiometer. That study constitutes an interesting approach to the issue of correcting UV measurements performed by means of shadow bands.

[10] The present study positively contributes in the same direction but now going one step further in regard to the validity and accuracy of the results. In addition to possible differences due to our continental location, our research extends the study to all sky conditions, while *Utrillas et al*. [2007] limited the comparison to clear cases. Moreover, this study improves the comparison by using highly reliable and suitable reference measurements. In contrast to the study by *Utrillas et al*. [2007], we use two radiometers of exactly the same model (Kipp & Zonen UVS-E-T) for directly measuring uncorrected and reference values, guaranteeing better comparability and, therefore, allowing more accurate validation.

[11] Therefore, to promote the performance of reliable measurements of solar UV irradiance, this study proposes a correction model for the solar UV diffuse irradiance measured using a shadow band. Specifically, the approaches originally proposed by *Drummond* [1956], *Steven* [1984], and *Batlles et al*. [1995] for the total solar range are revised and adapted to the UV range, and their performance for this new range is tested.

2. Data

[12] Data used in this study have been acquired at a radiometric station installed on the roof of the Physics building in the Campus of the University of Extremadura in Badajoz, south-western Spain (38.9º N; 7.01º W; 199 m a.s.l.). Suitable measuring conditions, open horizon, and periodic maintenance are guaranteed. The local climate is characterized by frequent cloud-free conditions mainly in summer, resulting in a high number of sunshine hours per year. This fact, together with a relatively low latitude, cause our site to have one of the highest annual solar UV irradiation in Europe and very high UV index near the summer solstice reaching values up to 11.

[13] The data set consists of one-minute measurements of horizontal global UV erythemal irradiance (UVER) and two simultaneous measurements of horizontal diffuse UVER irradiance. These measurements were recorded by Kipp & Zonen UVS-E-T radiometers. The first diffuse UVER irradiance dataset was recorded by a radiometer mounted on a semicircular shadow band. First, we tried to use a Kipp & Zonen CM121 shadow ring as blocking device, but it is specifically designed for CM pyranometers and could not be adapted to the model UVS-E-T. Thus, a 610-mm diameter and 75-mm width shadow band [*Horowitz*, 1969] was finally used. Although originally designed for total irradiance pyranometers, the shadow band was modified to function with the different height of the Kipp & Zonen UVS-E-T radiometer (Figure 1).

[14] Additionally, a second diffuse UVER irradiance dataset was measured using a Kipp & Zonen UVS-E-T radiometer installed on a Kipp & Zonen Solys 2 sun tracker. This device prevents the direct solar irradiance to reach the sensor by means of a ball which projects its shadow continuously on the sensor, not obstructing any other portion of

sky. The correction factor for these measurements is negligible [*Ineichen et al*., 1984], and therefore, they have been used as reference. The use of exactly the same model of radiometers for measuring band- and ball-shadowed diffuse irradiances contributes to minimize possible differences due to instrumentation.

[15] The period of study encompassed two complete years, from 7 August 2010 to 8 August 2012, ensuring that a variety of seasonal processes and meteorological conditions were sampled. Very different cloud types and amounts can be found throughout the year in our location, being very scarce in summer. Most of them are associated to frontal systems coming from the Atlantic Ocean or to more local convective systems, being the latter more frequent during spring and autumn. Regarding aerosols, our station is located in a low-turbidity continental region with some Atlantic maritime influence. The mean aerosol optical depth at 440 nm as measured at the nearest AERONET stations at Cáceres (Spain) and Évora (Portugal) is about 0.14, and the mean Angström exponent alpha is 1.2 [*Obregón et al*., 2012]. However, extreme optical depth values higher than 0.3 can be occasionally reached corresponding to desert dust intrusions from Sahara Desert (Northern Africa).

[16] The radiometers were employed in calibration campaigns every two years, ensuring the reliability of their measurements [*Antón et al*., 2011]. Specifically, to guarantee the quality and comparability of measurements, the UVS-E-T radiometers used in this study were intercompared and calibrated in a field campaign which took place in July 2011 at the Atmospheric Sounding Station of the National Institute for Aerospace Techniques (ESAt/ INTA) located at "El Arenosillo," Huelva, Spain (37.10ºN, 7.06ºW). This calibration followed a sound methodology [*Vilaplana et al*., 2009] based on the procedure recommended by the Working Group 4 of the COST Action 726 [*Webb et al*., 2006; *Gröbner et al*., 2007].

[17] Additionally, the data went through a quality control process to detect possible erroneous measurements. Subsequently, data were averaged on an hourly basis and divided in two subsets: the first year will be used for revising and adapting the models, and the second year will be used for their validation and comparison.

3. Methodology

[18] For the case of solar total irradiance measurements, reliable values of its diffuse component on a horizontal surface, $I_{d,r}$, can be obtained from the measurements recorded using a shadow band, $I_{d,u}$, as follows [*Batlles et al*., 1995]:

$$I_{d,r} = C \cdot I_{d,u} \tag{1}$$

where C is a factor that corrects for the diffuse radiation blocked by the band. For this spectral interval, the correction factor has been widely studied and quantified [*Drummond*, 1956; *Kasten et al*., 1983; *Steven*, 1984; *LeBaron et al*., 1980, 1990; *Kudish and Ianetz*, 1993; *Batlles et al*., 1995; *Muneer and Zhang*, 2002].

[19] In this study, we propose a similar correction factor, C_{UV} but specific for the UV spectral interval. The range of variation of this UV correction factor and its evolution throughout the period of study was analyzed. Taking into account the influencing factors such as the solar zenith angle, clouds, aerosols, and total ozone column (TOC), its dependence on these parameters was investigated. The total ozone column data used for this analysis was provided by the NASA Ozone Monitoring Instrument (OMI) through their website: *ozoneaq.gsfc.nasa.gov/index.md*. On the other hand, the dependence on clouds and aerosols were evaluated by means of the ultraviolet transmissivity, k_t^{UV}, and the ultraviolet diffuse fraction, k_d^{UV}, i.e., the ratio between diffuse and global ultraviolet irradiance. The ultraviolet transmissivity, k_t^{UV}, is a measure of the attenuation of the ultraviolet global irradiance due to its interaction with the atmospheric constituents. The definition of this parameter is analogue to the clearness index for the total solar spectrum. Meanwhile, k_d^{UV}, represents the contribution of the diffuse component to the ultraviolet global irradiance measured at the earth's surface. These parameters were calculated as follows:

$$k_t^{UV} = \frac{I_g^{UV}}{I_{TOA}^{UV}} \tag{2}$$

$$k_d^{UV} = \frac{I_d^{UV}}{I_g^{UV}} \tag{3}$$

where I_g^{UV} is the ultraviolet global irradiance, I_d^{UV} is the ultraviolet diffuse irradiance measured using the sun tracker, and I_{TOA}^{UV} is the ultraviolet irradiance at the top of the atmosphere. The latter variable depends on the hour of the day, day of the year, and latitude of the location under study [*Iqbal*, 1983]. It is calculated according to the following expression:

$$I_{TOA}^{UV} = S_{UV}\left(\frac{r_0}{r}\right)^2 \cos(\theta) \tag{4}$$

where θ in the solar zenith angle, $(r_0/r)^2$ is a factor which corrects for the eccentricity of the earth's orbit, and S_{uv} is the erythemally weighted solar constant, with an estimated value of 10.031 W/m^2.

[20] To find a suitable expression of the correction factor for shadow-band measurements in the ultraviolet region, C_{UV}, the models proposed by *Drummond* [1956], *Steven* [1984], and *Batlles et al*. [1995] were considered as first approach. These models were originally proposed by their respective authors for correcting total solar irradiance measurements. The first model was proposed by Drummond in 1956. Posterior models are improved versions which propose additional terms to account for the anisotropy not included in the Drummond's approach.

[21] To be suitable for UV measurements, these three models need to be adapted to account for the differences in scattering between total and UV regions. The dependence of scattering on wavelength induces differences in diffuse fraction between UV and total regions. The model proposed by *Drummond* [1956] resulted from a theoretical study which assumed isotropic sky radiance distribution and ring width small compared to its radius. When these hypotheses are assumed for the UV region, the resulting model only depends on shadow-band dimensions and geographical coordinates. Thus, the original expression proposed by Drummond can be applied to any location and wavelength. Conversely, the models proposed by *Steven* [1984] and *Batlles et al*. [1995] were developed for particular sites with specific local climate conditions. Thus, these models include coefficients which must be particularized for each location.

Therefore, it is necessary to adapt these models to our local conditions, which may have a large influence in the results [*Sanchez et al.*, 2012]. The mathematical expressions and the parameters involved in these models have been revised according to the wavelengths of interest, i.e., the UV region, and new regression coefficients have been calculated. For these fittings, the subdataset comprising the first year of measurements was used.

[22] Finally, modified Steven and Batlles models were included, together with the model proposed by *Drummond* [1956], in a comparative analysis carried out using the second year of measurements. The performance of the models was evaluated by means of statistical analysis and graphical plots such as the Taylor diagram [*Taylor*, 2001]. The relative root mean square error (rRMSE) and relative mean bias error (rMBE) were calculated to quantify the performance of the models. rRMSE is a measure of the magnitude of the differences between corrected and reference values. On the other hand, rMBE quantifies the mean deviation between the reference dataset and the corrected dataset. Negative values indicate underestimation with respect to the reference measurements while positive values indicate overestimation. Best models are those with these statistics close to zero. These statistics are calculated as follows:

$$rRMSE\ (\%) = \frac{100}{\overline{I^{UV}_{d,ref}}}\sqrt{\frac{1}{N}\sum_{i=1}^{N}\left(I^{UV}_{i,corr} - I^{UV}_{i,ref}\right)^2} \tag{5}$$

$$rMBE\ (\%) = \frac{100}{N\cdot\overline{I^{UV}_{d,ref}}}\sum_{i=1}^{N}\left(I^{UV}_{i,corr} - I^{UV}_{i,ref}\right) \tag{6}$$

where $I^{UV}_{d,ref}$ is the UV diffuse irradiance as measured by the pyranometer mounted on the sun tracker (reference values), $\overline{I^{UV}_{d,ref}}$ is the mean of those measurements, $I^{UV}_{d,cor}$ is the model-corrected UV diffuse irradiance, and N is the total number of measurements.

[23] Finally, the relative differences (RD) of both corrected and uncorrected UV diffuse irradiance measurements with respect to the reference measurements have been analyzed. The relative difference was defined as follows:

$$RD\ (\%) = 100\cdot\left(\frac{I^{UV}_{i,corr} - I^{UV}_{i,ref}}{I^{UV}_{i,ref}}\right) \tag{7}$$

[24] The magnitude of the differences and their behavior versus solar zenith angle, transmissivity of ultraviolet irradiance and ultraviolet diffuse fraction was also analyzed.

4. Models

4.1. Drummond [1956]

[25] The shadow-band correction factor proposed by *Drummond* [1956], C_D, is defined by the following expression:

$$C_D = \frac{1}{1-F} \tag{8}$$

where F represents the diffuse irradiance fraction blocked by a shadow band with an axis parallel to the polar axis. This magnitude is calculated under the assumptions that (1) the band width is small compared to its radius, (2) the sky radiance distribution is isotropic, (3) the sensor is negligible in size compared to the other dimensions, and (4) there is no back-reflection of radiation from the inner surface of the band. Assuming these hypotheses, the expression obtained is

$$F = \left(\frac{2b}{\pi r}\right)\cos^3\delta(\omega_s\sin\varphi\sin\delta + \cos\varphi\cos\delta\sin\omega_s) \tag{9}$$

where r is the radius of the band, b its width, ω_s the hour angle at sunset (in radians), δ the solar declination, and ϕ the latitude of the location.

[26] The hypotheses assumed in this model are independent of the spectral region of study, and therefore, equation (9) can be directly applied to UV measurements with no specific adaptation [*Utrillas et al.*, 2007].

4.2. Steven [1984]

[27] The model proposed by Steven introduces an additional factor that takes into account the anisotropy in the diffuse irradiance distribution at the circumsolar region. The correction factor proposed by this model is

$$C_S = \frac{I_{d,ref}}{I_{d,u}} = \frac{1}{1-FQ} \tag{10}$$

where F is the fraction of diffuse irradiance occluded by the band given by equation (9), and Q is the anisotropy correction factor. For the total solar region and under cloud-free conditions, Q is calculated as follows:

$$Q = 1 - C\xi' + \frac{C}{f'} \tag{11}$$

where C expresses the relative strength of the circumsolar component, and ξ' is the angular width of the circumsolar region. C and ξ' are obtained by linear fitting of equation (11). The function f′ is defined as follows:

$$f' = \omega_s\sin\varphi\sin\delta + \cos\varphi\cos\delta\sin\omega_s \tag{12}$$

[28] However, anisotropy in total and UV regions could be notably different since scattering highly depends on wavelength. Thus, the greater dispersion of radiation at shorter wavelengths could modify the contribution of the circumsolar region in the case of UV region. For this reason, it is necessary to adapt equation (11) for the UV spectral range, as will be discussed in section 5.2.

4.3. Batlles et al. [1995]

4.3.1. Batlles A

[29] *Batlles et al.* [1995] proposed two models to correct the diffuse irradiance measured with shadow-bands. The first one, called model Batlles A in this study, proposes the following expression for the correction factor:

$$C_{BA} = a\cdot C_D + b\cdot\log\Delta + c\cdot\log\varepsilon + d\cdot\exp(-1/\cos\theta) \tag{13}$$

where C_D is the isotropy correction proposed by *Drummond* [1956] in equation (9), ε is related to cloud conditions, Δ is a brightness index which is a function of cloud thickness and aerosol loading, and θ is the solar zenith angle. These three parameters account for different sources of anisotropy in the diffuse irradiance. a, b, c, and d are empirical coefficient that are obtained by regression analysis.

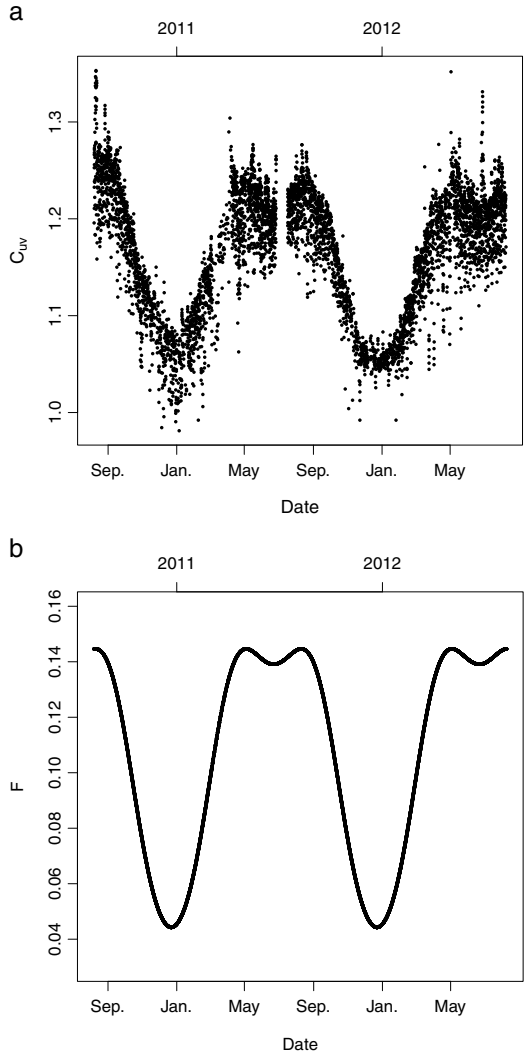

Figure 2. a) Evolution of the UV correction factor, C_{UV}, throughout the period of study. b) Evolution of the diffuse irradiance blocked by the I-profile band throughout the period of study.

[30] The parameters ε and Δ were originally defined for total irradiance measurements. We have adapted their original expressions to the ultraviolet region. The new parameters ε_{UV} and Δ_{UV} are defined as follows:

$$\varepsilon_{UV} = \frac{I_{d,u}^{UV} + I_{nb}^{UV}}{I_{d,u}^{UV}} \tag{14}$$

$$\Delta_{UV} = \frac{I_{d,u}^{UV} \cdot m}{I_{TOA}^{UV}} \tag{15}$$

where $I_{d,u}^{UV}$ is the uncorrected diffuse ultraviolet irradiance measured using the shadow band; I_{nb}^{UV} is the uncorrected normal beam ultraviolet irradiance, calculated subtracting uncorrected diffuse UV irradiance from global UV irradiance; m is the relative optical air mass; and I_{TOA}^{UV} is the UV irradiance at the top of the atmosphere (equation (4)).

[31] As mentioned above, due to the wavelength-dependence of scattering, clouds and aerosols will affect radiation differently in total and ultraviolet regions. These differences in spatial distribution and diffuse fraction induce differences in ε_{UV} and Δ_{UV} values with respect to their values in the case of total irradiance, subsequently affecting the correction factor.

4.3.2. Batlles B

[32] *Batlles et al.* [1995] proposed a second model, called Batlles B model in this study, based on the dependence of the correction factor with respect to ε. This model consists of a multiple linear model similar to equation (13) for each interval of ε. More details are given by *Batlles et al.* [1995]. Similar to the previous model, the expressions proposed in the Batlles B model were analyzed for the specific case of UV region. This will be discussed in section 5.2.

5. Results and Discussion

5.1. Analysis of the Shadow-Band Correction for Ultraviolet Region, C_{UV}.

[33] Several authors have analyzed the behavior of the shadow-band correction factor for total solar measurements [*Drummond*, 1956; *Ineichen et al.*, 1984; *Kasten et al.*, 1983; *Steven*, 1984; *LeBaron et al.*, 1980, 1990; *Batlles et al.*, 1995, *Muneer and Zhang*, 2002]. However, information about this correction factor in the UV region is scarce [*Utrillas et al.*, 2007]. Therefore, before proposing an expression specific for the ultraviolet region, the evolution of the correction factor throughout the period of study and its dependence on the atmospheric scattering must be analyzed.

[34] The correction factor for UV region, C_{UV}, was calculated from equation (1) as the ratio between the reference ultraviolet diffuse irradiance measured using the sun tracker and the ultraviolet diffuse irradiance measured using the shadow band. Figure 2 shows its evolution through the period of study. The highest correction occurs in spring and summer, with a mean value of 1.21.C_{UV} starts to decrease in October, reaches its minimum in January, and then starts to increase. This temporal pattern is characteristic of I-profile shadow bands as the one used in this study (Figure 1), being different from other band types such as U-profile [Kipp & Zonen, CM121 Shadow Ring Manual]. Figure 2b shows the diffuse irradiance fraction blocked by the I-profile band (equation (9)). The high similarity between Figures 2 and 2b reveals the high influence of the

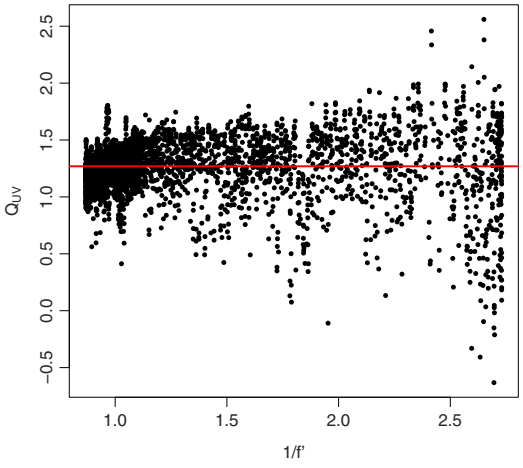

Figure 3. Ultraviolet anisotropy factor, Q_{UV}, versus $1/f'$.

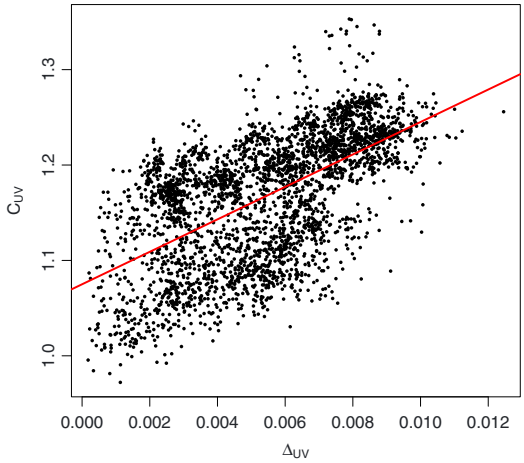

Figure 4. Ultraviolet correction factor dependence on Δ_{UV}.

geometric factors in the correction. As a result of these factors, the portion of sky blocked by I-profile bands is lower in autumn and winter than in spring and summer. Therefore, the uncorrected shadow-band measurements approach the true values in autumn and winter. This fact explains the lower correction during these seasons.

[35] Besides geometrical factors, the correction is affected by the anisotropy in the diffuse radiation at the earth's surface, mainly influenced by the solar zenith angle, clouds, aerosols, and ozone amount. These factors notably affect the distribution and the portion of the diffuse irradiance blocked by the shadow band. To evaluate their influence, the dependence of the UV correction factor on these variables has been investigated. No dependence on total ozone amount was observed. In contrast, the UV correction factor was weakly dependent on solar zenith angle, ultraviolet transmissivity and ultraviolet diffuse fraction. Thus, C_{UV} decreases about 7% as solar zenith angle varies from 20º to 70º, increases about 7% as k_t^{UV} increases from 0.005 to 0.020, and decreases about 8% as k_d^{UV} increases from 0.50 to 0.95. Lowest C_{UV} values correspond to cases with high UV diffuse irradiance and high isotropy. These conditions take place at high solar zenith angles, low ultraviolet transmissivity, and high ultraviolet diffuse fraction. This involves a decrease in the portion of ultraviolet diffuse irradiance blocked by the band and subsequently a decrease in the correction factor. Conversely, C_{UV} increases for situations in which the anisotropy of the ultraviolet diffuse irradiance increases, i.e., low solar zenith angle, high ultraviolet transmissivity, and low ultraviolet diffuse-to-global fraction. It is worth noting that the ultraviolet diffuse faction, k_d^{UV}, calculated in this study ranges from 0.45 to 1. This means that, at our location, the diffuse component is at least the 45% of the ultraviolet irradiance reaching the earth's surface. This fact emphasizes the importance of the diffuse component in the total ultraviolet amount.

[36] Scarce anomalous cases of $C_{UV} < 1$ (shadow-band measurements higher than sun-tracker measurements) were observed. These situations comprise the 0.15% of the data and correspond to clear sky conditions in winter at sunset or sunrise. These anomalous C_{UV} values could be associated with the pyranometer cosine error or multiple reflection on the inner surface of the shadow band [*LeBaron et al.*, 1980].

5.2. Adaptation of the Models

5.2.1. Steven [1984]

[37] This model proposes an anisotropy parameter, Q, which takes into account the anisotropy in the diffuse *radiance* distribution. Its dependence respect to the function $1/f'$ (equation (11)) in the UV region was analyzed using the experimental measurements. First, those cases with ultraviolet transmissivity higher than 0.02 and ultraviolet diffuse fraction lower than 0.65 were studied, being representative of clear sky conditions. However, these cases comprise only 20% of the data and showed no relationship between Q_{UV} and $1/f$. Therefore, the relationship was investigated using the complete dataset. Figure 3shows that the linear relationship described in equation (11) is not found in the UV region. In this spectral interval, the anisotropy factor, Q_{UV}, seems to be constant for the entire range of $1/f'$ values, with a median value of 1.27. Thus, this constant value was assumed in this model (equation (10)). The median instead of the mean value was considered because it is less affected by extreme anomalous values.

[38] Although the original Steven's model was proposed for clear sky conditions, the measurements used in this study to analyze the behavior of the ultraviolet anisotropy factor, Q_{UV}, correspond to all-sky conditions. Thus, the results obtained above can be applied to any sky condition. This modified Steven's model will be denoted as Steven* henceforth.

5.2.2. Batlles et al. [1995]

[39] For this model, the parameters ε and Δ corresponding to total and ultraviolet regions were evaluated for the same period and compared. Results indicated a notably shorter range of variation of ε_{UV} with respect to ε. While ε varies from 1.08 up to 28.30, ε_{UV} only ranges from 1.01 to 2.94. At the same time, there is an important difference in the order of magnitude of Δ between total and UV regions. These high differences could yield very different expressions when equation (13) is applied to each spectral region.

[40] In this study, in addition to adapting the coefficients to the UV range as in the paper by *Utrillas et al.* [2007], the mathematical expression was also revised.

[41] Thus, the relationship established by equation (13) between the ultraviolet correction factor, C_{UV}, and the parameters C_D, ε_{UV}, Δ_{UV} and $-1/cos(\theta)$ was analyzed. As

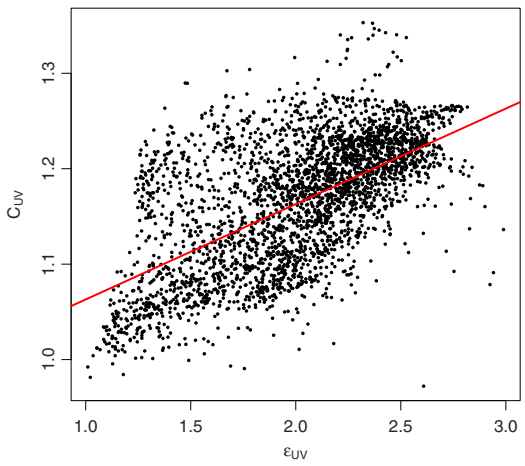

Figure 5. Ultraviolet correction factor dependence on ε_{UV}.

Table 1. Values of rRMSE and rMBE for Uncorrected Measurements and for Corrected Measurements Using the Three Models Analyzed

	rRMSE (%)	rMBE (%)
Uncorrected	20.16	−15.60
Drummond	5.46	−3.47
Steven*	2.20	0.46
Batlles A*	2.74	1.53

in the case of total solar irradiance measurements, the dependence with respect to the geometric correction, C_D, and the factor $-1/cos(\theta)$ are linear and exponential, respectively. However, in the ultraviolet region, the logarithmic dependence on ε_{UV} and Δ_{UV} is not observed (Figures 4 and 5). Thus, to account for the trend, a simple linear relationship is proposed. The high scatter in Figures 4 and 5 suggests not to use a more complex expression.

[42] Taking into account these results, the equation (13) was modified replacing the logarithmic dependence with a linear one as follows:

$$C_{modBA} = 0.94 \cdot C_D + 9.25 \cdot \Delta_{UV} + 0.025 \cdot \varepsilon_{UV} + 0.024 \cdot e^{(-1/cos\theta)} \quad (16)$$

[43] The coefficients were obtained by regression analysis, resulting a coefficient of determination, R^2, of 0.9996. The coefficient of C_D obtained in the fitting (0.94) notably differs from the value obtained by *Utrillas et al.* [2007] (1.24). This difference can be explained by the distinct mathematical model fitted to the data, since we have adapted the original expression (equation (13)) replacing the logarithmic functions by a more simple linear dependence (equation 16). This modified model Batlles A will be called Batlles A* in next sections.

[44] On the other hand, the model Batlles B relies on a nonlinear dependence between the shadow-band correction factor and ε. As mentioned above, for the ultraviolet region, the correction factor, C_{UV}, linearly depends on ε_{UV} (Figure 5), and therefore, Batlles B means no improvement with respect to model Batlles A*. Thus, in this paper, the model Batlles B is not used.

5.3. Comparative Analysis of the Models

[45] Finally, the model proposed by Drummond and the modified Steven* and Batlles A* models were applied to the comparison data set (second year of the period of study) and their results compared. Table 1 shows the rRMSE and rMBE for uncorrected and model-corrected measurements versus reference measurements. While rRMSE for uncorrected measurements is about 20%, for corrected measurements it decreases to values between 2.20% and 5.46%. According to this statistic, the model with best performance is the model Steven* followed by the model Batlles A* with rRMSE values of 2.20 and 2.74, respectively. On the contrary, the model proposed by Drummond presents the highest rRMSE values. The low values of rMBE confirm the good performance of the mentioned two best models.

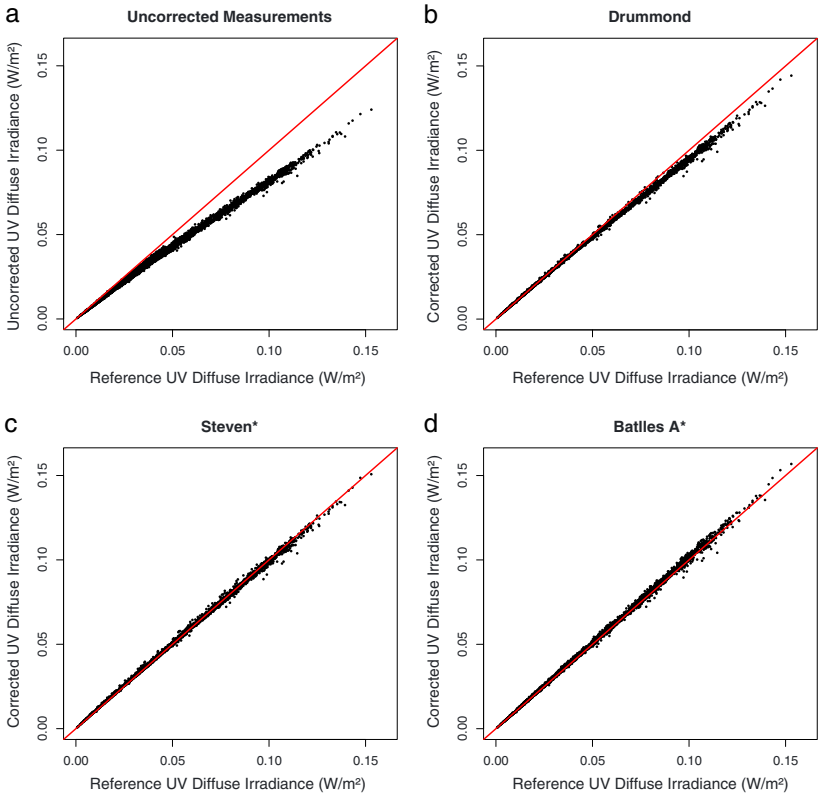

Figure 6. Uncorrected (a) and corrected (b-d) for the three models UV diffuse irradiance versus the reference UV diffuse irradiance.

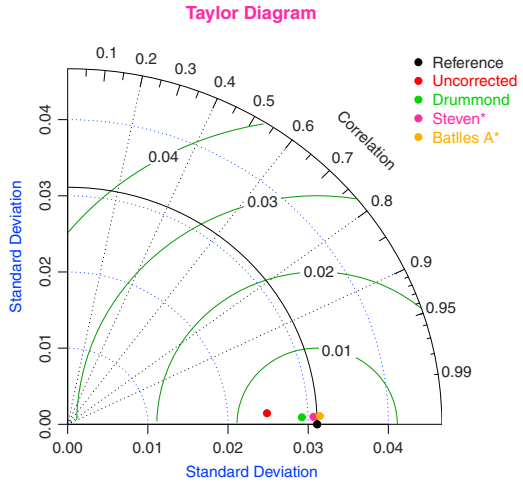

Figure 7. Taylor diagram summarizes three statistics about modeled and reference values: centered RMS difference between them, their correlation, and their standard deviations. RMS difference is proportional to their distance apart. Standard deviation is proportional to the radial distance from the origin. Correlation is given by the azimuthal position. The reference measurements are represented by a black point on the abscissa axis. Different models are represented by different colored points, being the closest to the reference point the one with best performance.

[46] The observation of rMBE values of Table 1 is consistent with values reported by *Utrillas et el*. [2007]. While they obtained underestimations between 1% and 5% for adapted LeBaron, Batlles, and Batlles 2 models, we obtain overestimations of 0.46% and 1.53% for modified Steven* and Batlles A* models respectively. However, in addition to the difference in the instrumentation used in the studies, we should bear in mind that their study is limited to clear days while ours covers all sky conditions and, therefore, results are not directly comparable. On the other hand, it is interesting to note that the Drummond underestimation obtained (3.47%) is notably lower that the value obtained by *Utrillas et al*. [2007] (9%) for the same model. This difference tends to support the idea that a higher accuracy has been achieved in this study due to the use of more comparable instrumentation.

[47] The different goodness of performance for the models are shown in Figures 6a–6d. They show the uncorrected and corrected values versus the reference values (measurements performed with the sun tracker) for the three models. These figures confirm the notable improvement achieved when corrections are applied. As mentioned above, a noticeable decrease in the underestimation is clearly observed for all models, although the correction applied by the Drummond's model still underestimates the reference values. These results indicate that the models Steven* and Batlles A*, which take into account the anisotropy in the ultraviolet diffuse irradiance distribution, show the best performance.

[48] To perform a complete comparison of the different models, the Taylor diagram was plotted (Figure 7). It is suitable tool for comparing several models. This diagram provides a graphical summary of different aspects of the performance of a model, such as the centered root mean square error (RMS), the correlation and the magnitude of its differences with respect to reference values [*Taylor*, 2001]. The Figure 7 shows the very good performance of models Steven* and Batlles A*, followed by Drummond's model, and ending with uncorrected measurements.

[49] The statistics rRMSE and rMBE and the Taylor diagram provide information about the general behavior of each model. To improve the knowledge of the behavior with respect to other factors, the relative differences (RD) of

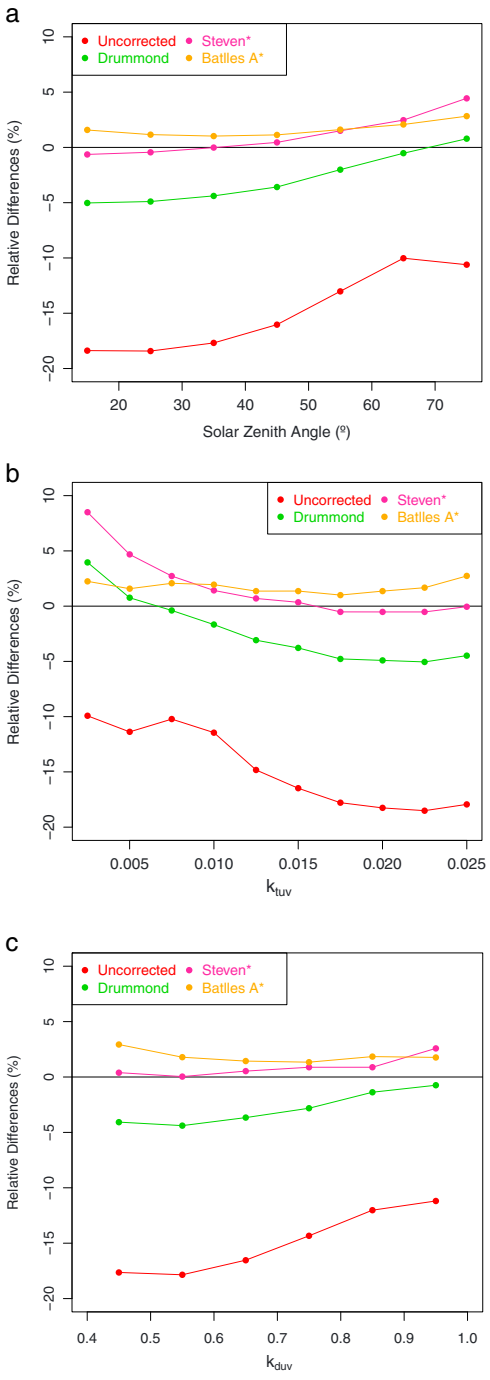

Figure 8. Relative difference dependence on solar zenith angle (a), ultraviolet transmissivity (b), and ultraviolet diffuse fraction (c).

uncorrected and corrected measurements with respect to the reference values have been analyzed. These relative differences have been calculated according to equation (7). As expected, relative differences of uncorrected measurements follow the annual pattern depicted in Figure 2, with a high underestimation shown in Table 1. Both effects are corrected by the proposed models. Thus, the absolute mean value of the relative differences decreases from 14% in uncorrected measurements to 1.53% and 1.70% in the measurements corrected with the models Steven* and Batlles A*, respectively.

[50] In addition, dependence of relative differences on solar zenith angle, ultraviolet transmissivity, and diffuse ultraviolet fraction were analyzed (Figures 8a–8c). For this analysis, the average of the relative differences has been computed over zenith angle, clearness index, and diffuse fraction bands. Figures 8a–8c show the remarkable improvement achieved when correction models are applied. The best results for Drummond's model are obtained in conditions of high solar zenith angle, low ultraviolet transmissivity, and high ultraviolet diffuse fraction. These situations are associated to a higher isotropy in the ultraviolet diffuse irradiance. This result was expected since the isotropy of the diffuse irradiance is the main hypothesis for this model. Drummond and Steven* models behave similarly due to the constant value of the ultraviolet anisotropy factor, Q_{UV}, in this region of the solar spectrum (Figure 3). Both models lower the relative differences but they do not completely correct the dependence with respect to solar zenith angle, k_t and k_d. This dependence is more suitably corrected by the model Batlles A*. Steven* and Batlles A* models show the lowest mean relative difference with respect to the mentioned three parameters.

6. Conclusions

[51] To evaluate the UV correction factor for shadow-band diffuse radiation values, experimental ultraviolet diffuse irradiance measurements were recorded using both a shadow-band and a sun tracker. Measurements indicated that the highest values of this factor were observed for low solar zenith angles, high ultraviolet transmissivity values, and low ultraviolet diffuse fraction.

[52] The shadow-band correction models proposed by Drummond, Steven, and Batlles et al. were revised and adapted to be applied to ultraviolet diffuse measurements. Drummond's model only implies geometric calculations and can be directly applied to any wavelength region. In contrast, the models proposed by Steven and Batlles et al. showed the need to be modified before being applied to the new spectral region of the study.

[53] A better performance was observed when the correction models proposed by Drummond and the modified Steven* and Batlles A* models were applied. This improvement is more notable with the application of the modified models Batlles A* and Steven*. These two models take into account the anisotropy of the ultraviolet irradiance distribution, achieving a better improvement, with the lowest rRMSE, 2.74% and 2.20%, respectively, and rMBE, 1.53% and 0.46%, respectively. The good performance of these two models was confirmed by the Taylor diagram and the analysis of relative differences. Batlles A* and Steven*'s models presented the lowest relative differences, although the latter does not completely correct the dependence with the solar zenith angle, the ultraviolet transmissivity and the diffuse fraction.

[54] This study positively contributes to a better knowledge of the ultraviolet diffuse irradiance and to improve the measurements obtained using shadow bands. The availability of precise diffuse measurements is essential for monitoring variations in the atmospheric components and their effects on the climate change.

[55] **Acknowledgments.** This study was partially supported by the research projects CGL2008-05939-C03-02/CLI and CGL2011-29921-C02-01 granted by the "Ministerio de Ciencia e Innovación" from Spain. The authors thank NASA for the total ozone column data. Thanks are due to anonymous reviewers for their constructive suggestions.

References

Alados-Arboledas, L., I. Alados, I. Foyo-Moreno, F. J. Olmo, and A. Alcántara (2003), The influence of clouds on surface UV etythemal irradiance, *Atmos. Res.*, *66*, 273–290.

Antón, M., A. Serrano, M. L. Cancillo, and J. M. Vilaplana (2011), Quality assurance of broadband erythemal radiometers at the Extremadura UV Monitoring Network (southwestern Spain), *Atmos. Res.*, *100*, 83–92.

Bais, A. R., C. S. Zerefos, C. Meleti, I. C. Ziomas, and K. Tourpali (1993), Spectral measurements of solar UVB radiation and its reations to total ozono, SO2 and clouds, *J. Geophys. Res.*, *98*, 5199–5204.

Batlles, F. J., F. J. Olmo, and L. Alados-Arboledas (1995), On shadow band correction methods for diffuse irradiance measurements, *Sol. Energy*, *54*, 105–114.

Blumthaler, M., and W. Ambach (1988), Solar UVB-albedo of various surfaces, *Photochem. Photobiol.*, *48*, 85–88.

Blumthaler, M., W. Ambach, and M. Salzgeber (1994), Effects of cloudiness on global and diffuse UV irradiance in a high-mountain area, *Theor. Appl. Climatol.*, *50*, 23–30.

Calbó, J., D. Pags, and J. A. Gonzalez (2005), Empirical studies of cloud effects on UV radiation: A review, *Rev. Geophys.*, *43*, RG2002, doi:10.1029/2004RG000155.

CIE (Commission Internationale d'Eclairage) (1987), Research Note. A reference action spectrum for ultraviolet induced erythema in human skin, *CIE J.*, *6*, 17–22.

Drummond, A. J. (1956), On the measurement of sky radiation, *Arch. Meteorol. Geophys. Bioklim. Ser. B*, *7*, 413–436.

Diffey, B. L. (1991), Solar ultraviolet radiation effects on biological systems, *Phys. Med. Biol.*, *36*, 299–328.

Diffey, B. L. (2004), Climate change, ozone depletion and the impact on ultraviolet exposure of human skin, *Phys. Med. Biol.*, *49*, 1–11.

Grant, R. H., and G. M. Heisler (1997), Obscured overcast sky radiance distributions for the UV and PAR wavebands, *J. Appl. Meteorol.*, *56*, 1336–1345.

Grant, R. H., and W. Gao (2003), Diffuse fraction of UV radiation under partly cloudy skies as defined by the Automated Surface Observation System (ASOS). *J. Geophys. Res.*, *108*(D2), 4046, doi:10.1029/2002JD002201.

Glerup, H., K. Mikkelsen, L. Poulsen, E. Hass, S. Overbeck, and J. Thomsen (2000), Commonly recommended daily intake of vitamin D is not sufficient if sunlight exposure is limited, *J. Intern. Med.*, *247*, 260–268.

Gröbner, J., G. Hülsen, L. Vuilleumier, M. Blumthaler, J. M. Vilaplana, D. Walker, and J. E. Gil (2007), Report of the PMOD/WRC-COST Calibration and Intercomparison of Erythemal radiometers. Available at: http//i115srv.vuwien.ac.at/uv/COST726/COST726 *Dateien/Results/PMOD WRC COST726 campaign 2006 R.pdf*.

Häder, D. P., E. W. Helbling, C. E. Williamson, and M. Ilyasd (2011), Effects of solar UV radiation on aquatic ecosystems and interactions with climate change, *Photochm. Photobiol. Sci.*, *10*, 242–260, doi:10.1039/c0pp90036b.

Harris, N. R. P., et al. (2008), Ozone trends at northern mid- and high latitudes - a European perspective, *Ann.Geophys.*, *26*, 1–14.

Heisler, G. M. Urban forest influence on exposure to UV radiation and potential consequences for human health, in *UV Radiation in Global Climate Change. Measurements, Modeling and Effects on Ecosystems*, edited by Gao, W., et al., pp. 331–369, Tsinghua University Press, Beijing, 2010.

Holick, M. F. (2004), Vitamin D: importance in the prevention of cancers, type 1 diabetes, heart disease and osteoposoris, *Am. J. Clin. Nutr.*, *79*, 362–371.

Horowitz, J. L. (1969), An easily constructed shadow-band for separating direct and diffuse solar radiation, *Sol. Energy*, *12*, 543–545.

Ineichen, P., J. M. Gremaud, O. Guisan, and A. Mermoud (1984), Study of the corrective factor involved when measuring the diffuse solar radiation by use of the ring method, *Sol. Energy*, *32*, 585–590.

Iqbal, M., (1983), *An Introduction to Solar Radiation*, Academic Press, Ontario, Canada.

Ireland, W., and R. Sacher (1996), The angular distribution of solar ultraviolet, visible and near-infrared radiation from cloudless skies, *Photochem. Photobiol.*, *63*, 483–486.

Kasten, F., K. Dehne, and W. Brettschneider (1983), Improvement of measurement of diffuse solar radiation, *Sol. Radiat. Data, Ser. F*, *2*, 221–225. D. Reidel, Dordrecht.

Krzyścin, J. W., and S. Puchalski (1998), Aerosol impact on the surface UV radiation from the ground-based measurements taken at Belk, Poland, 1980–1996, *J. Geophys. Res.*, *103*, 175–181.

Kudish, A. I., and A. Ianetz (1993), Analysis of diffuse radiation data for Beer Sheva: Measured (shadow ring) versus calculated (global-horizontal beam) values, *Sol. Energy*, *51*, 495–503.

Kudish, A. I., and E. G. Evseev (2008), The assessment of four different correction models applied to the diffuse radiation measured with a shadow ring using global and normal beam radiation measurements for Beer Sheva, Israel, *Sol. Energy*, *82*, 144–156.

Kudish, A. I., M. Harari, and E. G. Evseev (2011), The solar ultraviolet B radiation protection provided by shading devices with regard to its diffuse component, *Photodermatol. Photoimmunol. Photomed.*, *27*, 236–244, doi:10.1111/j.1600-0781.2011.00608.

Kylling, A., A. F. Bais, M. Blumthaler, J. Schreder, C. S. Zerefos, and E. Kosmidis (1998), Effect of aerosols on solar UV irradiances during the photochemical activity and solar ultraviolet radiation campaign, *J. Geophys. Res.*, *103*, 51–60.

LeBaron, B. A., W. A. Peterson, and I. Dirmhirn (1980), Corrections for diffuse irradiance measured with shadow bands, *Sol. Energy*, *25*, 1–13.

LeBaron, B. A., J. J. Michalsky, and R. Perez (1990), A simple procedure for correcting shadow band data for all sky conditions, *Sol. Energy*, *44*, 249–256.

López, G., T. Muneer, and R. Claywell (2004a), Assessment of four shadow band correction models using beam normal irradiance data from the United kingdom and Israel, *Energy Convers. Manage.*, *45*, 1963–1979.

López, G., T. Muneer, and R. Claywell (2004b), Comparative study of four shadow band diffuse irradiance corrections algorithms for Almeria, Spain, *J. Sol. Energ. Eng.*, *126*, 696–701.

McKenzie R. L., L. O. Björn, A. Bais, and M. Ilyasd (2003), Changes in biologically active ultraviolet radiation reaching the Earth's surface, *Phtochem. Photobiol. Sci.*, *2*, 5–15.

Muneer, T., and X. Zhang (2002), A new method for correcting shadow band diffuse irradiance data, *J. Sol. Energ. Eng.*, *124*, 34–43.

Musil, C. F., S. B. M. Chimphango, and F. D. Dalora (2002), Effects of elevated ultraviolet-B radiation on native and cultivate plants of Southern Africa, *Ann. Bot.*, *90*, 127–137, doi:10.1093/aob/mcf156.

Nuñez, M., M. P. Utrillas, and J. A. Martinez-Lozano (2012), *Approaches to partitioning the global UVER irradiance into its direct and diffuse components in Valencia*, Spain, J. of Geophys. Res., 117, doi:10.1029/2011JD016087.

Obregón, M. A., S. Pereira, F. Wagner, A. Serrano, M. L. Cancillo and A. M. Silva (2012). Regional differences of column aerosol parameters in western Iberian Peninsula. *Atmos. Environ.*, *62*, 208–219.

Parisi, A. V., M. G. kimlin, J. C. F. Wong, and M. Wilson (2000), Diffuse component of solar ultraviolet radiation in tree shade , *J. Photochem. Photobiol. B: Biol*, *54*, 116–120.

Parisi, A. V., A. Green, and M. G. Kimlin (2001), Diffuse Solar UV Radiation and Implications for Preventing Human Eye Damage, *Photochem. Photobiol.*, *73*, 135–139.

Sánchez, G., A. Serrano, M. L. Cancillo and J. A. García (2012), Comparison of shadow-ring models for diffuse solar irradiance, *J. Geophys. Res.*, *117*, D09206, doi:10.1029/2011JD017346, in press.

Steven, M. D. (1984), The anisotropy of diffuse solar radiation determined from shade-ring measurements, *Quart. J. R. Met. Soc.*, *110*, 261–270.

Turnbull, D. J., A. V. Parisi, and M. G. Kimlin (2005), Vitamin D effective ultraviolet wavelengths due to scattering in shade, *J. Steroid Biochem. Mol. Biol.*, *96*, 431–436.

Turnbull, D. J., and A. V. Parisi (2008), Utilising shade to optimize UV exposure for vitamin D, *Atmos. Chem. Phys.*, *8*, 2841–2846.

Taylor, K. E. (2001), Summarizing multiple aspects of model performance in a single diagram, *J. Geophys. Res.*, *106*, 7183–7192.

Utrillas, M. P., M. J. Marín, A. R. Esteve, F. Tena, J. Cañada, V. Estellés, and J. A. Martínez-Lozano (2007), Diffuse UV erythemal radiation experimental values, *J. Geophys. Res.*, *112*, doi:10.1029/2007JD008846.

Utrillas, M. P., M. J. Marín, A. R. Esteve, V. Estellés, F. Tena, J. Cañada, and J. A. Martínez-Lozano (2009), Diffuse Ultraviolet Erythemal Irradiance on Inclined Planes: A Comparison of Experimental and Modeled Data, *Phot. Pho.*, *85*(5), 1245, doi:10.1111/j.1751-1097.2009.00573.x.

Utrillas, M. P., J. A. Martınez-Lozano, and M. Nuñez (2010), Ultraviolet Radiation Protection by a Beach Umbrella, *Photochem. Photobiol.*, *86*, 449–456, doi:10.1111/j.1751-1097.2009.00677.x.

Vilaplana, J. M., A. Serrano, M. Antón, M. L. Cancillo, M. Parias, J. Gröbner, G. Hülsen, G. Zablocky, A. Díaz, and B. A. de la Morena (2009), COST Action 726 – Report of the "El Arenosillo"/INTA-COST calibration and intercomparison campaign of UVER broadband radiometers.

Webb, A. R., L. Kline, and M. F. Holick (1988), Influence of season and latitude on the cutaneous synthesis of Vitamin D3: exposure to winter sunlight in Boston and Edmonton will not promote Vitamin D3 synthesis in human skin, *J. Clin. Endocrinol. Metab.*, *67*, 373–378.

Webb, A., J. Gröbner, and M. Blumthaler (2006), A practical guide to operating broadband instruments measuring erythamally weighted irradiance, Producen by the join efforts of WMO SAG UV and Working Group 4 of the COST-726 Action: Long Term Changes and Climatology of the UV Radiation over Europe, vol.EUR 22595/WMO.

WMO: Scientific Assessment of Ozone Depletion (2010), Global Ozone Research and Monitoring Project - Report No. 52, 516 pp., Geneva, Switzerland, 2011.

Zerefos, C., C. Meleti, D. Balis, K. Tourpali, and A. F. Bais (1998), "Quasi-biennial and longer-term changes in clear sky UV-B solar irradiance", *Geophys. Res. Lett.*, *25* (23), 4345–4348.

Zerefos, S. C., K. Tourpali, K. Eleftheratos, S. Kazadzis, C. Meleti, U. Feister, T. Koskela, and A. Heikkilä (2012), "Evidence of a possible turning point in solar UV-B over Canada, Europe and Japan", *Atmos. Chem. Phys.*, *12*, 2469–2477.

4.3.4. Informe del Director de la Tesis Doctoral

El artículo "Shadow-band correction for diffuse ultraviolet radiation measurements", fue publicado en la revista Journal of Geophysical Research - Atmospheres en mayo de 2013, teniendo la revista un factor de impacto en 2013 de 3.440 y estando incluida en el primer cuartil (Q1, ranking 24 de 174 revistas) dentro de la categoría "Geosciences, Multidisciplinary".

La participación de la doctoranda Dña. Guadalupe Sánchez Hernández en este artículo ha sido muy elevada y diversa, colaborando muy activamente en todas las etapas desarrolladas para la obtención del artículo, como la preparación del experimento, toma de medidas, propuesta, implementación y adaptación de los modelos, cálculo, análisis de los resultados y comparativa entre modelos, extracción de conclusiones y elaboración del manuscrito. Merece la pena destacar las labores de preparación de una banda de sombra para la medida de la irradiancia difusa ultravioleta.

Todas estas las tareas han sido desarrolladas por la doctoranda bajo mi dirección y supervisión, pudiendo dar fe de que todo lo aquí expuesto es verídico.

Fdo.: El Director de la Tesis Doctoral

Por otra parte, D. Antonio Serrano Pérez y Dña. María Luisa Cancillo Fernández, coautores de este artículo, afirman mediante este escrito que han colaborado en este artículo pero que éste forma parte íntegra de la Tesis Doctoral de Dña. Guadalupe Sánchez Hernández y que no va a ser utilizado por ellos como parte de sus respectivas tesis doctorales.

Dña. Mª Luisa Cancillo Fernández D. Antonio Serrano Pérez

Capítulo 5

Modelos empíricos para la estimación de irradiacia difusa

5.1. Introducción

Como se comentó en el Capítulo 1, la modelización de la radiación difusa requiere de información precisa sobre la composición de la atmósfera con el fin de determinar los procesos de dispersión que en ella acontecen. Sin embargo, en la mayoría de las ocasiones, no se cuenta con toda la información necesaria, por lo que finalmente se selecciona un número reducido de variables que permitan, al menos, modelizar situaciones específicas.

Una de las variables más utilizadas para la estimación de valores de radiación difusa total es la radiación global total. Trabajar con esta magnitud presenta dos importantes ventajas. Por un lado, los valores de radiación global total contienen toda la información necesaria sobre los procesos de dispersión que tiene lugar en la atmósfera, ya que ha sido sometida a ellos. Por otro lado, la medida de esta magnitud está muy extendida, lo que permitiría la aplicación de los modelos construidos a partir de ella en numerosas localizaciones.

Una forma particular de este tipo de modelos consiste en expresiones que modelan la fracción difusa a partir de la transmisividad. Trabajar con estas variables normalizadas presenta algunas ventajas entre las que destacan: 1) una menor dependencia respecto a la posición solar y 2) una mayor sensibilidad a pequeñas variaciones en la distribución de las componentes difusa y directa de la radiación solar [Long y Ackerman, 2000].

Esta relación entre la fracción de irradiancia difusa total y la transmisividad en el espectro solar total (también denominada índice de claridad) fue sugerida por primera vez por Liu y Jordan [1960] y desde entonces ha sido utilizada como punto de partida de numerosos modelos. Entre los modelos de este tipo destacan los propuestos por Reinld et al. [1990], Boland et al. [2008] o Ridley et al. [2010]. Algunos estudios recientes han recopilado y comparado un gran número de este tipo de modelos poniendo de manifiesto su idoneidad para la estimación de la fracción difusa total [Engerer, 2015; Gueymard y Ruiz-Arias 2016].

Sin embargo, no existen modelos empíricos para la obtención de la fracción difusa a partir de la transmisividad en el rango de longitudes de onda ultravioleta. A priori, cabría esperar que en el rango ultravioleta este tipo los modelos también muestren buenos resultados, e incluso mejores que en el espectro total, debido al gran peso que la componente difusa tiene en este intervalo espectral. No obstante existen otros factores que podrían afectar negativamente a esta relación a la hora de proponer modelos para la estimación de la fracción difusa ultravioleta como, por ejemplo, el reducido rango de variación de los valores de transmisividad en este intervalo espectral. Este y otros aspectos de la relación entre la fracción difusa y la transmisividad en el rango ultravioleta han sido analizados en este capítulo con el fin proponer modelos empíricos para la estimación de la fracción difusa ultravioleta.

5.2. Artículo 7

5.2.1. Datos del artículo

Título: Modeling ultraviolet diffuse fraction

Autores: Guadalupe Sánchez[a]
Antonio Serrano[a]
Mª Luisa Cancillo[a]

Filiación: [a]Dpto. de Física, Universidad de Extremadura, Badajoz, España

Revista: *Journal of Geophysical Research-Atmospheres*

Estado: En revisión

5.2.2. Principales aportaciones del artículo

El principal objetivo de este trabajo es proponer modelos para la estimación de irradiancia difusa ultravioleta. En particular, se han propuesto modelos empíricos para la estimación de la fracción de irradiancia difusa eritemática (UVER) inspirados en expresiones empleadas habitualmente para la estimación de la fracción de irradiancia difusa total.

Los modelos propuestos parten de la relación entre la fracción de irradiancia difusa y la transmisividad de la radiación UVER. Se ha elegido la transmisividad como variable principal ya que esta magnitud se ve afectada por los mismos procesos de dispersión que la componente difusa. En los modelos propuestos en este estudio se han incorporado también otras variables que complementan la información aportada por la transmisividad como el ángulo cenital solar o parámetros de variabilidad obtenidos también a partir de valores de irradiancia global ultravioleta eritemática.

Para el desarrollo de este trabajo se ha contado con dos años de datos horarios de irradiancia global y difusa ultravioleta eritemática. Ambas magnitudes han sido medidas con el mismo modelo de radiómetro, el modelo UVS-E-T fabricado por Kipp & Zonen. Esto minimiza la posibilidad de que los modelos puedan verse afectados por diferencias en el comportamiento de los radiómetros. Además, ambos instrumentos han sido calibrados siguiendo el procedimiento establecido por Grupo de Trabajo 4 de la Acción COST 726 [Webb et al., 2006; Gröbner et al. 2007; Vilaplana et al., 2009]. La precisión de la medida no se verá afectada por el dispositivo de apantallamiento de la componente directa ya que para dicha labor se ha utilizado un seguidor solar equipado con un a bola de sombra.

Finalmente este trabajo propone tres expresiones lineales para la estimación de la fracción de difusa ultravioleta eritemática que reproducen los valores de referencia con un coeficiente de determinación de 0.8 y un error cuadrático medio relativo del 8 %.

Si bien la aplicación de los modelos propuestos en este trabajo se restringe a localizaciones con medidas de irradiancia global UV, esto supone cada vez menos una limitación. El creciente interés por los efectos de la radiación UV sobre la salud humana ha favorecido el aumento de estaciones para la medida de la radiación global UV, lo que favorece la aplicación de los modelos propuestos en este trabajo.

Es necesario validar estos modelos a partir de medidas tomadas con otros radiómetros y en otras localizaciones para confirmar su validez general. Además sería de gran interés comparar las expresiones propuestas en este artículo con otros modelos como por ejemplo el propuesto por Nuñez et al. [2012].

5.2.3. Copia original del artículo

MODELING ULTRAVIOLET DIFFUSE FRACTION

G. Sanchez[1], A. Serrano[1], M.L.Cancillo[1]

[1]Department of Physics, University of Extremadura, Badajoz, Spain

Corresponding author: Guadalupe Sanchez (guadalupesh@unex.es)

Key points:

.- Twenty-three empirical models are proposed to estimate hourly UVER diffuse fraction.

.- Models including k_{UV}, $cos(\theta)$ and $\Delta_{UV\text{-}2}$ as independent variables perform best.

.- Best models achieve an r^2 of 0.8 and *rRMSE* of 8%.

Abstract.- Although being extremely interesting, UV diffuse irradiance is scarcely measured at standard radiometric stations and, therefore, needs to be estimated. This study proposes and compares a plethora of empirical models to estimate the UV diffuse fraction. Thus, twenty-three models, originally inspired on mathematical expressions used to estimate total diffuse fraction, are adapted to the UV range and tested against experimental measurements. According to these expressions, the UV transmissivity (k_{UV}), the solar zenith angle, θ, three short-term variability parameters, the apparent solar time, the daily clearness index, and a persistence parameter are included as independent variables. Additionally, both linear and logistic functional forms are considered, showing the former a better performance. The performance of the models proposed is compared regarding its r^2, *rRMSE* and relative differences with experimental measurements of the UV diffuse fraction. The model M9, consisting of a fourth-order polynomial in determinate k_{UV} and including the cosine of the solar zenith angle, $cos(\theta)$, and $\Delta_{UV\text{-}2}$ short-term variability parameter as additional factors, performs best, with an r^2 of 0.8 and *rRMSE* of 7.8%. The relative importance of the factors is analyzed using the CAR scores, resulting in a 64.1% of the total correlation explained by the UV transmissivity, 13.4% by the solar zenith angle, and 22.5% by the short-term variability parameter $\Delta_{UV\text{-}2}$. This study provides empirical models for reliably estimate hourly UV diffuse fraction with errors under 10%.

Key words.- ultraviolet radition, diffuse fraction, erythemal irradiance, UV transmissivity

1.- Introduction

The knowledge of the ultraviolet (UV) solar radiation at the Earth's surface becomes a high priority since it affects many biological, ecological and photochemical processes [Williamson et al., 2014]. Essential ecosystems for Earth's life such as corals and phytoplankton are extremely sensitive to alterations in UV radiation [Häder et al., 2011 and 2015], notably affecting also plant growth [Diffey, 1991; Hollosy, 2002; Kataria et al., 2014]. Additionally, UV radiation is the main factor for the degradation of materials such as paints or plastics when exposed to the environmental conditions [Johnson and McIntyre, 1996; Verbeek et al., 2011].

On the other hand, low doses of UV radiation are beneficial for human health, particularly for the synthesis of vitamin D3, critical in maintaining blood calcium levels [Webb et al., 1988; Glerup et al., 2000; Holick, 2004]. However, an excessive exposure has adverse consequences such as favoring skin cancer, immune suppression and eye disorders [Diffey, 2004; Heisler, 2010]. The effectiveness of UV radiation in producing erythema on human skin is usually quantified by the erythemal action spectrum [McKinlay and Diffey, 1987], being the UV radiation weighted by this action spectrum named as erythemal ultraviolet (UVER) radiation.

Recent studies have shown that, in addition to ozone variability, changes in UV radiation in the last two decades have been influenced by variations in aerosols, clouds, and surface reflectivity [Arola et al., 2003; Herman, 2010]. Significant positive trends in UV radiation have been detected in different European countries and attributed to decreasing in cloud cover [Krzyscin et al., 2011; Smedley et al., 2012]. A positive trend in UVER of 2.1 % per decade has been detected in the Iberian Peninsula for the 1985 – 2011 period and attributed to aerosol reduction [Roman et al., 2015].

In the framework of the climate change, new variations are expected in ultraviolet irradiance at the Earth's surface for the next decades as a result of the changes predicted on clouds and aerosols [McKenzie et al., 2007; Bais et al., 2011; Craig et al., 2014]. These variations notably affect not only the amount but also the ultraviolet direct/diffuse partitioning due to the stronger effectiveness of scattering at shorter wavelengths.

The diffuse ultraviolet irradiance is of particular relevance since it is difficult to block [Utrillas 2010; Kudish 2011], in contrast to the direct component. Thus, diffuse UVER irradiance under a standard beach umbrella can reach 34% of global UVER irradiance [Utrillas 2007] and up to 60% in a tree shade [Parisi 2000]. This percentage increases notably with high load of aerosols and presence of clouds, especially in the case of broken-clouds [Piedehierro et al. 2014].

Very few studies focus on ultraviolet diffuse irradiance mainly due to the scarcity in experimental measurements. While global UV irradiance is commonly measured worldwide, its diffuse component is seldom measured. Therefore, modeling reveals as a good alternative to relieve this scarcity.

However, as far as we are aware, only a few studies have aimed at modeling the diffuse solar irradiance in the ultraviolet range [Grant and Gao, 2003; Nunez et al., 2012; Silva, 2015]. Moreover, these studies rely on spectral measurements [Silva, 2015] or require specific variables usually unavailable [Grant and Gao, 2003; Nunez et al., 2012]. In this context, comprehensive studies focused on the proposal of reliable models based on commonly available data are needed.

Therefore, this study aims to propose empirical expressions for modeling hourly UVER diffuse fraction under different sky conditions and to compare their performance against experimental measurements. The proposed expressions will be inspired on the empirical formulae commonly used to estimate the diffuse fraction for total solar irradiance. Several radiometric and geometrical variables will be essayed in order to address their contribution. Finally, the performance of the proposed expressions will be compared against experimental measurements.

2.- Instrumentation and data

Data used in this paper correspond to measurements registered at our radiometric station installed on the roof of the Physics Department building of the University of Extremadura in Badajoz, Spain. This experimental site is located in south-western Spain (38.9º N; 7.01º W; 199 m a.s.l.). It is characterized by a very dry summer with prevailing cloud-free conditions, leading to UVI values among the highest in Europe. Throughout the rest of the year very different cloud conditions can be found mainly

associated to frontal systems coming from the Atlantic Ocean and to local convective systems. This region is also influenced by different aerosol types such as industrial/urban, mineral and forest fire particles. The mean aerosol optical depth at 440 nm is 0.14 and the mean Angström exponent alpha is 1.2 [Obregón et al., 2012]. Extreme aerosol optical depth values higher than 0.3 can be occasionally reached as a result of desert dust intrusions from Sahara Desert (Northern Africa). This variety of situations guarantees the representativeness of the measurements to be used for the proposal and assessment of general empirical models.

The data set consists of simultaneous measurements of horizontal global and diffuse UVER irradiance recorded by two Kipp & Zonen UVS-E-T radiometers with serial numbers #000409 and #080017. The radiometer #080017 was installed on a Kipp & Zonen Solys 2 sun tracker and shaded by a small ball with the aim to measure diffuse UVER irradiance.

To ensure the reliability of the measurements, both pyranometers were accurately calibrated according to the standard procedure recommended by the Working Group 4 of the COST Action 726 [Webb et al., 2006; Gröbner et al. 2007; Vilaplana et al., 2009]. The calibration campaign was held in July 2011 at "El Arenosillo" Atmospheric Sounding Station of the National Institute for Aerospace Techniques (ESAt/ INTA) in Huelva, Spain (37.10º N, 7.06º W).

The period of study comprises years 2011 and 2012, ensuring the sampling of a great variety of seasonal processes and meteorological conditions. Diffuse UVER measurements were recorded every minute by a Campbell Scientific CR-1000 data logger.

One-minute values for the variables involved in this study such as UV diffuse fraction, UV transmissivity, solar zenith angle, and other sun-geometry parameters were calculated and subsequently averaged hourly. Hourly frequency was preferred since it suitably shows daily variations without been affected by the very fast short-term fluctuations.

3.- Methodology

3.1. Proposal of models

The diffuse component of the solar radiation is usually quantified by the diffuse fraction, defined as the ratio between the diffuse (D) and the global (G) solar irradiances. The present study focuses on estimating the diffuse fraction of the solar radiation at UV wavelengths at the Earth's surface, f_{UV}, defined as follows:

$$f_{UV} = \frac{D_{UV}}{G_{UV}} \qquad (1)$$

Although the models for estimating this UV diffuse fraction are very scarce, there are several expressions proposed for modeling the diffuse fraction integrated along the complete solar wavelength interval (termed as total diffuse fraction) [Engerer, 2015; Gueymard and Ruiz-Arias 2016]. These models attempt to describe the absorption and scattering suffered by the solar radiation when crossing the atmosphere. Since the mechanisms of absorption and scattering of UV solar radiation are similar to those affecting other solar wavelengths, the proposal of empirical models for the UV diffuse fraction will be inspired in the existing mathematical expressions used for modeling the total diffuse fraction. Towards this goal, a complete compilation of models for estimating total diffuse fraction was performed, and their functional form and variables involved were analyzed. Subsequently, similar models were proposed adapting the selected most representative mathematical expressions to the UV case, replacing the variables with their corresponding UV version.

Regarding its functional form, the empirical models for total diffuse fraction can be generally classified in two main groups: 1) those consisting of polynomials and linear combination of multiple variables, and 2) those based on logistic functions. Additionally, in this study, linear or linearizable models were preferred than highly nonlinear models such as those proposed by Boland et al. [2008] and Ruiz-Arias et al. [2010]. The non-linear fittings for these two models rely on non-trivial assumptions and highly depend on the preliminary values given to the fitting coefficients.

With respect to the independent variables, most empirical models for total diffuse fraction contain the total transmissivity, also named clearness index (k_t), as the main factor. Similarly, our proposed models will rely on the UV transmissivity (k_{UV}), defined as the ratio between the UV irradiance at the Earth's surface and the UV irradiance at the top of the atmosphere:

$$k_{UV} = \frac{G_{UV}(z=0)}{G_{UV}(z=TOA)} \qquad (2)$$

The UV irradiance at the top of the atmosphere can be calculated as follows [Iqbal, 1983]:

$$G_{UV}(z=TOA) = S_{UV}\left(\frac{r_0}{r}\right)^2 \cos(\theta) \qquad (3)$$

where θ is the solar zenith angle, $(r_0/r)^2$ is the eccentricity correction-factor of the Earth's orbit, and S_{UV} is the erythemally-weighted solar constant, with an estimated value of 10.031 W/m^2. The eccentricity correction-factor was calculated using the Spencer's formula [1971].

Figure 1 shows the relationship between the UV diffuse fraction, f_{UV}, and the UV transmissivity, k_{UV}. A general dependence can be clearly seen though the scatter suggests the influence of other factors as well. In order to account for this variability additional radiometric magnitudes and sun-geometry parameters directly related to the absorption and scattering of radiation in the atmosphere must be considered. Our proposal focuses on models relying on variables commonly available at standard radiometric stations, in order to ensure a large applicability.

Finally, according to the mentioned criteria regarding linear expressions and available variables, nineteen UV diffuse fraction models were proposed. They are inspired in the most representative functional forms used for modeling total diffuse fraction: polynomials and multiple linear combinations, and logistic functions. Table 1 shows their mathematical formulae and the next two subsections describe each model in detail.

3.1.a. Polynomials and multiple linear combinations

Many empirical models for estimating total diffuse fraction models use piecewise functions to suitably describe the particular behaviour shown for very low and very high diffuse transmissivity values [Orgill and Hollands, 1977; Erbs et al., 1982; Reindl et al., 1990; De Miguel et al., 2001]. As shown in Figure 2, this behaviour is not detected in the case of UV diffuse traction and, therefore, empirical models are proposed with the aim to be valid along the whole range of diffuse transmissivity.

Firstly, polynomials in the indeterminate k_{UV} with degrees from one to six were tested by fitting the experimental measurements. The findings suggested to select the fourth degree polynomial since it performed best. The first degree polynomial has been also analyzed in order to compare with the performance achieved by more simple expressions. First and fourth degree polynomials are plotted in Figure 2 and will be called M1 and M2, respectively.

Figure 2 shows large scatter, suggesting to consider additional factors. Reindl et al. [1990] proposed to use the term *cos(θ)* for total diffuse fraction since the scattering increases with the solar zenith angle, mainly in clear days. This effect is even more relevant in the UV range due to the stronger effectiveness of scattering at shorter wavelengths. Therefore, models M3 and M4 were built adding that term to the models M1 and M2.

Additionally, the diffuse fraction shows further variability due to short-term changes in clouds or atmospheric turbidity. Several authors [Skartveit and Olseth, 1987; Perez et al., 1990; Gonzalez and Calbo, 1999; Ridley et al., 2010] have proposed different approaches to account for this variability in the case of total diffuse fraction. In this study, the variables Δ_1, Δ_2 and Δ_3 originally suggested by Gonzalez and Calbo [1999] for the total solar range have been adapted to the UV wavelengths as follows:

$$\Delta_{UV-1} = \ln\left(\frac{\sigma}{\overline{k_{UV}}}\right) \tag{4}$$

$$\Delta_{UV-2} = \ln\left(\frac{1}{(N-1)\,\overline{k_{UV}}} \sum_{i=1}^{i=N} \left|k_{UV(i+1)} - k_{UV(i)}\right|\right) \tag{5}$$

$$\Delta_{UV-3}=\ln\left(\frac{1}{(N-1)\overline{k_{UV}}}\sum_{i=1}^{i=N}\left|k_{UV,max}-k_{UV,min}\right|\right) \quad (6)$$

where σ is the standar deviation, $\overline{k_{UV}}$ is the mean value, $k_{UV,max}$ is the maximmum value and $k_{UV,min}$ is the minimmum value of k_{UV} for each hour. Although looking similar, these variables mean different approaches to describe the short-term variability in the UV diffuse fraction. Thus, Δ_{UV-1} accounts for intermediate values between the minimum and the maximum, whereas Δ_{UV-3} only depends on the extreme values. On the other hand, the fast variations between consecutive measurements are only addressed by variable Δ_{UV-2}.

It should be noted that measurements at a frequency higher than one per hour are needed to calculate these variables. In this study the original one-minute data measurements have been used.

Similarly to the proposal of Gonzalez and Calbo [1999] for total diffuse fraction, the UV-adapted variables Δ_{UV-1}, Δ_{UV-2} and Δ_{UV-3} were added to our previously built models for UV diffuse fraction, resulting in new models M5 to M10 (see Table 1).

3.1.b.- Logistic models

Boland et al. [2001] proposed a logistic function to estimate the total diffuse fraction as function of the total transmissivity. This expression was later expanded by Ridley et al. [2010] to include four additional variables: 1) the solar zenith angle, 2) the apparent solar time (AST) to account for differences in the atmosphere between morning and afternoon, 3) the daily clearness index calculated as the ratio between the irradiation accumulated along the whole day at the Earth's surface and its value at the top of the atmosphere, and 4) a variable to account for the persistence at one hourly scale due to the very slow rate of change in the radiation under certain cloud conditions such as cloud-free or overcast skies.

Although this logistic function is highly non-linear, it can be linearized taken logarithms and, therefore, ordinary least squares regression can be use for the fitting. Hence, it has been included in this comparison. Towards this aim the UV daily clearness index, K_{UV}, and the atmospheric persistence from

UV measurements, Ψ_{UV}, have been adapted as follows:

$$\Psi_{UV} = \frac{k_{UV,i-1} + k_{UV,i+1}}{2} \tag{7}$$

$$K_{UV} = \frac{\sum_{sunrise}^{sunset} G_{UV}(z=0)}{\sum_{sunrise}^{sunset} G_{UV}(z=TOA)} \tag{8}$$

where $k_{UV,i-1}$ and $k_{UV,i+1}$ are the values before and after for each value of k_{UV}

In addition to adapting to the UV range the five-variable model originally proposed by Ridley et al. [2010], different more parsimonious combinations were considered, being named as models M11 to M15 (see Table 1). It has to be noted that, in this study, the variable θ used by Ridley et al. [2010] has been replaced by $cos(\theta)$ in order to facilitate the comparison with the other models. Models with θ and $cos(\theta)$ have been tested showing nearly equal performance (not shown here).

Additionally, following Kuo et al.'s [2014] suggestion, a multiple linear combination version of the models M11 to M15 was proposed resulting in models M16 to M19 (see Table 1). Similarly to the linear combination models described above, versions including first and fourth degree polynomials in determinate k_{UV} and the additional variables suggested by Kuo et al. were also tested.

3.2.-Fitting and comparison statistics

The performance of the models proposed to estimate the UV diffuse fraction were compared. Towards this aim, the hourly dataset was randomly divided in two subsets: 1) the fitting subset, containing the 75% of data, for fitting the coefficients of the models, and 2) the validation subset, containing the remaining 25% of data, for model validation and comparison.

The coefficient of determination, r^2, and the relative root-mean-square error, *rRMSE*, defined as:

$$r^2 = 1 - \frac{\sum_{i=1}^{i=N} (x_i - x_i^*)^2}{\sum_{i=1}^{i=N} (x_i - \overline{x})^2} \tag{9}$$

$$rRMSE() = \frac{100}{\overline{x}} \sqrt{\frac{1}{N} \sum_{i=1}^{i=N} (x_i - x_i^*)^2} \tag{10}$$

were used to assess the goodness of fit of the models and their performance. The coefficient of determination is a measure of the proportion of total variance explained by the model, while the relative root-mean-square error quantifies the difference between modeled and measured values.

Additionally, the Taylor diagram [Taylor, 2001] and the relative differences were used for model comparison. The Taylor diagram provides a concise graphical summary of different aspects of the performance of a model such as the centered root-mean-square error, the correlation and the standard deviation. On the other hand, the relative differences between modeled (x~i) and measured (xi) values are calculated as follows:

$$RD(\%) = 100 \cdot \frac{x_i - x_i^*}{x_i} \tag{11}$$

and can be analyzed as a function of the solar zenith angle, the UV transmissivity, and the UV diffuse fraction, providing interesting information about possible remaining dependences.

The contribution of the various factors included in the best performing models was analyzed. This contribution was quantified using the CAR score (Zuber and Strimmer, 2011). This statistic (Correlation-Adjusted (marginal) coRelation) is a natural measure of variable importance defined as the marginal correlation adjusted for correlation among explanatory variables. It provides a simple criterion for ranking and selecting variables in linear regression models (Zuber and Strimmer, 2011). CAR score comparison is widely applicable since it is untied from the specific estimation procedure like other model-selection regression approaches [Grömping, 2015].

Finally, the Akaike's Information Criterion (AIC) which describes the trade-off between precision and complexity of the best performing models were obtained.

4.- Results and Discussion

4.1.- Comparison of models

Table 1 shows the results of the models when fitted by ordinary least squares to the fitting subset. All models perform notably well with r^2 higher than 0.64 and *rRMSE* lower than 11.0%. This fact confirms the general suitability of the proposed models for estimating UV diffuse fraction. Regarding the functional form, the logistic function models perform somewhat worse than their analogous multiple linear combination version.

Subsequently, in order to address the performance of the models against independent data, they were applied to the validation subset. The resulting *rRMSE* values are also shown in Table 1. The validation results are very similar to the fitting results, indicating no overfitting effect. Taylor diagram (Figure 2) confirms the good general performance achieved by the proposed models, mainly the linear ones (M1 to M10, M16 to M23). Linear models show a correlation over 0.9 and centered root mean square error lower than logistic models (M11 to M15).

On the other hand, since polynomial models M1 and M2 include only the UV transmissivity as indeterminate variable, they show slightly worse performance than models involving additional factors. In fact the best performance is found for three-variable models M6 and M9. These models combine a first- and fourth-degree polynomial in k_{UV} with the terms $cos(\theta)$ and $\Delta_{UV\text{-}2}$. However, no significant improvement with respect to the three-variable model is achieved when a fourth and fifth variable is added such in models M15 and M23.

The comparisons of models M5, M6 and M7 among themselves, and M8, M9 and M10 among themselves indicate the better performance of $\Delta_{UV\text{-}2}$ with respect to $\Delta_{UV\text{-}1}$ and $\Delta_{UV\text{-}3}$ as descriptor of the variability at time periods shorter than one hour. This primacy of $\Delta_{UV\text{-}2}$ agrees with the case of total diffuse fraction, as reported by Gonzalez and Calbo [1999].

Differences among models with regard to r^2 and rRMSE are non significant and, therefore, further analyses are needed in order to select the best models. Thus, relative differences (RD) between measured and modeled values were calculated and their dependence with respect to solar zenith angle, UV transmissivity and UV diffuse fraction bands was analyzed. Figure 3 shows the relative differences for best performing and most representative models. Models including a first degree polynomial in determinate k_{UV} such as M1, M3, M6 and M17 are plotted on the left panel, whereas those including a fourth degree polynomial such as M2, M4, M9 and M20 are plotted on the right panel. In order to clearly show the dependence with a particular variable, relative differences were averaged by intervals in that variable.

In addition to showing the overall magnitude of the relative differences, Figure 3 provides interesting information about the variation in the relative differences with respect to certain variables. Significant trends are observed when the dependences with solar zenith angle and UV diffuse fraction are analyzed. Thus, relative differences are high for low solar zenith angle and generally decreases as the solar zenith angle increases. Concerning UV diffuse fraction, the models tend to underestimate for intermediate values and overestimate for high values over 0.8.

Models based on a first degree polynomial (Figure 3, left side) show large mean relative differences up to 10%. When a fourth degree polynomial is included (Figure 3, right side) mean relative differences are reduced to 5% and a more constant behaviour is obtained, mainly with respect to the UV diffuse fraction and solar zenith angle. This improvement is more significant in models M4 and M9.

On the other hand, including additional factors generally reduces the absolute relative differences (Figure 4). This improvement is clear in the case of adding the term $cos(\theta)$ as shown by models M3 versus M1, and M4 versus M2. However, the gain achieved by adding other additional factors is limited.

Therefore, M4, M9 and M20 were selected as best performance models. These models are analyzed in detail in the next subsection.

4.2. Analysis of best performing models

Table 2 shows the best performing empirical models M4, M9 and M20 with their corresponding fitting coefficients. All coefficients are statistically significant at the 95% confidence level. It is important to note that although the functional form can be generally suitable for other locations, the particular values of the coefficients are specific for the local conditions of Badajoz. Therefore, in order to apply the models to other locations, the coefficients should be calculated by fitting against local measurements.

Table 3 shows the magnitude of the terms included in the models M4, M9 and M20. The intercept is higher than 0.83, indicating most radiation is diffuse when the UV transmissivity is low (overcast conditions). Conversely, the polynomial in k_{UV} contributes negatively, in agreement with the increase in the direct component, and consequently decrease in the diffuse fraction, as the UV transmissivity increases (cloud-free conditions). Regarding the additional factors, as expected, the cosine of the solar zenith angle has a positive impact. Thus, the diffuse fraction increases at low solar altitude due to the longer atmospheric path and the subsequent intensified scattering. On the other hand, the short-term variability parameters $\Delta_{UV\text{-}2}$ and Ψ_{UV} contribute negatively since they are somewhat based on the UV transmissivity values.

In order to address the contribution of each term to the diffuse fraction, the CAR score was calculated (Table 3). This statistic quantifies the marginal correlation explained by each variable once adjusting for correlation among explanatory variables.

Among the set of variables, the polynomial in determinate k_{UV} shows the highest CAR score in all three models. It explains 88.6% of correlation in model M4 and decreases to 64.1% and 56.0% when short-term variability parameters $\Delta_{UV\text{-}2}$ or Ψ_{UV} are added, respectively. On the other hand, the additional factors show CAR scores between 6.2% and 37.8%.

Models M9 and M20 allow to analyze the improvement achieved when additional variables are added to model M4 in order to describe the short-term variability in f_{UV}. It is to note that, although Ψ_{UV} shows a high CAR score in model M20, the statistics *rRMSE*, r^2 and *AIC* of model M20 seldom improve the values obtained by model M4 (Table 3). Conversely, including $\Delta_{UV\text{-}2}$ results in the best performance model M9. In this model the UV transmissivity is responsible for 64.1% of the correlation, the cosine

of the solar angle explains a 13.4% and the Δ_{UV-2} parameter explains the 22.5% (Table 3).

5.- Summary and conclusions

This study aims to accurately estimate hourly UVER diffuse fraction at the Earth's surface using empirical models. Towards this goal, a plethora of mathematical expressions were proposed and their performance compared against experimental measurements. Since very few empirical models for the UV diffuse fraction have been proposed in the literature, our functional forms were inspired on mathematical expressions suggested for the total diffuse fraction by Reindl. et al [1990], Gonzalez and Calbo [1999], Ridley et al. [2010] and Kuo [2014].

The empirical models proposed in this study were primarily based on the UV transmissivity (k_{UV}) as the main factor. Then, other additional factors such as the solar zenith angle, the apparent solar time, the persistence, and different short-term variability parameters were added resulting a total of 23 different linear and logistic mathematical expressions to be tested.

The fitting to experimental measurements revealed a better performance of linear than logistic models. In the case of total integrated radiation, logistic models were proposed since they reliably describe the abrupt change shown by the relationship between the total diffuse fraction and the total transmissivity. However, in the UV range that relationship is much smoother and, therefore, logistic models provide no improvement with respect to more simple linear models.

The validation against independent set of measurements showed that polynomial models M1 and M2 with only UV transmissivity as indeterminate variable performed reasonably well, with r^2 of 0.75 and rRMSE around 9.4%. These statistics were improved by including additional factors in the formula. Taking into account the convenience of parsimonious expressions, models with two or three independent variables are generally prefered than those with five variables (such as M15 and M23). Thus, models M6 and M9 with k_{UV}, $cos(\theta)$ and Δ_{UV-2} as independent variables best performed, showing a r^2 of 0.81 and 0.83, and rRMSE of 8.3% and 7.9%, respectively. These two models performed better than those including Δ_{UV-1} or Δ_{UV-3} as short-term variability parameters, in line with the case of total

solar irradiance [Gonzalez and Calbo 1999].

With regard to the fundamental dependence with k_{UV}, a fourth degree polynomial performed notably better than using only a first degree polynomial, showing a better behaviour of the relative differences between modeled and measured values. These relative differences are generally reduced by including additional factors, mainly when the term $cos(\theta)$ is added. Finally, models M6, M9 and M20 are the ones with best performance.

The CAR scores were applied to quantify the relative importance of each term in the global magnitude. They were applied to models M6, M9 and M20, and identified k_{UV} as the main term explaining 88.6% of the total correlation in model M4, decreasing to 64.1% and 56.0% when short-term variability parameters $\Delta_{UV\text{-}2}$ or Ψ_{UV} are added, respectively. The additional factors show moderate CAR scores between 6.2% and 37.8%. The analysis of the AIC values for these three models confirms variable $\Delta_{UV\text{-}2}$ as the best descriptor for the short-term variability.

It can be concluded that M9 is the best model of the plethora of empirical expressions proposed. Its r^2 value of 0.83 is similar to the value obtained by the model proposed by Nunez et al. [2012] for the UV diffuse fraction. It is to note that, in contrast to Nunez et al.'s models, M9 requires no additional measurements of aerosols nor ozone.

This study positively contributes to estimate UV diffuse irradiance and UV diffuse fraction in locations where only UV global irradiance measurements are available. Additionally, the models proposed here can be used to expand time series of UV diffuse radiation to periods when global but not diffuse UV irradiance was being measured. In order to assess the general validity of the proposed models, similar research must be conducted in other locations.

6.- Acknowledgements

This study was partially supported by the research projects CGL2011-29921-C02-01 and CGL2014-56255-C2-1-R granted by the Ministerio de Economía y Competitividad from Spain and by Ayuda a

Grupos GR15137 granted by Junta de Extremadura and Fondo Social Europeo (FEDER). Guadalupe Sanchez Hernandez thanks the Ministerio de Economía y Competitividad for the predoctoral FPI grant BES-2012-054975. The data analyzed in this study are available from authors upon request (guadalupesh@unex.es).

7.- References

Bais A.F., K.Tourpali, A. Kazantzidis, H. Akiyoshi, S. Bekki, P. Braesicke, M.P. Chipperfield, M. Dameris, V. Eyring, H. Garny, D. Iachetti, P. Jöckel, A. Kubin, U. Langematz, E. Mancini, M. Michou, O. Morgenstern, T. Nakamura, P.A. Newman, G. Pitari, D.A. Plummer, E. Rozanov, T.G. Shepherd, K. Shibata, W. Tian, and Y. Yamashita (2011), Projections of UV radiation changes in the 21st century: impact of ozone recovery and cloud effects, *Atmos. Chem. Phys.*, 11, 7533-7545.

Boland, J., L. Scott, and M. Luther (2001), Modelling the diffuse fraction of global solar radiation on a horizontal surface, *Environmetrics*, 12, 103–116.

Boland, J., B. Ridley, and B. Brown (2008), Models of diffuse solar radiation, *Renew. Energy*, 33, 575–584.

De Miguel, A., J. Bilbao, R. Aguiar, H.D. Kambezidis, and E. Negro (2001), Diffuse solar irradiation model evaluation in the north Mediterranean belt area, *Sol. Energy*, 70, 143–153.

Diffey B.L. (1991), Solar ultraviolet radiation effects on biological systems, *Phys. Med. Biol.*, 36, 299-328.

Diffey, B. L. (2004), Climate change, ozone depletion and the impact on ultraviolet exposure of human skin, *Phys. Med. Biol.*, 49, 1–11.

Engerer, N.A. (2015), Minute resolution estimates of the diffuse fraction of global irradiance for

southeastern Australia, *Sol. Energy*, 116, 215–237.

Erbs, D., S.A. Klein, and J.A. Duffie (1982), Estimation of the diffuse radiation fraction for hourly, daily and monthly average global radiation, *Sol. Energy*, 28, 293–302.

Glerup, H., K. Mikkelsen, L. Poulsen, E. Hass, S. Overbeck and J. Thomsen (2000), Commonly recommended daily intake of vitamin D is not sufficient if sunlight exposure is limited, *J. Intern. Med.*, 247, 260-268.

Gonzalez, J.A., and J. Calbo (1999), Influence of the global radiation variability on the hourly diffuse fraction correlations, *Sol. Energy,* 65, 119–131.

Grant, R. H., and W. Gao (2003), Diffuse fraction of UV radiation under partly cloudy skies as defined by the Automated Surface Observation System (ASOS), *J. Geophys. Res.,* 108(D2), 4046, doi:10.1029/2002JD002201.

Gröbner, J., G. Hülsen, L. Vuilleumier, M. Blumthaler, J. M. Vilaplana, D. Walker, and J. E. Gil (2007), Report of the PMOD/WRC-COST Calibration and Intercomparison of Erythemal radiometers. Available at: http//i115srv.vuwien.ac.at/uv/COST726/COST726 Dateien/Results/PMOD WRC COST726 campaign 2006 R.pdf.

Gueymard C.A., and J.A. Ruiz-Arias (2016), Extensive worldwide validation and climate sensitivity a climate sensitivity analysis of direct irradiance predictions from 1-min global irradiance, *Solar Energy*, 128, 1–30

Häder D.P., E.W. Helbling, C.E. Williamson, and R.C. Worrest (2011), Effects of UV radiation on aquatic ecosystems and interactions with climate change, *Photochem. Photobiol. Sci.*, 10, 242 -260, doi: 10.1039/c0pp90036b.

Häder D.P., C.E. Williamson, S.Ä. Wängberg, M. Rautio, K.C. Rose, K. Gao, E.W. Helbling, R.P. Sinha, R.C. Worrest (2015), Effects of UV radiation on aquatic ecosystems and interactions with other environmental factors, *Photochem. Photobiol. Sci.,* 14, 108-126, doi: 10.1039/c4pp90035a.

Herman, J. R. (2010), Global increase in UV irradiance during the past 30 years (1979–2008) estimated from satellite data, *J. Geophys. Res.*, 115, doi:10.1029/2009JD012219.

Heisler, G. M. (2010), Urban forest influence on exposure to UV radiation and potential consequences for human health, in UV Radiation in Global Climate Change. Measurements, Modeling and Effects on Ecosystems, edited by Gao, W., et al., pp. 331–369, Tsinghua University Press, Beijing.

Holick, M. F. (2004), Vitamin D: importance in the prevention of cancers, type 1 diabetes, heart disease and osteoposoris, *Am. J. Clin. Nutr.*, 79, 362–371.

Hollósy F. (2002), Effects of ultraviolet radiation on plant cells, *Micron*, 33, 179 -197.

Iqbal, M. (1983), An Introduction to Solar Radiation, Academic Press, Ontario, Canada.

Johnson B.W., and R. McIntyre (1996), Analysis of test methods for UV durability predictions of polymer coatings, *Prog. Org. Coat.*, 27, 95 -106.

Kataria, S., A. Jajoo, and K.N. Guruprasad, 2014, Impact of increasing Ultraviolet-B (UV-B) radiation on photosynthetic processes, Journal of Photochemistry and Photobiology, 137, 55-66.

Krzyścin J.W., P.S. Sobolewski, J. Jarosławski, J. Podgórski, and B. Rajewska-Więch (2011), Erythemal UV observations at Belsk, Poland, in the period 1976–2008: Data homogenization, climatology, and trends, *Acta Geophysica*, 59, 155-182.

Kudish, A. I., M. Harari, and E. G. Evseev (2011), The solar ultraviolet B radiation protection provided by shading devices with regard to its diffuse component, *Photodermatol. Photoimmunol. Photomed.*, 27, 236–244, doi:10.1111/j.1600-0781.2011.00608.

Kuo, C.-W., W.-C. Chang, ad K.-C. Chang (2014), Modeling the hourly solar diffuse fraction in

Taiwan, *Renew. Energy,* 66, 56–61.

McKenzie R.L., P.J. Aucamp, A.F. Bais, L.O. Björn, and M. Ilyas (2007), Changes in biologically-active ultraviolet radiation reaching the Earth's surface, *Photochem. Photobiol. Sci.,* 6, 218 - 231. doi.:10.1039/B700017K

McKinlay A.F. and B.L. Diffey (1987), Human Exposure to Ultraviolet Radiation: Risks and Regulations Edited by W. F. Passchier and B. F. M. Bosnajakovic, pp.83–87, Elsevier, Amsterdam.

Nuñez, M., M. P. Utrillas, and J. A. Martinez-Lozano (2012), Approaches to partitioning the global UVER irradiance into its direct and diffuse components in Valencia, Spain, *J. Geophys. Res.*, 117, doi:10.1029/2011JD016087.

Obregón, M.A., S. Pereira, F. Wagner, A. Serrano, M.L. Cancillo, and A.M. Silva (2012), Regional differences of column aerosol parameters in western Iberian Peninsula, *Atmos. Environ.,* 12, 1 – 10. http://dx.doi.org/10.1016/j.atmosenv.2012.08.016.

Orgill, J.F., and K.G.T. Hollands (1977), Correlation equation for hourly diffuse radiation on a horizontal surface, *Sol. Energy,* 19, 357–359.

Parisi, A. V., M. G. Kimlin, J. C. F. Wong, and M. Wilson (2000), Diffuse component of solar ultraviolet radiation in tree shade , *J. Photochem. Photobiol. Biol.*, 54, 116–120.

Perez, R., P. Ineichen, R. Seals, and A. Zelenka (1990), Making full use of the clearness index for parameterizing hourly insolation conditions, *Sol. Energy,* 45, 111–114.

Piedehierro A.A., M. Anton, A. Cazorla, L. Alados-Arboleda L., and F.J. Olmo (2014), Evaluation of enhancement events of total solar irradiance during cloudy conditions at Granada (Southeastern Spain), *Atmospheric Research*, 135-136,1-7.

Reindl, D.T., W.A. Beckman, and J.A. Duffie (1990), Diffuse fraction correlations, *Sol. Energy*, 45, 1–7.

Ridley, B., J. Boland, and P. Lauret (2010), Modelling of diffuse solar fraction with multiple predictors, *Renew. Energy,* 35, 478–483.

Román R., J. Bilbao and A. de Miguel (2015), Erythemal ultraviolet irradiation trends in the Iberian Peninsula from 1950 to 2011, *Atmos. Chem. Phys.*, 15, 375–391, doi:10.5194/acp-15-375-2015

Ruiz-Arias, J.A., H. Alsamamra, J. Tovar-Pescador, and D. Pozo-Vazquez (2010), Proposal of a regressive model for the hourly diffuse solar radiation under all sky conditions, *Energy Convers. Manag.*, 51, 881–893.

Silva A. (2015), The diffuse component of erythemal ultraviolet radiation, *Photochem. Photobiol. Sci.,* doi: 10.1039/c5pp00131e

Skartveit, A., and J.A. Olseth (1987), A model for the diffuse fraction of hourly global radiation, *Sol. Energy,* 38, 271–274.

Smedley A.R.D., J.S. Rimmer, D. Moore, R. Toumi, and A.R. Webb (2012), Total ozone and surface UV trends in the United Kingdom: 1979–2008, *Int. J Climatol.,* 32, 338-346.

Spencer, J. W. (1971), Fourier series representation of the position of the sun, *Search,* 2(5), 172.

Taylor, K.E. (2001), Summarizing multiple aspects of model performance in a single diagram, *J. Geophys. Res.,* 106D, 7183–7192.

Utrillas, M. P., M. J. Marín, A. R. Esteve, F. Tena, J. Cañada, V. Estellés, and J. A. Martínez-Lozano (2007), Diffuse UV erythemal radiation experimental values, *J. Geophys. Res.,* 112, doi:10.1029/2007JD008846.

Utrillas, M. P., J. A. Martınez-Lozano, and M. Nuñez (2010), Ultraviolet Radiation Protection by a Beach Umbrella, *Photochem. Photobiol.,* 86, 449–456, doi:10.1111/j.1751-1097.2009.00677.x.

Verbeek C.J.R., T. Hick, and A. Langdon (2011), Degradation as a result of UV radiation of bloodmeal-based thermoplastics, *Polym. Degrad. Stab.*, 96, 515-522.

Vilaplana, J. M., A. Serrano, M. Antón, M. L. Cancillo, M. Parias, J. Gröbner, G. Hülsen, G. Zablocky, A. Díaz, and B. A. de la Morena (2009), COST Action 726 – Report of the "El Arenosillo"/INTA-COST calibration and intercomparison campaign of UVER broadband radiometers.

Webb, A. R., L. Kline, and M. F. Holick (1988), Influence of season and latitude on the cutaneous synthesis of Vitamin D3: exposure to winter sunlight in Boston and Edmonton will not promote Vitamin D3 synthesis in human skin, *J. Clin. Endocrinol. Metab.*, 67, 373–378.

Webb, A., J. Gröbner, and M. Blumthaler (2006), A practical guide to operating broadband instruments measuring erythemally weighted irradiance, Produced by the join efforts of WMO SAG UV and Working Group 4 of the COST-726 Action: Long Term Changes and Climatology of the UV Radiation over Europe, vol.EUR 22595/WMO.

Williamson, C.E., R. G. Zepp, R. M. Lucas, S. Madronich, A. T. Austin, C. L. Ballaré, M. Norval, B. Sulzberger, A. F. Bais, R. L. McKenzie, S. A. Robinson, D.-P. Häder, N. D. Paul and J. F. Bornman, Solar ultraviolet radiation in a changing climate, Nat. Clim. Change, 2014, 4, 434–441

Zuber, V., and K. Strimmer (2011), High-dimensional regression and variable selection using CAR scores, *Statist. Appl. Genet. Mol. Biol*., 10: 34.

Tables

Table 1. Mathematical formula, coefficient of determination and relative root mean squared error of the ordinary least squares regression and validation for each proposed model.

Model	Mathematical Formulae	Fitting	Validation
		rRMSE (%)	rRMSE (%)
M1	$f_{UV}=a_1+b_1\cdot k_{UV}$	9.5	9.5
M2	$f_{UV}=a_2+b_2\cdot k_{UV}+c_2\cdot k_{UV}^2+d_2\cdot k_{UV}^3+g_2\cdot k_{UV}^4$	9.2	9.3
M3	$f_{UV}=a_3+b_3\cdot k_{UV}+c_3\cdot\cos(\theta)$	8.9	8.8
M4	$f_{UV}=a_4+b_4\cdot k_{UV}+c_4\cdot k_{UV}^2+d_4\cdot k_{UV}^3+g_4\cdot k_{UV}^4+h_4\cdot\cos(\theta)$	8.6	8.5
M5	$f_{UV}=a_5+b_5\cdot k_{UV}+c_5\cdot\cos(\theta)+d_5\cdot\Delta_{UV-1}$	8.9	8.8
M6	$f_{UV}=a_6+b_6\cdot k_{UV}+c_6\cdot\cos(\theta)+d_6\cdot\Delta_{UV-2}$	8.3	8.3
M7	$f_{UV}=a_7+b_7\cdot k_{UV}+c_7\cdot\cos(\theta)+d_7\cdot\Delta_{UV-3}$	8.8	8.7
M8	$f_{UV}=a_8+b_8\cdot k_{UV}+c_8\cdot k_{UV}^2+d_8\cdot k_{UV}^3+g_8\cdot k_{UV}^4+h_8\cdot\cos(\theta)+j_8\cdot\Delta_{UV-1}$	8.4	8.4
M9	$f_{UV}=a_9+b_9\cdot k_{UV}+c_9\cdot k_{UV}^2+d_9\cdot k_{UV}^3+g_9\cdot k_{UV}^4+h_9\cdot\cos(\theta)+j_9\cdot\Delta_{UV-2}$	7.8	7.9
M10	$f_{UV}=a_{10}+b_{10}\cdot k_{UV}+c_{10}\cdot k_{UV}^2+d_{10}\cdot k_{UV}^3+g_{10}\cdot k_{UV}^4+h_{10}\cdot\cos(\theta)+j_{10}\cdot\Delta_{UV-3}$	8.4	8.4
M11	$f_{UV}=\frac{1}{1+\exp(a_{11}+b_{11}\cdot k_{UV}+c_{11}\cdot\cos(\theta))}$	10.8	10.6
M12	$f_{UV}=\frac{1}{1+\exp(a_{12}+b_{12}\cdot k_{UV}+c_{12}\cdot\cos(\theta)+d_{12}\cdot AST)}$	10.8	10.6
M13	$f_{UV}=\frac{1}{1+\exp(a_{13}+b_{13}\cdot k_{UV}+c_{13}\cdot\cos(\theta)+d_{13}\cdot\Psi_{UV})}$	10.8	10.6
M14	$f_{UV}=\frac{1}{1+\exp(a_{12}+b_{14}\cdot k_{UV}+c_{14}\cdot\cos(\theta)+d_{14}\cdot K_{UV})}$	10.8	10.6
M15	$f_{UV}=\frac{1}{1+\exp(a_{15}+b_{15}\cdot k_{UV}+c_{15}\cdot\cos(\theta)+d_{15}\cdot AST+g_{15}\cdot\Psi_{UV}+h_{15}\cdot K_{UV})}$	10.8	10.6
M16	$f_{UV}=a_{16}+b_{16}\cdot k_{UV}+c_{16}\cdot\cos(\theta)+d_{16}\cdot AST$	8.9	8.8
M17	$f_{UV}=a_{17}+b_{17}\cdot k_{UV}+c_{17}\cdot\cos(\theta)+d_{17}\cdot\Psi_{UV}$	8.9	8.8
M18	$f_{UV}=a_{18}+b_{18}\cdot k_{UV}+c_{18}\cdot\cos(\theta)+d_{18}\cdot K_{UV}$	8.9	8.8
M19	$f_{UV}=a_{19}+b_{19}\cdot k_{UV}+c_{19}\cdot k_{UV}^2+d_{19}\cdot k_{UV}^3+g_{19}\cdot k_{UV}^4+h_{19}\cdot\cos(\theta)+j_{19}\cdot AST$	8.6	8.5

M20	$f_{UV}=a_{20}+b_{20}\cdot k_{UV}+c_{20}\cdot k_{UV}^2+d_{20}\cdot k_{UV}^3+g_{20}\cdot k_{UV}^4+h_{20}\cdot\cos(\theta)+j_{20}\cdot\Psi_{UV}$	8.5	8.5
M21	$f_{UV}=a_{21}+b_{21}\cdot k_{UV}+c_{21}\cdot k_{UV}^2+d_{21}\cdot k_{UV}^3+g_{21}\cdot k_{UV}^4+h_{21}\cdot\cos(\theta)+j_{21}\cdot K_{UV}$	8.5	8.4
M22	$f_{UV}=a_{22}+b_{22}\cdot k_{UV}+c_{22}\cdot\cos(\theta)+d_{22}\cdot AST+g_{22}\cdot\Psi_{UV}+h_{22}\cdot K_{UV}$	8.9	8.7
M23	$f_{UV}=a_{23}+b_{23}\cdot k_{UV}+c_{23}\cdot k_{UV}^2+d_{23}\cdot k_{UV}^3+g_{23}\cdot k_{UV}^4+h_{24}\cdot\cos(\theta)+j_{23}\cdot AST+l_{22}\cdot\Psi_{UV}+m_{22}\cdot K_{UV}$	8.4	8.3

Table 2. Empirical fitting coefficients and their corresponding stadard error for the best modes M4, M9 and M20

Model	**Mathematical Formulae**
M4	$f_{UV}=(80\pm1)\times10^{-2}+(17\pm5)\cdot k_{UV}+(-73\pm7)\times10^{2}\cdot k_{UV}^2+(40\pm4)\times10^{4}\cdot k_{UV}^3+(-71\pm8)\times10^{5}\cdot k_{UV}^4+(27\pm1)\times10^{-2}\cdot\cos(\theta)$
M9	$f_{UV}=(98\pm1)\times10^{-2}+(21\pm5)\cdot k_{UV}+(-70\pm7)\times10^{2}\cdot k_{UV}^2+(38\pm4)\times10^{4}\cdot k_{UV}^3+(-65\pm7)\times10^{5}\cdot k_{UV}^4+(13\pm1)\times10^{-2}\cdot\cos(\theta)+(30\pm1)\times10^{-3}\cdot\Delta_{UV-2}$
M20	$f_{UV}=(85\pm1)\times10^{-2}+(23\pm5)\cdot k_{UV}+(-75\pm7)\times10^{2}\cdot k_{UV}^2+(42\pm4)\times10^{4}\cdot k_{UV}^3+(-73\pm7)\times10^{5}\cdot k_{UV}^4+(26\pm1)\times10^{-2}\cdot\cos(\theta)+(-75\pm8)\times10^{-1}\cdot\Psi_{UV}$

Table 3. Magnitude and CAR score of the terms and AIC for models M4, M9 and M20

Model	**Term contribution**				***r²***	***rRMSE (%)***	***AIC***
	$b\cdot\overline{k_{UV}}+c\cdot\overline{k_{UV}^2}+d\cdot\overline{k_{UV}^3}+g\cdot\overline{k_{UV}^4}$	$h\cdot\overline{\cos(\theta)}$	$j\cdot\overline{\Delta_{UV-2}}$	$j\cdot\overline{\Psi_{UV}}$			
M4	-0.27 (88.6%)	0.18 (11.4%)			0.79	8.6	- 20942
M9	-0.20 (64.1%)	0.09 (13.4%)	-0.13 (22.5%)		0.83	7.8	- 21639
M20	-0.11 (56.0%)	0.16 (6.2%)		-0.08 (37.1%)	0.79	8.5	- 21020

Figures

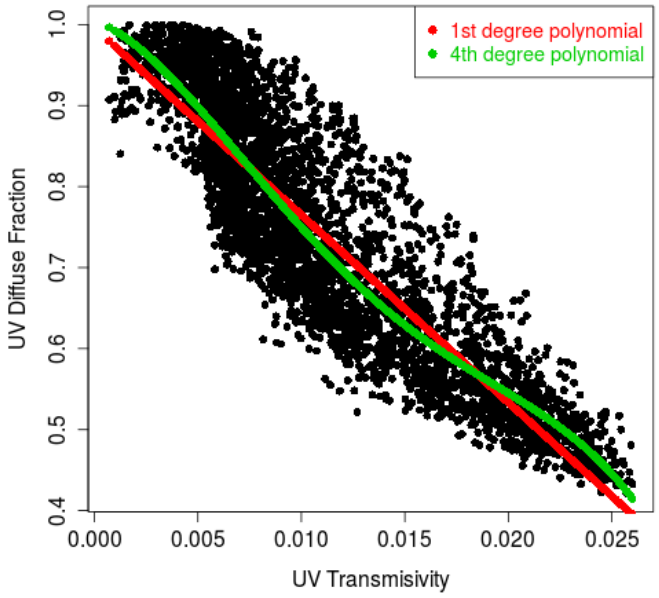

Figure 1. UV diffuse fraction, f_{UV}, versus UV transmissivity, k_{UV}.

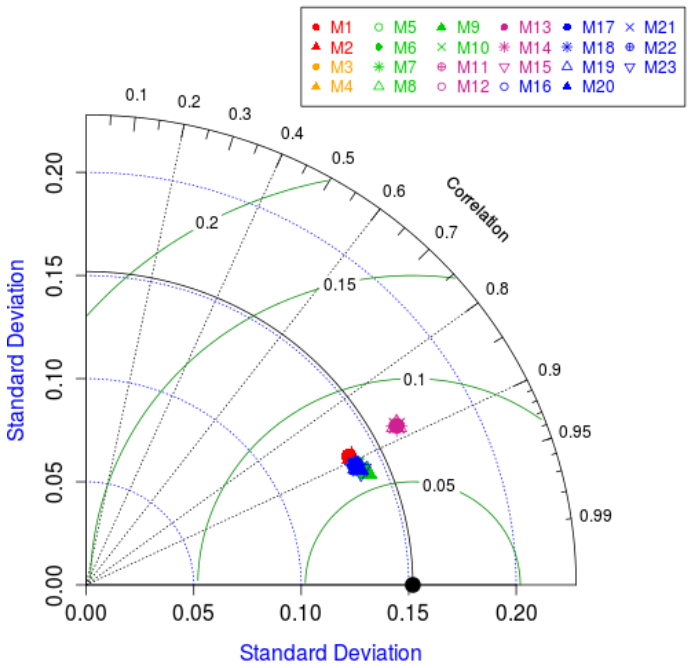

Figure 2. Taylor diagram

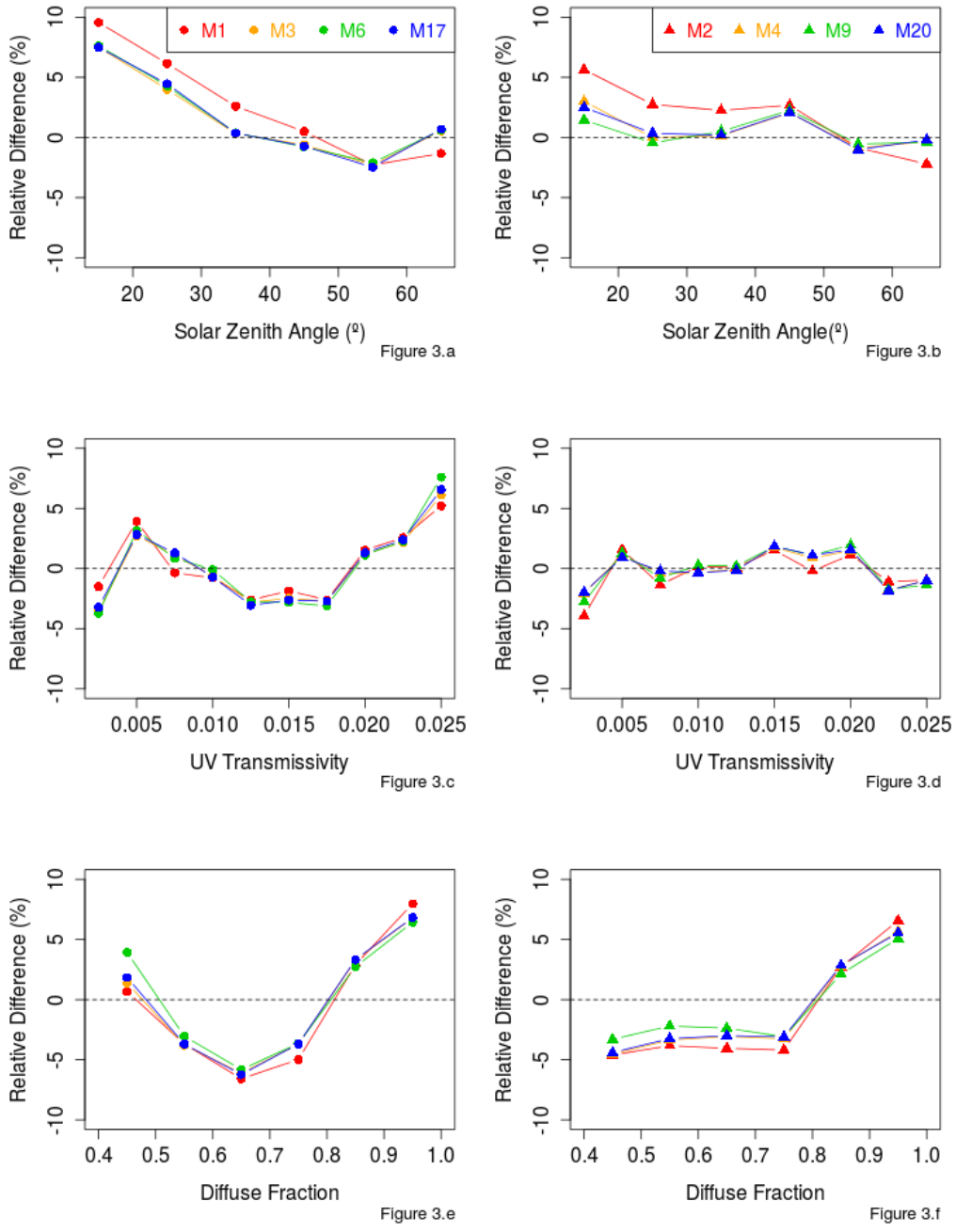

Figure 3. Relative differences versus a, b) solar zenith angle; c, d) UV transmissivity and e, f) UV diffuse fraction

5.2.4. Informe del Director de la Tesis Doctoral

El artículo "Modeling ultraviolet diffuse fraction", ha sido enviado para su publicación en la revista Journal of Geophysical Research - Atmospheres y se encuentra actualmente en fase de revisión, teniendo la revista un factor de impacto en 2015 de 3.318 y estando incluida en el primer cuartil (Q1, ranking 27 de 184 revistas) dentro de la categoría "Geosciences, Multidisciplinary".

La participación de la doctoranda Dña. Guadalupe Sánchez Hernández en este artículo ha sido muy elevada y diversa, colaborando muy activamente en todas las etapas desarrolladas para la obtención del artículo, desde la concepción de la idea original hasta la toma de medidas, propuesta y adaptación de modelos, cálculo, análisis de resultados y comparativa entre modelos, extracción de las principales conclusiones y elaboración del manuscrito.

Todas estas las tareas han sido desarrolladas por la doctoranda bajo mi dirección y supervisión, pudiendo dar fe de que todo lo aquí expuesto es verídico.

Fdo.: El Director de la Tesis Doctoral

Por otra parte, D. Antonio Serrano Pérez y Dña. María Luisa Cancillo Fernández, coautores de este artículo, afirman mediante este escrito que han colaborado en este artículo pero que éste forma parte íntegra de la Tesis Doctoral de Dña. Guadalupe Sánchez Hernández y que no va a ser utilizado por ellos como parte de sus respectivas tesis doctorales.

Dña. Mª Luisa Cancillo Fernández D. Antonio Serrano Pérez

Capítulo 6

Principales resultados y conclusiones

A continuación se resumen los principales resultados y conclusiones obtenidos en esta Tesis Doctoral:

- Es necesario corregir el cero térmico diurno de las medidas registradas por un piranómetro, pues puede alcanzar valores de hasta 15 W/m^2, lo que puede suponer un error de hasta un 20 % en las medidas de irradiancia difusa.

- El valor del cero térmico diurno de los piranómetros estudiados es significativamente diferente del valor nocturno y, por lo tanto, no puede ser estimado a partir de la señal registrada por el piranómetro durante la noche.

- Se puede estimar el cero térmico a partir de expresiones empíricas basadas en variables meteorológicas del ambiente. En este sentido se ha propuesto un conjunto de modelos que predicen el cero térmico con un coeficiente de correlación en torno a 0.92 y un error cuadrático medio en torno a 2.0 W/m^2.

- La utilización de ventilación artificial reduce la magnitud y variabilidad del cero térmico, así como sus diferencias entre distintos modelos de piranómetros. Las diferencias en el cero térmico de un mismo piranómetro con y sin ventilación pueden variar entre 1 W/m^2 y 9 W/m^2.

- La aplicación de los modelos empíricos para la corrección del error introducido por el anillo de sombra en la medida de irradiancia solar difusa total requiere su particularización a las condiciones locales, consiguiendo reducir el valor medio de dicho error de un 11 % a un 0.6 %.

- Se pueden obtener medidas precisas de irradiancia solar difusa ultravioleta usando bandas de sombra. Así, se han propuesto dos modelos empíricos originales para la corrección del error introducido por el anillo de sombra en las medidas de irradiancia solar difusa ultravioleta, que corrigen dicho error reduciéndolo de un 14 % a un 1.6 %.

- Es posible estimar la fracción de irradiancia solar difusa ultravioleta a partir de valores de irradiancia solar global ultravioleta. Para ello, se han propuesto tres modelos empíricos originales que estiman dicha fracción difusa, obteniendo un coeficiente de correlación de 0.9 y un error cuadrático medio relativo en torno al 8 %.

Summary of results and main conclusions

The main results and conclusions obtained in this Doctoral Thesis are summarized below:

- It is necessary to correct the daytime thermal offset in measurements recorded by pyranometers, as it can reach values up to 15 W/m^2.which yields an error of up to 20 % in total diffuse irradiance measurements.
- The daytime thermal offset value of the pyranometers analyzed in this study is significantly different from the nighttime value and, therefore, no reliable estimation can be derived from the nighttime pyranometer signal.
- Thermal offset can be estimated using empirical expressions based on environmental variables. In this sense, a set of models have been proposed to predict the thermal offset with a correlation coefficient around 0.92 and a mean squared error around 2.0 W/m^2.
- The use of artificial ventilation reduces the magnitude and variability of thermal offset, as well as differences between pyranometer models. The differences in the thermal offset of one pyranometer with and without ventilation can vary between 1 W/m^2 and 9 W/m^2.
- In order to correct the error associated to the use of a shadow ring for solar diffuse irradiance measurements, the empirical models need to be adjusted to local conditions. Once adjusted, the mean error is reduced from 11 % to 0.6 %.
- Accurate measurements of ultraviolet diffuse solar irradiance can be obtained using a shadow band. Thus, two original empirical models have been proposed to correct the error caused by the use of a shadow ring for ultraviolet diffuse solar irradiance measurements, with the relative error being reduced from 14 % to 1.6 %.

- The solar ultraviolet diffuse fraction can be reliably estimated using global ultraviolet irradiance values. To this end, three original empirical models have been proposed to estimate the diffuse fraction,achieving a correlation coefficient of 0.9 and a relative root mean squared error around 8 %.